

**UNIVERSIDADE FEDERAL DE MINAS GERAIS
INSTITUTO DE CIÊNCIAS BIOLÓGICAS
DEPARTAMENTO DE BIOQUÍMICA IMUNOLOGIA**

**CÁLCIO INTRACELULAR NA PROLIFERAÇÃO
DE CÉLULAS HEPÁTICAS**

Viviane Aguiar Andrade

**BELO HORIZONTE
MINAS GERAIS – BRASIL
2010**

VIVIANE AGUIAR ANDRADE

**CÁLCIO INTRACELULAR NA PROLIFERAÇÃO
DE CÉLULAS HEPÁTICAS**

Tese apresentada ao programa de pós-graduação em Bioquímica e Imunologia do Instituto de Ciências Biológicas da Universidade Federal de Minas Gerais, como requisito parcial para obtenção do título de Doutor em Bioquímica e Imunologia.

Área de concentração: Biologia Molecular

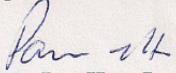
Orientadora: Maria de Fátima Leite

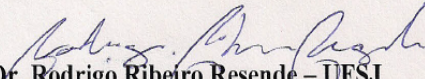
Co-orientador: José Miguel Ortega

**BELO HORIZONTE
MINAS GERAIS – BRASIL
2010**



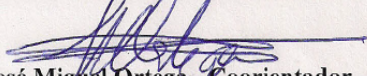
ATA DA DEFESA DA TESE DE DOUTORADO DE VIVIANE AGUIAR ANDRADE. Aos sete dias do mês de dezembro de 2010, às 13:30 horas, reuniu-se no Instituto de Ciências Biológicas da Universidade Federal de Minas Gerais, a Comissão Examinadora da tese de Doutorado, indicada *ad referendum* do Colegiado do Curso, para julgar, em exame final, o trabalho intitulado “Cálcio intracelular na proliferação de células hepáticas”, requisito final para a obtenção do grau de *Doutor em Ciências: Biologia Molecular*. Abrindo a sessão, a Presidente da Comissão, Profa. Maria de Fátima Leite, da Universidade Federal de Minas Gerais, após dar a conhecer aos presentes o teor das Normas Regulamentares do Trabalho Final, passou a palavra à candidata, para apresentação de seu trabalho. Seguiu-se a arguição pelos examinadores, com a respectiva defesa da candidata. Logo após, a Comissão se reuniu, sem a presença da candidata e do público, para julgamento e expedição do resultado final. Foram atribuídas as seguintes indicações: Dr. Paulo Lee Ho, do Instituto Butantan, aprovada; Dr. Rodrigo Ribeiro Resende, da Universidade Federal de São João Del Rey, aprovada; Dra. Elaine Maria de Souza Fagundes, da Universidade Federal de Minas Gerais, aprovada; Dra. Santuza Maria Ribeiro Teixeira, da Universidade Federal de Minas Gerais, aprovada; Dr. José Miguel Ortega, Coorientador, da Universidade Federal de Minas Gerais, aprovada e Dra. Maria de Fátima Leite, Orientadora, da Universidade Federal de Minas Gerais, aprovada. Pelas indicações, a candidata foi considerada APROVADA. O resultado final foi comunicado publicamente à candidata pela Presidente da Comissão. Nada mais havendo a tratar, a Presidente da Comissão encerrou a reunião e lavrou a presente Ata que será assinada por todos os membros participantes da Comissão Examinadora. Belo Horizonte, 07 de dezembro de 2010.

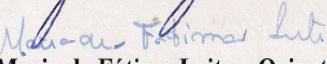

Dr. Paulo Lee Ho - Instituto Butantan

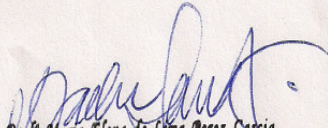

Dr. Rodrigo Ribeiro Resende - UFSJ


Dra. Elaine Maria de Souza Fagundes - UFMG


Dra. Santuza Maria Ribeiro Teixeira - UFMG


Dr. José Miguel Ortega - Coorientador - UFMG


Dra. Maria de Fátima Leite - Orientadora - UFMG


Prof. Maria Elena de Lima Perez Garcia
Coordenadora do Curso de Pós-Graduação
em Bioquímica e Imunologia
ICB - UFMG

*“Os limites do mundo meus pés não ultrapassam, mas o
que de mais alto existe minha alma alcança.”*

Padre Fábio de Melo

*“Dedico a minha mãe amada, Dorinha, que mesmo não
estando presente, me fortalece e incentiva a
lutar por cada vitória.”
Sinto saudades mãe...*

AGRADECIMENTOS

A minha sempre amada mãe... Ao meu pai, Fernando, e meus irmãos Carla e Júnior, pelo amor, confiança e carinho constantes em todos os momentos de minha vida. Aos sobrinhos Caio, Juju, Luis Fernando e Marcos Felipe, luz e alegria de nossas vidas. Ao meu cunhado Regi por completar nossa família.

Ao Fabrício, presença mais que necessária; imprescindível em meus melhores e piores momentos. Obrigada pela paciência, carinho e amor; e também pela preocupação, compreensão e dedicação durante todo o tempo em que estamos juntos e principalmente, durante estes longos anos de doutorado.

Ao Mateus “Antônio”, por tudo! Pela paciência, convivência, ensinamentos, incentivo e colaboração. Sem você teria sido bem mais difícil!

A Flávia e a Camila, pela amizade e companherismo e pela imensa ajuda no desenvolvimento deste trabalho.

À Maria Jimena, pela amizade e carinho e pelas mensagens de força e apoio. E a Romina Fiorotto pela amizade e dedicação.

A Elaine “Maria”, Márcia “Maria” e Nilo “Antônio” companheiros de república, pela amizade, preocupação, companherismo, união e convivência e por proporcionarem momentos felizes e inesquecíveis.

À minha orientadora Maria de Fátima Leite pela confiança, ensinamentos, conselhos e oportunidade e acima de tudo pela amizade.

Ao meu grande orientador e amigo José Miguel Ortega pela orientação científica e pessoal; pela dedicação, amizade e confiança demonstradas durante toda minha trajetória acadêmica, desde a iniciação científica. Valeu Miguel!!!!

Ao Dr. Michael Nathanson pela confiança e oportunidade e aos demais membros do Nathanson’s Lab: Emma Kruglov, Michael Fiedler, Máira e Denise por me acolherem durante minha temporada na Universidade de Yale. E a todos de Yale que me ajudaram no desenvolvimento do meu trabalho.

Aos professores Alfredo Góes, Oscar Bruna-Romero, Silvia Guatimosim e Elaine Fagundes por sempre estarem dispostos a esclarecer minhas dúvidas, e pela disponibilização dos seus laboratórios para que eu pudesse realizar meu trabalho. E aos membros de seus laboratórios por sempre me ajudarem quando solicitados.

Aos demais professores do departamento de Bioquímica e Imunologia pelos ensinamentos compartilhados e pela preocupação com minha formação acadêmica.

Aos professores Paulo Lee Ho, Rodrigo Resende, Santuza Teixeira e Elaine Fagundes de Sousa por aceitarem participar da minha banca examinadora e contribuírem para minha formação pessoal, profissional e acadêmica.

Aos amigos do Laboratório de Sinalização de Cálcio: Carla, Sandhra, Vanessa, Aninha, Lídia “Maria”, Emerson “Antônio”, Marisa, Lili, Fernanda, Douglas e Rafael. Obrigado pela convivência. E ao Gilson por sempre nos auxiliar na questão burocrática e organizacional do laboratório. À Michele pelo exemplo de dedicação e serenidade e a Dawidson pelos ensinamentos e sugestões científicas.

Aos amigos, companheiros inesquecíveis: Enéas, Marina, Marcinha, Ricardo e Rose. E a todos do Eletrocel pela amizade, companherismo e solidariedade.

Aos colegas e amigos do departamento de Bioquímica e Imunologia por andarem junto comigo neste caminho; e departamento de Fisiologia por me adotarem durante meu doutorado.

A Celise Maria Costa, pela presteza, dedicação e boa vontade constantes para resolver todos os problemas departamentais. E aos demais funcionários do departamento de Bioquímica pela competência no desenvolvimento dos seus trabalhos.

Aos funcionários do Biotério, pelo cuidado com os animais e por sempre me atenderem com o fornecimento de animais para os experimentos *in vivo*.

E a todos os amigos e demais pessoas que, de alguma maneira, contribuíram para a conclusão de mais uma etapa de minha vida.

Agradeço também a Deus, luz maior de minha vida, responsável por todas as coisas, e por me guiar até o fim desta jornada.

Este trabalho foi realizado com o apoio das seguintes instituições:

- Conselho Nacional do Desenvolvimento Científico e Tecnológico (CNPq)
- Coordenação de Aperfeiçoamento de Nível Superior (CAPES)
- Fundação de Amparo à Pesquisa do Estado de Minas Gerais (FAPEMIG)
- Howard Hughes Medical Institute (HHMI)

SUMÁRIO

Lista de abreviaturas	ix
Lista de figuras	x
Lista de tabelas	xii
Resumo	xiii
Abstract	xv
1. Introdução	1
1.1. Ciclo celular	2
1.2. Sinais de Ca²⁺	4
1.3. Receptores de RyR	4
1.4. Receptores de InsP₃	5
1.5. Ca²⁺ nuclear	6
1.6. Expressão gênica	10
1.7. O Ca²⁺ e a expressão gênica	13
1.8. Proliferação de células hepáticas	15
1.9. Regeneração do fígado	16
1.10. Justificativa	17
2. Objetivos	19
3. Materiais e Métodos	21
3.1. Materiais e reagentes	22
3.2. Linhagens celulares	23
3.3. Extração de DNA plasmidial	23
3.4. RaSH	24
3.5. RT e PCR semi-quantitativo	30
3.6. Real time PCR	30
3.7. Imunofluorescência	31
3.8. Western blot	32
3.9. Medidas de incorporação de BrdU	32
3.10. Medidas do índice mitótico	33
3.11. Análises do ciclo celular	33
3.12. Ensaio de apoptose	33
3.13. Imunofluorescência em tecido humano	34

3.14. Ensaio de luciferase	34
3.15. Construção de adenovírus recombinantes.....	35
3.16. Infecção das células com adenovírus.....	38
3.17. Hepatectomia parcial	38
3.18. Medidas de sinais de Ca ²⁺ intracelular	39
3.19. Análises estatísticas	40
4. Resultados	41
4.1. Verificar a influência do Ca ²⁺ nuclear, sobre a expressão de genes envolvidos na proliferação celular	42
4.1.1. Identificação de genes com expressão modulada pelo Ca ²⁺ nuclear.....	42
4.1.2. Validação dos clones selecionados pelo RaSH	44
4.1.3. Tamponamento do Ca ²⁺ nuclear altera a expressão da LGMN	48
4.1.4. Silenciamento da LGMN altera a proliferação celular	52
4.1.5. Silenciamento da LGMN altera a cinética do ciclo celular	55
4.1.6. Silenciamento da LGMN modula expressão das proteínas do ciclo célula	57
4.1.7. Expressão da LGMN em fígado humano normal e em hepatocarcinoma	59
4.2. Investigar o papel que o Ca ²⁺ intracelular liberado a partir da ativação dos InsP ₃ RI exerce sobre a regeneração hepática	59
4.2.1. Construção e teste dos adenovirus Ad-siRNA-I	59
4.2.2. Silenciamento dos InsP ₃ RI	64
4.2.3. Alterações dos sinais de Ca ²⁺ intracelulares após silenciamento dos InsP ₃ RI	65
4.2.4. Silenciamento dos InsP ₃ RI altera a regeneração hepática	68
5. Discussão	71
6. Referências bibliográficas.....	78
7. Anexos.....	86
7.1. Certificado do CETEA	
8. Produção bibliográfica	88
8.1. Artigo: Nucleoplasmic calcium regulates cell proliferation through legumain	
8.2. Artigo: Mitochondrial calcium regulates liver regeneration through modulation of apoptosis.	

- 8.3.** Artigo: Insulin induces calcium signals in the nucleus of rat hepatocytes
- 8.4.** Artigo: Highly efficient siRNA delivery system into human and murine cells using single-wall carbon nanotubes
- 8.5.** Capítulo de livro: Signaling pathways in biliary epithelial cells

LISTA DE ABREVIATURAS

- Ad-GFP:** adenovírus com a sequência GFP (*green fluorescent protein*)
- Ad-PV-NLS:** adenovírus com a construção parvalbumina, e sequência NLS (*nuclear localization sequence*)
- Ad-PV-NLS-Cd:** adenovírus com a construção parvalbumina mutada e sequência NLS
- AdsiRNA-I:** adenovírus contendo siRNA para InsP₃RI
- ARID1A:** domínio de ligação ao DNA rico em A-T
- AVP:** arginina-vasopressina
- BLAST:** *basic local alignment search tool*; compara sequências biológicas primárias
- Ca²⁺:** cálcio
- CHO:** células de ovário de Hamster
- c-Met:** receptor do fator de crescimento do hepatócito (HGFR)
- HEK293:** células renais embrionárias humanas
- HepG2:** linhagem hepática humana
- HGF:** fator de crescimento do hepatócito
- HX:** hepatectomia parcial
- InsP₃:** inositol 1,4,5-trifosfato
- InsP₃R:** receptor de inositol 1,4,5-trifosfato
- LGMN:** legumaina
- MOI:** multiplicidade de infecção
- RaSH:** rápida subtração por hibridização
- RTN4:** reticulom
- RyR:** receptor de rianodina
- siRNA:** pequeno RNA de interferência
- SKHep1:** linhagem celular derivada de hepatocarcinoma humano
- TBRG4:** fator regulador do TGFβ₄ (fator de crescimento transformante β₄)

LISTA DE FIGURAS

- Figura 1** - Mecanismo de sinalização de Ca^{2+} em hepatócitos
- Figura 2** - Sinalização de Ca^{2+} no núcleo de hepatócitos induzida por hormônio
- Figura 3** - Controle da expressão gênica
- Figura 4** - Elementos *cis* e *trans* que atuam na regulação da expressão gênica
- Figura 5** - Metodologia RaSH
- Figura 6** - Tamponamento de Ca^{2+} nuclear pela proteína Parvalbumina (PV)
- Figura 7** - Diagrama esquemático da região promotora do gene da LGMN
- Figura 8** - Desenho dos *primers* para o gene do RTN4
- Figura 9** - Validação do resultado do RaSH para o gene do RTN4
- Figura 10** - Expressão do mRNA do RTN4
- Figura 11** - Validação do resultado do RaSH para os genes da LGMN e do TBRG4
- Figura 12** - Expressão protéica de LGMN
- Figura 13** - Expressão de LGMN em células SKHep1
- Figura 14** - Ativação do promotor de LGMN
- Figura 15** - Indução da expressão de LGMN por mitógenos
- Figura 16** - Expressão de LGMN após silenciamento
- Figura 17** - LGMN afeta a proliferação celular
- Figura 18** - Atividade enzimática da LGMN não altera a proliferação celular
- Figura 19** - Cinética do ciclo celular após silenciamento da LGMN
- Figura 20** - Apoptose após silenciamento da LGMN
- Figura 21** - Expressão de proteínas *checkpoints* do ciclo celular
- Figura 22** - Expressão de LGMN em fígado humano normal e com hepatocarcinoma
- Figura 23** - Seqüenciamento do siRNA desenhado para o InsP₃RI
- Figura 24** - Silenciamento do InsP₃RI
- Figura 25** - Expressão de InsP₃R-I em fígado

Figura 26 - Expressão de InsP₃R-I em hepatócitos

Figura 27 - Expressão de InsP₃R-I em hepatócitos após hepatectomia parcial

Figura 28 - Sinalização de Ca²⁺ em hepatócitos

Figura 29 - Regeneração hepática.

LISTA DE TABELAS

Tabela 1. *Primers* específicos utilizados no seqüenciamento e nas reações de RT-PCR

Tabela 2. *Primers* específicos utilizados nas reações de Real-Time PCR

Tabela 3. Número de clones selecionados na subtração pelo método RaSH

Tabela 4. Clones selecionados pelo RaSH

RESUMO

A regeneração do fígado depende de fatores de crescimento como o fator de crescimento hepático (HGF) e a insulina, que induzem sinais de Ca^{2+} necessários para a proliferação celular. Sinais de Ca^{2+} em hepatócitos dependem da atividade dos receptores de inositol 1,4,5-trifosfato (InsP_3Rs), porém os mecanismos pelos quais os sinais de Ca^{2+} regulam a regeneração hepática não são conhecidos. Neste trabalho examinamos se o Ca^{2+} nuclear modula a expressão de genes envolvidos na proliferação celular e avaliamos também a contribuição dos sinais de Ca^{2+} mediados pelo InsP_3RI na regulação da regeneração hepática. Para investigar alterações de expressão gênica pelo Ca^{2+} nuclear utilizamos o protocolo de RaSH (*Rapid Subtraction Hybridization*) que permite selecionar genes expressos em células SKHep1 que tiveram o Ca^{2+} nuclear tamponado. A subtração permitiu identificar 154 genes cuja expressão foi afetada por pequena alteração na concentração do Ca^{2+} nuclear. Dentre estes, foram selecionados 3 clones, legumina (LGMN), reticulom (RTN4) e o regulador do fator de crescimento transformante (TBRG), que através de pesquisa de similaridade utilizando o programa BLASTN, mostraram envolvimento em processos de proliferação celular. A LGMN foi alvo de futuros estudos. Observamos que o tamponamento do Ca^{2+} nuclear reduziu os níveis de mRNA e os níveis protéicos da LGMN. Por outro lado, o aumento de Ca^{2+} nuclear, pela estimulação das células SKHep1 com HGF aumentou a expressão de LGMN. O silenciamento da LGMN por siRNA diminuiu a proliferação de células SKHep1, por um mecanismo que independe da atividade da LGMN como endopeptidase. Além disso, foi observado que na ausência da LGMN, houve redução do índice mitótico, com significativa redução na fração de células na fase G2/M. Isto foi associado ao aumento na expressão das ciclinas A e E e ausência de apoptose. O papel da LGMN na proliferação celular foi confirmado em tecido humano, no qual observamos expressão aumentada de LGMN em células de hepatocarcinomas comparados a hepatócitos normais na mesma amostra. Como o aumento de Ca^{2+} intracelular em células hepáticas é mediado primordialmente por InsP_3R , investigamos a contribuição relativa da isoforma tipo I do InsP_3R na capacidade proliferativa de hepatócitos durante a regeneração hepática. Utilizamos siRNA acoplados ao sistema adenoviral para promover a redução na expressão InsP_3R tanto *in vitro* quanto *in vivo*. Os adenovirus AdsiRNA-I foram eficientes e específicos para reduzir a expressão do receptor tanto em células CHO quanto em hepatócitos. A sinalização de Ca^{2+} foi

deficiente em animais com InsP₃RI silenciado e isto comprometeu o processo de regeneração do fígado. Em conjunto, esses dados mostram que o Ca²⁺ nuclear, regula o processo de proliferação de células hepáticas, ao menos em parte pela modulação do gene da LGMN. Além disso, demonstramos que a sinalização de Ca²⁺ mediada por InsP₃RI é importante para regulação da regeneração do fígado.

ABSTRACT

Liver regeneration depends upon growth factors such as hepatic growth factor (HGF) and insulin that induce Ca^{2+} signals are necessary for proliferation of cells. Ca^{2+} signals in hepatocytes are mediated by inositol 1,4,5-triphosphate receptors (InP_3Rs) activity, therefore, the mechanism by which nuclear Ca^{2+} regulates liver regeneration is not known. Here we examined whether nuclear Ca^{2+} modulates expression of genes involved in cell proliferation and evaluated the contribution of InP_3RI -mediated Ca^{2+} signaling to the regulation of liver regeneration. To investigate the role of nuclear Ca^{2+} in gene expression we used Rapid Subtraction Hybridization (RaSH) protocol that permit subtract genes expressed in SKHep1 cells with nuclear Ca^{2+} buffered. The subtraction permitted identification of 154 genes whose expression was affected by a small alteration in nuclear Ca^{2+} concentration. Among the selected clones, 3 clones were chosen, legumain (LGMN), reticulon 4 (RTN4) and transforming growth factor beta regulator 4 (TBRG4). These clones showed involvement in proliferative process by BLASTN analysis. The LGMN was chosen to investigate in details studies. We observed that buffering of nuclear Ca^{2+} reduced mRNA and protein LGMN levels. On the other hand, increases in nuclear Ca^{2+} , by HGF stimulation, increased the LGMN expression. Silencing of LGMN by siRNA decreased proliferation of SKHep1 cells, by a mechanism that not depends of endopeptidase activity of LGMN. The inhibitor of LGMN activity did not affect BrdU incorporation. Moreover, was observed that in LGMN absence there was reduction in mitotic index, with a significant reduction on fraction of cells in G2/M phase. This was associated with an increase in expression of cyclins A and E and no apoptosis. The role of LGN in proliferation was confirmed in human tissue, where we observed increased expression of LGMN in hepatocellular carcinoma cells relative to normal hepatocytes in the same specimens. As the increase of intracellular Ca^{2+} in liver cells is mediated primarily by InP_3R , we investigated the relative contribution of isoform type I InP_3R in the proliferative capacity of hepatocytes during liver regeneration. We used siRNA coupled to the adenoviral system to decrease the expression InP_3R both in vitro and in vivo. Adenoviruses AdsiRNA-I were effective and specific to reduce both receptor expression in CHO cells and in hepatocytes. The Ca^{2+} signaling was impaired in animals with InP_3RI silenced and this affected the process of liver regeneration. Together, these data show that the nuclear Ca^{2+} regulates the process of proliferation of liver cells, at least in part by the

modulation of gene LGMN. Furthermore, we demonstrated that Ca^{2+} signaling mediated by InsP_3RI is important for regulation of liver regeneration.

1. INTRODUÇÃO

A capacidade de crescer e se reproduzir são propriedades fundamentais de todas as células não maduras. Esta reprodução ocorre através da duplicação de seus conteúdos e posterior divisão em duas células filhas. Este processo é a garantia de uma sucessão contínua de células identicamente dotadas. As células originadas repetem o ciclo e o número de células aumenta exponencialmente. O ciclo de duplicação e divisão das células, denominado ciclo celular, é o mecanismo pelo qual todos os tecidos, os órgãos e os organismos crescem (Junqueira e Carneiro, 1995). Em organismos unicelulares, existe uma pressão seletiva para que cada célula cresça e se divida o mais rápido possível, porque a reprodução celular é responsável pelo aumento do número de indivíduos. Já nos organismos multicelulares, a produção de novas células através da duplicação permite a divisão do trabalho, no qual grupos de células tornam-se especializados em determinada função. Em um organismo adulto, a divisão celular é também necessária para repor as células que morreram e manter o organismo em equilíbrio.

1.1. Ciclo celular

Essa multiplicação celular é ordenada e regulada por complexas redes de proteínas que permitem que a passagem da informação genética para a próxima geração ocorra adequadamente. Porém, as células se dividem em níveis diferentes, algumas não se dividem como os neurônios, enquanto outras apresentam divisão rápida e contínua, como as células epiteliais. O ciclo de divisão celular apresenta duas etapas fundamentais, a fase M que compreende a mitose (divisão do núcleo) e a citocinese (divisão do citoplasma), e a interfase (crescimento celular, duplicação do DNA e síntese de proteínas). Em uma típica célula humana proliferativa em cultura, a interfase pode durar de 23 a 24 horas, compreendendo as fases G1, S e G2 do ciclo celular; e 1 hora a fase M (Junqueira e Carneiro, 1995).

O ciclo celular é regulado pelas interações de diversas proteínas. Essas proteínas compõem o sistema de controle que conduz e coordena o desenvolvimento do ciclo celular. Embora as proteínas que regulam o início da replicação do DNA sejam conservadas desde leveduras até mamíferos, as seqüências que são utilizadas como

sítios de iniciação são altamente divergentes (Gilbert, 2002). Pouco é conhecido sobre como os sítios de replicação são determinados ou o que regula a ordem na qual a replicação irá começar (Li et al., 2003). Pouco se sabe também sobre a estabilidade dos domínios cromossômicos durante os processos de replicação e como cada domínio é submetido à replicação. Mas é sabido que a transição entre as fases do ciclo celular é altamente regulada.

Durante o ciclo celular as proteínas *checkpoints* permitem a célula determinar se está tudo de acordo para que a nova fase se inicie. Por exemplo, se ocorre dano no DNA durante a fase G2 do ciclo, as células páram o ciclo e reparam o DNA antes de entrarem na mitose (Elledge, 1996; Nigg, 2001). Um grupo de proteínas que agem como reguladoras do ciclo celular são as cinases dependentes de ciclinas (cdk). As cdks são cinases da família de proteínas serina/treonina, que dependem da ligação de uma ciclina para sua atividade (Nigg, 2001).

Células de mamíferos possuem múltiplas cdks e ciclinas que agem em diferentes fases do ciclo celular. Enquanto as células progridem através do G1, o complexo ciclina D/cdk4 é ativado e fosforila a proteína supressora de tumor retinoblastoma (Rb) (Ekholm and Reed, 2000). Depois, o complexo ciclina E/cdk2 é ativado e a célula entra na fase S. Durante a fase S ocorre a ativação do complexo ciclina A/cdk2 que fica ativado até a entrada na fase G2 (Yam et al., 2002). Na fase G2, o complexo ciclina B/cdk1 é ativado permitindo a entrada e progressão do ciclo celular pela mitose (Ekholm and Reed, 2000).

Apesar de toda essa regulação, em organismos multicelulares a divisão e escolha dos sítios de replicação a serem ativados são controladas por proteínas altamente específicas, denominadas de fatores de crescimento. Os fatores de crescimento regulam a proliferação celular através de uma rede complexa de cascatas bioquímicas que por sua vez regulam a transcrição gênica e a montagem e desmontagem de um sistema de controle (Ekholm and Reed, 2000). Sabe-se que a regulação da proliferação celular requer vários fatores como hormônios, fatores de crescimento e citocinas, mas a maioria das cascatas de sinalização ativadas para as repostas de proliferação são aquelas iniciadas pelo aumento transiente dos níveis de Ca^{2+} intracelular (Kahl and Means, 2003).

1.2. Sinais de cálcio

O cálcio (Ca^{2+}) é uma das mais importantes moléculas de transdução de sinais. Sua função como segundo mensageiro é fundamental em diversas respostas celulares, influenciando eventos como secreção, contração muscular, fertilização, exocitose, plasticidade sináptica, expressão gênica, diferenciação e proliferação celular e apoptose (Pusch and Nathanson, 2004). Em hepatócitos, Ca^{2+} regula funções como secreção biliar, motilidade canalicular, transcrição gênica, apoptose, liberação de glicose, potencial de membrana mitocondrial, entre outras (revisado por Leite e Nathanson, 2009). Ainda não está completamente elucidado como o Ca^{2+} pode coordenar diferentes funções dentro da célula, mas a amplitude e a frequência dos sinais de Ca^{2+} , bem como o padrão espacial e temporal desses sinais, parecem estar diretamente relacionadas a esta especificidade (Pusch et al., 2002; Berridge et al., 2000).

Os mecanismos de sinalização de Ca^{2+} são, na sua grande maioria, ativados por canais intracelulares de Ca^{2+} (Leite and Nathanson, 2009). Os receptores de rianodina (RyR) e os receptores de inositol 1,4,5-trifosfato (InsP_3R) são os principais canais intracelulares de Ca^{2+} presentes nas células.

1.3. Receptores de rianodina

Os RyRs, apesar de estarem presentes em células epiteliais como ácino pancreático (Leite et al., 2002), são de primordial importância para a sinalização de Ca^{2+} em células excitáveis como células do músculo cardíaco e de células neuro-endócrinas (revisado por Leite e Nathanson, 2009). Existem três isoformas de RyRs: I, II e III. Todas são ativadas pelo Ca^{2+} e promovem sua liberação do retículo endo/sarcoplasmático para o citosol por um processo conhecido por liberação de Ca^{2+} induzida por Ca^{2+} (CIRC). Os RyRs tipos II e III também são sensíveis à adenosina trifosfato cíclica (cADP-ribose) (revisado por Leite e Nathanson, 2009).

A presença de RyRs em fígado é controversa. A enzima que catalisa a formação de cADP-ribose a partir da oxidação de adenina nicotinamida dinucleotídeo (NAD^+) é expressa em todos os tecidos, incluindo o fígado. Entretanto, seu papel direto na sinalização mediada pelo cADP-ribose, com conseqüente ativação de RyRs, ainda não foi estabelecida em hepatócitos (revisado por Leite e Nathanson, 2009)

Mas estudos realizados por Pierobon e colaboradores (Pierobon et al., 2006), mostraram por análises de RT-PCR a presença de uma proteína truncada de RyR tipo I em hepatócitos de ratos. Foi demonstrado que estes receptores são importantes na amplificação das respostas de Ca^{2+} induzidas por InsP_3 no fígado. Os RyRs criam microdomínios de Ca^{2+} próximos ao retículo endoplasmático que promovem o recrutamento de InsP_3Rs . Como consequência, ocorre uma maior liberação de Ca^{2+} pelos InsP_3Rs . Este Ca^{2+} é requerido para ativar as diversas repostas celulares do hepatócito em divisão. Contudo, ainda não foi comprovada a localização exata dessa proteína truncada de RyRsI em hepatócitos nem como ela é ativada.

1.4. Receptores de inositol 1,4,5-trifosfato

Os InsP_3R pertencem a uma família de canais de liberação de Ca^{2+} localizados predominantemente no retículo endoplasmático de todos os tipos celulares. Eles funcionam ao liberar Ca^{2+} em resposta ao inositol 1,4,5-trifosfato (InsP_3) produzido por diversos estímulos e geram sinais de Ca^{2+} locais ou globais. Estes sinais regulam numerosos processos fisiológicos, desde a transcrição de genes à secreção, aprendizagem e memória (revisado por Choe and Ehrlich, 2006).

O InsP_3 é formado quando algum ligante, de receptores acoplados à proteína G, se liga a este receptor e ativa a fosfolipase C (PLC), que hidroliza o fosfatidil inositol 4,5-bisfosfato (PIP_2) de membrana para formar diacilglicerol (DAG) e o InsP_3 . O InsP_3 se difunde pelo citoplasma e se liga ao seu receptor tetramérico no retículo endoplasmático que age como um canal, permitindo a liberação do Ca^{2+} para o citosol (revisado por Leite e Nathanson, 2009) (Figura 1).

Existem três isoformas de InsP_3Rs : Tipo I, II ou III. Já foi demonstrado que a distribuição espacial dos InsP_3R e a presença de diferentes isoformas resultam em diferenças nos parâmetros da sinalização de Ca^{2+} (Leite et al., 2003; Mendes et al., 2005). As isoformas de InsP_3Rs possuem uma considerável homologia na seqüência gênica, de aproximadamente 65%, mas cada subtipo é expresso e regulado de maneira distinta em cada tecido (Leite et al., 2003; Mendes et al., 2005). As diferenças e especificidades de cada isoforma, bem como a expressão e distribuição sub-celular apresentado por cada uma sugerem que as isoformas servem a diferentes papéis na sinalização de Ca^{2+} (Choe and Ehrlich, 2006; Leite and Nathanson, 2009).

Após a ligação do InsP_3 , o receptor sofre uma grande mudança conformacional que resulta na abertura do canal de Ca^{2+} . Embora cada isoforma funcione como um canal de Ca^{2+} , elas apresentam sensibilidades diferentes ao InsP_3 . A ordem de afinidade pelo InsP_3 é tipo II maior que tipo I que é maior que tipo III (revisado por Leite e Nathanson, 2009). Apesar do InsP_3 ser um requerimento absoluto para ativar o canal, a ativação dos InsP_3Rs é modulada de forma diferenciada por várias moléculas, entre elas o próprio Ca^{2+} . Outros ligantes como o ATP, regulam a atividade do canal principalmente por modificar a sensibilidade do receptor e controlar a liberação do Ca^{2+} (Foskett et al., 2007). Numerosas proteínas reguladoras como IRBIT (proteínas de ligação ao InsP_3R), ERp44, Homer, 4.1N e NCS-1 (sensor de cálcio neuronal 1) têm sido mostradas interagirem com diferentes isoformas do receptor e modificar suas propriedades (Choe and Ehrlich, 2006).

Estudos realizados por Hirata e colaboradores (Hirata et al., 2002) identificaram a presença de duas isoformas de InsP_3Rs em hepatócitos de ratos, InsP_3RI e InsP_3RII . Foi investigada também a distribuição dos receptores e foi constatado que o InsP_3RI encontra-se difusamente distribuído pelo citosol do hepatócito enquanto que o InsP_3RII concentra-se na região pericanicular da célula. O InsP_3RIII não é expresso em hepatócitos. Foi demonstrado que a distribuição dos InsP_3RI e InsP_3RII pela célula hepática contribui para o padrão de polarização das ondas de Ca^{2+} que se iniciam na região apical e seguem até a região basolateral da célula (Hernandez et al., 2007; Hirata et al., 2002).

1.5. Cálcio nuclear

Inicialmente pensava-se que o núcleo funcionava como um compartimento passivo no que diz respeito à passagem de Ca^{2+} originada no citoplasma. Sabe-se hoje que o núcleo é capaz de gerar e controlar sinais de Ca^{2+} locais. Estudo em núcleos isolados de hepatócitos de ratos demonstrou que o núcleo celular armazena Ca^{2+} , cuja liberação é dependente de InsP_3R (Gerasimenko et al., 1995).

Leite e colaboradores (2003), estudando a regulação do Ca^{2+} em diferentes compartimentos sub-celulares, verificaram que a presença de InsP_3Rs no envelope nuclear (NE) promove aumento dos níveis de Ca^{2+} no núcleo independente dos níveis de Ca^{2+} citoplasmático. A liberação deste íon no núcleo está ligado à existência de um compartimento membranoso, rico em receptores de InsP_3 tipo II, destinado a reservar

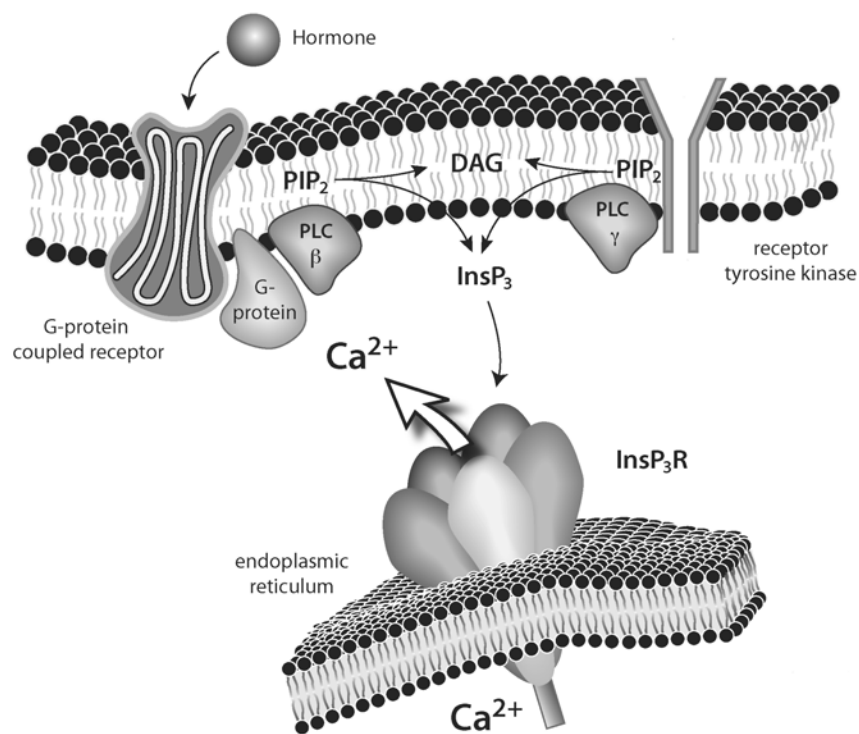


Figura 1. Mecanismo de sinalização de Ca^{2+} em hepatócitos. Após ligação ao seu receptor específico acoplado à proteína G, o hormônio induz a hidrólise do fosfatidil inositol difosfato (PIP₂) pela fosfolipase C. Há a formação de diacilglicerol (DAG) e inositol 1,4,5-trifosfato (InsP₃R). O InsP₃ se liga ao seu receptor (InsP₃R) no retículo endoplasmático que age como canal que permite a liberação de Ca^{2+} para o citosol. Fonte: Leite e Nathanson, 2009.

cálcio. Este compartimento, identificado por Echevarria e colaboradores (2003), é uma rede que se estende do retículo endoplasmático e do NE para o interior do núcleo, caracterizado em células epiteliais SKHep1 e denominado “retículo nucleoplasmático”.

A sinalização ativada pelo Ca^{2+} nuclear regula diretamente a ativação de cinases, como a CaM-cinase IV (Kahl and Means, 2003), que são capazes de ativar a transcrição de genes específicos (revisado por Berridge et al., 2000; Bootman et al., 2000); promove a indução e a translocação da proteína cinase C (PKC) para a membrana nuclear (Echevarria et al., 2003); regula negativamente o fator de transcrição TEF/TEAD (Thompson et al., 2003); promove impactos no crescimento e na proliferação celular (Rodrigues et al., 2007).

Já foi demonstrado em SKHep1 que o núcleo desta célula possui predominantemente o InsP₃RII (Echevarria et al., 2003). A localização e a isoforma presente na célula induz uma sinalização de Ca^{2+} distinta que desencadeia respostas

celulares específicas. Estudos revelam que o Ca^{2+} nuclear controla a proliferação de células SKHep1 e seu tamponamento promove um bloqueio do ciclo celular na transição G2/M (Rodrigues et al., 2007). A regulação da progressão do ciclo celular pelo Ca^{2+} afeta diretamente o processo de proliferação celular. Outros estudos em HepG2, linhagem de células hepáticas, mostraram que com baixa concentração de adenosina trifosfato, os sinais de Ca^{2+} nucleares precediam os sinais citosólicos (Leite et al., 2003). Este efeito foi atribuído à expressão majoritariamente nuclear de InsP_3RII , isoforma que apresenta maior afinidade por InsP_3 .

A presença de InsP_3Rs no NE já está bem documentada (revisado por (Vermassen et al., 2004) bem como sua localização na membrana externa do NE (Malviya et al., 1990; Gerasimenko et al., 1995) mas é importante observar que, para que a sinalização ocorra é necessário a presença de todos os componentes para liberação de Ca^{2+} mediada por InsP_3R no núcleo. Já foi demonstrado que o NE contém a fosfatidilinositol fosfato cinase (PIPK) (Cocco et al., 1987; Divecha et al., 1991; Boronenkov et al., 1998) que sintetiza fosfatidilinositol-4,5-bifosfato (PIP_2), o lipídio precursor do InsP_3 . A enzima fosfolipase C (PLC) que hidrolisa o PIP_2 para formar o InsP_3 (Martelli et al., 2000; Berridge, 1993). Além de apresentar InsP_3Rs funcionais (Foskett and Mak, 2004) e a SERCA (bomba sarco(endo)plasmática que repleenche os reservatórios da Ca^{2+} após sua liberação no meio intracelular) (Gensburger et al., 2003). Todos estes componentes presentes no núcleo da célula possibilita a formação de InsP_3 dentro do núcleo, o que pode causar um aumento transitório de Ca^{2+} independente dos níveis citoplasmáticos de InsP_3 .

A liberação de Ca^{2+} mediada por InsP_3 no núcleo da célula depende da produção nuclear do InsP_3 . Essa produção pode ser alcançada pela ativação de receptores de tirosina cinases (RTKs) (Gomes et al., 2008). Já foi demonstrado que os RTKs estão presentes na membrana nuclear. Receptores de insulina, receptores para o fator de crescimento epidermal (EGF) e para o fator de crescimento do fibroblasto são alguns exemplos de RTKs presentes no NE (Lin et al., 2000; Reilly and Maher, 2001). Em hepatócitos, o fator de crescimento do hepatócito (HGF) é secretado pelas células do estroma e se liga ao seu receptor c-Met, que é um receptor de tirosina cinase (Maher, 1993). Gomes e colaboradores (2008) demonstraram que o c-Met transloca para o núcleo após estimulação com HGF. Os sinais de Ca^{2+} induzidos por HGF resultam da hidrólise do PIP_2 para formar o InsP_3 dentro do núcleo da célula (Gomes et al., 2008) (Figura 2).

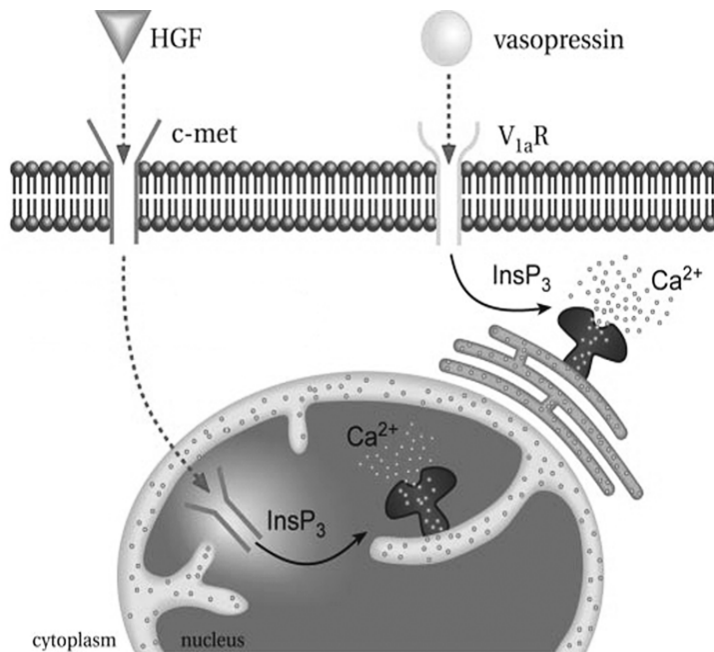


Figura 2. Sinalização de Ca^{2+} no núcleo de hepatócitos induzida por hormônio. Estimulação com HGF induz translocação do c-Met para o núcleo. No núcleo, c-Met ativo forma InsP_3 que se liga ao seu receptor na membrana nuclear e libera Ca^{2+} dos estoques nucleares. Em contraste, vasopressina ativa receptores $V_{1a}R$ que formam InsP_3 que ativa InsP_3Rs da membrana do RE e libera Ca^{2+} no citoplasma da célula. Fonte: modificado de Gomes et. al., 2008.

A geração de InsP_3 intranuclear pode fornecer um mecanismo para ativar seletivamente eventos dependentes de Ca^{2+} que ocorrem no núcleo e não em outro lugar. A versatilidade do Ca^{2+} para funcionar como segundo mensageiro é devido ao perfil da onda de Ca^{2+} que forma o sinal, e à localização sub-celular dos InsP_3Rs . Estes eventos juntos ajudam no padrão espacial e do tipo de onda que é liberado. No entanto, a demonstração de que fatores de crescimento podem seletivamente aumentar InsP_3 no núcleo revela um nível de regulação mais sofisticado no qual InsP_3Rs podem ser ativados não por virtude de sua localização sub-celular mas sim pela produção localizada de InsP_3 (Gomes et al., 2008).

Tem sido demonstrado que a proliferação celular depende dos sinais de Ca^{2+} nucleares mais do que os sinais citoplasmáticos e isso ocorre tanto em células *in vitro* como também em células *in vivo* e regula o ciclo celular e a progressão do tumor

(Rodrigues et al., 2007). No entanto permanece incerto se o Ca^{2+} nuclear regula e expressão de genes envolvidos nos processos de proliferação celular.

1.6. Expressão gênica

A expressão individual de um gene é regulada por um repertório de proteínas e outros elementos genéticos que tornam as células capazes de ajustar a taxa de transcrição e tradução de diferentes genes independentemente, de acordo com a necessidade.

Em procariotos a expressão gênica serve para que as células se ajustem às mudanças no ambiente e assim o seu crescimento e divisão sejam otimizados. Ocorre a expressão de vários genes ao mesmo tempo porque nestes organismos a estrutura gênica está organizada em *operons* (unidades de expressão gênica coordenada). O operon consiste de regiões reguladoras (operador e promotor) e grupo de genes estruturais. A modulação da expressão exige a interação DNA-proteína. Uma dessas interações determina o início da transcrição e é ativado quando a RNA-polimerase se liga ao segmento de DNA denominado promotor. A outra interação permite ou não o início da transcrição dos genes. Isto ocorre porque proteínas regulatórias, ativadoras ou repressoras, reconhecem as condições fisiológicas presentes na célula e no seu ambiente. Assim, a regulação da expressão gênica em procariotos ocorre de maneira coordenada com o ambiente onde está inserido.

Já em eucariotos, a regulação da expressão gênica é mais complexa e requer um número maior de proteínas regulatórias e diferentes interações com as regiões regulatórias. Isto ocorre porque os genomas eucarióticos são maiores e têm um grau mais complexo de organização estrutural do que os procariotos (Strayer, 1996). Por possuir em seu genoma a informação necessária para codificar centenas de proteínas diferentes, eucariotos requerem um controle rigoroso para decidir quais devem ser os genes que devem ser expressos e quando eles devem ser expressos. Por isso, as células podem mudar o padrão de expressão gênica em resposta a mudanças no seu ambiente ou por perceber sinais emitidos por outras células (Alberts et al., 2002). No processo de codificação de uma proteína, partindo da informação contida no DNA, existe vários pontos passíveis de regulação. Todos estes pontos podem ser submetidos a algum tipo de regulação (Alberts et al., 2002) (Figura 3). Na maioria dos casos, o início da

transcrição do RNA é o controle mais importante. No entanto, nucleossomos e outras proteínas associadas à cromatina contribuem para o processo de regulação transcricional. Nos eucariontes, a estrutura da cromatina é dinâmica e é um ingrediente essencial na regulação gênica (Kahl and Means, 2003).

Os mecanismos que controlam a expressão gênica operam em vários níveis, porém, a atividade gênica é primeiramente regulada em nível de transcrição (Strayer, 1996) (Figura 3). A transcrição é o primeiro ponto de regulação da expressão gênica em eucariotos. Os dois componentes fundamentais da regulação da transcrição são: os elementos *cis*-regulatórios, que são as seqüências de DNA regulatórias; e os *trans*-regulatórios, que são as proteínas regulatórias.

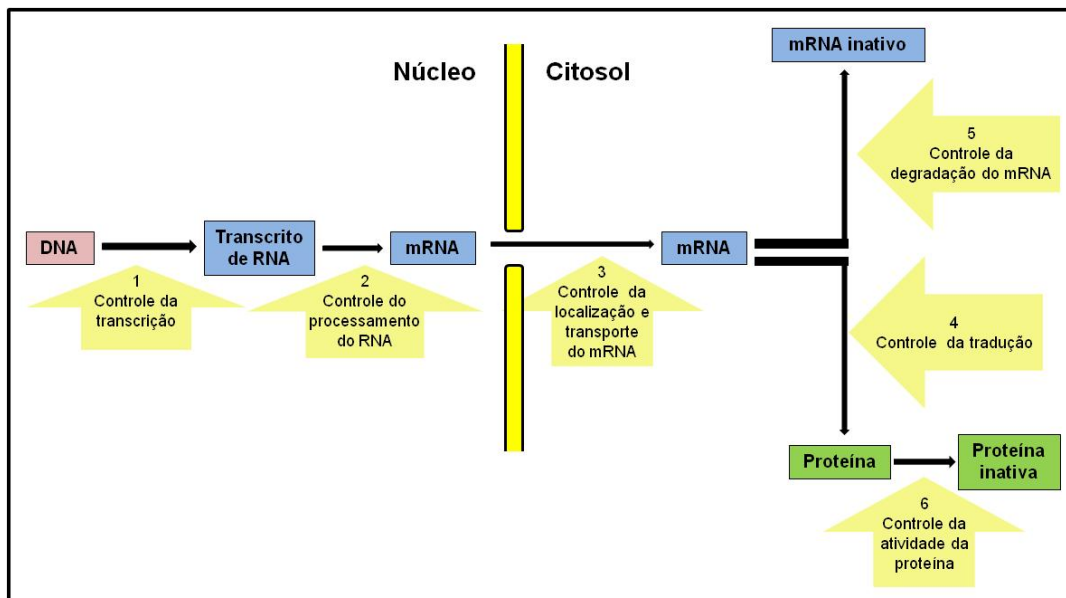


Figura 3. Controle da expressão gênica. Seis passos onde a expressão gênica eucariótica pode ser controlada (modificado de Alberts et. al., 2002).

Os elementos *cis*-regulatórios compreendem a região promotora mínima, os *enhancers* (regiões ativadoras ou inibidoras da transcrição) e os insuladores. A região promotora mínima fica acima do ponto de início da transcrição. Nesta região que a RNA polimerase e as demais proteínas acessórias irão se ligar para iniciar a montagem da maquinaria de transcrição e iniciar a síntese do pré-RNA (Alberts et al., 2002). No entanto, nenhuma RNA polimerase eucariótica é capaz de transcrição independente,

pois ela requer proteínas adicionais (os fatores de transcrição), que com exceção do TATA-binding protein (TBP), é diferente para cada enzima.

O *core* do promotor inclui o TATA-box (Aso et al., 1994; Butler and Kadonaga, 2002) que fica localizado aproximadamente a 30 pb do nucleotídeo inicial da transcrição (Aso et al., 1994) e o elemento iniciador (*Inr element*) (Levine and Tjian, 2003). Numerosos dados da literatura mostram uma variabilidade no elemento TATA, sugerindo que promotores com seqüências variantes no TATA-box e diferentes estabilidades do complexo TBP-DNA apresentem um mecanismo comum de regulação transcricional (Basehoar et al., 2004); (Gershenzon and Ioshikhes, 2005). Os *enhancers* podem ser localizados próximos ou distantes do seu gene, a mais de 100 pb. Podem estar acima ou abaixo do gene ou dentro de íntron. Já as seqüências insuladoras protegem a região promotora de um gene da ação das proteínas regulatórias de outros genes (Alberts et al., 2002).

Os elementos *trans*-regulatórios são os fatores de transcrição que possuem uma seqüência de aminoácidos capazes de reconhecerem e se ligarem a curtas seqüências conservadas contidas em cada promotor (Alberts et al., 2002). Os diferentes motivos estruturais utilizados pelos fatores de transcrição para reconhecerem seus sítios de ligação permitiram que estas proteínas fossem classificadas em “famílias de fatores de transcrição”. A presença desses sítios de ligação próximos uns dos outros permite que diferentes fatores de transcrição atuem em uma mesma região reguladora, potencializando a atividade do complexo transcricional (Schrem et al., 2002). A ligação dos fatores de transcrição ao DNA recruta várias outras proteínas regulatórias e forma assim o complexo de transcrição basal (Figura 4). Uma vez ligados ao DNA, os fatores de transcrição irão atuar ativando ou reprimindo a transcrição. Eles facilitam ou dificultam a montagem do complexo de transcrição basal ou modulam a acessibilidade das demais proteínas reguladoras ao DNA (Schrem et al., 2002).

Vários fatores de transcrição se ligam a sítios ubíquos, presentes em todos os tipos de células. O *Specificity protein 1* (SP1), o *Octamer factor 1* (Oct1), GATA-1 e 2 e o ELK1 são exemplos de fatores de transcrição que participam da transcrição da maioria dos genes (Schrem et al., 2002). No fígado, existem alguns fatores de transcrição exclusivos como o *CAAT enhancer proteins* (C/EBPC) e o *hepatocyte nuclear proteins* (HNF) que pertencem a famílias de fatores de transcrição envolvidos na transcrição de genes hepato-específicos (Krivan and Wasserman, 2001). Como regulam genes como a

albumina, estes fatores são fortes candidatos a atuarem na regulação de genes expressos por hepatócitos.

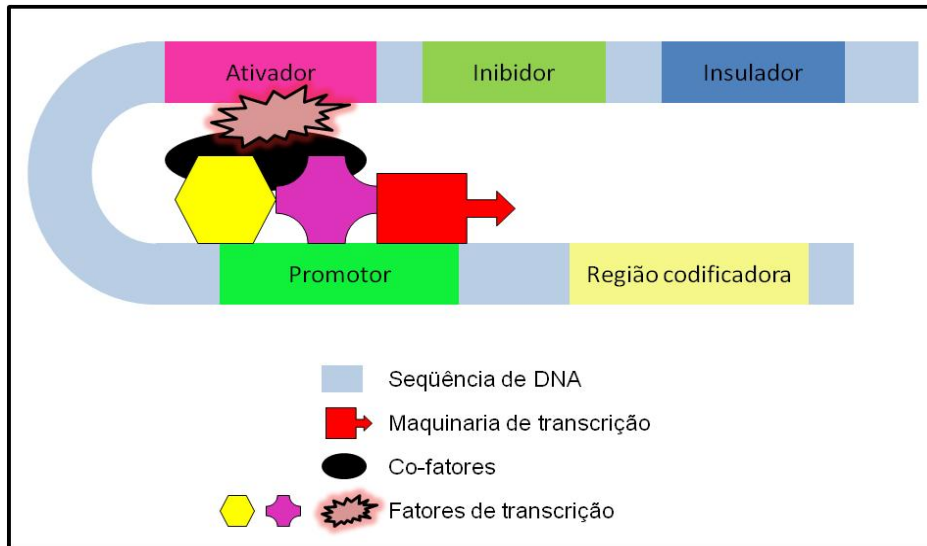


Figura 4. Elementos *cis* e *trans* que atuam na regulação da expressão gênica. A figura esquematiza a formação do complexo de transcrição basal no qual, diferentes fatores de transcrição se ligam ao promotor do gene e com o auxílio de proteínas ativadoras recrutam a maquinaria responsável por iniciar a transcrição do gene.

1.7. O cálcio e a expressão gênica

Vias de sinalização são complexas redes de reações bioquímicas que culminam na alteração dos padrões de expressão de um gene mediado por mecanismos transcricionais. Fatores de transcrição funcionam como a interface entre a informação contida no DNA e o sistema de sinalização de resposta a estímulos internos ou externos. Em resposta a diversos estímulos, as células geram aumentos transitórios na concentração de Ca^{2+} intracelular livre. Este Ca^{2+} atua então como um segundo mensageiro na ativação das vias de sinalização. Vários perfis espaços-temporais variam a amplitude, frequência, duração, localização intracelular e velocidade do transiente de Ca^{2+} (Bading et al., 1993; Lerea and McNamara, 1993; Hardingham et al., 1997; Evans et al., 2001).

Estes sinais são decodificados e transmitidos por um sistema de proteínas que se ligam ao Ca^{2+} e transmitem esta informação em respostas *downstream*. As principais

rotas de transdução sinais de Ca^{2+} envolvem cinases reguladas pelo Ca^{2+} que mediam eventos de fosforilação. Estes eventos organizam as respostas ou modulam a regulação gênica via fatores de transcrição. Muitos desses fatores de transcrição são regulados pelo Ca^{2+} ou possuem promotores responsivos ao Ca^{2+} intracelular (Thiel et al., 2010).

Um exemplo de como o Ca^{2+} modula a atividade transcricional das células é o efeito sobre a expressão do gene da renina. Aumento da concentração do Ca^{2+} citosólico pode inibir a expressão do gene da renina de maneira independente da atividade da proteína cinase C (PKC) (Klar et al., 2005). Utilizando o gene do fator neurotrófico derivado do cérebro (BDNF) como modelo, West e colaboradores (2001) descobriram que um influxo de Ca^{2+} induz a transcrição deste gene (West et al., 2001). A expressão do gene BDNF é possível porque o influxo de Ca^{2+} é regulado pela rota de entrada de Ca^{2+} , pelo padrão de fosforilação induzido no CREB e pelo recrutamento de fatores de transcrição ativos para o promotor do *BDNF* (Klar et al., 2005).

O efeito do Ca^{2+} extracelular na expressão do gene MMP-9, que pertence à família de genes de metaloproteinases de matrix (MMP), em células escamosas oral cancerígenas (OSCC) revelou que o aumento do Ca^{2+} extracelular induz, de maneira concentração-dependente, a expressão do MMP-9 (Mukhopadhyay et al., 2004). Esta expressão é diferencialmente regulada pela ERK1/2 e via da MAPK p38, sugerindo que a perda deste mecanismo regulatório está acompanhada de transformação maligna das células do epitélio oral (Mukhopadhyay et al., 2004).

Já a influência do Ca^{2+} nuclear foi estudada em células do sistema imune. Nestas células a duração dos sinais de Ca^{2+} nuclear contribui para a especificidade da indução transcricional: apenas um pequeno aumento na concentração intracelular de Ca^{2+} , mas não um breve sinal de Ca^{2+} , induz translocação nuclear do fator de transcrição NFAT (Dolmetsch et al., 1997). Dolmetsch e colaboradores (1997) demonstraram em neurônios, que a via de sinalização ERK1/2 é sensível a apenas um pulso de Ca^{2+} . Este pulso é suficiente para ativar a fosforilação de ERK1/2 e CREB. Fosforilação de CREB é importante para o recrutamento do co-ativador transcricional a proteína de ligação ao CREB (CPB). Já foi demonstrado que o CPB é regulado por sinais de Ca^{2+} (Chawla et al., 1998; Hardingham et al., 1999) e é suficiente para mediar expressão gênica induzida por Ca^{2+} (Chawla et al., 1998). A expressão gênica mediada por CREB e CBP requer Ca^{2+} nuclear e a forma como os neurônios codificam estes sinais determina a expressão gênica. Também foi demonstrado que o tamponamento do Ca^{2+} nuclear aumenta a expressão da calcineurina (fosfatase dependente de Ca^{2+} /calmodulina utilizada como

marcador de estresse celular) e induz translocação do NFAT para o núcleo da célula promovendo crescimento nuclear de cardiomiócitos (Guatimosim et al., 2008). Além disso, já foi demonstrado que o Ca^{2+} nuclear regula negativamente o fator de transcrição TEAD que tem uma variedade de funções durante o desenvolvimento e a diferenciação celular (Thompson et al., 2003). Entretanto, ainda permanece incerto se o Ca^{2+} nuclear regula a expressão de genes envolvidos em processos proliferativos.

1.8. Proliferação de células hepáticas

O fígado é o maior órgão do corpo humano, com massa média de 1,5 a 1,8 Kg em um indivíduo adulto, correspondendo a 2% da massa total do corpo e possui uma localização anatômica relacionada à sua função (Ramadori and Saile, 2005). É um órgão multifuncional e dentre suas principais funções destacam-se a síntese e secreção protéica, a secreção biliar, a regulação dos níveis glicêmicos e a metabolização de drogas e carboidratos. Por produzir grandes quantidades de proteínas do soro, como albumina, o fígado influencia a pressão oncótica e a retenção de líquidos de água dentro das veias (Ramadori and Saile, 2005) e, quando há necessidade, fornece glicose para o organismo por ser um reservatório de glicogênio (revisado por Taub R, 2004).

Dentre os diversos tipos celulares que compõem a massa parenquimal do fígado, o hepatócito é o tipo celular mais abundante, correspondendo a cerca de 80% da massa total do órgão. São células altamente especializadas e estáveis que, apesar de apresentarem um baixo índice mitótico, entram em divisão celular mediante estímulo de natureza física, infecciosa ou tóxica. O restante do órgão é constituído por células endoteliais, células de Kupffer, linfócitos e células estelares. As células endoteliais estão localizadas nos vasos da circulação intra-hepática (sinusóides) e fornecem uma grande área de superfície para a absorção de nutrientes. As células de Kupffer são os macrófagos residentes do fígado, localizados próximos aos sinusóides e são essenciais para a fagocitose de partículas estranhas ao organismo e para a produção de citosinas. Os linfócitos do fígado fazem parte do sistema imune e participam da resistência a infecções. As células estelares apresentam várias funções, incluindo o estoque de vitamina A e produção da matriz extracelular (revisado por (Taub, 2004).

1.9. Regeneração do fígado

Desde a antiguidade já se conhecia o processo de regeneração hepática através da Mitologia Grega. Como punição a Prometeu, um titã que roubou o segredo do fogo dos deuses para levá-lo aos homens. Zeus, o deus dos deuses, ordenou que Prometeu fosse acorrentado ao Monte Cáucaso, e que todos os dias um abutre viesse comer partes do seu fígado, que seria regenerado durante a noite, para que o seu suplício fosse eterno. A regeneração hepática, no entanto, não é apenas um mito, mas sim um fato.

A capacidade regenerativa do fígado é imensa e reflete uma complexa resposta para promover a replicação celular e o crescimento suficiente para restaurar a massa funcional do fígado (Fausto et al., 2006). Quando ocorre uma lesão do parênquima hepático, induzido por qualquer estímulo, é desencadeado o processo de reparação. Este processo começou a ser elucidado com o advento da biologia molecular e com o avanço das técnicas que investigam os processos de divisão celular. Conhecer todo o mecanismo de regeneração facilita o prognóstico e a patogênese das mais frequentes doenças do órgão como hepatite, cirrose e hepatomas (Taub, 2004).

A geração de novas células de um fígado injuriado depende da pré-existência de células que possam recompor o tecido perdido. Diferente do conceito clássico de regeneração, que é a neo-formação de tecidos e órgãos perdidos, após a perda de massa hepática o fígado entra em replicação conduzindo a uma hiperplasia compensatória que envolve as células maduras da parte intacta do órgão. Isto promove o repovoamento celular e tecidual, ou seja, os lobos removidos não crescem novamente, o que ocorre é o crescimento do lobo restante (Fausto et al., 2006).

No fígado adulto, os hepatócitos são células quiescentes que rapidamente re-entram no ciclo celular após uma injúria no tecido. Após remoção cirúrgica de dois-terços do fígado de ratos, os hepatócitos saem da fase G_0 (estágio mitoticamente inativo) e passam pelas fases G_1 , S (de síntese de DNA), mitose e citocinese. O reestabelecimento de células perdidas e a restauração da massa hepática excisada ocorrem dentro de uma a duas semanas após a cirurgia (Fausto et al., 2006).

Vários são os eventos que ocorrem durante a regeneração hepática. Os fatores mais importantes presentes na regeneração hepática são: fatores de crescimento, citocinas e alguns genes. Fatores de crescimento como HGF, fator de crescimento transformante α (TGF α) e fator anti-proliferativo TGF β estão envolvidos nos processos

regenerativos do fígado. O HGF é um importante fator de crescimento que dirige a progressão do ciclo celular durante a regeneração. Ele é produzido pelas células estelares e age de forma parácrina nos hepatócitos. HGF liga-se ao seu receptor *c-met* na membrana do hepatócito e ativa uma cascata de sinalização, via ERK1/2. ERK1/2 por sua vez, ativa genes responsáveis pela regeneração do fígado (Huh et al., 2004). Além disso, HGF aumenta Ca^{2+} intracelular, preferencialmente no núcleo da célula hepática (Echevarria et al., 2003). Sabemos que o aumento intracelular de Ca^{2+} é importante para a proliferação celular. Porém, o papel relativo do Ca^{2+} nuclear ou citosólico na proliferação de hepatócito ainda não foi esclarecido.

Estudos moleculares de expressão gênica, aliados às técnicas de *microarrays* indicam genes que são rapidamente ativados em hepatócitos submetidos à hepatectomia. Estes genes estão envolvidos principalmente em respostas proliferativas. Outros genes ativados durante a regeneração do fígado estão envolvidos nas cadeias ativadas por citocinas. Ainda não está claro como isto ocorre, mas acredita-se que a interleucina 6 (IL-6) é a responsável por ativar o fator transcricional STAT 3 dentro do hepatócito depois que o fator de necrose de tumor (TNF) é liberado pelas células de Kupffer. Isto induz a liberação da citocina pelo hepatócito. Uma vez ativado o STAT 3 forma homodímeros que translocam para o núcleo e induz a transcrição de vários genes alvos (Fausto et al., 2006). Mas os efeitos exercidos pela IL-6 durante a regeneração hepática podem estar sendo modulados por outras moléculas como o *stem cell factor* (SCF) e a oncostatina M (OSM) (Fausto et al., 2006) demonstrando a complexidade do mecanismo.

1.10. Justificativa

Já foi demonstrado o papel dos sinais de Ca^{2+} nucleares sobre a proliferação de células SKHep1 (Rodrigues et al., 2007). No entanto, permanece incerto se a expressão dos genes responsáveis pelo processo de proliferação celular pode apresentar alterações em decorrência da modulação dos sinais de Ca^{2+} nucleares. Sabemos também que após uma injúria, as citocinas, os fatores de crescimento e as vias metabólicas ativadas formam uma grande rede de interação que promovem a regeneração do fígado.

Muito já se sabe a respeito do processo regenerativo, mas novos conhecimentos sobre os mecanismos celulares e moleculares envolvidos na regeneração hepática

conceitualmente e diretamente relevantes para o desenvolvimento de novas terapias para as doenças hepáticas são necessários. Bem como estudar o papel dos sinais de Ca^{2+} nuclear sobre a expressão de genes importante para a proliferação celular e para a regeneração do fígado. Estes estudos podem fornecer dados que levem à elucidação de mecanismos que regulam o desenvolvimento e a proliferação de células hepáticas.

2. OBJETIVOS

Diante das mais variadas funções que o Ca^{2+} intracelular exerce dentro da célula, decidimos verificar a influência direta que este íon exerce sobre a proliferação de células hepáticas e sobre o controle da expressão de genes importantes para que os mecanismos de regeneração hepática ocorram.

Assim, esse estudo teve como objetivos principais:

- A) Verificar a influência do Ca^{2+} nuclear, sobre a expressão de genes envolvidos na proliferação celular.
- B) Investigar o papel que o Ca^{2+} intracelular liberado a partir da ativação dos InsP_3RI exerce sobre a regeneração hepática.

3. MATERIAIS E MÉTODOS

3.1. Materiais e reagentes

Utilizamos o kit Effectene transfection Kit da Quiagen para experimentos de transfecção e o kit pSilencer™ adeno 1.0-CMV System da Ambion's (Austin, TX) para construção de adenovírus. Para síntese de cDNA foi utilizado o kit SuperScript™-III First-Strand Syntesis System for RT-PCR da Invitrogen (Carlsbad, CA) e o Wizard® Plus SV Minipreps DNA Purification System da Promega (Madison, Wisconsin) foi utilizado para extração de DNA plasmidial.

Para reações de sequenciamento foi utilizado o kit Dyenamic ET Dye Terminator GE Healthcare (Buckinghamshire, UK). A membrana Spectrapor (12 a 14000 KDa de corte molecular; 1 a 2 cm de largura) da BioAgency (Houston, TX) foi utilizada para a diálise das partículas virais e a membrana de PVDF (Hercules, CA) foi utilizada em transferências de western blot. Para extração de proteínas foi utilizado o coquetel de inibidor de protease da Sigma Roche Applied Science (Saint Louis, MO). O kit ECL plus da GE Healthcare (Buckinghamshire, UK) foi utilizado para revelação do western blot em filme de raio-X da Bio Max™ML, KODAK (Buckinghamshire, UK). A vasopressina Sigma (Sant Louis, MO) foi utilizada para mobilizar Ca²⁺ intracelular via InsP₃Rs. As enzimas de restrição utilizadas foram da Invitrogen (Carisbad, CA). O reagente Trizol Invitrogen (Carisbad, CA) foi utilizado para extração de RNA.

Reagente TRizol e lipofectamine 2000 foram obtidos da Invitrogen (Eugene, OR). Anticorpo policlonal contra LGMN foi obtido da ABCAM (Cambridge, MA). Anticorpo policlonal contra InsP₃RI foi obtido da Affinity BioReagents (Golden, CO). Anticorpos secundários Alexa-488 e Alexa-568, e a sonda Fluo-4/AM foram obtidos da Molecular Probes Inc (Eugene, Oregon) e os anticorpos secundários conjugados à peroxidase foram obtidos da Amershan Biosciences. Estes anticorpos foram utilizados para ensaios de imunofluorescência e western blot.

Os plasmídeos pShuttle-1.0-CMV e pAdeno LacZ Backbone foram obtidos do Kit pSilencer™ adeno 1.0-CMV System da Ambion's (Austin, TX) e os plasmídeos PV-NLS e PV-NLS-Cd e os adenovirus recombinantes pAd-PV-NLS-DsRed e pAd-PV-NLS-Cd-DsRed foram fornecidos pelo laboratório do Dr. Michael H. Nathanson da Universidade de Yale, (New Haven, NY). O plasmídeo pZeRo.1 foi obtido da Invitrogen (Carlsbad, CA). Plasmídeos pGL4.10[Luc] e pRL-CMV, que promove expressão constitutiva da *Renilla luciferase*, foram obtidos da Promega (Madison, WI).

3.2. Linhagens celulares

As células HEK293 (células renais embrionárias humanas), SKHep1 (linhagem epitelial de células hepáticas) e CHO (células de ovário de Hamster) foram obtidas do banco de células da American Type Culture Collection (Manassas, VA) e cultivadas em meio DMEM (Dulbecco's modified Eagle's medium) ou RPMI 1640 suplementados com 100 U/ml de penicilina, 100 µg/ml de estreptomicina e 0,25 µg/ml de anfotericina-b, 10% de soro fetal bovino (SFB) e mantidos à temperatura de 37°C e 5% de CO₂. Hepatócitos foram isolados de fígado de ratos Holzman machos (50-80 gramas) por perfusão com colagenase como descrito por Boyer e colaboradores (1990). Hepatócitos primários foram cultivados em meio L15 (Leibovitz) da Sigma-Aldrich (Sant Louis, MO) sob condições normais de cultivo celular.

3.3. Extração de DNA plasmidial

A extração do DNA plasmidial foi utilizada para a obtenção do DNA dos plasmídeos e para a obtenção do DNA dos clones selecionados na metodologia do RaSH (descrita a seguir).

O isolamento do DNA plasmidial foi realizado pelo método de purificação em colunas, de acordo com o Wizard® Plus SV Minipreps DNA Purification System (Promega). Células hospedeiras *E. coli* DH10B foram submetidas à lise alcalina após crescimento em meio LB, contendo 100 µg/ml de ampicilina, por 12 a 16 horas. Em seguida, foram centrifugadas a 5.000 RPM, por 2 minutos, a 4°C. A ressuspensão foi realizada em solução contendo glicose 50 mM, Tris-HCl 25 mM pH 8, EDTA 20 mM e RNase A na concentração final de 100 mg/ml. Em seguida, a solução de lise (NaOH 0,2 M e SDS 1%) foi adicionada à mistura com incubação por 5 minutos à temperatura ambiente. A esta mistura foi adicionada a solução de protease alcalina, prolongando a incubação por mais 5 minutos. Posteriormente, a solução de neutralização (hidroclorato de guanidina 4,09 M, acetato de potássio 0,75 M e ácido acético glacial 2,12 M) foi incorporada ao sistema. Uma centrifugação a 13.000 RPM, por 10 minutos foi realizada para separar o DNA dos resíduos insolúveis e do DNA cromossômico. As resinas pré-empacotadas foram utilizadas para isolar o DNA plasmidial, que foi lavado com a solução de lavagens contendo acetato de potássio 162,8 mM, Tris-HCl 22,6 mM pH 7,5,

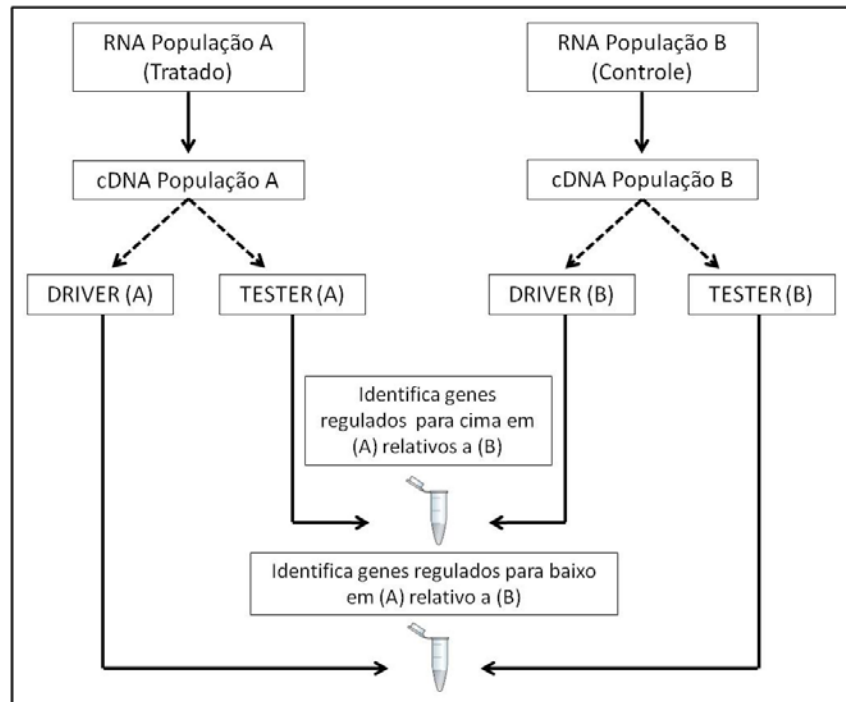
EDTA 0,109 mM pH 8,0 e etanol 95%, conforme as recomendações do fabricante. A eluição foi realizada com água livre de nucleases. O DNA plasmidial foi digerido com enzimas de restrição para confirmar os clones positivos e estimar seus tamanhos. A integridade dos plasmídeos foi confirmada em gel de agarose 1,5%.

3.4. RaSH

Esta técnica, denominada RaSH (*rapid subtraction hybridization*) permite a análise de expressão diferencial através de subtração por hibridização capaz de isolar genes que são expressos em uma determinada condição pré estabelecida. A metodologia do RaSH está representada na forma de esquema na figura 5A. A figura 5B indica as condições experimentais (PV-NLS ou PV-NLS-Cd) e a alteração na expressão gênica (regulados para cima ou para baixo) que a metodologia RaSH possibilitou para este trabalho. Para obtermos uma condição de redução de Ca^{2+} no interior da célula utilizamos uma construção adenoviral, fornecida pelo laboratório do Dr. Nathanson. Para realizarmos a subtração utilizamos amostras de RNAs extraídos de células SKHep1 infectadas com Ad-PV-NLS-DsRed contra amostras de RNA extraídas de células infectadas com Ad-PV-NLS-Cd-DsRed.

A primeira construção adenoviral possui uma proteína capaz de tamponar o Ca^{2+} em compartimentos celulares específicos. O cassete de expressão montado nesta construção possui a seqüência gênica que codifica a parvalbumina (PV) que é uma proteína com alta afinidade pelo Ca^{2+} . A PV é uma proteína Ca^{2+} -binding de baixa massa molecular (12 KDa) presente no músculo esquelético dos vertebrados (Pechere et al., 1971). Quantificação da ligação de Ca^{2+} pela PV tem mostrado que sua constante de afinidade aparente é de $K_{ca} = 2,8 \times 10^7 \text{ M}^{-1}$ na presença de 1 mM de Mg^{2+} , ou $K_{ca} = 2,7 \times 10^9 \text{ M}^{-1}$ na ausência de magnésio (Moeschler et al., 1979). Há também uma seqüência que codifica a proteína vermelha DsRed seguida por três repetições da seqüência NLS (seqüência de localização nuclear) que direciona todo o cassete para o núcleo da célula (Figura 6A). Com a expressão da proteína DsRed apenas no núcleo da célula (Figura 6B) podemos afirmar que a parvalbumina promove a redução de Ca^{2+} nuclear sem afetar os níveis de Ca^{2+} citosólico porque a proteína é expressa exclusivamente no núcleo da célula (Figura 6B). No caso da seqüência NLS-Cd, a expressão também ocorre no núcleo da célula porém, não há alteração do sinal de Ca^{2+} .

A)



B)

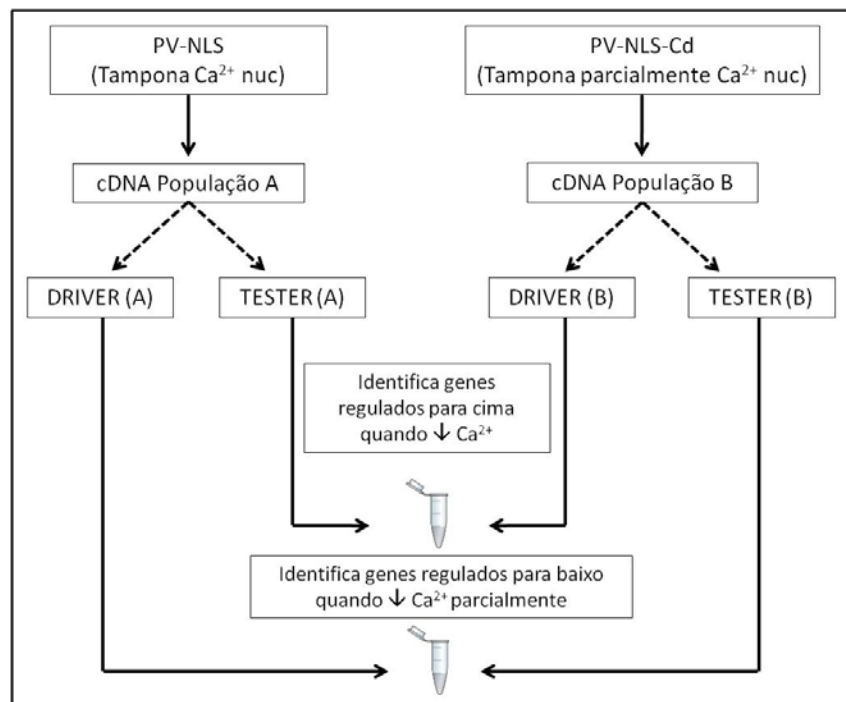


Figura 5. Metodologia RaSH. A) Representação esquemática da metodologia RaSH (modificado de (Pastorian et al., 2000)). B) Condições experimentais utilizadas neste trabalho.

A figura 6C mostra que o adenovírus Ad-PV-NLS-DsRed promove o tamponamento de Ca^{2+} apenas no núcleo. Neste perfil podemos observar que os sinais nucleares estão quase próximos à linha basal (Figura 6C). Utilizamos como controle o Ad-PV-NLS-Cd-DsRed, esse adenovirus possui dois sítios da parvalbumina mutados e promove apenas ligeira redução dos níveis do Ca^{2+} nuclear, mas esta redução não é significativa. Assim, esperamos selecionar genes que têm expressão modulada por alterações nos níveis nucleares de Ca^{2+} .

3.4.1. Extração de RNA total

O RNA total foi extraído utilizando o reagente Trizol e o método desenvolvido por Chomczynski e Sacchi (1987). Após homogeneização das amostras de tecido ou células com o trizol, o complexo formado foi incubado por 5 minutos a 30°C e centrifugados por 15 minutos a 4°C e 13000 RPM. A fase superior foi coletada e o RNA foi precipitado com álcool isopropílico por 16 horas a -20°C . Nova centrifugação a $8.000g$ por 10 minutos e lavagem com etanol 70% foram realizadas e o RNA foi ressuspenso em água tratada com DEPC (dietilpirocarbonato). O RNA foi quantificado por espectrofotometria a 260 nm e armazenado a -80°C até seu uso. A concentração do RNA foi estimada pela fórmula: $[\text{RNA}] \mu\text{g}/\mu\text{l} = (A_{260} f \times 40/1000)$, onde f é o fator de diluição e 40 é o fator de conversão.

3.4.2. Síntese da primeira e segunda fitas de cDNA

A primeira fita de cDNA foi sintetizada usando o SuperScriptTM-III First-Strand Syntesis System for RT-PCR, de acordo com as recomendações do fabricante. Dois microgramas de cada amostra de RNA total foram incubados com $0,5 \mu\text{g}$ de oligo(dT)₁₂₋₁₈ a 70°C por 10 minutos e, em seguida, as amostras foram incubadas no gelo. Logo após, foi adicionado às amostras, tampão PCR 1X (Tris-HCl 20 mM pH 8,4 e KCl 50 mM), MgCl_2 5 mM, os quatro dNTPs 0,5 mM cada e DTT (ditiotretol) 5 mM, e foram incubadas a 42°C por 5 minutos. Em seguida, foram adicionadas 200 unidades da enzima SuperScript III RNaseH⁻ Reverse Transcriptase (Invitrogen) e as amostras foram incubadas por mais 50 minutos a 42°C .

Após a síntese da primeira fita de cDNA, o RNA do híbrido DNA/RNA foi degradado por incubação com duas unidades de RNase H (Invitrogen) a 37°C, por 20 minutos. Para cada reação de síntese da primeira fita foi feito um controle negativo que continha todos os reagentes exceto a enzima transcriptase reversa.

Para a síntese da segunda fita, foram adicionados ao volume total obtido na reação de primeira fita, 0,3 mM de dNTPs, uma unidade de DNA ligase (10U/μl) (Invitrogen), 40 unidades de DNA polimerase I de *E. Coli* (10U/μl) uma unidade de Rnase H (2U/μl) em um volume final de 100 μl. Esta reação foi incubada por 2 horas a 16°C e depois foi acrescentado 5 unidades de T4 DNA ligase (Invitrogen). A reação foi extraída com fenol/clorofórmio, precipitada em etanol e ressuspensa em água DEPC.

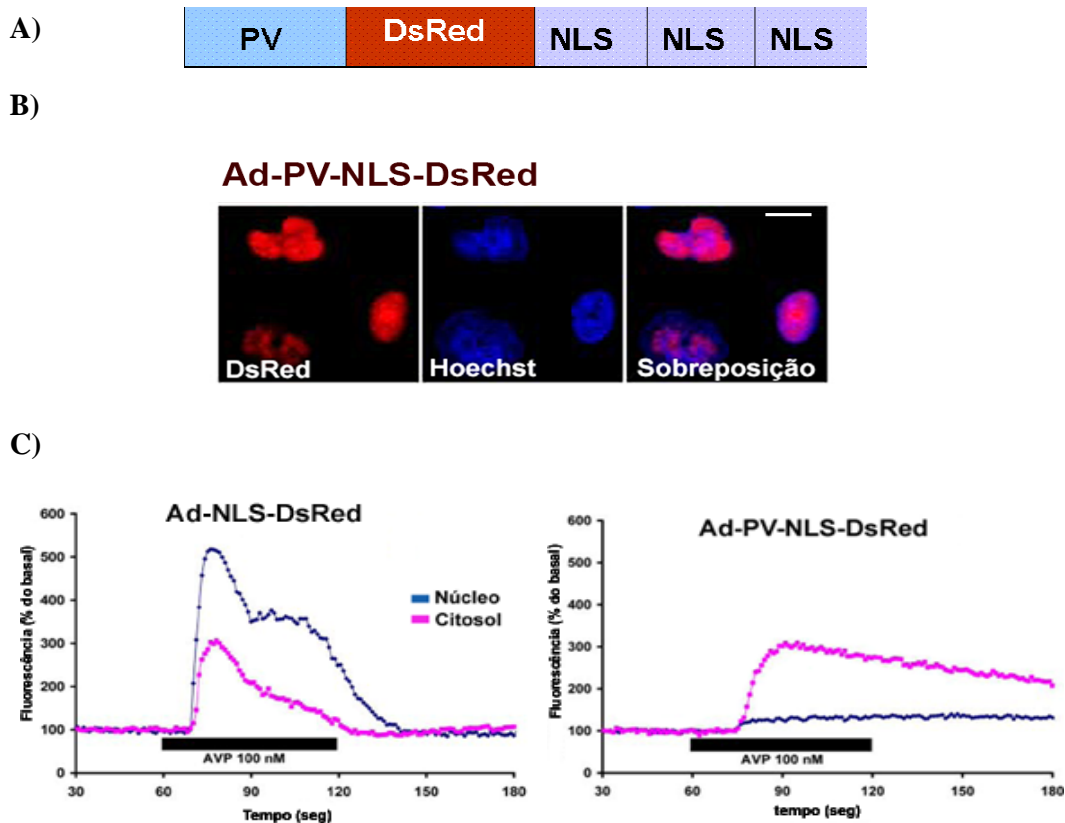


Figura 6. Tamponamento de Ca^{2+} nuclear pela proteína Parvalbumina (PV). A) Representação esquemática da construção do cassete. B) A cor vermelha no núcleo da célula indica que a construção Ad-PV-NLS-DsRed está corretamente sendo expressa no núcleo. C) Traços representativos dos sinais de Ca^{2+} em células SKHepl após estimulação com 100nM de vasopressina. Células foram examinadas 48 horas após infecção com a construção adenoviral contendo apenas o controle DsRed ou o DsRed fusionado ao NLS. O Ca^{2+} foi monitorando com Fluo-4/AM e microscopia confocal. Barra de escala = 10μm (Rodrigues et al., 2007).

3.4.3. Preparação da biblioteca de cDNA baseada em PCR

A subtração, descrita por Jiang e colaboradores (2000), foi realizada entre os cDNAs TESTER e DRIVER obtidos de RNA de células SKHep1 infectadas com adenovírus contendo parvalbumina, proteína quelante de Ca^{2+} . Usamos também a construção adenoviral Ad-PV-NLS-Cd-DsRed, mesma construção que contém um dos dois sítios de ligação ao Ca^{2+} da parvalbumina mutado (glutamato por valina na posição 12 de cada *loop* de ligação ao Ca^{2+}), como tratamento controle. Após a síntese do cDNA, todo o volume de cDNA obtido foi digerido com a enzima de restrição *Mbo*I (Invitrogen) a 37°C por 1 hora, seguido por extração com fenol/clorofórmio e precipitação em etanol. O cDNA digerido foi ligado a adaptadores XDPN₁₂ e XDPN₁₄ (Tabela 1) na concentração final de 20 μM em 30 μl de tampão de ligação, aquecido a 55°C por 1 minuto e incubado a 14°C por 1 hora. T4 DNA ligase (15 unidades) foram adicionados à reação e deixados a 14°C por 16 horas. A mistura foi diluída para 100 μl com tampão Tris 10mM, EDTA 1mM pH 7. Desta reação, 40 μl foram utilizados para amplificação por PCR.

As reações de amplificação foram realizadas em um volume final de 50 μL contendo 1,0 μM de cada dNTP, 1 unidade de *Taq* DNA Polimerase, 10 μM do *primer* XDPN₁₈ (Tabela 1), tampão PCR 1X (Tris-HCl 20 mM pH 8,4 e KCl 50 mM) e MgCl_2 2,5 mM. As seqüências dos oligonucleotídeos utilizados estão descritas na Tabela 1. Os parâmetros da reação de PCR foram: 1 ciclo de 5 min a 72°C, seguidos por 25 ciclos de 1 min a 94°C, 1 min a 55°C e 1 min a 72°C, e 1 ciclo de 3 min a 72°C. O produto de PCR foi purificado por extração com fenol/clorofórmio e precipitado em etanol. Uma porção do produto de PCR TESTER foi digerida com a enzima de restrição *Xho* I. Dois grupos de bibliotecas de cDNA foram preparados: um com sítios de restrição para *Xho* I e outro sem o sítio.

3.4.4. Hibridização subtrativa e geração de biblioteca subtraída

Três microgramas do cDNA TESTER foi misturado a 10 μg de cDNA DRIVER em 10 μl de solução de hibridização [NaCl 0,5 M, Tris 50 mM pH 7,5, SDS 0,2% e formamida 40% (vol/vol)], fervido por 5 minutos e incubados a 42°C por 48 horas. A mistura de hibridização foi extraída com fenol/clorofórmio, precipitada em etanol e dissolvida em 20 μl de tampão Tris 10 mM/EDTA 1mM pH 7. Parte desta mistura foi

ligada a 1µg do vetor pZeRo.1 previamente digerido com a enzima *Xho* I, a 14°C por 16 horas e transformado em bactéria *E. coli* DH10B.

Tabela 1. *Primers* específicos utilizados no seqüenciamento e nas reações de RT-PCR.

Adaptadores	Sequência (5'→3')
XDPN12	GATCTCTCGAGT
XDPN14	CTGATCACTCGAGA
XDPN18	CTGATCACTCGAGAGATC
Primers	Sequência (5'→3')
Actina Foward	CCCCTCAACCCAAAGGTCAACAG
Actina Reverse	GGAATCTCTCTGCCCAATTGTG
RTN4 Foward	GATGTGGGTATTTACCTATGTTGGTGCC
RTN4 Reverse	GATGAACACATGGCAGTCAAGACAGG
LG MN Foward	CGGACCCACTGCTTCAACCTGG
LG MN Reverse	CCCCATGAGCTTCCTGCTCC
TBRG Foward	CTGCTGGACAGTGACGGCGAG
TBRG Rverse	GGCCCAAGGTCCTGCACAGAGGT

3.4.5. *Screening* das colônias

Colônias de bactérias foram selecionadas randomicamente e submetidas à amplificação por PCR de colônia utilizando *primers* universais M13 (*forward* e *reverse*). Clones selecionados foram submetidos ao seqüenciamento.

3.4.6. Seqüenciamento e análise dos resultados

O DNA plasmidial dos clones selecionados foi extraído e seqüenciado utilizando o *primer* M13 *forward*. As reações de seqüenciamento foram conduzidas com o kit Dyenamic ET Dye Terminator (GE Healthcare) conforme recomendações do fabricante, e analisadas pelo seqüenciador MegaBace. As seqüências obtidas mostraram alta qualidade de nucleotídeos e a busca por similaridades foi feita com outras seqüências depositadas no *GenBank* através do programa BLASTn (Altschul et al., 1997) do

“National Center for Biotechnology Information”– NCBI -
(<http://www.ncbi.nlm.nih.gov>).

3.5. RT e PCR semi-quantitativo

RNA total de células SKHep1 foram extraídos em diferentes tempos de exposição ao adenovírus Ad-PV-NLS e Ad-PV-NLScd. O cDNA foi produzido com o kit SuperScriptTM-III First-Strand Syntesis System for RT-PCR. A amplificação foi realizada com o termociclador PTC-100 (MJ Research, Watermown, MA) utilizando 1-3 µl de cDNA, 200 µM de dNTPs, 2,5 mM de MgCl₂, 1 unidade de *Taq* DNA polimerase e 400 nM de cada *primer* para um volume final de 25 µl. Os *primers* utilizados foram específicos para cada gene e estão descritos na Tabela 1. As amostras foram submetidas a aquecimento inicial de 94°C por 1 min, seguido por 30 ciclos de 94°C por 1 min, 60°C para RTN4 ou ARID1A, 72°C por 1 min. A reação foi terminada por um período de extensão de 10 min a 72°C. Os produtos foram analisados em gel de agarose 1,5%.

Para PCR semi-quantitativo, a reação foi feita como descrito acima, mas os ciclos foram de 15, 20, 25 e 30 vezes. O produto de PCR foi fracionado em gel de poliacrilamida 6% e visualizado com coloração de nitrato de prata.

3.6. Real Time PCR.

RNA total foi isolado conforme descrito acima (sessão 3.4.1). Oligonucleotídeos forward e reverse para β-actina e para os genes RTN4, TBRG e LGMN estão descritos na tabela 2. Amostras de DNA foram amplificadas por PCR usando Sybr Green método. β-actina foi utilizada como controle interno. Experimentos foram realizados em triplicata. Após amplificação, o produto amplificado foi submetido a eletroforese em gel de agarose e corado com brometo de etídeo. Real time PCR foi realizado em Real-Time Rotary Analyzer - Rotor-Gene 6000 (Corbett Robotics Inc., San Francisco, USA).

Tabela 2. *Primers* específicos utilizados nas reações de Real-Time PCR.

<i>Primer</i>	<i>Sequência (5'→ 3')</i>
Actina Foward	GACGGCCAGGTCATCCTA
Actina reverse	AGGAAGGCTGGAAAAGAGCC
RTN4 Foward	GCAGTGTGATGTGGGTATTTACC
RTN4 reverse	GAGTGAAATGAGAGCCAAAATCAG
LGMN Forward	CATAGGATCCGGCAAAGTC
LGMN Reverse	TCCAGTAGATCCA TGGTCAGTGA
TBRG Foward	TGCTGTCTGAGAAGCCAGAAGAT
TBRG Reverse	TTCCAAGTTGCTCTCGATTTTACC

3.7. Imunofluorescência

Ensaio de imunofluorescência foram conduzidos conforme métodos padrão (Leite et al., 2003; Mendes et al., 2005). Células foram crescidas em lamínulas de vidro 22X22 mm e os experimentos foram conduzidos 48 horas após o plaqueamento. As células foram lavadas 3X com PBS e fixadas com paraformaldeído 4% por 15 minutos à temperatura ambiente. A permeabilização da membrana plasmática foi feita com solução de PBS/Triton 0,5% através de 3 lavagens de 5 minutos cada. O bloqueio foi feito com solução PBS, BSA 10%, Triton 0,5%, soro de cabra 5%, por 1 hora em câmara úmida. Em seguida, as células foram incubadas por 2 horas em câmara úmida contendo um dos seguintes anticorpos diluídos em leite 1%/PBS, anticorpo policlonal anti-InsP₃RI (diluído 1:100); anticorpos policlonais anti-RTN4 (1:200), anti-LGMN (1:100) e anti-TBRG (1:200). Três lavagens de 5 minutos cada com PBS foram feitas antes de incubar o anticorpo secundário conjugado ao Alexa-488 (diluído 1:500). Três lavagens de 5 minutos cada com PBS foram feitas para retirar o excesso de anticorpos e 1 gota de Hidromount foi colocada sobre a lâmina, previamente identificada para montagem das lâminas. Após secar as lâminas foram deixadas a 4°C até análise no microscópio confocal. Controles negativos foram feitos com o anticorpo secundário sozinho. As imagens foram obtidas por microscópio confocal MRC-1024 (Bio Rad) usando objetiva de 63X com imersão em óleo. O comprimento de onda de 488 do laser Kryton/Argon foi utilizado par excitar Alexa-488 e a emissão foi coletada entre 505 e 530 nm. Para medir a especificidade da marcação, as imagens foram obtidas

padronizando os parâmetros do microscópio, o *pinhole* e o detector de ganho foram mantidos idênticos para a captura das imagens do controle e do tratamento.

3.8. Western Blot

Western blots foram realizados conforme metodologia padronizada por Mendes (2005) e Leite (2003). Células crescidas em placas de 35 mm foram lavadas com PBS e solubilizadas em 150 µl de solução detergente: Nonide P40 1% contendo 2% de inibidor de protease (Roche Applied Science). A concentração de proteína foi determinada espectrofotometricamente pelo método de Bradford. 50-80 µg de proteína foram separados em gel de poliacrilamida 6% e transferidos para membrana de PVDF (Bio Rad). As membranas foram bloqueadas com 5% de leite diluído em tampão TBST (tampão salino Tris base 20 mM acrescido de 0,05% de Tween 20) por 1 hora e depois, incubadas com anticorpos primários: anticorpo policlonal anti-InsP₃RI (1:1000); anticorpos policlonais anti-RTN4 (1:500), anti-LGMN (1:500) e anti-TBRG (1:1000); ou anticorpo monoclonal β-actina (1:5000). Para análise da expressão protéica das ciclinas diferentes concentrações e anticorpos foram utilizados. Esta incubação ocorreu por 2 horas à temperatura ambiente. Após 3 lavagens com PBS, a membrana foi incubada por 1 hora com anticorpo secundário conjugado à peroxidase (1:5000) à temperatura ambiente. As membranas lavadas foram expostas ao reagente de detecção ECL *plus* (GE Healthcare), 30 µl/cm² por 5 minutos. Após este tempo, o excesso de reagente foi removido e as membranas foram expostas ao filme de raio-X (Bio MaxTMML, KODAK) por tempos determinados. Nessa etapa, a peroxidase reage com o seu substrato formando um composto quimiluminescente. O filme foi revelado com solução reveladora até o aparecimento de bandas, em seguida lavada em água e colocada em solução fixadora por mais 2 minutos, e então, colocados para secar.

3.9. Medidas da incorporação de BrdU

A proliferação celular foi avaliada pela incorporação de BrdU, um análogo da timidina que é incorporado ao DNA durante a replicação do DNA. Esta medida foi avaliada usando ELISA (Roche Applied Science). Células SKHep1 foram plaqueadas

em placas de cultura de 96 poços, privadas de soro por 24 horas e então transfectadas com siRNA. Setenta e duas horas após a transfecção, as células foram tratadas com solução de BrdU (10 μ M diluído 1:100) por 4 horas. As células foram fixadas e anticorpo anti-BrdU (1:100) foi adicionado. A incorporação do BrdU foi medido por ensaio colorimétrico. Em experimentos com inibidor de legumaina, as células foram tratadas por 24 horas com 25 ou 50 μ M do inibidor. Células controle foram tratadas com DMSO sozinho.

3.10. Medidas do índice mitótico

Células SKHep1 que foram tratadas com siRNA foram marcadas para a fosfo-histona-3 (Upstate Biotechnology, Chicago, IL) por imunofluorescência e então examinados por microscopia confocal. Células em mitose foram definidas pela presença de DNA condensado e positivo para fosfo-histona-3 (Hendzel et. al., 1997). Índice mitótico foi calculado como a porcentagem de células em mitose pelo número total de células. Pelo menos 20 campos, representando um total >100 células foram visualizados para cada condição.

3.11. Análises do ciclo celular

Células SKHep1 tratadas com siRNA foram tripsinizadas, lavadas com PBS, fixadas em etanol 70% a 4°C e novamente lavadas com PBS. Após centrifugação, as células foram suplementadas com RNase (100 μ g/ml Sigma) por 5 min e coradas com iodeto de propídio (50 μ g/ml). O conteúdo de DNA foi determinado usando FACSCalibur (BD Bioscience) e os dados foram analisados usando Flowjo software.

3.12. Ensaio de apoptose

A apoptose foi medida usando detecção colorimétrica da atividade da Caspase-3 utilizando o kit ApoAlert Caspase Colorimetric Assay (Chontec, Waterford, CT). Apoptose foi induzida usando 500 nM de estaurosporina (Sigma-Aldrich) como controle positivo.

3.13. Imunofluorescência em amostras de tecido humano

Secções embebidas em parafina de carcinoma hepatocelular (HCC) de fígado humano foram de-parafinizado com xilol e lavagens seqüenciais com etanol em concentrações de 100 a 50% e depois pré-tratados com tampão Tris/EDTA (10 nmol/L Tris; EDTA 1 mmol/L). Após recuperação dos epitopos, foram incubadas com anticorpo anti-LGMN e então tratadas com anticorpo secundário Alexa 488 (Shibao et al., 2003). Os núcleos das células foram marcados com Topro-3. Para medir a especificidade da marcação, imagens foram obtidas usando configurações do microscópio no qual nenhuma fluorescência foi detectada em controles negativos com anticorpo secundário sozinho. Espécimes foram observadas em microscópio confocal e quantificadas usando ImageJ software. O diagnóstico de carcinoma hepatocelular foi realizado em cada caso usando critérios histopatológicos padrão. É caracterizado pela presença de uma discreta massa do fígado composta de uma proliferação de hepatócitos que exibem uma variedade de desordens nos padrões de crescimento. Perda da arquitetura lobular, artérias aberrantes, inclusões citológicas aberrantes e múltiplas formas nucleares foram observadas em variados graus em cada caso.

3.14. Ensaio de luciferase

Para o estudo da atividade do promotor de LGMN foi gerado um vetor que possui o gene da luciferase como gene repórter. Um fragmento de 750 pb, *upstream* ao códon de iniciação do gene da LGMN, foi amplificado por PCR, a partir do DNA genômico de células SKHep1, com os seguintes oligonucleotídeos: 5'-GGACCACCCAGAAACACC-3' e 5'-CTCGCTTAAGGGCCACTG-3'. O produto amplificado foi utilizado como *template* em uma segunda reação de PCR, na qual foram utilizados os óligos: 5'-GCGCCTCGAGTTGGCATTCTAAAATAGGGAAGTTAA-3' e 5'-GCGCAGATCTGCGTGGCATCTGCCAAAA-3'. Para introduzir os sítios de restrição *XhoI* e *BglII* respectivamente (Figura 7). O fragmento foi então inserido no plasmídeo pGL4.10[Luc2] para gerar o vetor pGLMNprom. A seqüência foi verificada por seqüenciamento. Lipofectamina 2000 foi usada para transfectar células SKHep1 com 10 µg de pGLMNprom sozinho ou em combinação com 3 µg de pAd-PV-NLS-DsRed, que expressa a proteína parvalbumina no núcleo da célula junto com a proteína DsRed. A atividade de luciferase foi medida com o Dual-Luciferase Reporter Assay

(Promega, Madison, WI). A atividade de luciferase foi normalizada pela atividade da *Renilla* luciferase. Cada experimento foi realizado em triplicata e os dados foram comparados com os controles de vetor vazio.

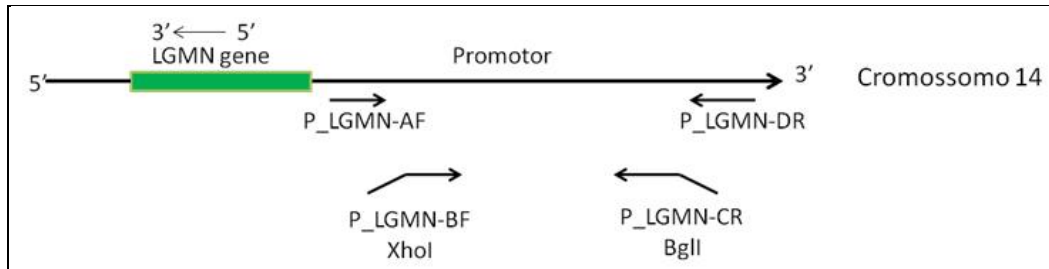


Figura 7. Diagrama esquemático da região promotora do gene da LGMN. O gene está localizado no cromossomo 14 na fita invertida. O produto de PCR amplificado com os *primers* P_LGMN-BF e P_LGMN-CR possuem sítios de restrição para as enzimas *XhoI* e *BglII* e amplifica um fragmento de 750 pb.

3.15. Construção dos Adenovírus Recombinantes

Com esta técnica objetivamos a produção de um vetor adenoviral capaz de maximizar o processo de entrega de siRNAs que contêm como seqüência alvo o mRNA das diferentes isoformas de receptores de InsP_3 para promover o silenciamento das proteínas traduzidas a partir deste mRNAs. Um dos maiores desafios para o uso de RNA de interferência no estudo da função dos genes em mamíferos é a dificuldade de entregar estes pequenos RNAs ou vetores que expressam siRNA nas células *in vivo*. A transferência de genes mediada por adenovírus é um sistema bem caracterizado e muito utilizado como vetor de entrega de seqüências de DNA *in vivo* e *in vitro* (Graham and Prevec, 1992; McConnell and Imperiale, 2004).

3.15.1. Desenho do siRNA e clonagem no pShuttle

Os siRNAs foram desenhados após estudos da seqüências gênicas codificadoras de receptores de InsP_3 , na qual foram escolhidas várias seqüências de 21 nucleotídeos para possíveis alvos contra InsP_3 s. Destas seqüências as que apresentaram maior porcentagem de silenciamento da proteína foram selecionadas para clonagem no vetor pShuttle tratado previamente com as enzimas de restrição *XhoI* e *SpeI*. Após a

clonagem, as seqüências foram confirmadas por sequenciamento com o kit Dyenamic ET Dye Terminator (GE Healthcare) conforme recomendações do fabricante, e analisadas pelo sequenciador MegaBace.

3.15.2. Linearização dos plasmídeos

Quatro microgramas de plasmídeo pAdeno LacZ backbone foi linearizado em reação de restrição com a enzima *Pac I* (10U/ μ l), em um volume final de 20 μ l de reação. Para o plasmídeo pShuttle, que contém o inserto de siRNA de interesse, foram linearizados 15 μ g em um volume final de reação de 50 μ l, também com a enzima *Pac I*. A digestão dos plasmídeos ocorreu a 37°C por 1,5 horas com 10 unidades da enzima. A eficiência da restrição foi confirmada em gel de agarose 1,0 %.

3.15.3. Transfecção em células HEK-293

Um dia antes da transfecção, $1,5 \times 10^6$ células HEK293 foram plaqueadas em frasco de cultura de 25 cm² com meio DMEM, suplementado com 10% de SFB. A confluência das células no dia da transfecção era de aproximadamente 60%, nunca sendo maior que 70%. Um complexo de transfecção foi preparado com 500 μ l de tampão salino HEPES, 4 μ g do plasmídeo pAdeno LacZ e 15 μ g do plasmídeo pShuttle digeridos com a enzima *Pac I*, e 25 μ l de cloreto de cálcio. Este complexo foi homogeneizado em vortex e incubado à temperatura ambiente por 25 minutos. Durante este tempo, as células foram lavadas e deixadas em meio de cultura, suplementado com 2% de SFB. O complexo de transfecção foi misturado ao meio e as células foram incubadas em condições normais de cultura por 4 horas. Após este tempo, o meio foi removido e as células foram deixadas em meio de cultura com 10% SFB a 37°C e 5% de CO₂ por 14-20 dias. Durante este período o meio não foi trocado, 1 ml de meio DMEM completo era adicionado a cada 3 dias. As células contendo adenovírus recombinantes formados foram coletadas quando mais que 60% delas se desprenderam da placa.

3.15.4. Coleta dos adenovírus recombinantes

As células foram coletadas junto com o meio de cultura e centrifugadas a 1500 RPM por 10 minutos. O meio foi reservado (-80°C) e o pellet de células lavado com 1 mL de PBS, centrifugados por 5 minutos a 1500 RPM e ressuspensionado em 1 mL de Tris 10 mM pH 8. O volume ressuspensionado foi congelado e descongelado 3X para lise das células e centrifugado a 13000 RPM por 10 minutos. O sobrenadante foi coletado e armazenado a -20°C até a etapa de expansão viral.

3.15.5. Expansão viral

O lisado de células coletado foi utilizado para a expansão inicial dos adenovírus. 500 µl de lisado contendo os vírus foram misturados a 50 mL de meio de cultura suplementado com 10 % de SFB e distribuídos em 5 frascos de cultura de 75 cm² (T₇₅), plaqueados com 1,5 x 10⁷ células HEK293 no dia anterior e incubados em condições normais por 24-48 horas. Após formação das placas de lise, as células foram coletadas e lisadas como descrito no item 3.3.2. O procedimento foi repetido e o lisado foi utilizado para infectar 20 novos frascos T₇₅. As células infectadas foram coletadas, centrifugadas, o sobrenadante foi reservado e o *pellet* foi ressuspensionado em 8 mL de Tris 10 mM pH 8 e congelado a -80°C até o momento da purificação.

3.15.6. Purificação dos adenovírus recombinantes

O lisado de células contendo os adenovírus foi congelado e descongelado rapidamente e imediatamente incubado com 1/10 do seu volume com Deoxicolato de sódio 5% (preparado no momento do uso) e deixado no gelo por 30 minutos. A suspensão foi homogeneizada manualmente em gelo e a ela foi adicionado 5,8 mL de solução de cloreto de céσιο saturado para cada 10 mL de suspensão viral. Todo o volume de solução foi colocado em tubos de ultracentrífuga que foram devidamente calibrados e centrifugados a 35000 RPM, a 4°C por 16 horas. A banda de vírus formada no gradiente de céσιο foi coletada e dializada em membrana Spectrapor (12 a 14000 KDa de capacidade para peso molecular; 1 a 2 cm de largura) com Tris 10 mM pH 8 por

4 horas a 4°C. Ao volume dializado foi adicionado glicerol 10%. Os adenovírus purificados foram aliquotados e armazenados no -80°C.

3.15.7. Titulação

A densidade de $3,0 \times 10^6$ células HEK293 foram plaqueadas 24 horas antes em placa de 24 poços. Os adenovírus foram descongelados em gelo (4°C) durante 10 minutos e brevemente sonicados em banho de água por 20 segundos antes de preparar as diluições. 10 µl da solução estoque de vírus foram adicionados a 990 µl de meio contendo 10% de SFB. Desta solução foram retirados 25 µl e colocados em 225 µl de meio completo para fazer as diluições seriadas (1-10). O meio de cultura das células foi retirado e a elas foi adicionado 200 µl de cada diluição. A placa foi deixada na estufa CO₂ por 7-10 dias até o aparecimento de placas de lise. O título, determinado em pfu/ml, foi obtido por contagem das placas de lise na última diluição positiva e este número foi multiplicado pelo correspondente fator de diluição.

3.16. Condições de infecção das células com Adenovírus recombinantes

As células foram plaqueadas 24 horas antes da infecção em placas de cultura celular de 35 mm, contendo lamínulas de 22x22 mm. No dia da infecção as células foram lavadas com tampão PBS (solução salina de fosfato) e incubadas com diferentes MOI (multiplicidade de infecção) de adenovírus recombinantes em 1,5 ml de meio de cultura suplementado com 10% SFB. As células infectadas foram incubadas por 1 hora em estufa de CO₂. Posteriormente, foram adicionados 1,5 ml de meio com soro às células e deixadas em condições ideais de cultura por 48 horas.

3.17. Hepatectomia parcial

3.17.1. Animais experimentais e procedimentos cirúrgicos

Ratos Holtzman machos de 80 gramas foram cedidos pelo biotério CEBIO (Centro de Bioterismo da UFMG). Após os tratamentos todos os animais permaneceram no biotério do Departamento de Fisiologia-ICB/UFMG onde foram mantidos em

condições laboratoriais com ração e água e ciclo circadiano de 12 horas claro e 12 horas escuro, com temperatura controlada de acordo com as normas padrão. Para a realização dos procedimentos cirúrgicos, os ratos foram sedados com 10 mg/kg de mistura anestésica de Ketamina 5% e cloridrato de Xilasina 2% (proporção 4:1), injetados pela via intra-peritoneal. Experimentos com animais foram conduzidos segundo princípios da ética experimental, e aprovados pelo Comitê de Ética em Experimentação Animal da Universidade Federal de Minas Gerais (CETEA).

3.17.2. Hepatectomia parcial (HX)

Foi feita uma incisão na cavidade abdominal dos ratos para a retirada de dois-terços (lóbulo médio e esquerdo) do fígado dos animais de acordo com o método descrito por Higgins e Anderson (1971) com adaptações. Ratos controles sham foram submetidos ao processo cirúrgico, tendo seu fígado manipulado, porém sem nenhuma ressecção (Higgins and Banks, Jr., 1971). A cavidade abdominal foi fechada por sutura. Em diferentes tempos, de 24 horas a 5 dias, após a hepatectomia, os animais foram anestesiados e o fígado foi rapidamente removido para isolar proteínas e RNA.

3.17.3 Razão peso fígado/peso animal

A massa do corpo do animal e a massa do fígado extraído foram pesados após o sacrifício dos ratos para comparar a taxa de regeneração do fígado. A massa do fígado foi expressa como porcentagem da massa total do corpo.

3.18. Medidas dos sinais de Ca^{2+} intracelular

Ca^{2+} nuclear e citosólico foram monitorados em células plaqueadas em lamínulas (22X22 mm) e infectadas com as construção adenoviral AdsiRNA-I. Após a infecção, as células foram deixadas em condições normais de cultura por 48 horas. Para realização dos experimentos as células foram incubadas por 30 minutos na presença de 6µl de Fluo-4/AM para monitorar o Ca^{2+} nuclear e citosólico e então foram transferidas para câmara de perfusão do microscópio confocal MRC-1024 (Bio-Rad). As células

foram mantidas em tampão HEPES (130 mM NaCl, 5 mM KCl, 1 mM MgSO₄, 1,2 mM KH₂PO₄, 1,2 mM CaCl₂ suplementado com 4,7 g de HEPES e 0,9 g de dextrose) durante o experimento e observadas utilizando objetiva de 63X imersa em óleo. Os comprimentos de onda 488 nm do laser Krypton/Argon foram utilizados para excitar a sonda e os sinais foram capturados entre 505 e 530 nm. As células foram estimuladas com 5 e 50 nM de vasopressina (Sigma).

Experimentos com células SKHep1 transfectadas com pAd-PV-NLS e incubadas por 48 horas, foram realizados para verificar os sinais de Ca²⁺ no núcleo das células. Estes plasmídeos são fusionados ao DsRed que codifica uma proteína vermelha que permite a localização da Parvalbumina no correto compartimento celular. Assim, as células foram excitadas à 568 nm e as imagens foram coletadas a 605 nm para identificação das células infectadas. Nestas células foram realizados os experimentos de avaliação do Ca²⁺ intracelular. As células foram incubadas com Fluo4/AM e estimuladas com 50 nM de vasopressina. O comprimento de onda de 488 nm foi utilizado para excitar as células e as imagens foram coletadas em comprimentos de onda de 503 a 530 nm.

3.19. Análises estatísticas

Todos os resultados foram analisados pelo Teste *t* de Student's para comparações entre os grupos estudados, enquanto medidas repetidas foram analisadas por ANOVA para comparações entre grupos maiores. Um valor de $p < 0,05$ foi utilizado para indicar significância estatística. Todos os testes estatísticos foram realizados pelo software GraphPad Prism (San Diego, CA).

4. RESULTADOS

4.1. Verificar a influência do Ca^{2+} nuclear, sobre a expressão de genes envolvidos na proliferação celular

4.1.1. Identificação de genes com expressão modulada pelo Ca^{2+} nuclear

Com o objetivo de investigar quais os genes têm sua expressão modulada pelo Ca^{2+} nuclear, foi realizado um estudo de expressão diferencial baseado em uma metodologia de análise por subtração. O método utilizado, denominado RaSH (*Rapid subtraction hybridization*), indica quais são os genes expressos em uma determinada situação.

Trabalhos publicados pelo nosso grupo em células SKHep1, indicam que sinais de Ca^{2+} nucleares regulam a progressão do ciclo celular não permitindo a passagem da transição G2/M quando seus níveis estão diminuídos no núcleo das células (Rodrigues et al., 2007). Sendo assim, fizemos uma análise de expressão diferencial na qual alteramos a concentração de Ca^{2+} intracelular de células SKHep1 para investigarmos os genes que têm sua expressão modulada pelo Ca^{2+} nuclear. As condições utilizadas para fazer o tamponamento de Ca^{2+} e para a obtenção dos clones diferencialmente expressos estão descritas em Materiais e Métodos.

Brevemente, as células foram infectadas e após 48 horas o RNA total foi extraído. A subtração ocorreu por hibridização de fragmentos derivados das populações TESTER e DRIVER. Estes fragmentos foram incubados por 48 horas a 14°C. Após obtenção da biblioteca de cDNA, as colônias de bactérias foram selecionadas randomicamente e submetidas à amplificação por PCR de colônia (dados não mostrados). Um total de 145 insertos de fragmentos de DNA foi amplificado por PCR. Na tabela 3 está a relação do número de clones que foram selecionados em cada condição de subtração. A metodologia do RaSH permite duas condições diferentes para os níveis de Ca^{2+} . Quando utilizamos o Ad-PV-NLS-DsRed como TESTER selecionamos genes que são expressos quando o nível de Ca^{2+} é reduzido, e utilizando o Ad-PV-NLS-Cd-DsRed como TESTER selecionamos genes que são expressos na presença de Ca^{2+} , pois a proteína parvalbumina possui uma capacidade reduzida de tamponar o Ca^{2+} .

Tabela 3. Número de clones selecionados na subtração pelo método RaSH.

Subtração	Tratamento	Clones
A (NLS TESTER)	Ausência de Ca ²⁺	43
B (NLS-Cd TESTER)	Presença de Ca ²⁺	102

Deste *pool* de clones positivos, isolados e seqüenciados, 13 apresentaram similaridades com proteínas conhecidas presentes no banco de dados do GeneBank (Tabela 4). A identidade dos genes com as seqüência depositadas no banco de dados variou de 93 a 100%. Estes clones foram diferencialmente expressos sendo que três deles mostraram regulação para baixo enquanto outros 10 mostraram regulação para cima quando tamponamos o Ca²⁺ nuclear. A condição de Ca²⁺ em que cada clone foi isolado está identificada na tabela 4, bem como a alteração da expressão destes clones apresentada após o tamponamento do Ca²⁺ nuclear. Escolhemos dois genes de cada condição, expressão aumentada ou diminuída, para fazermos um estudo preliminar e determinar a relevância destes genes na proliferação celular. Dados da literatura indicaram quatro candidatos com possíveis ações em processos de proliferação celular e progressão de tumores. Esses quatro genes foram validados por PCR semi-quantitativo e real time PCR.

Os genes ARID-1A e Reticulon 4 (RTN4) foram selecionados na ausência de Ca²⁺. ARID-1A pertence à família de proteínas ARID que apresentam importante papel nos processos de desenvolvimento, diferenciação, regulação transcricional e remodelamento da cromatina (Wilsker et al., 2004). O RTN4 pertence a uma família de genes que codificam o reticulon. Reticulons são proteínas ancoradoras da membrana do retículo endoplasmático envolvidas na secreção neuroendócrina ou no tráfico entre células neuroendócrinas (Yan et al., 2006). O produto deste gene é um potente inibidor do crescimento dos axônios (GrandPre et al., 2000).

Os genes que apresentam expressão diminuída quando o Ca²⁺ nuclear é tamponado, selecionados para validação foram, o gene da Legumaina e o gene do Regulador do TGFβ 4 (TBRG4). Legumaina é uma endopeptidase presente na matriz extracelular que auxilia a migração e capacidade invasiva de células tumorais (Liu et al., 2003). Já o gene TBRG4, também conhecido por CPR2 (*cell cycle progression restoration*), é um regulador dos fatores de crescimento de tumor e está relacionado com

proliferação e diferenciação celular (Edwards et al., 1997) e controle tecido-específico da expressão gênica (Montazer-Torbati et al., 2008).

Tabela 4. Clones selecionados pelo RaSH.

Clones – <i>GeneBank</i>	Nomenclatura	Níveis de Ca ²⁺	Expressão**
Domínio interativo rico em AT - 1A *	ARID 1A	Ausente	↑
Legumaina *	LGMN	Presente	↓
Regulador TGFβ 4 *	TBRG4	Presente	↓
Reticulon 4 *	RTN4	Ausente	↑
Gama tubulina	TUBG1	Ausente	↑
Gene homólogo ao membro A-família Ras	RHOA	Ausente	↑
Mps One binder activator-like 1B	MOB1	Ausente	↑
Proteína similar a proteína L3 ribossomal	-	Ausente	↑
Fator de splicing 3b	-	Ausente	↑
Alanil tRNA sintetase	AARS	Ausente	↑
Serpina inibidor membro 1	SERPINE1	Ausente	↑
Proibitina 2	PBHB2	Presente	↓
Proteína similar a proteína ribossomal L27	-	Ausente	↑

* Indica genes envolvidos em respostas proliferativas. Coluna **Níveis de Ca²⁺** indica a condição de subtração na qual o clone foi selecionado. ** Indica mudanças no nível de expressão gênica comparado ao controle. ↑ significa regulados para cima; ↓ significa regulados para baixo após o tamponamento do Ca²⁺ nuclear.

4.1.2. Validação dos clones selecionados pelo RaSH

O primeiro gene a ser validado foi o gene do Reticulon 4 (RTN4). A análise do *blast* revelou que a seqüência do clone obtido apresentou identidade com as diferentes isoformas deste gene. Procuramos então na seqüência N-terminal do gene uma boa seqüência para desenharmos os *primers*. Foram escolhidas regiões nos éxons 4 e 7 como sítios de ancoramento para os *primers* (Figura 8). Amplificar esta região não permite discriminar qual isoformas de RTN4 será amplificada. Como não sabíamos qual isoforma foi selecionada no RaSH optamos primeiro em verificar se o gene é induzido pelo decréscimo de Ca²⁺ nuclear e depois, caso seja relevante, fazer a determinação da

isoforma específica que tem sua expressão regulada pelo Ca^{2+} nuclear. Para os demais genes que apresentaram mais de uma isoforma, também desenhamos os *primers* em éxons que permitiam a amplificação de qualquer uma das isoformas, assim como foi feito para o gene do RTN4.

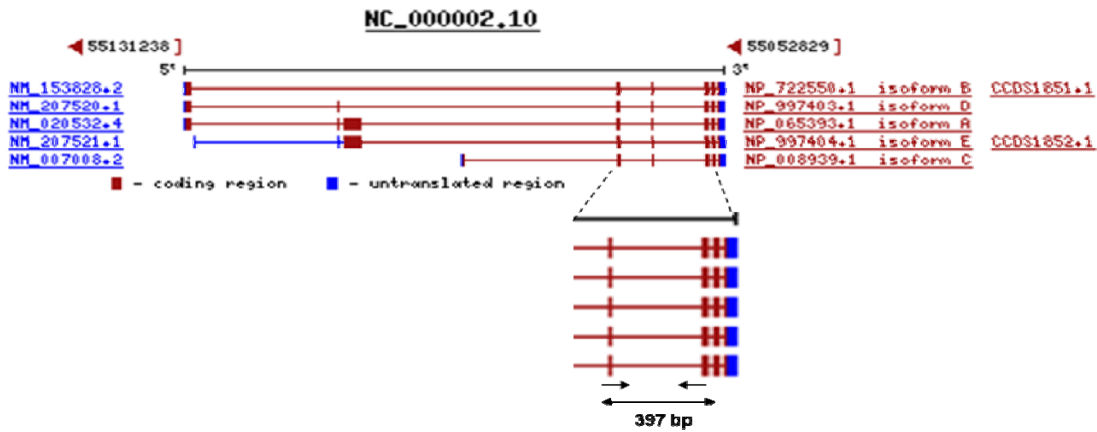


Figura 8. Desenho dos *primers* para o gene do RTN4. Éxons 5 e 7 foram escolhidos para desenhar os oligonucleotídeos. Nesta posição não há discriminação de qual isoforma está sendo amplificada. O produto de 397 pb foi obtido na PCR.

Os resultados do PCR semi-quantitativo confirmaram que o gene RTN4 é mais expresso quando a concentração de Ca^{2+} é diminuída no núcleo da célula. À medida que aumenta o tempo de infecção com o Ad-PV-NLS-DsRed, aumenta a expressão da PV, e conseqüentemente, a concentração de Ca^{2+} diminui. Com um nível menor de Ca^{2+} no núcleo da célula verificamos que a expressão do RTN4 aumenta em 55% e 74% após 12 e 48 horas de infecção com o Ad-PV-NLS-DsRed, respectivamente, comparados ao controle zero hora ($p < 0,05$) (Figura 9 A e B). Estes resultados sugerem que a ausência de Ca^{2+} está modulando a expressão deste gene, ou seja, quando analisamos a cinética de expressão temporal apresentada pelo RTN4, percebemos que este gene é induzido quando há diminuição dos níveis de Ca^{2+} nuclear.

O mesmo não ocorre com o gene da actina, que foi utilizada como controle interno para os experimentos de PCR semi-quantitativo. A expressão da actina apresentou apenas uma pequena variação, não significativa, durante todo o tempo de infecção. Análises de real time PCR confirmaram este resultado e também demonstrou

aumento nos níveis de mRNA do RTN4 em $91\% \pm 9,5$ ($p < 0,005$) comparados ao controle, quando o Ca^{2+} nuclear foi tamponado (Figura 10).

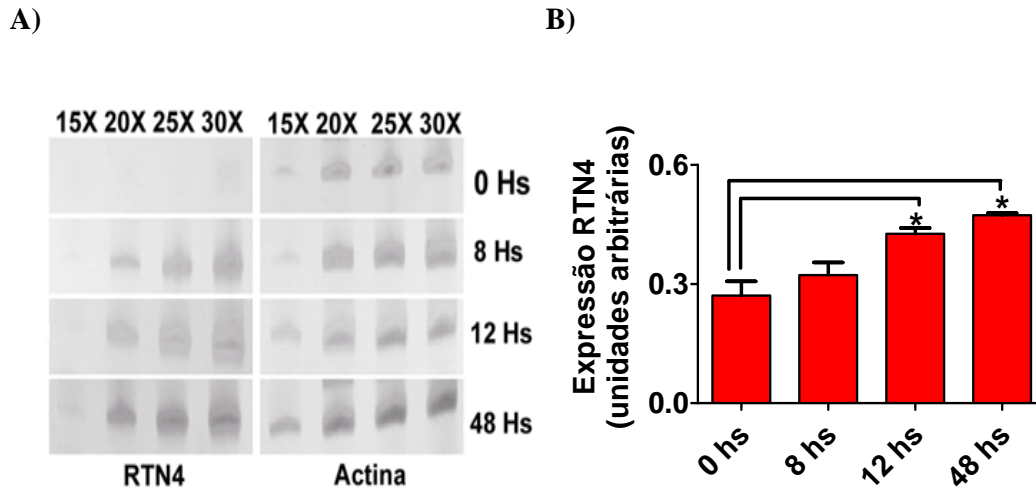


Figura 9. Validação do resultado do RaSH para o gene do RTN4. **A).** Análises de PCR semi-quantitativo indicam que o gene RTN4 tem sua expressão aumentada quando o Ca^{2+} é tamponado no núcleo da célula. Igual quantidade de produto de PCR (2 μl) submetidos a eletroforese em gel de poliacrilamida 6% e corados com prata. Os ciclos do PCR foram 15, 20, 25 e 30 vezes, e o tempo de incubação com o adenovírus de 0, 8, 12 e 48 horas. **B)** Análises de densitometria indicam aumento da expressão do RTN4 após 12 e 48 horas de infecção com o Ad-PV-NLS-DsRed, respectivamente. Asterisco indica significância de ($p < 0,05$) comparado ao controle. Todos os resultados são representativos da média \pm desvio padrão de três experimentos individuais.

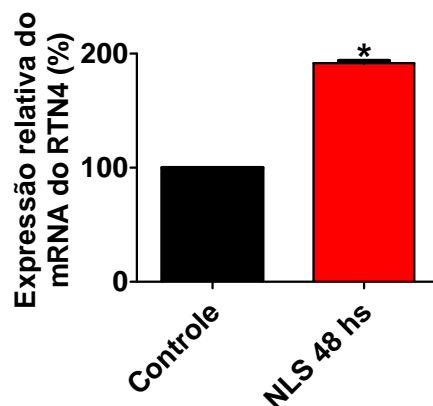


Figura 10. Expressão do mRNA do RTN4. Real time PCR foi utilizado para medir a expressão relativa do mRNA do RTN4 em células SKHep1. mRNA do RTN4 aumentou quando o Ca^{2+} nuclear foi tamponado ($p < 0,005$). Expressão de β -actina foi utilizada como controle. Todos os resultados são representativos da média \pm desvio padrão de três experimentos individuais.

Os mesmos experimentos foram realizados para os genes ARID1A, LGMN e TBRG4. O gene ARID1A não alterou sua expressão quando o Ca^{2+} nuclear foi tamponado (dados não mostrados). Já os genes LGMN e TBRG4 apresentaram uma diminuição na sua expressão. Os dados de PCR semi-quantitativo mostraram uma redução 15% para a LGMN e 32,5% para o TBRG, na expressão destes genes após tamponamento do Ca^{2+} nuclear (Figura 11 A e B). Já os resultados de real time PCR mostraram que os níveis de mRNA foram reduzidos em $97\pm 2\%$ para a LGMN, enquanto TBRG4 diminuiu em $88\pm 4,4\%$ comparados ao controle ($p < 0,0001$ e $p < 0,013$ respectivamente).

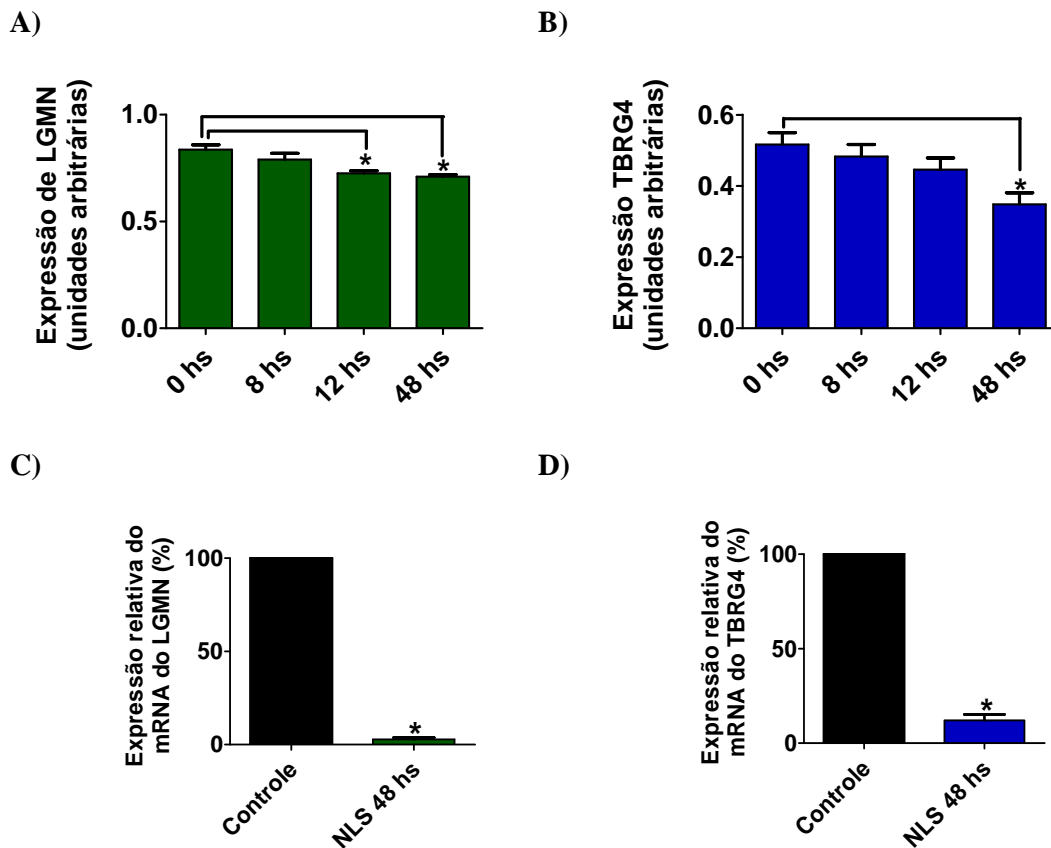


Figura 11 Validação do resultado do RaSH para os genes da LGMN e do TBRG4. **A-B)** Análises de densitometria do PCR semi-quantitativo indicam que os genes LGMN e TBRG4 tiveram diminuição da expressão quando o Ca^{2+} . Asterisco indica significância de ($p < 0,03$) comparado ao controle. **C-D)** PCR em tempo real foi utilizado para medir a expressão relativa do mRNA dos genes. LGMN e TBRG4 indicam redução nos níveis de mRNA destes genes ($p < 0,0001$; $p < 0,013$ respectivamente). Expressão de β -actina foi utilizada como controle. Todos os resultados são representativos da média \pm desvio padrão de três experimentos individuais.

4.1.3. Tamponamento do Ca^{2+} nuclear altera expressão da LGMN

Embora os genes validados tenham sido demonstrados pela literatura participarem direta ou indiretamente de processos proliferativos ou na progressão de tumores sólidos nós escolhemos apenas o gene da LGMN para demonstrar se sua expressão afeta a proliferação celular. Esta proteína foi então escolhida para ser estudada em maiores detalhes. A partir disso, nosso primeiro passo foi avaliar se os níveis de proteínas também estavam alterados pelo tamponamento do Ca^{2+} .

Assim como aconteceu com os níveis de mRNA, também foi observado uma redução nos níveis da proteínas LGMN 48 horas após a infecção com o adenovírus Ad-PV-NLS-DsRed (Figura 12). A expressão da proteína diminuiu $52 \pm 9\%$ ($p < 0,01$) depois que o Ca^{2+} nuclear foi tamponado comparado com o controle. Para confirmar que a expressão desse gene foi alterada em células SKHep1 que expressam PV fusionada ao DsRed dentro do núcleo, imagens de microscopia confocal foram realizadas. Marcação para LGMN com anticorpos específicos para este gene indicou que a expressão da proteína foi mais baixa em células que expressavam PV-DsRed dentro do núcleo quando comparado com células controle transfectadas com o DsRed sozinho (Figura 13A). Quantificação da imunofluorescência mostrou que o tamponamento do Ca^{2+} nuclear reduziu a expressão da LGMN em 45% ($11,1 \pm 0,4$ nos grupos DsRed versus $6,1 \pm 0,6$ unidades arbitrárias em células Pv-NLS-DsRed ($p < 0,001$) (Figura 13B).

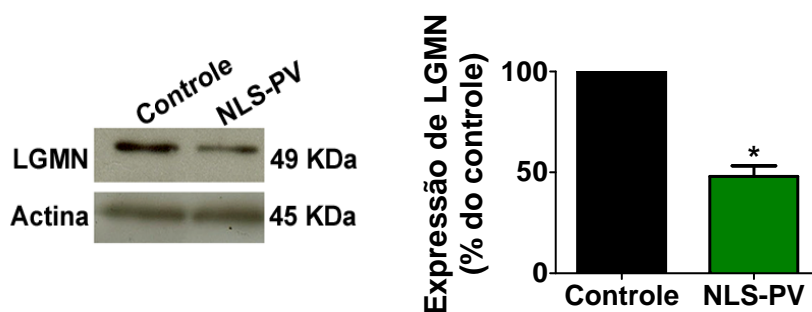
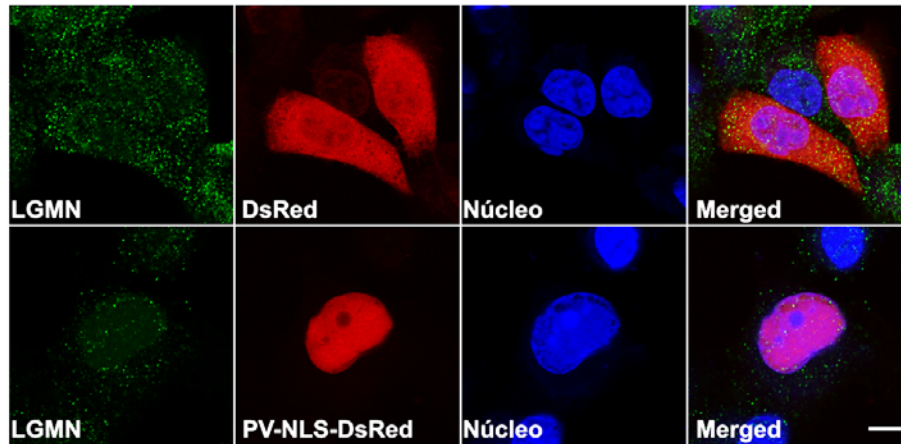


Figura 12. Expressão protéica de LGMN. Análises de western blot de proteínas totais extraídas de células SKHep1 48 horas após a infecção com Ad-PV-NLS-DsRed demonstram que a expressão de LGMN diminui após tamponamento do Ca^{2+} nuclear. Análises de densitometria confirmam redução na expressão da proteína comparada ao controle ($p < 0,01$). Expressão de β -actina foi utilizada como controle. Todos os resultados são representativos da média \pm desvio padrão de três experimentos individuais.

A)



B)

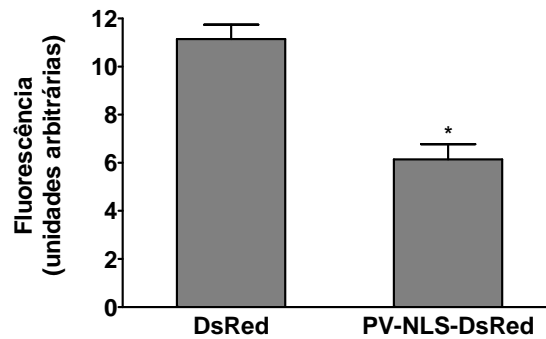


Figura 13. Expressão de LGMN em células SKHeP1. **A)** Confocal imunofluorescência confirma diminuição da expressão de LGMN (verde) em células SKHeP1 infectadas com Ad-PV-NLS-DsRed (vermelho). O núcleo foi identificado por marcação com Topro-3 (azul). Detecção da proteína DsRed confirma que ela está localizada no núcleo. Resultados são representativos de quatro experimentos independentes. Barra de escala = 10 μ m. **B)** Quantificação da imunofluorescência mostra que o tamponamento do Ca²⁺ nuclear reduz a expressão da LGMN (p<0,001).

Uma vez que o tamponamento do Ca²⁺ nuclear está associado com redução dos níveis de mRNA e protéicos da LGMN, investigamos se esse íon exerce algum papel na ativação da expressão da LGMN a nível transcricional. Para isso utilizamos ensaio de luciferase para quantificar a atividade do promotor do gene da LGMN quando o Ca²⁺ nuclear é tamponado. Análises computacionais da região que flanqueia o sítio de iniciação da transcrição do LGMN foram realizadas para determinar o promotor mínimo e a presença de *cis*-elementos regulatórios nessa seqüência. Para testar se a região vizinha ao sítio de iniciação do pré-mRNA do LGMN tinha atividade de promotor *in vitro*, um fragmento de 750 pb, acima ao códon de início da transcrição do gene da

LGMN, foi escolhido como um promotor mínimo e ligado a um plasmídeo repórter luciferase (pGL4.10[Luc2]). Foi gerado um vetor (pLGMN(prom)) que possui o fragmento da região promotora da LGMN fusionado ao gene da luciferase de vaga-lume. Os plasmídeos foram transientemente transfectados em células SKHep1 e a atividade de luciferase foi quantificada 24 horas depois. Para controle da eficiência de transfecção, as células foram co-transfectadas com plasmídeo pRL-CMV que codifica a *Renilla* luciferase. A atividade de luciferase dirigida pelo promotor da LGMN foi significativamente reduzida quando o Ca^{2+} nuclear foi tamponado pela expressão da PV no núcleo da célula (Figura 14). A atividade de luciferase foi de $20,57 \pm 5,34$ para o promotor (pLGMN(prom)) sozinho e de $6,89 \pm 0,88$ para o promotor mais a construção PV-NLS-DsRed que tampona o Ca^{2+} nuclear ($p < 0,005$). A atividade da luciferase de vaga-lume foi normalizada pela atividade da *Renilla* luciferase. Estes dados sugerem que o tamponamento do Ca^{2+} nuclear reduziu a expressão da LGMN em parte através da regulação da transcrição deste gene.

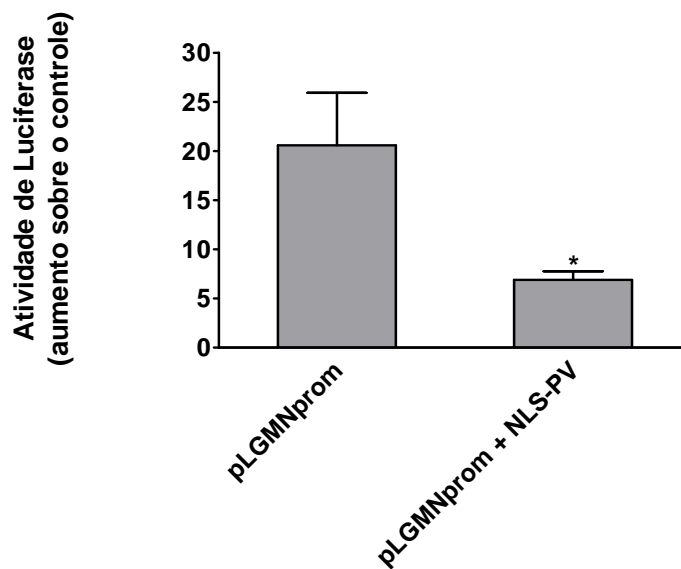


Figura 14. Ativação do promotor de LGMN. O ensaio de luciferase mostrou que a atividade do promotor de LGMN é inibida quando o Ca^{2+} nuclear é tamponado ($p < 0,05$). Os dados foram expressos como média do aumento da atividade \pm desvio padrão em relação ao vetor vazio. Os resultados são representativos de cinco experimentos individuais, cada realizado em triplicata.

Nossa próxima questão era determinar se a expressão do gene da LGMN pode ser induzida por algum outro mitógeno. Verificamos então, se o fator de crescimento do hepatócito (HGF), que é um potente mitógeno para os hepatócitos e que seletivamente aumenta Ca^{2+} nuclear em células SKHep1 (Gome DA et. al, 2008), modula a expressão da LGMN. Nós observamos que HGF (100 ng/ml) promoveu um aumento na expressão da LGMN de uma maneira tempo-dependente, alcançando seu máximo em 60 minutos (Figura 15A-B).

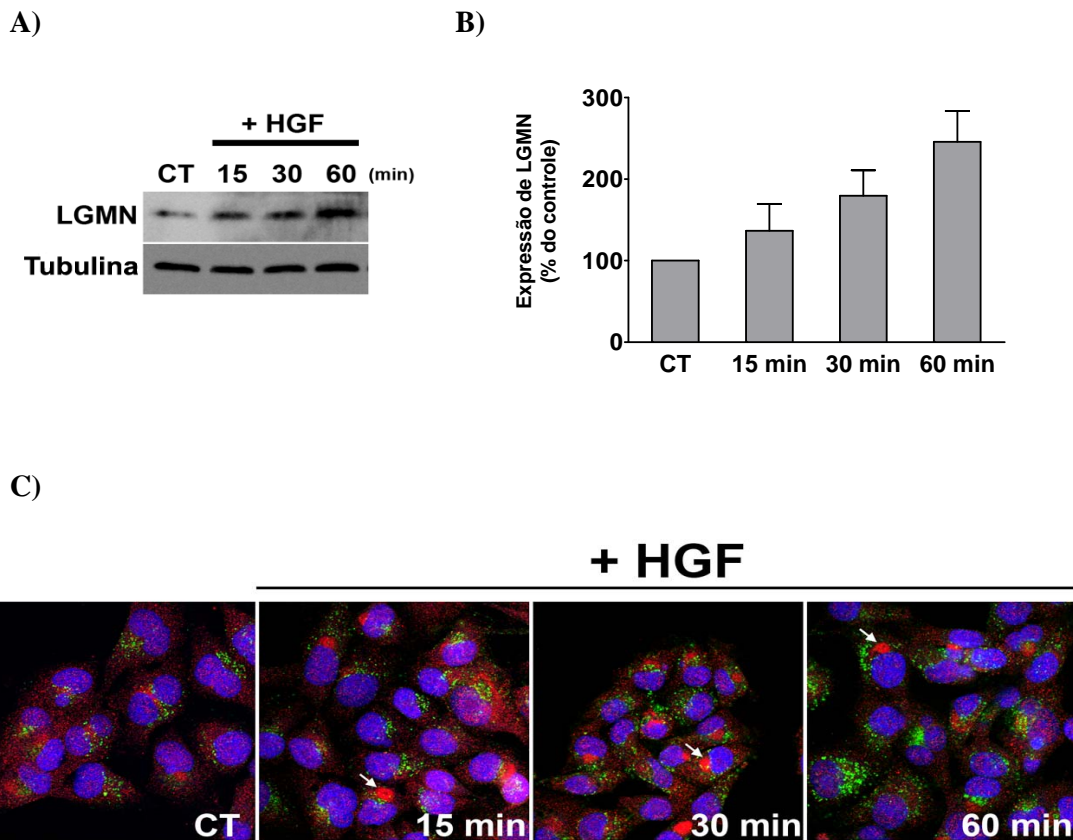


Figura 15. Indução da expressão de LGMN por mitógenos. **A)** Análises de western blot de lisado total de células não estimuladas e estimuladas com 100 ng/ml de HGF, pelo tempo indicado na figura, demonstram aumento na expressão da LGMN tempo-dependente. **B)** Gráfico de barras indica a quantificação densitométrica do aumento da expressão da LGMN de quatro experimentos independentes ($p < 0,05$). **C)** A localização da LGMN é alterada após tratamento com HGF. Células SKHep1 foram estimuladas e examinada por imunofluorescência confocal. LGMN (vermelho) está presente em estruturas pontilhadas que não apresentam co-localização com marcador lisossomal Lamp-1 (verde), nem em células controle nem em células estimuladas com HGF. O núcleo foi marcado com Topro-3 (azul). Após estimulação com HGF, LGMN se acumulou próximo ao núcleo das células (setas).

Este aumento na expressão de LGMN foi de $245,7 \pm 37,9\%$ ($p < 0,05$) 60 minutos após indução com HGF. Para mensurar a expressão da LGMN, proteínas foram extraídas 24 horas após o tratamento com HGF. Este aumento na expressão aconteceu associado com uma parcial redistribuição da LGMN, que mudou de um padrão pontilhado, observado em células não transfectadas, para a formação de grandes agregados peri-nucleares em células tratadas com HGF (Figura 15C). Não foi demonstrada a co-localização da LGMN com a proteína lisossomal Lamp-1 (Figura 15C). Estes resultados sugerem que a LGMN pode ter sua expressão modulada por algum estímulo celular que induza a proliferação celular.

4.1.4. Silenciamento da LGMN altera a proliferação celular

Já foi demonstrado que a proliferação celular depende dos sinais de Ca^{2+} nucleares para regular o ciclo celular e controlar a progressão de tumores (Rodrigues et al., 2007). Entretanto, a relação entre expressão de LGMN e a proliferação de células SKHep1 ainda não tinha sido demonstrada. Assim, decidimos investigar qual era a relação existente entre a LGMN e a proliferação celular. Para este estudo utilizamos a tecnologia do RNA de interferência. Constructos de siRNA específicos para mRNA da LGMN foram transfectados em células SKHep1 e o silenciamento foi verificado 72 horas após a transfecção. A expressão da LGMN reduziu em $78 \pm 6\%$ ($p < 0,0001$) quando comparado a células não transfectadas, como demonstrado pelos resultados de western blot (Figura 16).

A proliferação celular foi verificada através da incorporação de BrdU em células que teve a LGMN silenciada. O silenciamento da LGMN diminuiu a incorporação do BrdU 49% em relação a células não transfectadas (Figura 17A). Células cultivadas sem soro (0% FBS) foram utilizadas como controle negativo. Da mesma maneira a fração de células em mitose diminuiu para $2,2 \pm 0,7\%$ do controle após silenciamento da LGMN (Figura 17B). O número de células em mitose foi calculado por meio da determinação do índice mitótico. Resultados similares foram obtidos da contagem manual das células, demonstrando que a proliferação das células SKHep1 diminuiu após silenciamento da LGMN (Figura 17C).

O único efeito biológico descrito para a LGMN na literatura é de ser uma endopeptidase responsável por degradar a matriz extracelular e auxiliar na migração de células tumorais (Liu et al., 2003). Para elucidar se o efeito anti-proliferativo da LGMN é decorrente de sua atividade de endopeptidase nós verificamos como a proliferação celular seria afetada quando a LGMN estivesse com sua atividade inibida. Para isso, utilizamos o inibidor químico da LGMN, o MV026630 (Loak et al., 2003), e realizamos um ensaio de proliferação celular por incorporação de BrdU. Um único ensaio para verificar a eficiência do inibidor foi realizado, e este experimento indicou boa eficiência do inibidor MV026630 em inativar a atividade enzimática da LGMN (dados não mostrados). Para os experimentos de proliferação celular na presença do inibidor células SKHep1 foram tratadas com 25 ou 50 μM do inibidor por 24 horas e depois foi medida a proliferação celular. O ensaio de BrdU indicou que a inibição da atividade enzimática da LGMN não alterou a incorporação de BrdU ($p < 0,05$) (Figura 18). Este resultado sugere que o efeito proliferativo da LGMN é independente de sua atividade de endopeptidase. Juntos, estes resultados fornecem evidência de que a LGMN promove a proliferação e sugere que o Ca^{2+} nuclear regula a proliferação de células SKHep1 em parte por modular a expressão da LGMN.

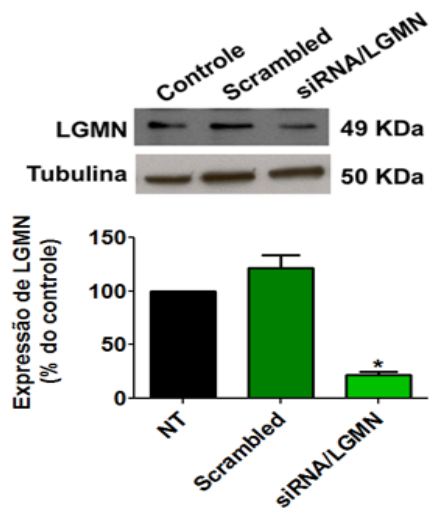


Figura 16. Expressão de LGMN após silenciamento. Análises de western blot de proteínas totais extraídas de células SKHep1 72 horas após transfecção de 20 nM de siRNA para LGMN demonstram que a expressão de LGMN, mas não a do siRNA scrambled, silencia a expressão da LGMN. Análises de densitometria confirmam redução na expressão da proteína comparada ao controle de células não transfectadas ($p < 0,0001$). Expressão da tubulina foi utilizada como controle. Todos os resultados são representativos da média \pm desvio padrão de três experimentos individuais.

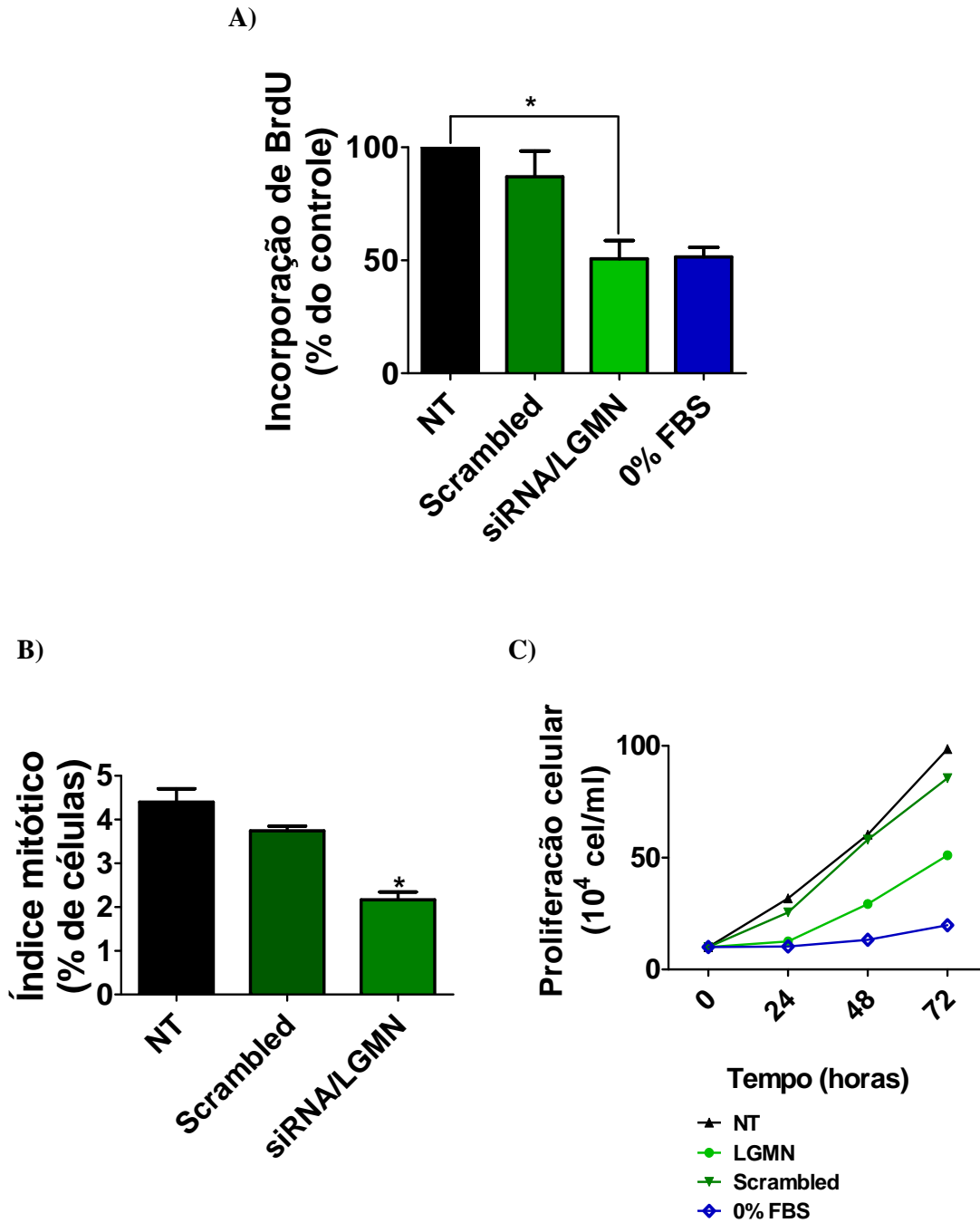


Figura 17. LGMN afeta a proliferação celular. **A)** A proliferação celular foi quantificada pela incorporação de BrdU durante a replicação. Silenciamento da LGMN reduziu a incorporação do BrdU em células SKHep1 comparado ao controle ($p < 0,0034$). **B)** Células SKHep1 em mitose foram identificadas por imagens de confocal da marcação da fosfo-histona-3 medida 72 horas após o silenciamento da LGMN. O índice mitótico foi reduzido comparado ao controle em células nas quais a LGMN foi silenciada ($p < 0,0001$). Um total de 300 células foi examinado em três experimentos separados. **C)** Número de células é menor no grupo tratado com siRNA para LGMN.

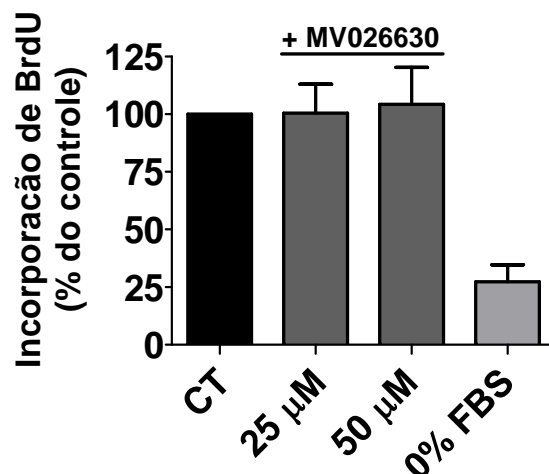


Figura 18. Atividade enzimática da LGMN não altera a proliferação celular. Inibição da atividade da LGMN com MV026630, 25 ou 50 μ M, não altera a incorporação do BrdU em células SKHep1 ($p < 0,05$, one-way ANOVA). Células controle foram tratadas com DMSO sozinho. Os resultados são representativos da média \pm desvio padrão de três experimentos individuais.

4.1.5. Silenciamento da LGMN altera a cinética do ciclo celular

Para tentar entender porque a redução da expressão da LGMN inibe a proliferação celular, investigamos se a diminuição da proliferação celular era devido a apoptose ou por alterações no perfil do ciclo celular. Análises de citometria de fluxo foram utilizadas para examinar se a redução na expressão de LGMN altera a distribuição das células dentro das fases do ciclo celular. As células foram privadas de soro por 24 horas para serem sincronizadas em G_0 , e o ciclo celular foi iniciado por adição de soro. As células foram transfectadas com siRNA e 72 horas depois elas foram fixadas e coradas com iodeto de propídio e submetidas a análises de FACs (Figura 19A).

Nas células em que a LGMN foi silenciada houve uma significativa redução na fração de células em G_2/M ($25 \pm 2\%$ das células não transfectadas, comparada a $7 \pm 6\%$ das células tratadas com siRNA; $p < 0,05$) (Figura 19B). Apesar da redução na fração de células na fase G_2/M , não houve nenhuma alteração significativa na fração de células nas fases G_1 ou S. Nenhuma mudança foi observada nas células transfectadas com o siRNA scrambled.

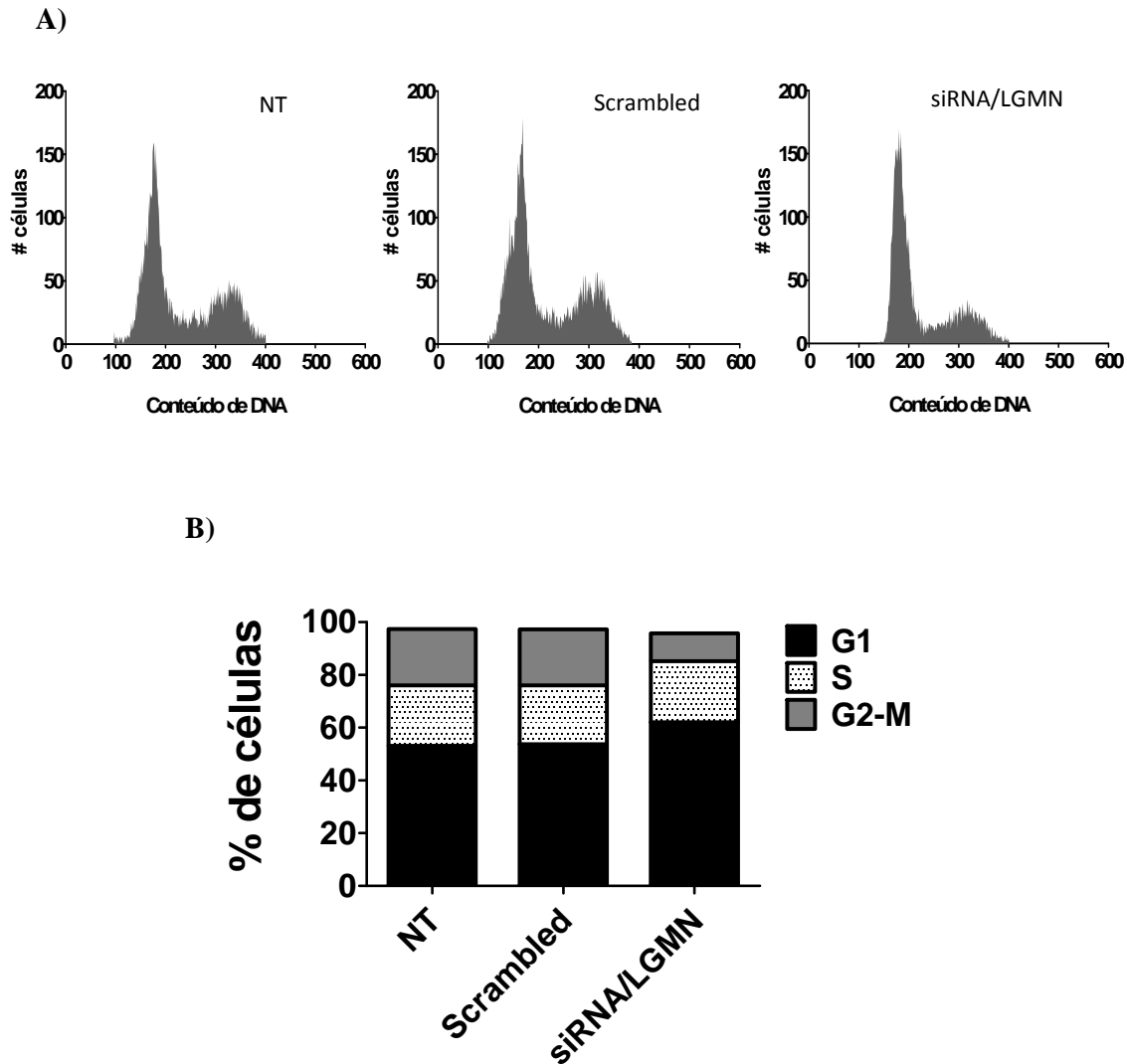


Figura 19. Cinética do ciclo celular após silenciamento da LGMN. **A)** Perfil representativo do ciclo celular de células SKHep1 não transfectadas (NT) e transfectadas com siRNA, 72 horas após tratamento com siRNA para LGMn ou scrambled. **B)** As células nas quais a LGMN foi silenciada houve uma redução na fração de células em G₂/M (<0,05) sem um significativo aumento da fração de células nas fases G₁ ou S. Perfil do ciclo celular não foi alterado em células transfectadas com siRNA scrambled. Os dados são representativos da média ± desvio padrão de três experimentos independentes.

Para verificarmos se os mecanismos de apoptose estavam envolvidos com a diminuição da proliferação celular utilizamos ensaio de caspase-3. Como observado na figura 20, nenhum aumento da atividade da caspase-3 foi observada nas células tratadas com siRNA para LGMN. Juntos, estes achados sugerem que a ausência da LGMN causa uma diminuição na proliferação de células SKHep1 que resulta de uma prejudicada progressão através do ciclo celular e não por aumento da apoptose.

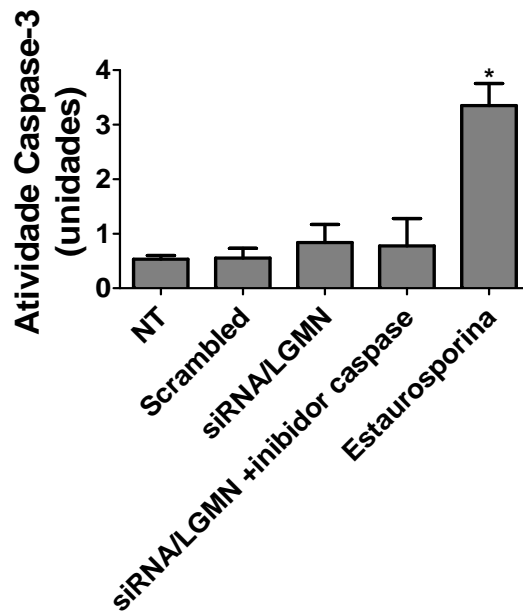


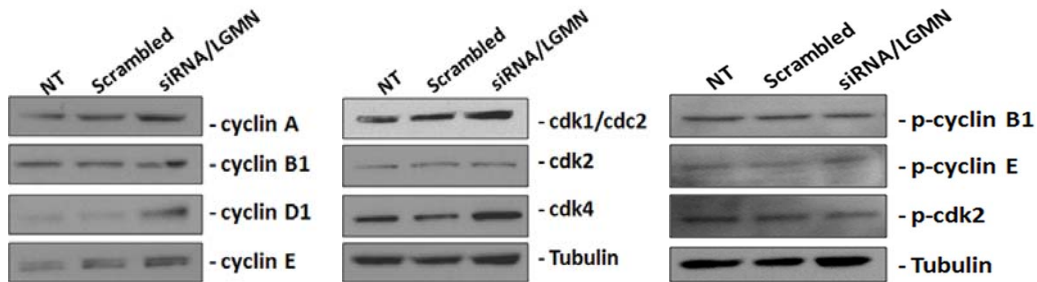
Figura 20. Apoptose após silenciamento da LGMN. A atividade de caspase-3 quantificada em células SKHep1 não transfectadas (NT) e transfectadas com siRNA, 72 horas após tratamento com siRNA para LGMN ou scrambled. Silenciamento de LGMN não induz apoptose. Estaurosporina (500 nM) foi usado como controle positivo e inibidor de caspase-3 foi utilizado como controle negativo. Gráfico de barras mostra que a atividade de caspase-3 não aumenta em resposta ao silenciamento da LGMN ($p > 0,05$, one-way ANOVA). Resultados são representativos de quatro experimentos independentes (* $p < 0,001$).

4.1.6. Silenciamento da LGMN modula expressão das proteínas do ciclo celular

As mudanças observadas no perfil do ciclo celular após o silenciamento da LGMN sugerem que a regulação negativa do ciclo celular pode ser decorrente da expressão de proteínas *checkpoint* do ciclo celular. Para investigar se ausência de LGMN estava afetando a expressão destas proteínas verificamos por western blot a expressão das principais ciclinas e cinases do ciclo celular (Figura 21A). A expressão da ciclina D1 e da cdk4, que juntas formam o complexo que regula a progressão pela fase G₁, não foi significativamente alterada (Figura 21A). A expressão da ciclina B₁ também não apresentou alteração. Esta ciclina regula a transição da fase G₂ para a fase M (Figura 21A). Entretanto, as proteínas *checkpoints* da fase S mostraram aumento de sua expressão quando a LGMN foi silenciada. Ambas, ciclina A e ciclina E foram significativamente aumentadas ($p < 0,05$) (Figura 21B). Este aumento na expressão destas proteínas não foi seguido de aumento na fosforilação de cdk2, sugerindo um bloqueio

da transição da fase S para a fase G₂/M. Essas alterações no perfil de expressão das proteínas *checkpoints* sugerem que a LGMN pode contribuir diretamente na regulação do ciclo celular.

A)



B)

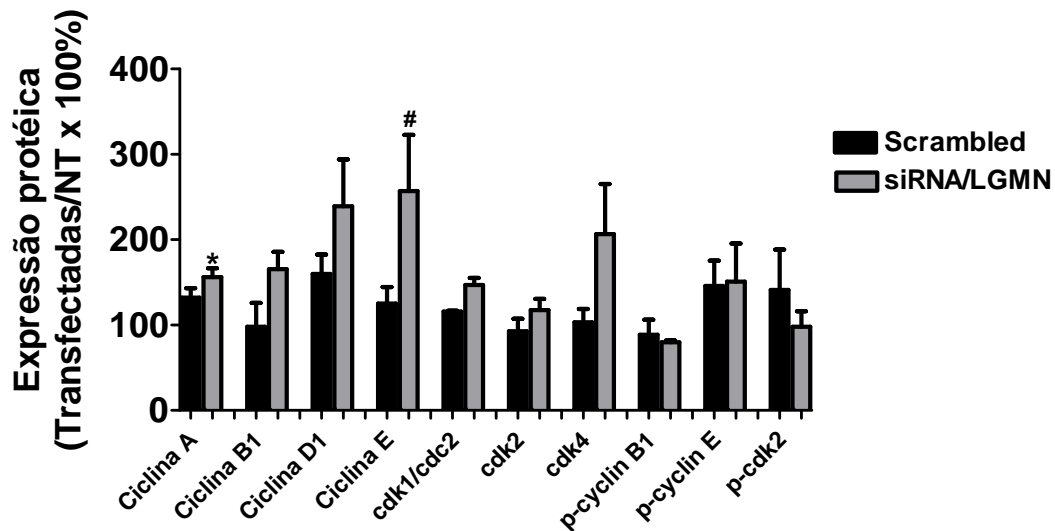


Figura 21. Expressão de proteínas *checkpoints* do ciclo celular. **A)** Análises de western blot de proteínas totais extraídas de células SKHepl 72 horas após silenciamento da LGMN para várias proteínas regulatórias do ciclo celular. **B)** Análises de densitometria sumarizam os resultados do western blot. Houve um significativo aumento na expressão das ciclina A ($p < 0,01$) e da ciclina E ($p < 0,05$) em células transfectadas com siRNA para LGMN em relação a células não transfectadas. Expressão da tubulina foi utilizada como controle. Todos os resultados são representativos da média \pm desvio padrão de três experimentos independentes.

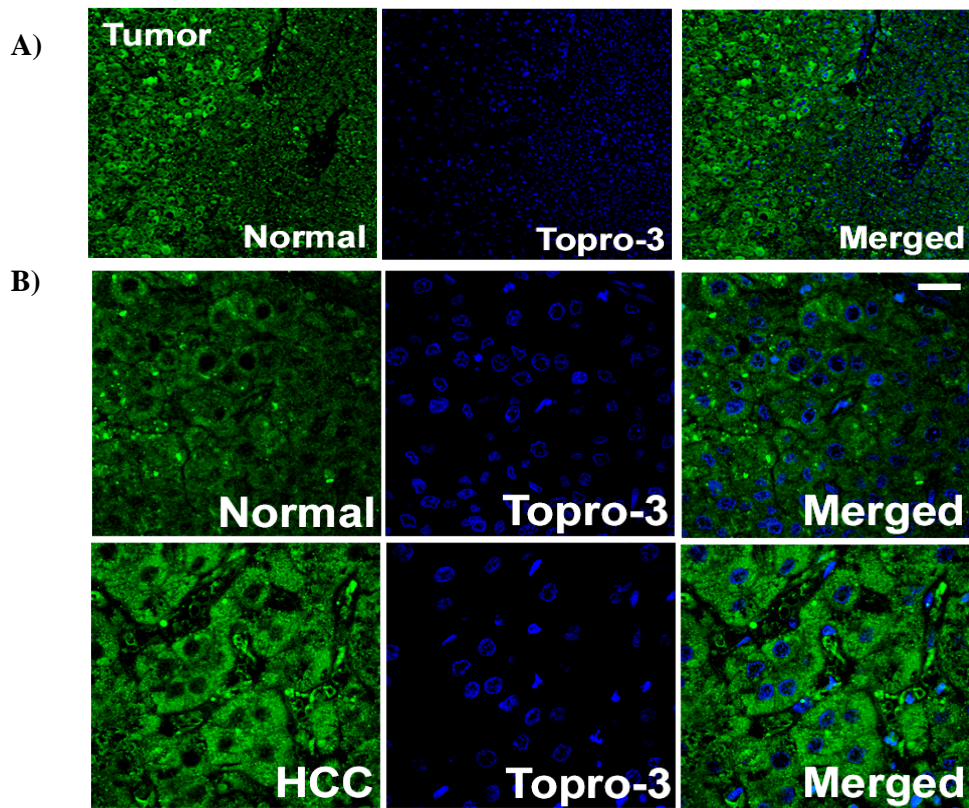
4.1.7. Expressão de LGMN em fígado humano normal e em hepatocarcinomas

Entre os cDNAs identificados pelo RaSH, LGMN é destacada porque este gene é altamente expresso em vários tipos de tumores. Sua presença está correlacionada com um pobre prognóstico e aumento da capacidade invasiva dos tumores (Liu et al., 2003) e pode ser utilizado como fator prognóstico em câncer de mama (Gawenda et al., 2007). Já foi demonstrado também que LGMN pode estar envolvido com desenvolvimento inicial de câncer colo-retal (Murthy et al., 2005). Por isso, investigamos a expressão de LGMN em hepatocarcinoma (HCC). HCC é o quinto tipo de tumor em frequência mundial, com maior incidência na África sub-saariana e sudeste asiático devido à alta incidência de infecção com o vírus da hepatite B (HBV) e da contaminação de alimentos com aflotoxinas (Rocken and Carl-McGrath, 2001). É o tumor hepático mais freqüente e é altamente vascularizado (Tanigawa et al., 1997). Para identificar expressão de LGMN em HCC amostras de fígado de pacientes diagnosticados com HCC foram examinadas por imunofluorescência confocal. As áreas de tumor e normal foram identificadas por meio de histopatologia com coloração hematoxilina-eosina (HE). Três amostras que contêm tecido normal e com tumor, de cinco diferentes pacientes foram examinadas. Expressão de LGMN estava aumentada em células tumorais ($53,9 \pm 6,5$ unidades arbitrárias) quando comparadas aos hepatócitos normais ($38,3 \pm 4,3$ unidades arbitrárias) na mesma amostra de tecido ($p < 0,01$, teste *t* pareado) (Figura 22). Estes resultados sugerem que a expressão de LGMN é aumentada em carcinoma hepatocelular, similar ao que foi observado em outros tumores sólidos. Isto é consistente com a idéia de que o efeito positivo da LGMN na proliferação celular pode promover carcinogênese.

4.2. Investigar o papel que o Ca^{2+} intracelular liberado a partir da ativação dos $InsP_3RI$ exerce sobre a regeneração hepática

4.2.1. Construção e teste dos adenovírus Ad-siRNA-I

O aumento na concentração de Ca^{2+} resultante da ativação de $InsP_3Rs$ ativa centenas de alvos que tem papel em muitos processos celulares incluindo desenvolvimento, proliferação, secreção e plasticidade sináptica (revisado por Leite e



C)

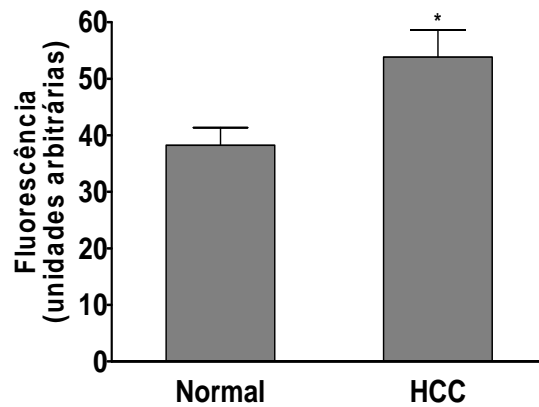


Figura 22. Expressão de LGMN em fígado humano normal e em hepatocarcinomas. **A)** Imagens de imunofluorescência confocal foram obtidas de amostras de tumores, embebidas em parafina, de pacientes com HCC. Marcação imunohistoquímica foi realizada para determinar a expressão de LGMN (verde) em células tumorais e em hepatócitos adjacentes. Topro-3 foi utilizado para identificar o núcleo da célula (azul). Painel superior: Imagem de baixa magnitude (10x) de células de carcinoma e hepatócitos normais no mesmo campo de visão mostram que a marcação de LGMN é maior em HCC. Painel inferior: Imagens de alta magnitude (63x) confirmam aumento na expressão de LGMN e mostra que ela está distribuída através do citoplasma em células HCC (escala da barra= 30 μ m). Resultados são representativos do que foi observado em 3 campos diferentes de cada amostra de 5 pacientes separados. **B)** Quantificação da média de fluorescência de áreas normal e afetadas com HCC na mesma amostra mostra redução na expressão de LGMN em células tumorais comparadas aos hepatócitos normais.

Nathanson, 2001). Em hepatócitos, os sinais de Ca^{2+} são decorrentes da abertura de InsP_3Rs tipos I e II que se encontram distribuídos por toda a célula, principalmente pelo tipo II que é o predominante e localiza-se na região pericanalicular da célula (Hirata et al., 2002). Porém, já foi visto que a expressão dos InsP_3RII também ocorre no núcleo dos hepatócitos (Echevarria et al., 2003). Estes receptores nos hepatócitos podem influenciar a liberação do Ca^{2+} nuclear e, conseqüentemente, a proliferação destas células durante o processo de regeneração.

No entanto, é importante observar que o fígado é populado por outros tipos celulares: células estelares, fibroblastos portais, colangiócitos, etc. Durante a regeneração hepática as células fornecedoras do HGF são as células estelares. Nessas células a principal isoforma de InsP_3Rs que é expressa é o tipo I (Bosanac et al., 2002), tornando o InsP_3RI o receptor mais importante para a exocitose do HGF. Por isso, decidimos verificar se o silenciamento do receptor de InsP_3 do tipo I influencia a sinalização de Ca^{2+} durante a regeneração hepática.

Para conseguirmos elucidar este objetivo, optamos pelo silenciamento dos InsP_3Rs tipo I utilizando RNA de interferência inserido em um sistema adenoviral. Utilizamos o sistema adenoviral como vetor para a entrega de siRNAs que possuem como alvo os RNAs que codificam a isoforma I dos InsP_3Rs . Para o desenho destes siRNAs foi realizado uma triagem por toda a seqüência do RNA mensageiro do InsP_3RI . Foram selecionadas algumas seqüências com 21 pb ditas como potenciais sítios alvos para o siRNA. A partir destes 21 nucleotídeos, foi desenhado um oligonucleotídeo de 55 pb, com sítios de restrição para as enzimas *Xho* I e *Spe* I o que possibilitou a clonagem deste fragmento no vetor pShuttle.

O seqüenciamento do inserto presente no vetor possibilitou a confirmação de que a seqüência de siRNA foi clonada corretamente (Figura 23). A seqüência de siRNA selecionada apresentou alta eficiência de silenciamento das proteínas dos InsP_3R . Mendes e colaboradores (2005) utilizaram esta mesma seqüência para estudo da influência do InsP_3R em processos apoptóticos em células CHO e mostraram que após transfecção com o siRNA houve redução de 99% na expressão do $\text{InsP}_3\text{R-I}$ quando comparadas ao controle, demonstrando que a construção de siRNA selecionada é altamente eficiente e específica para o silenciamento da isoforma de InsP_3R .

Após a confirmação da seqüência, os plasmídeos foram transformados em *E. coli* e purificados. Depois, eles foram linearizados e transfectados em células HEK293 junto com o plasmídeo pAdeno LacZ Backbone. Dentro destas células os dois plasmídeos sofreram recombinação homóloga resultando na produção de um adenovírus recombinante capaz de silenciar o InsP₃RI.

```

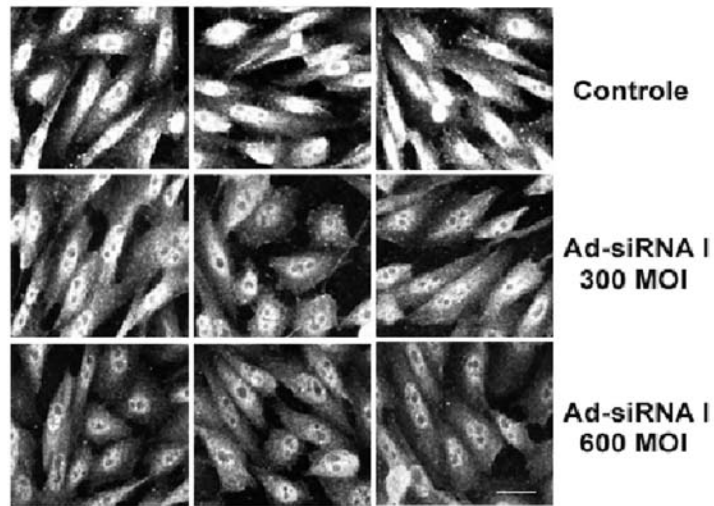
Sequenciado      AACCGTCTCGAGAGCACCAGCAGCTACAACCTTCAAGAGAAGTTGTAGCTGCTGGTGCTT 180
siRNA-I          -----TCGAGAGCACCAGCAGCTACAACCTTCAAGAGAAGTTGTAGCTGCTGGTGCTT 53
                  *****
Sequenciado      TACTAGTAATAAAGGATCCTTTATTTTCATTGGATCCGTGTGTTGGTTTTTTGTGTGCGG 240
siRNA-I          TA-----
                  **

```

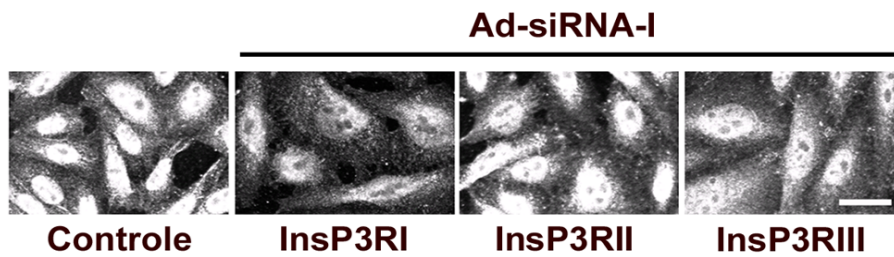
Figura 23. Sequenciamento do siRNA desenhado para o InsP₃RI. Sequenciamento do siRNA-I; na primeira linha está a seqüência obtida, na segunda linha está a seqüência do siRNA desenhado. Asterisco indica homologia entre as seqüências.

Após todo o processo de produção e expansão dos adenovírus, conforme descrito em Materiais e Métodos, as partículas virais foram testadas quanto à sua eficácia em silenciar os InsP₃RI. Células CHO foram utilizadas para verificar a eficiência dos adenovírus porque estas células expressam todas as três isoformas de InsP₃Rs. As células foram infectadas com diferentes MOI a fim de determinar a melhor condição de silenciamento. Ensaio de imunofluorescência indicaram que InsP₃RI apresentou uma redução na sua expressão após tratamento com 300 e 600 MOI de AdsiRNA-I (Figura 24A). O efeito de silenciamento do adenovírus mostrou ser específico para a isoforma tipo I, pois a expressão dos outros receptores, tipo 2 e 3, não foi afetada (Figura 24B). Quantificação da imunofluorescência mostrou que o AdsiRNA-I reduziu a expressão da receptor de InsP₃ tipo I em 48% comparado ao controle (5,4±2,13 unidades arbitrárias para InsP₃RI versus 12,9±1,8 para o InsP₃RII; 11,9±1,4 para o InsP₃RIII e 10,4±5,4 para o controle) (p<0,0001) (Figura 24C). Os resultados indicam que os adenovírus construídos e purificados são capazes de promover o silenciamento dos InsP₃RI de forma específica.

A)



B)



C)

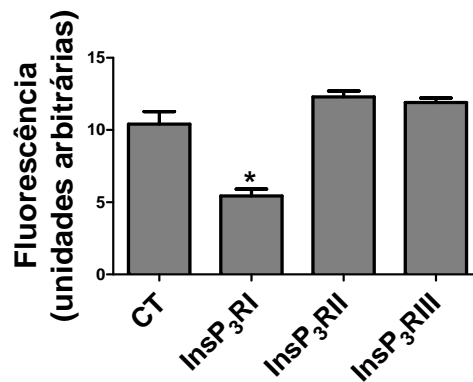


Figura 24. Silenciamento do InsP₃RI. **A)** Células CHO infectadas com 300 e 600 MOI de adenovírus específicos para o tipo I. Painéis de diferentes campos de células controle (superior) exibem uma maior intensidade de fluorescência quando comparado com os painéis de células infectadas com 300 (meio) e 600 (inferior) MOI, indicando redução da expressão do receptor. **B)** Confocal imunofluorescência confirma redução apenas na expressão do InsP₃RI sem alterar a expressão dos InsP₃Rs tipo 2 e 3, indicando a especificidade do silenciamento. **C)** Quantificação da imunofluorescência mostra que o AdsiRNA-I reduz a expressão deste receptor ($p < 0,001$). A barra representa 10 μ m.

4.2.2. Silenciamento dos InsP₃RI

O próximo passo então foi utilizar estes vírus para silenciar as proteínas *in vivo*. Para determinar a eficiência em silenciar os receptores diretamente no fígado dos animais, diferentes concentrações do AdsiRNA-I foram injetadas pela veia caudal e depois de 48 horas os animais foram sacrificados e o fígado foi extraído. Análises de western blot revelaram que 100 µl de solução contendo 1×10^9 pfu/animal resultou em $42 \pm 6,3\%$ ($p < 0,001$) de redução na expressão do InsP₃RI no fígado comparado ao controle enquanto que a concentração de 1×10^8 pfu/animal não alterou a expressão do receptor (Figura 25A). Injeção de grandes quantidades de adenovírus (1×10^{11} ou 1×10^{12} pfu/animal) em dose única causou toxicidade aos animais enquanto que a administração de baixas doses (1×10^6 ou 1×10^7 pfu/animal) repetidas vezes, não apresentou resultados de silenciamento mais expressivos (dados não mostrados).

Para verificar se a transferência gênica do siRNA estava ocorrendo por todo o fígado, foi realizado um ensaio de β-galactosidase. O genoma adenoviral do kit utilizado para construção dos adenovírus possuem o gene LacZ inserido na sua sequência e permite quantificar a atividade da enzima β-galactosidase. Este método foi utilizado para determinar se todo o fígado estava sendo infectado. Quarenta e oito horas depois da infecção com 1×10^9 pfu/animal de Ad-siRNA-I, pedaços de fígado foram analisados (Figura 25B imagens). A atividade de β-gal foi normalizada pela concentração de proteína em cada amostra e sua quantificação foi realizada por leitura no espectrofotômetro no comprimento de onda de 615 nm. A injeção de 1×10^9 pfu/animal mostrou ter uma maior concentração de β-gal sugerindo uma maior e mais extensiva infecção (Figura 25B). Estes resultados indicam que injeção pela veia caudal dos constructos adenovirais pode ser usada para eficiente entrega dos AdsiRNA-I dentro do fígado dos animais para promover o silenciamento dos InsP₃RI.

Para confirmarmos se o AdsiRNA-I também promovia o silenciamento dos InsP₃Rs nos hepatócitos isolamos estas células e verificamos a expressão do receptor um, quatro e seis dias após a infecção. Assim como aconteceu no fígado, os níveis de InsP₃RI nos hepatócitos reduziu nos dias quatro ($48 \pm 15\%$) e seis ($38,5 \pm 4,03\%$) após a infecção com AdsiRNA-I ($p < 0,0036$) (Figura 26A). Quantificação da imunofluorescência mostrou que o adenovírus foi capaz de silenciar o receptor por seis dias após a infecção (Figura 26B).

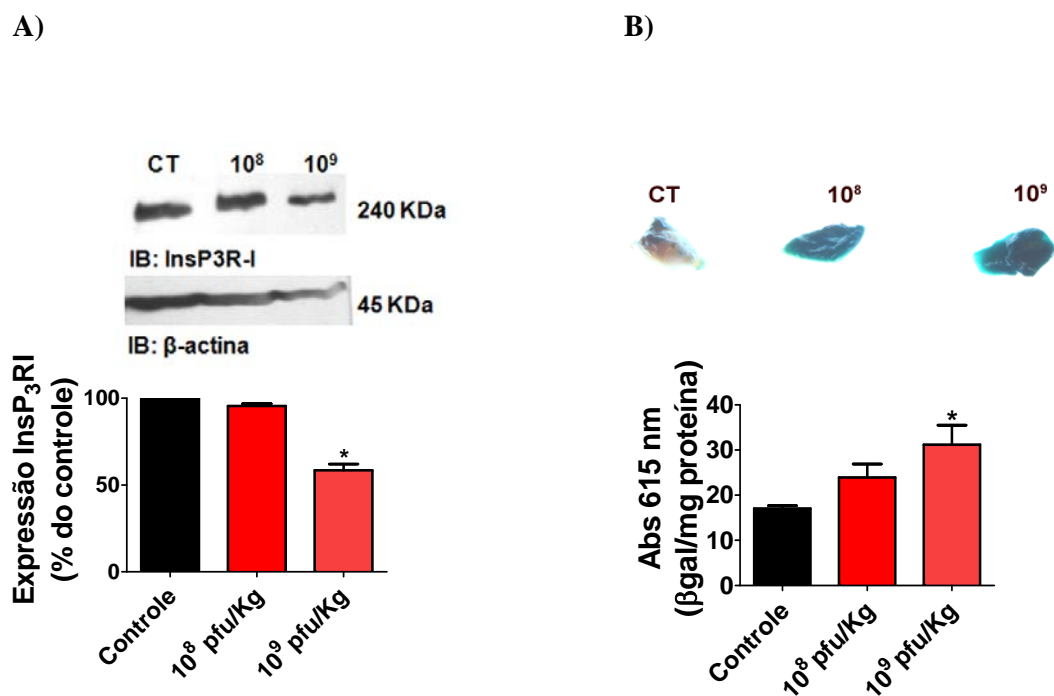


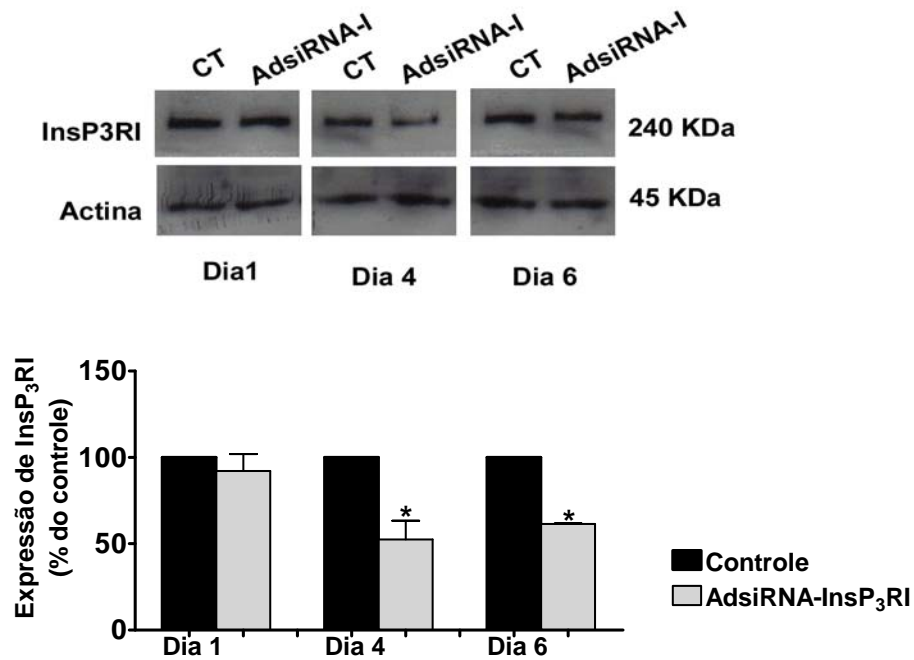
Figura 25. Expressão de InsP₃R-I em fígado. **A)** Imunoblot com proteínas totais extraídas de fígados infectados com 10^8 ou 10^9 pfu/animal de adenovírus, 48 horas depois da infecção indica redução na expressão do receptor comparado ao controle ($p < 0,05$) ($n = 3$ animais para cada tratamento). **B)** Animais foram infectados com AdsiRNA-I e a transferência gênica foi quantificada por espectrofotometria (gráfico de barras) e visualizadas por ensaio de β galactosidase (imagens) ($p < 0,05$).

4.2.3. Alterações dos sinais de Ca^{2+} intracelulares após silenciamento dos InsP₃RI

O fígado exibe uma imensa capacidade regenerativa que envolve a ativação de uma complexa resposta para promover a replicação celular e o crescimento suficiente para restaurar a massa funcional do fígado (Fausto et al., 2006). Vários são os eventos que ocorrem durante a regeneração hepática. HGF é um importante fator de crescimento que dirige a progressão do ciclo celular durante a regeneração. Ele é produzido pelas células estelares e age de forma parácrina nos hepatócitos. Sabemos que o aumento intracelular de Ca^{2+} é importante para a proliferação celular. Porém, o papel relativo do Ca^{2+} intracelular na proliferação de hepatócitos ainda não foi esclarecido.

Para verificar a sinalização de Ca^{2+} em hepatócitos de ratos em processo de regeneração hepática foram realizadas análises de western blot para verificar o nível de

A)



B)

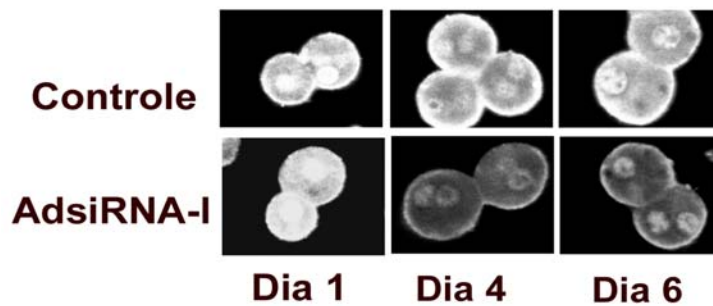


Figura 26. Expressão de InsP₃R-I em hepatócitos. **A)** Análises de western blot de proteínas totais extraídas de hepatócitos infectados com 1×10^9 pfu/animal de adenovírus, 4 e 6 dias após infecção indica redução na expressão do receptor comparado ao controle ($p < 0,05$) ($n=3$ animais para cada tratamento). **B)** Análises de densitometria sumarizam os resultados de western blot. Houve uma significativa redução na expressão dos InsP₃RI durante 6 dias de infecção comparada ao controle ($p < 0,05$). Expressão da actina foi utilizada como controle. Todos os resultados são representativos da média \pm desvio padrão de três experimentos independentes.

expressão deste receptor nas diferentes condições de tratamento. Utilizamos também a técnica de hepatectomia parcial que consiste na remoção de 2/3 do órgão (retirada dos lóbulos esquerdo e médio). Os dados indicam que a expressão dos InsP_3RI reduziu após infecção com AdsiRNA-I , porém esta redução não foi significativamente diferente da redução observada nos animais apenas submetidos à hepatectomia parcial ou apenas infectados com o AdsiRNA-I (Figura 27). A expressão reduziu para $71 \pm 5,3\%$ em animais submetidos à hepatectomia; $58,51 \pm 8,4\%$ em animais infectados com AdsiRNA-I e $56,75 \pm 9,1$ em animais que sofreram hepatectomia e tiveram os receptores de InsP_3 silenciados comparados ao controle ($p < 0,05$).

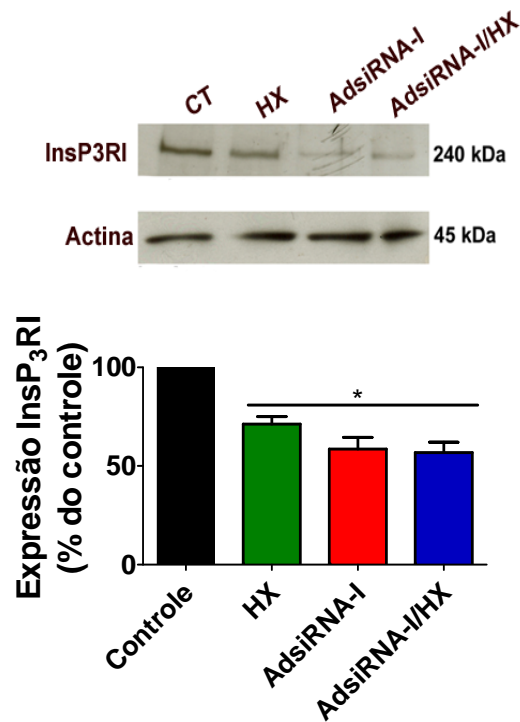


Figura 27. Expressão de $\text{InsP}_3\text{R-I}$ em hepatócitos após hepatectomia parcial. Análises de western blot de proteínas totais extraídas de hepatócitos infectados com 1×10^9 pfu/animal e submetidos à hepatectomia parcial (barra azul) indicam redução na expressão do receptor comparado ao controle ($p < 0,05$) ($n=3$ animais para cada tratamento). Expressão da actina foi utilizada como controle. Todos os resultados são representativos da média \pm desvio padrão de três experimentos independentes.

Para avaliar o efeito direto do silenciamento do InsP_3RI nos sinais de Ca^{2+} animais foram infectados e 48 horas depois foram submetidos a hepatectomia. Vinte e quatro horas depois da cirurgia os hepatócitos foram isolados e marcados com indicador

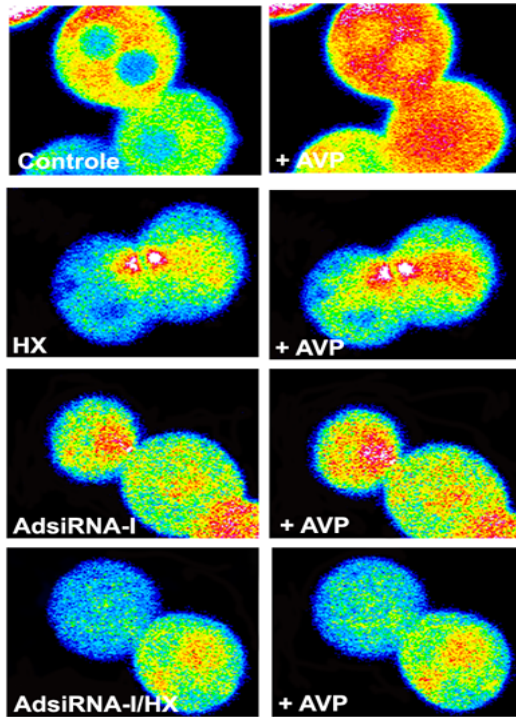
fluorescente de Ca^{2+} (Fluo-4/AM) e analisados por microscopia confocal. As células foram estimuladas com 50 nM de vasopressina (n=30-80 células). A figura 28A mostra que todas as células respondem ao estímulo e liberam Ca^{2+} intracelular. O perfil de cada resposta pode ser observado pelos traços representativos de cada resposta (Figura 28B). O perfil de resposta apresentado pelas células infectadas e hepatectomizadas ou com os dois tratamentos simultâneos foi diferente daquele apresentado por células controle indicando que tanto a hepatectomia quanto o silenciamento do receptor tipo I altera a amplitude do sinal de Ca^{2+} e a duração deste sinal na célula (Figura 28B). É possível observar que os sinais de Ca^{2+} após silenciamento dos InsP_3RI e hepatectomia demoram mais para se iniciar. O tempo de subida dos sinais de Ca^{2+} para o controle e para os tratamentos AdsiRNA-I e HX foi de aproximadamente 80 segundos, já para as células submetidas aos dois tratamentos simultaneamente esse tempo foi maior, chegando a 120 segundos para iniciar a resposta (Figura 28B).

O silenciamento do InsP_3RI e a hepatectomia parcial reduziram significativamente a amplitude dos sinais de Ca^{2+} (Figura 28C). A amplitude é definida como a diferença entre o valor basal e o valor máximo da fluorescência. A amplitude do sinal no grupo AdsiRNA-I/HX reduziu 45% do valor do controle ($92,147 \pm 25,03$ para AdsiRNA-I/HX versus $168 \pm 31,36$ para o controle). Os tratamentos AdsiRNA-I e HX também reduziram sua amplitude variando de $125,26 \pm 10,04$ e $126,21 \pm 10,49$ respectivamente em relação ao controle (Figura 28C). Ambos os eventos, mudança no perfil de liberação de Ca^{2+} e diminuição da amplitude, são importantes para definir uma resposta fisiológica a ser desencadeada após aumento de Ca^{2+} intracelular. Em conjunto, os resultados demonstram que a redução na expressão dos InsP_3RI reduzem ou dificultam a liberação de Ca^{2+} intracelular em hepatócitos e isto é agravado quando o fígado está em processo de regeneração.

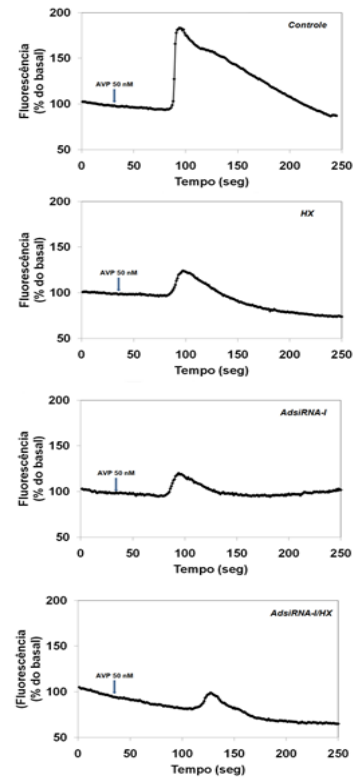
4.2.4. Silenciamento dos InsP_3RI altera a regeneração hepática

Para investigar como a modulação da sinalização de Ca^{2+} exercida pela ausência dos InsP_3Rs do tipo I pode influenciar a proliferação dos hepatócitos determinamos qual o impacto que estes receptores podem causar no processo de regeneração hepática. A avaliação do processo regenerativo foi realizada calculando a razão entre a massa do

A)



B)



C)

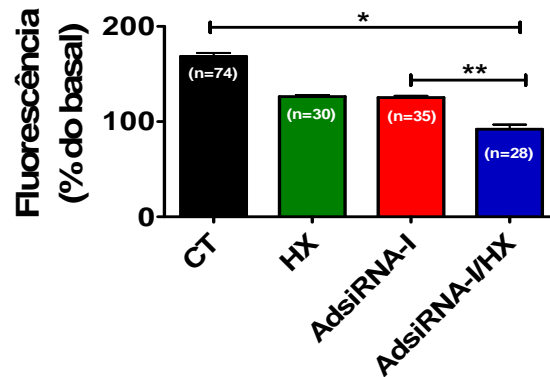


Figura 28. Sinalização de Ca^{2+} em hepatócitos. **A)** Padrão do aumento de Ca^{2+} em células com InsP_3RI silenciados apresentam menor amplitude dos sinais de Ca^{2+} em resposta a estimulação com AVP. As imagens foram pseudocoloridas de acordo com a escala de cores. **B)** Traço representativo do aumento de Ca^{2+} em uma única célula controle (preto), ou em células que foram infectadas com AdsiRNA-I (vermelho); submetidas a hepatectomia parcial (verde) ou infectadas e submetidas a hepatectomia parcial (azul). A amplitude dos sinais de Ca^{2+} diminuiu em células submetidas aos tratamentos quando comparadas ao controle. **C)** O gráfico sumariza a porcentagem de aumento da amplitude do sinal de Ca^{2+} . Asterisco (*) indica diferença significativa em relação ao controle; ** representa diferença significativa entre animais infectados com AdsiRNA-I e animais infectados e submetidos a hepatectomia parcial. ($p < 0,0001$). Resultados decorrentes da análise de 30-80 células, indicados em cada barra.

figado pela massa do corpo do animal. Foi verificado que, após a retirada parcial do figado, a razão de massa do figado pelo massa total do animal foi aumentando gradativamente em todas as condições experimentais (animais infectados, hepatectomizados e com ambos os tratamentos) indicando que estes animais estavam em processo de proliferação hepático para reestruturação da massa tecidual do figado. Porém, a regeneração foi mais lenta após silenciamento do $\text{InsP}_3\text{R-I}$ (Figura 29). A taxa de regeneração em animais com InsP_3RI silenciado e submetidos a hepatectomia parcial foi $32\pm 12,9\%$ menor que o controle SHAM, Já a redução dos sinais de Ca^{2+} foi de $89,9\pm 11,3$ para HX e $96,07\pm 4,07$ para Ad-GFP. O resultado indica que a ausência do receptor de InsP_3 do tipo I é importante para o processo de regeneração hepática. Sem este receptor todo o processo de regeneração fica mais atrasado sugerindo que o Ca^{2+} intracelular liberado por este receptor apresenta um papel fundamental no processo de proliferação dos hepatócitos.

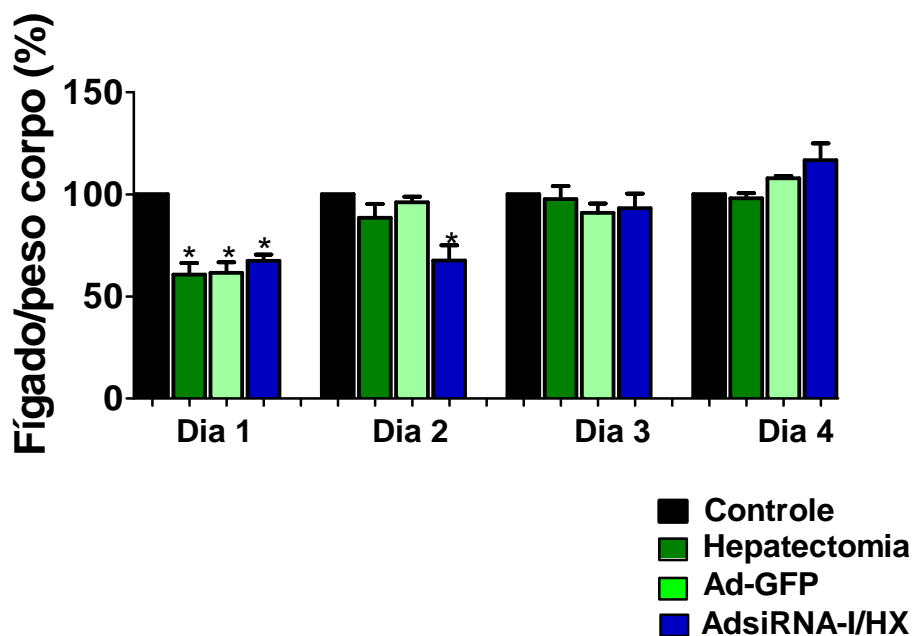


Figura 29. Regeneração hepática. Razão fígado/peso corpo apresentada pelos animais que sofreram hepatectomia parcial é menor do que o controle no dia 2 indicando uma regeneração mais lenta nos animais submetidos a hepatectomia que tiveram o InsP_3RI silenciado. Experimento realizado com $n=3$ animais para cada condição experimental. Hepatectomia (HX).

5. DISCUSSÃO

Rápida subtração por hibridização (RaSH) é um método utilizado para identificar diferenças no padrão de expressão gênica. A relativa simplicidade, baixo custo e sensibilidade do método permitiram que examinássemos o papel do Ca^{2+} nuclear na transcrição de genes envolvidos em respostas proliferativas. A transcrição de muitos genes está correlacionada com as funções das proteínas codificadas por eles. Mudanças na atividade transcricional dos genes refletem mudanças nos processos biológicos e no ambiente celular. Identificar alterações transcricionais permite novas idéias para esclarecer as respostas celulares mediadas por alterações da concentração de Ca^{2+} nuclear, como por exemplo, bloqueio ou aumento da proliferação de células hepáticas.

Neste trabalho nós utilizamos a parvalbumina (PV), que é uma proteína que se liga ao Ca^{2+} , não expressa em fígado, que tampona o Ca^{2+} intracelular. Essa proteína foi fusionada a um sistema adenoviral, para maximizar o número de células que expressam a PV, e foi dirigida para o núcleo da célula pela seqüência de localização nuclear (NLS). Sua correta localização foi determinada pelo gene repórter que codifica a proteína vermelha DsRed. Essa estratégia, juntamente com o metodologia do RaSH, possibilitou a determinação de genes que apresentam expressão modulada pelo Ca^{2+} nuclear.

Após varredura da biblioteca de cDNA, nós identificamos pelo programa BLASTN, 13 clones diferencialmente expressos após tamponamento do Ca^{2+} nuclear (Tabela 4). Nós verificamos que esses clones foram regulados positiva ou negativamente quando o Ca^{2+} nuclear foi tamponado. Escolhemos alguns genes selecionados pelo RaSH para serem validados e os resultados mostraram que o reticulon (RTN4) aumentou sua expressão (Figuras 9 e 10) enquanto que os genes da legumaina (LGMN) (Figuras 11A-C; 12 e 13) e do Regulator $\text{TGF}\beta$ 4 (TBRG4) (Figuras 11B-D) diminuíram sua expressão após o tamponamento do Ca^{2+} nuclear.

Sinais intracelulares de Ca^{2+} regulam crescimento celular (Patel et al., 1999) e em hepatócitos, sinais nucleares de Ca^{2+} , mais que sinais citoplasmáticos, são os responsáveis por esta regulação (Rodrigues et al., 2007). O núcleo contém toda a maquinaria necessária para gerar sinais de Ca^{2+} e pode formar estes sinais independentes dos sinais de Ca^{2+} do citoplasma (Echevarria et al., 2003; Leite et al., 2003; Rodrigues et al., 2009). Mitógenos hepáticos como a insulina (Rodrigues et al., 2008) e o HGF (Gomes et al., 2008) ativam seletivamente essa maquinaria. Já foi demonstrado que o tamponamento do Ca^{2+} nuclear inibe o crescimento de tumores no

figado (Rodrigues et al., 2007). Tumores de fígado implantados em ratos nudos cresceram mais lentamente quando expressaram parvalbumina no seu núcleo, mas o mesmo não ocorreu quando a parvalbumina foi expressa no seu citosol (Rodrigues et al., 2007).

Embora existam alguns estudos que mostram que sinais de Ca^{2+} apresentam efeitos que podem estimular a proliferação celular. Por exemplo, Ca^{2+} nuclear ativa fatores de transcrição CREB (Hardingham et al., 1997) e Elk-1 (Pusl et al., 2002) e estimula a atividade intracelular da PKC (Echevarria et al., 2003) e CaMK-IV (Deisseroth et al., 1998). As proteínas que fazem a ligação entre Ca^{2+} nuclear e proliferação celular ainda estão sendo identificadas. O presente trabalho identificou a expressão da LGMN como um novo alvo para o Ca^{2+} nuclear e mostrou que a inibição da expressão de LGMN prejudica a proliferação de células SKHep1 (Figuras 17 e 18).

Nossos achados mostraram que o promotor da LGMN é sensível ao Ca^{2+} nuclear (Figura 14). Análises de bioinformática foram utilizadas para verificar a presença de potenciais sítios de ligação de fatores de transcrição que são modulados pelo Ca^{2+} nuclear. Utilizamos o TESS (Transcription Element Search System) que é uma ferramenta usada para prever sítios de ligação para fatores de transcrição nas seqüências de DNA (www.cbil.upenn.edu/cgi-bin/tess/). Este programa se baseia em matrizes de sítios de ligação consenso de fatores de transcrição dos bancos de dados do TRANSFAC, JASPAR, IMD, e CBIL-GibbsMat para prever os putativos sítios presentes em um fragmento de DNA.

Vários potenciais sítios de ligação de fatores de transcrição foram identificados no fragmento da região promotora extraída da região promotora do gene da LGMN. Entre estes sítios estavam presentes o CCAAT box, o sítio para o *Specificity protein 1* (SP1), o sítio para o *Octamer factor 1* (Oct1), para o GATA-1 e 2 e também o sítio para a ligação do fator de transcrição ELK1 (dados não mostrados). Também foi previsto os sítios *CAAT enhancer proteins* (C/EBPC) e *hepatocyte nuclear proteins* (HNFs) ao qual se ligam fatores de transcrição específicos para a transcrição de genes hepato-específicos (Krivan and Wasserman, 2001; Schrem et al., 2002). Com a identificação do putativo sítio de ligação da Elk-1 no promotor da LGMN é possível que o Ca^{2+} nuclear regule a expressão da LGMN através da modulação da atividade do fator de transcrição Elk-1. Neste aspecto, já foi demonstrado que a transativação da Elk-1 depende de Ca^{2+}

nuclear. Sinais de Ca^{2+} nuclear e citosólico foram seletivamente bloqueados através da expressão da proteína quelante de Ca^{2+} , a parvalbumina (PV), e foi encontrado que a redução de Ca^{2+} nuclear inibiu a ativação da Elk-1 pelo fator de crescimento epidermal (EGF) (Pusl et al., 2002). Então, as ações do Ca^{2+} quando localizadas no núcleo podem ser distintas daquelas localizadas no citosol. Isso pode explicar a modulação da sinalização exercida pelo fator de transcrição Elk-1 durante a mitogênese.

Embora o tamponamento de Ca^{2+} nuclear e o silenciamento da LGMN promovam a redução da proliferação celular, a redução da expressão da LGMN não mimetiza exatamente o efeito da construção PV-NLS-DsRed. Como já demonstrado por Rodrigues (2007), transfecção de células com PV-NLS-DsRed aumenta a fração de células na fase G_2 do ciclo celular e isso está associado com o bloqueio no início da prófase e aumento no índice mitótico. O presente trabalho mostra que, por outro lado, que o silenciamento da LGMN por siRNA reduz a fração de células em G_2 (Figura 19) e o índice mitótico (Figura 17).

Além disso, PV-NLS-DsRed reduz a expressão de p-cdk1, mas não altera a expressão de ciclinas, enquanto a ausência da LGMN aumenta a expressão das ciclinas A e E (Figura 21). Estes achados são contrários ao modelo clássico de regulação do ciclo celular que prediz aumento na proliferação celular em células com altos níveis de ciclinas (Hochegger et al., 2008). No entanto, superexpressão de ciclina E tem sido demonstrada promover parada do ciclo celular no início da mitose (Keck et al., 2007). Além do mais, o aumento na expressão de inibidores do ciclo celular como p27 e p21 pode contra-atacar a superexpressão das ciclinas A e E, resultando em menor proliferação. Tomados juntos, os resultados sugerem que Ca^{2+} nuclear age na proliferação celular talvez apenas parcialmente, por ser capaz de regular a expressão da LGMN. Uma investigação mais aprofundada a partir destes dados seria interessante para determinar se de fato a LGMN é capaz de influenciar a proliferação celular por atuar diretamente sobre proteínas reguladoras do ciclo celular e assim prejudicar a progressão do ciclo.

Neste trabalho demonstramos que a LGMN está aumentada em hepatocarcinomas (Figura 22) ou após o tratamento com o mitógeno HGF (Figura 15). Esse fato sugere que a LGMN pode ter um papel na carcinogênese no fígado. LGMN é uma asparaginil endopeptidase que hidrolisa peptídeos e proteínas nos resíduos de

asparagina no terminal carboxílico (Chen et al., 1998). Estudos com animais *knockout* têm mostrado que LGMN é expressa predominantemente em endossomos tardios e em lisossomos, onde está envolvida no processamento de catepsinas e na degradação lisosomal (Shirahama-Noda et al., 2003). LGMN é altamente expressa em carcinomas da mama, cólon e próstata e em vários neoplasmas do sistema nervoso central, comparado com os tecidos normais correspondentes, nos quais há pouca ou nenhuma expressão de LGMN (Liu et al., 2003). Estes achados em outros tipos de tumores são similares ao que reportamos no presente trabalho em hepatocarcinomas (HCC). Animais *knockout* para LGMN apresentam hepatomegalia, que é atribuída a uma hematopoiese extracelular e não a proliferação do hepatócito, uma vez que a morfologia do fígado nestes ratos é normal (Chan et al., 2009). Entretanto, a incidência de HCC não tem sido estudada nestes animais, nem tem sido estudada a expressão de LGMN em modelos xenográficos de tumores de fígado. Mesmo assim, nossos estudos indicam que expressão de LGMN pode estar relacionada com a presença de hepatocarcinomas.

LGMN está envolvida no remodelamento da matrix extracelular, e já foi visto que a degradação da fibronectina aumenta quando há superexpressão da LGMN (Morita et al., 2007). Vesículas contendo LGMN são localizadas no broto de invaginação de células tumorais, e células tumorais que superexpressam LGMN têm aumentada capacidade invasiva e alta atividade migratória (Liu et al., 2003). Coletivamente, dados de superexpressão em HCC e outros tumores sólidos e das funções da LGMN em diferentes tumores têm sido interpretados para sugerir que a LGMN promove neoplasia por criar um microambiente que facilita o comportamento metastático das células tumorais. Entretanto, o presente trabalho sugere que LGMN pode ter um efeito direto na proliferação celular. Já foi demonstrado que integrinas podem modular diretamente o crescimento celular e já foi visto também que LGMN co-localiza com integrinas (Liu et al., 2003). Esta pode ser uma evidência para a atuação direta na proliferação celular da LGMN.

Neste trabalho nós também investigamos o papel dos receptores de InsP₃ tipo I na liberação do Ca²⁺ intracelular que é requerido para o processo de regeneração hepática. O processo de regeneração pode ser determinado pela geração de novas células a partir de células pré-existentes. Diferente do conceito clássico de regeneração, que é a neo-formação de tecidos e órgãos perdidos, após a perda de massa hepática o fígado entra em replicação conduzindo a uma hiperplasia compensatória que envolve as

células maduras da parte intacta do órgão. Isto promove o repovoamento celular e tecidual, ou seja, os lobos removidos não crescem novamente, o que ocorre é o crescimento do lobo restante a partir da proliferação dos hepatócitos (Fausto et al., 2006).

Nós demonstramos que as técnicas de silenciamento gênico acopladas ao sistema adenoviral podem ser utilizadas para eficiente e especificamente reduzir a expressão dos InsP_3RI (Figuras 24; 25; 26 e 27). O fígado é o único órgão com capacidade de regular seu próprio crescimento e massa. Vários são os eventos que ocorrem para que ocorra a regeneração hepática. Os fatores mais importantes presentes na regeneração hepática são: fatores de crescimento, citocinas e alguns genes. Fatores de crescimento como HGF, $\text{TGF}\alpha$ e $\text{TGF}\beta$ estão envolvidos nos processos regenerativos do fígado. HGF é um importante fator de crescimento que dirige a progressão do ciclo celular durante a regeneração. Ele é produzido pelas células estelares e age de forma parácrina nos hepatócitos.

HGF liga-se ao seu receptor *c-met* na membrana do hepatócito e ativa uma cascata de sinalização, via ERK1/2. ERK1/2 por sua vez, ativa genes responsáveis pela regeneração do fígado (Huh et al., 2004). Além disso, HGF aumenta Ca^{2+} intracelular, preferencialmente no núcleo da célula hepática (Echevarria et al., 2003) e faz com que o aumento intracelular de Ca^{2+} seja fundamental para a proliferação dos hepatócitos. Uma vez que os InsP_3RI estão em níveis reduzidos devido ao silenciamento pelo AdsiRNA-I , o Ca^{2+} intracelular liberado por estes receptores apresenta um padrão de sinalização diferente, com amplitudes menores e duração dos sinais mais curtos (Figura 28). Este fenômeno pode sugerir que a excitose do HGF pode estar sendo afetada pela ausência dos níveis normais das concentrações de Ca^{2+} e isso pode impedir que o hormônio aja nos hepatócitos desencadeando os mecanismos de sinalização necessários para a proliferação do hepatócito.

Neste trabalho foi demonstrado também que o silenciamento dos InsP_3RI atrasou o processo de regeneração do fígado de animais submetidos a hepatectomia parcial (Figura 29). Isso pode ter acontecido provavelmente devido à redução dos sinais de Ca^{2+} intracelulares. Imagens de hepatócitos marcados com Flou-4/AM mostraram que após estimulação com arginina-vasopressina (AVP) os níveis citoplasmáticos de Ca^{2+} são menores em células que foram submetidas à hepatectomia parcial e tiveram os InsP_3RI

silenciados (Figura28). Esses resultados indicam que a *down*-regulação da expressão dos InsP₃RI está correlacionada com a redução da liberação de Ca²⁺ mediada por InsP₃ e essa oscilação no padrão de sinalização é importante para que o hepatócito entre na fase S do ciclo celular durante o processo de regeneração do fígado. Juntos estes achados sugerem que a sinalização de Ca²⁺ mediada pela ativação de receptores de InsP₃ apresentam um papel relevante para o processo de regeneração hepática.

Em resumo, a liberação de Ca²⁺ de reservas nucleares regula a proliferação celular por modular a expressão de genes que atuam diretamente em respostas proliferativas. O papel efetivo do Ca²⁺ na regulação de expressão gênica e conseqüentemente na proliferação celular reflete a importância dos receptores de InsP₃ do tipo I na regeneração hepática. Deficiente liberação de Ca²⁺ intracelular, mediada por InsP₃RI durante o processo de proliferação de células hepáticas compromete a regeneração do fígado.

6. REFERÊNCIAS BIBLIOGRÁFICAS

- Alberts,B., Johnson,A., Lewis,J., Raff,M., Roberts,K., and Walter,P. (2002). *Molecular Biology of the Cell*. (New York: Garland Science).
- Aso,T., Conaway,J.W., and Conaway,R.C. (1994). Role of core promoter structure in assembly of the RNA polymerase II preinitiation complex. A common pathway for formation of preinitiation intermediates at many TATA and TATA-less promoters. *J. Biol. Chem.* *269*, 26575-26583.
- Bading,H., Ginty,D.D., and Greenberg,M.E. (1993). Regulation of gene expression in hippocampal neurons by distinct calcium signaling pathways. *Science* *260*, 181-186.
- Basehoar,A.D., Zanton,S.J., and Pugh,B.F. (2004). Identification and distinct regulation of yeast TATA box-containing genes. *Cell* *116*, 699-709.
- Berridge,M.J. (1993). Inositol trisphosphate and calcium signalling. *Nature* *361*, 315-325.
- Berridge,M.J., Lipp,P., and Bootman,M.D. (2000). The versatility and universality of calcium signalling. *Nat. Rev. Mol. Cell Biol.* *1*, 11-21.
- Bootman,M.D., Thomas,D., Tovey,S.C., Berridge,M.J., and Lipp,P. (2000). Nuclear calcium signalling. *Cell Mol. Life Sci.* *57*, 371-378.
- Boronenkov,I.V., Loijens,J.C., Umeda,M., and Anderson,R.A. (1998). Phosphoinositide signaling pathways in nuclei are associated with nuclear speckles containing pre-mRNA processing factors. *Mol. Biol. Cell* *9*, 3547-3560.
- Bosanac,I., Alattia,J.R., Mal,T.K., Chan,J., Talarico,S., Tong,F.K., Tong,K.I., Yoshikawa,F., Furuichi,T., Iwai,M., Michikawa,T., Mikoshiba,K., and Ikura,M. (2002). Structure of the inositol 1,4,5-trisphosphate receptor binding core in complex with its ligand. *Nature* *420*, 696-700.
- Butler,J.E. and Kadonaga,J.T. (2002). The RNA polymerase II core promoter: a key component in the regulation of gene expression. *Genes Dev.* *16*, 2583-2592.
- Chan,C.B., Abe,M., Hashimoto,N., Hao,C., Williams,I.R., Liu,X., Nakao,S., Yamamoto,A., Zheng,C., Henter,J.I., Meeths,M., Nordenskjold,M., Li,S.Y., Hara-Nishimura,I., Asano,M., and Ye,K. (2009). Mice lacking asparaginyl endopeptidase develop disorders resembling hemophagocytic syndrome. *Proc. Natl. Acad. Sci. U. S. A* *106*, 468-473.
- Chawla,S., Gairola,M., Nachiappan,P.L., Deshpande,A., Rathi,A.K., and Rath,G.K. (1998). Pancreatic leiomyosarcoma in a middle-aged lady. *Trop. Gastroenterol.* *19*, 118-119.
- Chen,J.M., Dando,P.M., Stevens,R.A., Fortunato,M., and Barrett,A.J. (1998). Cloning and expression of mouse legumain, a lysosomal endopeptidase. *Biochem. J.* *335 (Pt 1)*, 111-117.

- Choe,C.U. and Ehrlich,B.E. (2006). The inositol 1,4,5-trisphosphate receptor (IP3R) and its regulators: sometimes good and sometimes bad teamwork. *Sci. STKE*. 2006, re15.
- Cocco,L., Gilmour,R.S., Ognibene,A., Letcher,A.J., Manzoli,F.A., and Irvine,R.F. (1987). Synthesis of polyphosphoinositides in nuclei of Friend cells. Evidence for polyphosphoinositide metabolism inside the nucleus which changes with cell differentiation. *Biochem. J.* 248, 765-770.
- Deisseroth,K., Heist,E.K., and Tsien,R.W. (1998). Translocation of calmodulin to the nucleus supports CREB phosphorylation in hippocampal neurons. *Nature* 392, 198-202.
- Divecha,N., Banfic,H., and Irvine,R.F. (1991). The polyphosphoinositide cycle exists in the nuclei of Swiss 3T3 cells under the control of a receptor (for IGF-I) in the plasma membrane, and stimulation of the cycle increases nuclear diacylglycerol and apparently induces translocation of protein kinase C to the nucleus. *EMBO J.* 10, 3207-3214.
- Dolmetsch,R.E., Lewis,R.S., Goodnow,C.C., and Healy,J.I. (1997). Differential activation of transcription factors induced by Ca²⁺ response amplitude and duration. *Nature* 386, 855-858.
- Echevarria,W., Leite,M.F., Guerra,M.T., Zipfel,W.R., and Nathanson,M.H. (2003). Regulation of calcium signals in the nucleus by a nucleoplasmic reticulum. *Nat. Cell Biol.* 5, 440-446.
- Edwards,M.C., Liegeois,N., Horecka,J., DePinho,R.A., Sprague,G.F., Jr., Tyers,M., and Elledge,S.J. (1997). Human CPR (cell cycle progression restoration) genes impart a Far-phenotype on yeast cells. *Genetics* 147, 1063-1076.
- Ekholm,S.V. and Reed,S.I. (2000). Regulation of G(1) cyclin-dependent kinases in the mammalian cell cycle. *Curr. Opin. Cell Biol.* 12, 676-684.
- Elledge,S.J. (1996). Cell cycle checkpoints: preventing an identity crisis. *Science* 274, 1664-1672.
- Evans,N.H., McAinsh,M.R., and Hetherington,A.M. (2001). Calcium oscillations in higher plants. *Curr. Opin. Plant Biol.* 4, 415-420.
- Fausto,N., Campbell,J.S., and Riehle,K.J. (2006). Liver regeneration. *Hepatology* 43, S45-S53.
- Foskett,J.K. and Mak,D.O. (2004). Novel model of calcium and inositol 1,4,5-trisphosphate regulation of InsP3 receptor channel gating in native endoplasmic reticulum. *Biol. Res.* 37, 513-519.
- Gawenda,J., Traub,F., Luck,H.J., Kreipe,H., and von Wasielewski,R. (2007). Legumain expression as a prognostic factor in breast cancer patients. *Breast Cancer Res. Treat.* 102, 1-6.
- Gensburger,C., Freyermuth,S., Klein,C., and Malviya,A.N. (2003). In vivo nuclear Ca²⁺-ATPase phosphorylation triggers intermediate size molecular transport to the nucleus. *Biochem. Biophys. Res. Commun.* 303, 1225-1228.

- Gerasimenko,O.V., Gerasimenko,J.V., Tepikin,A.V., and Petersen,O.H. (1995). ATP-dependent accumulation and inositol trisphosphate- or cyclic ADP-ribose-mediated release of Ca²⁺ from the nuclear envelope. *Cell* 80, 439-444.
- Gershenzon,N.I. and Ioshikhes,I.P. (2005). Promoter classifier: software package for promoter database analysis. *Appl. Bioinformatics*. 4, 205-209.
- Gilbert,D.M. (2002). Replication timing and transcriptional control: beyond cause and effect. *Curr. Opin. Cell Biol.* 14, 377-383.
- Gomes,D.A., Rodrigues,M.A., Leite,M.F., Gomez,M.V., Varnai,P., Balla,T., Bennett,A.M., and Nathanson,M.H. (2008). c-Met must translocate to the nucleus to initiate calcium signals. *J. Biol. Chem.* 283, 4344-4351.
- Graham,F.L. and Prevec,L. (1992). Adenovirus-based expression vectors and recombinant vaccines. *Biotechnology* 20, 363-390.
- GrandPre,T., Nakamura,F., Vartanian,T., and Strittmatter,S.M. (2000). Identification of the Nogo inhibitor of axon regeneration as a Reticulon protein. *Nature* 403, 439-444.
- Guatimosim,S., Amaya,M.J., Guerra,M.T., Aguiar,C.J., Goes,A.M., Gomez-Viquez,N.L., Rodrigues,M.A., Gomes,D.A., Martins-Cruz,J., Lederer,W.J., and Leite,M.F. (2008). Nuclear Ca²⁺ regulates cardiomyocyte function. *Cell Calcium* 44, 230-242.
- Hardingham,G.E., Chawla,S., Cruzalegui,F.H., and Bading,H. (1999). Control of recruitment and transcription-activating function of CBP determines gene regulation by NMDA receptors and L-type calcium channels. *Neuron* 22, 789-798.
- Hardingham,G.E., Chawla,S., Johnson,C.M., and Bading,H. (1997). Distinct functions of nuclear and cytoplasmic calcium in the control of gene expression. *Nature* 385, 260-265.
- Hernandez,E., Leite,M.F., Guerra,M.T., Kruglov,E.A., Bruna-Romero,O., Rodrigues,M.A., Gomes,D.A., Giordano,F.J., Dranoff,J.A., and Nathanson,M.H. (2007). The spatial distribution of inositol 1,4,5-trisphosphate receptor isoforms shapes Ca²⁺ waves. *J. Biol. Chem.* 282, 10057-10067.
- Higgins,E.S. and Banks,W.L., Jr. (1971). Cognate effects of ethanol, hydrazine and tissue regeneration on hepatic mitochondrial activities. *Biochem. Pharmacol.* 20, 1513-1524.
- Hirata,K., Pusch,T., O'Neill,A.F., Dranoff,J.A., and Nathanson,M.H. (2002). The type II inositol 1,4,5-trisphosphate receptor can trigger Ca²⁺ waves in rat hepatocytes. *Gastroenterology* 122, 1088-1100.
- Hochegger,H., Takeda,S., and Hunt,T. (2008). Cyclin-dependent kinases and cell-cycle transitions: does one fit all? *Nat. Rev. Mol. Cell Biol.* 9, 910-916.
- Huh,C.G., Factor,V.M., Sanchez,A., Uchida,K., Conner,E.A., and Thorgeirsson,S.S. (2004). Hepatocyte growth factor/c-met signaling pathway is required for efficient liver regeneration and repair. *Proc. Natl. Acad. Sci. U. S. A* 101, 4477-4482.

- Junqueira,L.C. and Carneiro,J. (1995). *Histologia Básica*. (Rio de Janeiro: Guanabara-Koogan).
- Kahl,C.R. and Means,A.R. (2003). Regulation of cell cycle progression by calcium/calmodulin-dependent pathways. *Endocr. Rev.* *24*, 719-736.
- Keck,J.M., Summers,M.K., Tedesco,D., Ekholm-Reed,S., Chuang,L.C., Jackson,P.K., and Reed,S.I. (2007). Cyclin E overexpression impairs progression through mitosis by inhibiting APC(Cdh1). *J. Cell Biol.* *178*, 371-385.
- Klar,J., Sigl,M., Obermayer,B., Schweda,F., Kramer,B.K., and Kurtz,A. (2005). Calcium inhibits renin gene expression by transcriptional and posttranscriptional mechanisms. *Hypertension* *46*, 1340-1346.
- Krivan,W. and Wasserman,W.W. (2001). A predictive model for regulatory sequences directing liver-specific transcription. *Genome Res.* *11*, 1559-1566.
- Leite,M.F., Burgstahler,A.D., and Nathanson,M.H. (2002). Ca²⁺ waves require sequential activation of inositol trisphosphate receptors and ryanodine receptors in pancreatic acini. *Gastroenterology* *122*, 415-427.
- Leite,M.F. and Nathanson,M.H. (2009). Ca²⁺ signaling in the liver. In *The Liver: Biology and Pathology*, I.M.Arias, J.L.Boyer, N.F.V.Chisari, N.Fausto, D.Schater, and D.A.Shafritz, eds.: pp. 537-554.
- Leite,M.F., Thrower,E.C., Echevarria,W., Koulen,P., Hirata,K., Bennett,A.M., Ehrlich,B.E., and Nathanson,M.H. (2003). Nuclear and cytosolic calcium are regulated independently. *Proc. Natl. Acad. Sci. U. S. A* *100*, 2975-2980.
- Lerea,L.S. and McNamara,J.O. (1993). Ionotropic glutamate receptor subtypes activate c-fos transcription by distinct calcium-requiring intracellular signaling pathways. *Neuron* *10*, 31-41.
- Levine,M. and Tjian,R. (2003). Transcription regulation and animal diversity. *Nature* *424*, 147-151.
- Li,F., Chen,J., Solessio,E., and Gilbert,D.M. (2003). Spatial distribution and specification of mammalian replication origins during G1 phase. *J. Cell Biol.* *161*, 257-266.
- Lin,S.Y., Chen,K.S., and Run-Chu,L. (2000). Organic esters of plasticizers affecting the water absorption, adhesive property, glass transition temperature and plasticizer permanence of eudragit acrylic films. *J. Control Release* *68*, 343-350.
- Liu,C., Sun,C., Huang,H., Janda,K., and Edgington,T. (2003). Overexpression of legumain in tumors is significant for invasion/metastasis and a candidate enzymatic target for prodrug therapy. *Cancer Res.* *63*, 2957-2964.
- Loak,K., Li,D.N., Manoury,B., Billson,J., Morton,F., Hewitt,E., and Watts,C. (2003). Novel cell-permeable acyloxymethylketone inhibitors of asparaginyl endopeptidase. *Biol. Chem.* *384*, 1239-1246.

- Maher,P.A. (1993). Inhibition of the tyrosine kinase activity of the fibroblast growth factor receptor by the methyltransferase inhibitor 5'-methylthioadenosine. *J. Biol. Chem.* *268*, 4244-4249.
- Malviya,A.N., Rogue,P., and Vincendon,G. (1990). Stereospecific inositol 1,4,5-[³²P]trisphosphate binding to isolated rat liver nuclei: evidence for inositol trisphosphate receptor-mediated calcium release from the nucleus. *Proc. Natl. Acad. Sci. U. S. A* *87*, 9270-9274.
- Martelli,A.M., Billi,A.M., Manzoli,L., Faenza,I., Aluigi,M., Falconi,M., De Pol,A., Gilmour,R.S., and Cocco,L. (2000). Insulin selectively stimulates nuclear phosphoinositide-specific phospholipase C (PI-PLC) beta1 activity through a mitogen-activated protein (MAP) kinase-dependent serine phosphorylation. *FEBS Lett.* *486*, 230-236.
- McConnell,M.J. and Imperiale,M.J. (2004). Biology of adenovirus and its use as a vector for gene therapy. *Hum. Gene Ther.* *15*, 1022-1033.
- Mendes,C.C., Gomes,D.A., Thompson,M., Souto,N.C., Goes,T.S., Goes,A.M., Rodrigues,M.A., Gomez,M.V., Nathanson,M.H., and Leite,M.F. (2005). The type III inositol 1,4,5-trisphosphate receptor preferentially transmits apoptotic Ca²⁺ signals into mitochondria. *J. Biol. Chem.* *280*, 40892-40900.
- Moeschler,H.J., Malencik,D.A., Pocinwong,S., Alaba,O., Kerrick,G.L., and Fischer,E.H. (1979). Exchange of calcium between muscle Ca²⁺-binding proteins. *Biochimie* *61*, 615-624.
- Montazer-Torbati,M.B., Hue-Beauvais,C., Droineau,S., Ballester,M., Coant,N., Aujean,E., Petitbarat,M., Rijnkels,M., and Devinoy,E. (2008). Epigenetic modifications and chromatin loop organization explain the different expression profiles of the *Tbrg4*, *WAP* and *Ramp3* genes. *Exp. Cell Res.* *314*, 975-987.
- Morita,Y., Araki,H., Sugimoto,T., Takeuchi,K., Yamane,T., Maeda,T., Yamamoto,Y., Nishi,K., Asano,M., Shirahama-Noda,K., Nishimura,M., Uzu,T., Hara-Nishimura,I., Koya,D., Kashiwagi,A., and Ohkubo,I. (2007). Legumain/asparaginyl endopeptidase controls extracellular matrix remodeling through the degradation of fibronectin in mouse renal proximal tubular cells. *FEBS Lett.* *581*, 1417-1424.
- Mukhopadhyay,S., Munshi,H.G., Kambhampati,S., Sassano,A., Plataniias,L.C., and Stack,M.S. (2004). Calcium-induced matrix metalloproteinase 9 gene expression is differentially regulated by ERK1/2 and p38 MAPK in oral keratinocytes and oral squamous cell carcinoma. *J. Biol. Chem.* *279*, 33139-33146.
- Murthy,R.V., Arberman,G., Gao,J., Roodman,G.D., and Sun,X.F. (2005). Legumain expression in relation to clinicopathologic and biological variables in colorectal cancer. *Clin. Cancer Res.* *11*, 2293-2299.
- Nigg,E.A. (2001). Mitotic kinases as regulators of cell division and its checkpoints. *Nat. Rev. Mol. Cell Biol.* *2*, 21-32.

- Pastorian,K., Hawel,L., III, and Byus,C.V. (2000). Optimization of cDNA representational difference analysis for the identification of differentially expressed mRNAs. *Anal. Biochem.* 283, 89-98.
- Patel,R., Holt,M., Philipova,R., Moss,S., Schulman,H., Hidaka,H., and Whitaker,M. (1999). Calcium/calmodulin-dependent phosphorylation and activation of human Cdc25-C at the G2/M phase transition in HeLa cells. *J. Biol. Chem.* 274, 7958-7968.
- Pechere,J.F., Capony,J.P., and Ryden,L. (1971). The primary structure of the major parvalbumin from hake muscle. Isolation and general properties of the protein. *Eur. J. Biochem.* 23, 421-428.
- Pierobon,N., Renard-Rooney,D.C., Gaspers,L.D., and Thomas,A.P. (2006). Ryanodine receptors in liver. *J. Biol. Chem.* 281, 34086-34095.
- Pusl,T. and Nathanson,M.H. (2004). The role of inositol 1,4,5-trisphosphate receptors in the regulation of bile secretion in health and disease. *Biochem. Biophys. Res. Commun.* 322, 1318-1325.
- Pusl,T., Wu,J.J., Zimmerman,T.L., Zhang,L., Ehrlich,B.E., Berchtold,M.W., Hoek,J.B., Karpen,S.J., Nathanson,M.H., and Bennett,A.M. (2002). Epidermal growth factor-mediated activation of the ETS domain transcription factor Elk-1 requires nuclear calcium. *J. Biol. Chem.* 277, 27517-27527.
- Ramadori,G. and Saile,B. (2005). Hepatocytes. In *Signaling Pathways in Liver Diseases*, J.F.Dufour and P.A.Clavien, eds. (Berlin: Springer Verlag), pp. 3-16.
- Reilly,J.F. and Maher,P.A. (2001). Importin beta-mediated nuclear import of fibroblast growth factor receptor: role in cell proliferation. *J. Cell Biol.* 152, 1307-1312.
- Rocken,C. and Carl-McGrath,S. (2001). Pathology and pathogenesis of hepatocellular carcinoma. *Dig. Dis.* 19, 269-278.
- Rodrigues,M.A., Gomes,D.A., Andrade,V.A., Leite,M.F., and Nathanson,M.H. (2008). Insulin induces calcium signals in the nucleus of rat hepatocytes. *Hepatology* 48, 1621-1631.
- Rodrigues,M.A., Gomes,D.A., Leite,M.F., Grant,W., Zhang,L., Lam,W., Cheng,Y.C., Bennett,A.M., and Nathanson,M.H. (2007). Nucleoplasmic calcium is required for cell proliferation. *J. Biol. Chem.* 282, 17061-17068.
- Rodrigues,M.A., Gomes,D.A., Nathanson,M.H., and Leite,M.F. (2009). Nuclear calcium signaling: a cell within a cell. *Braz. J. Med. Biol. Res.* 42, 17-20.
- Schrem,H., Klempnauer,J., and Borlak,J. (2002). Liver-enriched transcription factors in liver function and development. Part I: the hepatocyte nuclear factor network and liver-specific gene expression. *Pharmacol. Rev.* 54, 129-158.
- Shibao,K., Hirata,K., Robert,M.E., and Nathanson,M.H. (2003). Loss of inositol 1,4,5-trisphosphate receptors from bile duct epithelia is a common event in cholestasis. *Gastroenterology* 125, 1175-1187.

Shirahama-Noda,K., Yamamoto,A., Sugihara,K., Hashimoto,N., Asano,M., Nishimura,M., and Hara-Nishimura,I. (2003). Biosynthetic processing of cathepsins and lysosomal degradation are abolished in asparaginyl endopeptidase-deficient mice. *J. Biol. Chem.* 278, 33194-33199.

Strayer,L. (1996). *Bioquímica*. (New York: W.H. Freeman and Company).

Tanigawa,N., Lu,C., Mitsui,T., and Miura,S. (1997). Quantitation of sinusoid-like vessels in hepatocellular carcinoma: its clinical and prognostic significance. *Hepatology* 26, 1216-1223.

Taub,R. (2004). Liver regeneration: from myth to mechanism. *Nat. Rev. Mol. Cell Biol.* 5, 836-847.

Thiel,G., Mayer,S.I., Muller,I., Stefano,L., and Rössler,O.G. (2010). Egr-1-A Ca(2+)-regulated transcription factor. *Cell Calcium* 47, 397-403.

Thompson,M., Andrade,V.A., Andrade,S.J., Pusch,T., Ortega,J.M., Goes,A.M., and Leite,M.F. (2003). Inhibition of the TEF/TEAD transcription factor activity by nuclear calcium and distinct kinase pathways. *Biochem. Biophys. Res. Commun.* 301, 267-274.

Vermassen,E., Parys,J.B., and Mauger,J.P. (2004). Subcellular distribution of the inositol 1,4,5-trisphosphate receptors: functional relevance and molecular determinants. *Biol. Cell* 96, 3-17.

West,A.E., Chen,W.G., Dalva,M.B., Dolmetsch,R.E., Kornhauser,J.M., Shaywitz,A.J., Takasu,M.A., Tao,X., and Greenberg,M.E. (2001). Calcium regulation of neuronal gene expression. *Proc. Natl. Acad. Sci. U. S. A* 98, 11024-11031.

Wilsker,D., Patsialou,A., Zumbun,S.D., Kim,S., Chen,Y., Dallas,P.B., and Moran,E. (2004). The DNA-binding properties of the ARID-containing subunits of yeast and mammalian SWI/SNF complexes. *Nucleic Acids Res.* 32, 1345-1353.

Yam,C.H., Fung,T.K., and Poon,R.Y. (2002). Cyclin A in cell cycle control and cancer. *Cell Mol. Life Sci.* 59, 1317-1326.

Yan,R., Shi,Q., Hu,X., and Zhou,X. (2006). Reticulon proteins: emerging players in neurodegenerative diseases. *Cell Mol. Life Sci.* 63, 877-889.

7. ANEXOS

7.1. Certificado do CETEA



UNIVERSIDADE FEDERAL DE MINAS GERAIS
COMITÊ DE ÉTICA EM EXPERIMENTAÇÃO ANIMAL
- C E T E A -

CERTIFICADO

Certificamos que o **Protocolo nº 136/2007**, relativo ao projeto intitulado "**Regeneração hepática por sinais de cálcio**", que tem como responsável **Maria de Fátima Leite**, está de acordo com os Princípios Éticos da Experimentação Animal, adotados pelo **Comitê de Ética em Experimentação Animal (CETEA/UFMG)**, tendo sido aprovado na reunião de **21/ 11/2007**.

Este certificado expira-se em **21/ 11 / 2012**.

CERTIFICATE

We hereby certify that the **Protocol nº 136/2007**, related to the project entitled "**Hepatic regeneration by calcium signalling**", under the supervision of **Maria de Fátima Leite**, is in agreement with the Ethical Principles in Animal Experimentation, adopted by the **Ethics Committee in Animal Experimentation (CETEA/UFMG)**, and was approved in **November 21, 2007**.

This certificate expires in **November 21, 2012**.

Belo Horizonte, 26 de Novembro de 2007.

Prof. Humberto Pereira Oliveira
Coordenador do CETEA/UFMG

Universidade Federal de Minas Gerais
Avenida Antônio Carlos, 6627 – Campus Pampulha
Unidade Administrativa II – 2º Andar, Sala 2005
31270-901 - Belo Horizonte, MG - Brasil
Telefone: (31) 3499-4516 – Fax: (31) 3499-4516
www.ufmg.br/bioetica/cetea - cetea@prpq.ufmg.br

(Mod.Cert. v1 0)

8. PRODUÇÃO BIBLIOGRÁFICA

Nucleoplasmic calcium regulates cell proliferation through legumain

Viviane Andrade¹, Mateus Guerra^{5,6}, Camila Jardim², Flavia Melo², Wamberto Silva³, Jose M. Ortega¹, Marie Robert⁴, Michael H. Nathanson^{5,6,*}, Fatima Leite²

¹Department of Biochemistry and Immunology, Federal University of Minas Gerais, Belo Horizonte, MG, Brazil; ²Department of Physiology and Biophysics, Federal University of Minas Gerais, Belo Horizonte, MG, Brazil; ³Department of Genetics, Center for Cell Based Therapy, University of São Paulo, Ribeirão Preto, SP, Brazil; ⁴Department of Pathology, Yale University School of Medicine, New Haven, CT, USA; ⁵Section of Digestive Diseases, Department of Internal Medicine, Yale University School of Medicine, New Haven, CT, USA; ⁶Department of Cell Biology, Yale University School of Medicine, New Haven, CT, USA

Background & Aims: Nucleoplasmic Ca²⁺ regulates cell growth in the liver, but the proteins through which this occurs are unknown.

Methods: We used Rapid Subtraction Hybridization (RaSH) to subtract genes in SKHep1 liver cells expressing the Ca²⁺ buffer protein parvalbumin (PV) targeted to the nucleus, from genes in cells expressing a mutated form of nuclear-targeted PV which has one of two Ca²⁺-binding sites inactivated. The subtraction permitted the selection of genes whose expression was affected by a small alteration in nuclear Ca²⁺ concentration.

Results: The asparaginyl endopeptidase legumain (LGMN) was identified in this screening. When Ca²⁺ was buffered in the nucleus of SKHep1 cells, LGMN mRNA was decreased by 97%, in part by a transcriptional mechanism, and decreased expression at the protein level was observed by immunoblot and immunofluorescence. Treatment with hepatocyte growth factor increased LGMN expression. Knockdown of LGMN by siRNA decreased proliferation of SKHep1 cells by ~50% as measured both by BrdU uptake and mitotic index, although an inhibitor of LGMN activity did not affect BrdU incorporation. A significant reduction in the fraction of cells in G2/M phase was seen as well. This was associated with increases in the expression of cyclins A and E. Furthermore, LGMN expression was increased in hepatocellular carcinoma cells relative to normal hepatocytes in the same specimens.

Conclusions: These findings suggest a new role for LGMN and provide evidence that nuclear Ca²⁺ signals regulate cell proliferation in part through the modulation of LGMN expression. Increased expression of LGMN may be involved in liver carcinogenesis.

© 2011 European Association for the Study of the Liver. Published by Elsevier B.V. All rights reserved.

Keywords: Nuclear calcium; Legumain; Hepatocellular carcinoma.

Received 13 April 2010; received in revised form 9 December 2010; accepted 11 December 2010

* Corresponding author. Address: Section of Digestive Diseases, Department of Internal Medicine, Yale University School of Medicine, 300 Cedar Street, TAC S241D, New Haven, CT 06520-8019, USA. Tel.: +1 203 785 7312; fax: +1 203 785 7273.

E-mail address: michael.nathanson@yale.edu (M.H. Nathanson).

Abbreviations: RaSH, Rapid Subtraction Hybridization; PV, parvalbumin; LGMN, legumain; BrdU, 5-bromo-2'-deoxyuridine; HCC, hepatocellular carcinoma.

Introduction

Ca²⁺ regulates a wide range of activities in the liver, including bile secretion [1,2], canalicular contraction [3], metabolism [4], gene transcription [5,6], apoptosis [7,8], and growth of liver tumors [9]. The spatial patterns of Ca²⁺ signals determine the specificity of these signals and which responses are activated [10,11]. Increases in nucleoplasmic Ca²⁺ have specific biological effects that differ from the effects of increases in cytosolic Ca²⁺. These effects include activation of distinct genes and transcription factors [5,6,12,13], activation of intranuclear kinases [14,15] and regulation of cell proliferation [9]. The nucleus contains the machinery required for local formation of Ca²⁺ signals, including PIP2, PLC, and InsP₃R-gated Ca²⁺ stores [16–18], and several mechanisms permit selective activation of Ca²⁺ signaling pathways within the nucleus. This includes direct coupling between integrin receptors and the nucleus [19] and translocation of receptor tyrosine kinases such as c-met and the insulin receptor to the nucleus [17,18]. However, the specific targets of Ca²⁺ signals in the nucleus that are responsible for regulating cell proliferation are not clear.

Legumain (LGMN) is an endopeptidase that was first identified in plants [20] and later in humans and mice [21], and parasites [22] and helminthes [23]. LGMN hydrolyzes peptides and proteins on the carboxyl side of asparaginyl residues. This enzyme is predominantly localized in late endosomes and lysosomes [24] and has been implicated in antigen processing [25,26], regulation of biosynthesis of lysosomal proteins [27], and extracellular matrix turnover [28]. LGMN also is present in the tumor microenvironment where it is expressed by macrophages and contributes to metastatic behavior by promoting cell migration and tissue invasion [29]. Increased expression of LGMN is associated with poorer differentiation of tumors and a higher degree of necrosis and apoptosis. LGMN co-localizes with integrins at the invading front of tumors and expression of this enzyme is associated with increased invasiveness [30,31]. Thus, until now the effects of LGMN have been related to its actions as an endopeptidase that modulates the invasive and metastatic potential of cells. Here we identified LGMN as one target of nuclear Ca²⁺ and characterize the role of this gene in regulating cell proliferation.



ELSEVIER

Journal of Hepatology 2011 vol. xxx | xxx–xxx

Research Article

Materials and methods

Materials, reagents and cell lines

The SKHep1 liver cell line was from ATCC (Manassas, VA). Cells were grown at 37 °C with 5% CO₂ in DMEM supplemented with 1% penicillin–streptomycin and 10% fetal bovine serum (Gibco, Grand Island, NY). SuperScript First-Strand Synthesis System for RT-PCR, TRizol reagent and lipofectamine 2000 were from Invitrogen (Eugene, OR). Anti-LGMN polyclonal antibody was from ABCAM (Cambridge, MA). Enhanced chemiluminescence reagent (ECL plus) and horseradish peroxidase (HRP) antibodies were from GE Biosciences (Buckinghamshire, UK). Mouse monoclonal antibodies to α -tubulin, β -actin, and anti-gamma tubulin were purchased from Sigma–Aldrich (St. Louis, MO).

PV-DsRed adenovirus constructs and infection conditions

Ca²⁺ was selectively buffered within the nucleoplasm by expressing parvalbumin (PV) with a nuclear localization sequence fused to DsRed [6]. One of the two Ca²⁺ binding sites of PV is disrupted in the CD mutant, which was used as well. Recombinant adenoviruses pAd-PV-NLS-DsRed and pAd-PV-NLS-CD-DsRed [9] were used for delivery to SKHep1 cells, which were infected at a multiplicity of infection (MOI) of 100. Cells were used 48 h after infection. It has previously been demonstrated that PV-NLS effectively and selectively buffers Ca²⁺ in the nucleus of transfected cells [6].

Rapid Subtraction Hybridization (RaSH)

RaSH was performed using a modification of the method previously described [32]. Total RNA (25 μ g), isolated from cells infected with pAd-PV-NLS-DsRed or pAd-PV-NLS-CD-DsRed (control adenovirus), was used for cDNA synthesis. cDNA then was digested with *Mbol* (Fermentas, Glen Burnie, MD) followed by ligation to adapters XDPN-14 (5'-CTGATCACTCGAGA-3') and XDPN-12 (5'-GATCTCTC-GAGT-3') at 4 °C overnight. Mixtures were diluted in 100 μ l of 10 mM Tris/1 mM EDTA, pH 7 and used for PCR amplification with 10 μ M XDPN-18 (5'-CTGATCACTCGAGAGATC-3'). To obtain TESTER samples, 3 μ g of the PCR products (DRIVER) were digested with *Xho*I. The TESTER cDNA (3 μ g) was mixed with 10 μ g of the DRIVER cDNA in 10 μ l of a hybridization solution [0.5 M NaCl/50 mM Tris, pH 7.5/0.2% SDS/40% (vol/vol) formamide] and boiled for 5 min, then incubated at 42 °C for 48 h. Part of the mixture (3 μ l) was ligated with 1 μ g of *Xho*I-digested pZErO-1 (Invitrogen, Carlsbad, CA) plasmids and transformed into DH-10B bacteria. The colonies with positive clones were subjected to DNA plasmid extraction and submitted for automated sequencing. Sequences were confirmed by BLASTN.

Real time PCR

Total RNA was isolated from cells using TRIzol and reverse-transcribed using SuperScript II (Invitrogen). Sense and antisense primer sequences for PCR amplification of β -actin were: 5'-GACGGCCAGGTCATCTATTG-3' and 5'-AGGAAGGCTG-GAAAAGAGCC-3' and 5'-GCATAGGATCCGCCAAAGTC-3' and 5'-TCCAGTAGATCCA TGGTCAGTGA-3' for *LGMN*. DNA templates were amplified by real time PCR using the Sybr Green Method. β -Actin was used as an internal control. Experiments were performed in triplicate. After amplification, 10 μ l of reaction mixture were subjected to electrophoresis on agarose gels and visualized after ethidium bromide staining.

Western blot and CDK2 kinase assay

Standard methods were used for immunoblots [33]. Cells were lysed at 4 °C and 50 μ g of total cellular protein was separated by SDS-PAGE. Membranes were blocked and then incubated with an affinity-purified polyclonal antibody against human *LGMN* (1:1000). Membranes were then incubated with peroxidase-conjugated secondary antibody (1:5000). Bands were revealed by enhanced chemiluminescence. For experiments involving HGF stimulation, cells were starved overnight and treated with HGF (100 ng/ml, at 37 °C) for the indicated time points prior to protein extraction. CDK2 activity was evaluated by a modified *in vitro* Histone H1 phosphorylation assay [34].

Immunofluorescence

Confocal immunofluorescence was performed as described [7]. SKHep1 cells were fixed with 4% paraformaldehyde and incubated with anti-LGMN antibody (1:200) for 2 h at room temperature followed by incubation with goat anti-rabbit second-

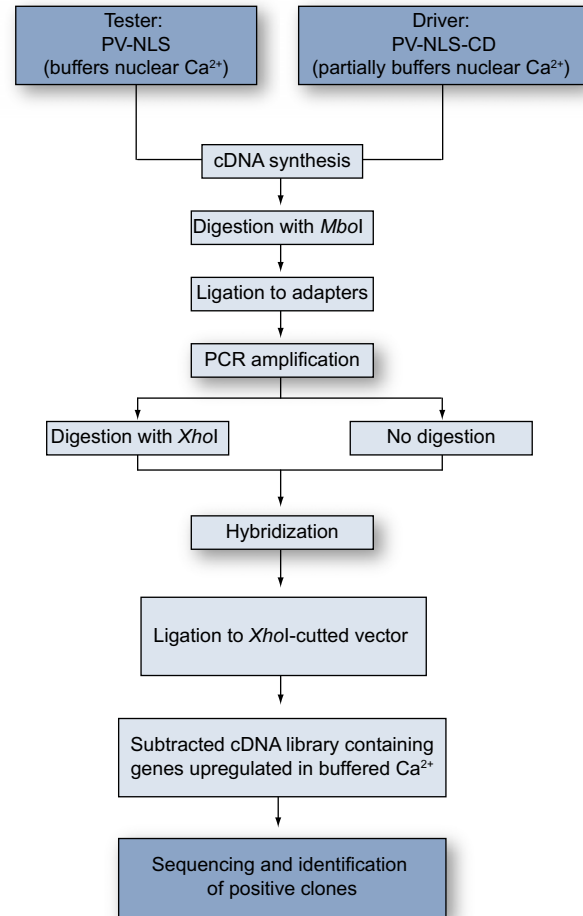


Fig. 1. Schematic outline of the RaSH protocol. Tester and driver libraries were constructed, followed by digestion of only the tester library with *Xho*I. After hybridization, differentially expressed sequences were cloned into *Xho*I-digested vectors, resulting in a subtracted cDNA library enriched in genes displaying differential expression. By using the PV-NLS library as the tester and the PV-NLS-CD library as the driver, RaSH was used to produce a subtracted cDNA library enriched in genes up-regulated when nuclear Ca²⁺ is buffered (adapted from [32]). Down-regulated genes can be isolated using the PV-NLS-CD library as the tester and the PV-NLS library as the driver.

ary antibody conjugated with Alexa 488 (1:500), for 1 h. Images were obtained using a Zeiss LSM 510 confocal microscope (Thornwood, NY) and mean fluorescence was quantified with ImageJ software (NIH, Bethesda, MD).

Transfection of siRNA

Silencer select siRNA sequences specific for *LGMN* or scrambled control sequences were acquired from Ambion (Austin, TX). Cell cultures were treated with 20 nM of siRNA using lipofectamine 2000 (Invitrogen). Cells were incubated at 37 °C in an atmosphere of 5% CO₂ for 72 h prior to use.

Measurement of BrdU incorporation

Cell proliferation was measured by BrdU incorporation using ELISA (Roche Applied Science). SKHep1 cells were plated in 96-well culture plates, starved for 24 h and transfected with siRNA. Seventy hours afterward, cells were treated for 2 h with BrdU labeling solution. Cells were then fixed, and anti-BrdU antibody was added. BrdU incorporation was measured colorimetrically. For experiments employing the legumain inhibitor MV026630, cells were treated for 24 h with the inhibitor at 25 or 50 μ M. Control cells were treated with DMSO alone.

Table 1. Sequences identified by RaSH.

Clone GeneBank	Nomenclature	GeneBank Access	Change*
AT rich interactive domain 1A	<i>ARID 1A</i>	NM_006015.4	↑
Legumain	<i>LGMN</i>	NM_005606.5	↓
Transforming growth factor beta regulator 4	<i>TBRG4</i>	NM_030900.2	↓
Reticulon 4	<i>RTN4</i>	NM_207521.1	↑
Tubulin gamma	<i>TUB1</i>	NM_001070.3	↑
Ras homolog gene family member A	<i>RHOA</i>	NM_001664.2	↑
Mps One Binder kinase activator-like 1B	<i>MOB1</i>	NM_018221.3	↑
Similar to ribosomal protein L3	-	CX816870	↑
Splicing factor 3B	-	NM_012426.3	↑
Alanyl-tRNA synthetase	<i>AARS</i>	NM_001605.2	↑
Serpin peptidase inhibitor member 1	<i>SERPINE 1</i>	NM_000602.1	↑
Prohibitin 2	<i>PBHB2</i>	NM_007531.2	↓
Similar to ribosomal protein L27	-	CX816883	↑

*Change means gene expression level compared to normal control. ↑means up-regulated; ↓means down-regulated when nuclear Ca^{2+} is buffered.

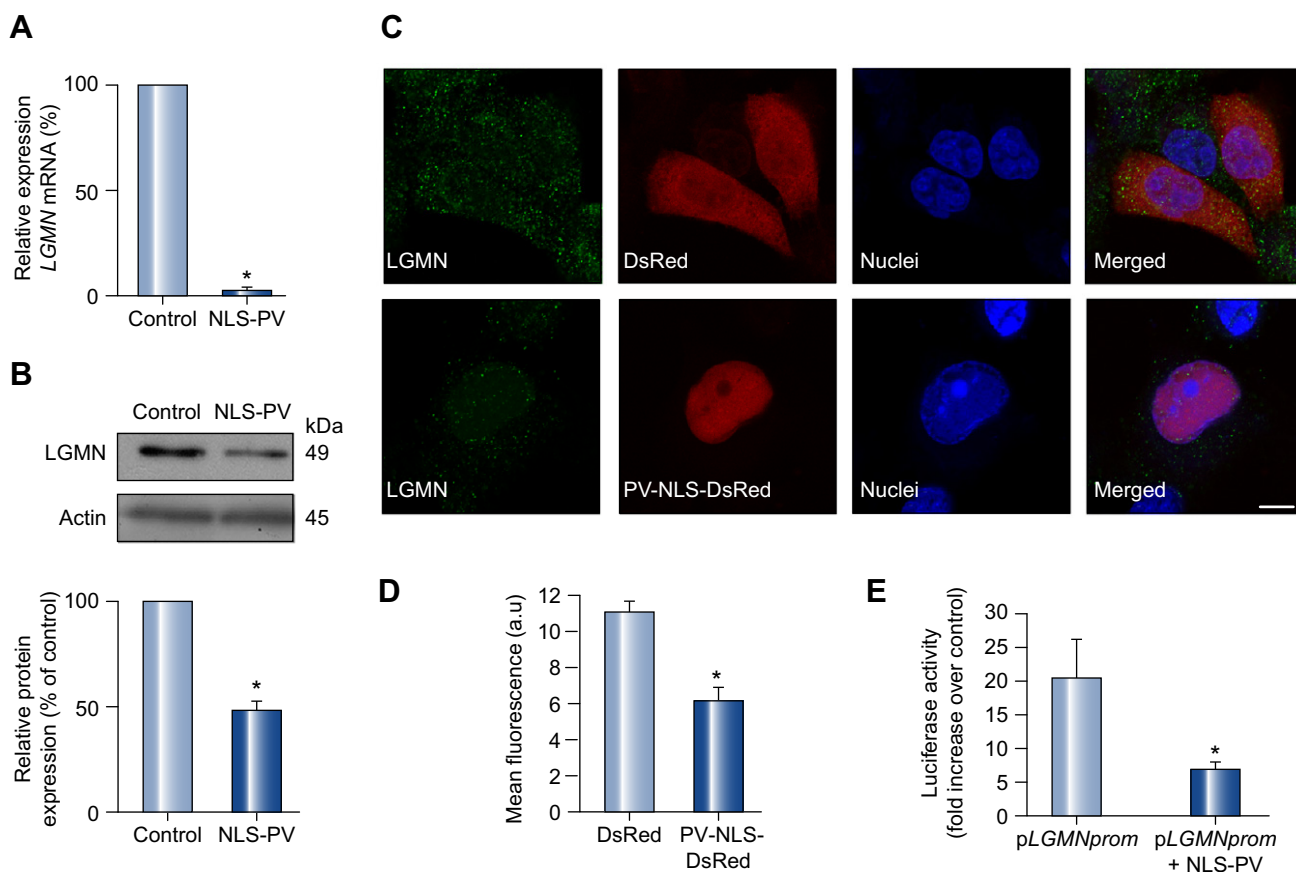


Fig. 2. LGMN expression is decreased by buffering nuclear Ca^{2+} . (A) Real time quantitative PCR was used to measure the relative expression of *LGMN* mRNA in the SKHep1 liver cell line. *LGMN* mRNA was decreased by $97 \pm 2\%$ in cells transfected with PV-NLS, relative to non-transfected controls ($p < 0.0001$). β -Actin gene was used to normalize expression in both groups. The data are expressed as mean \pm SEM of triplicate measurements and are representative of three separate experiments ($p < 0.05$). (B) Immunoblot of whole-cell protein from SKHep1 cells 48 h after infection demonstrates that *LGMN* protein expression is decreased after buffering nuclear Ca^{2+} . Densitometric analysis confirms reduction of *LGMN* protein expression to $52 \pm 9\%$ of controls ($p < 0.01$). Expression of β -actin was used as a loading control. (C) Confocal immunofluorescence confirms decreased *LGMN* expression (green) in SKHep1 cells transfected with PV-NLS (red). Nuclei are identified by TO-PRO-3 staining (blue). Detection of the DsRed tag on PV-NLS confirms that it is localized to the nucleus. Results are representative of four independent experiments. Scale bar = $10 \mu m$. (D) Quantification of *LGMN* immunofluorescence shows that buffering nuclear Ca^{2+} reduces *LGMN* expression by 45% (11.1 ± 0.4 in DsRed group versus 6.1 ± 0.6 a.u. in PV-NLS-DsRed cells; $p < 0.001$). (E) Luciferase assay shows that *LGMN* promoter activity is inhibited when nuclear Ca^{2+} is buffered (20.6 ± 5.3 pLGMNprom versus 6.9 ± 0.9 pLGMNprom + PV-NLS; $p < 0.05$). Data are expressed as mean fold increase \pm SEM over empty vector in five separate experiments.

Research Article

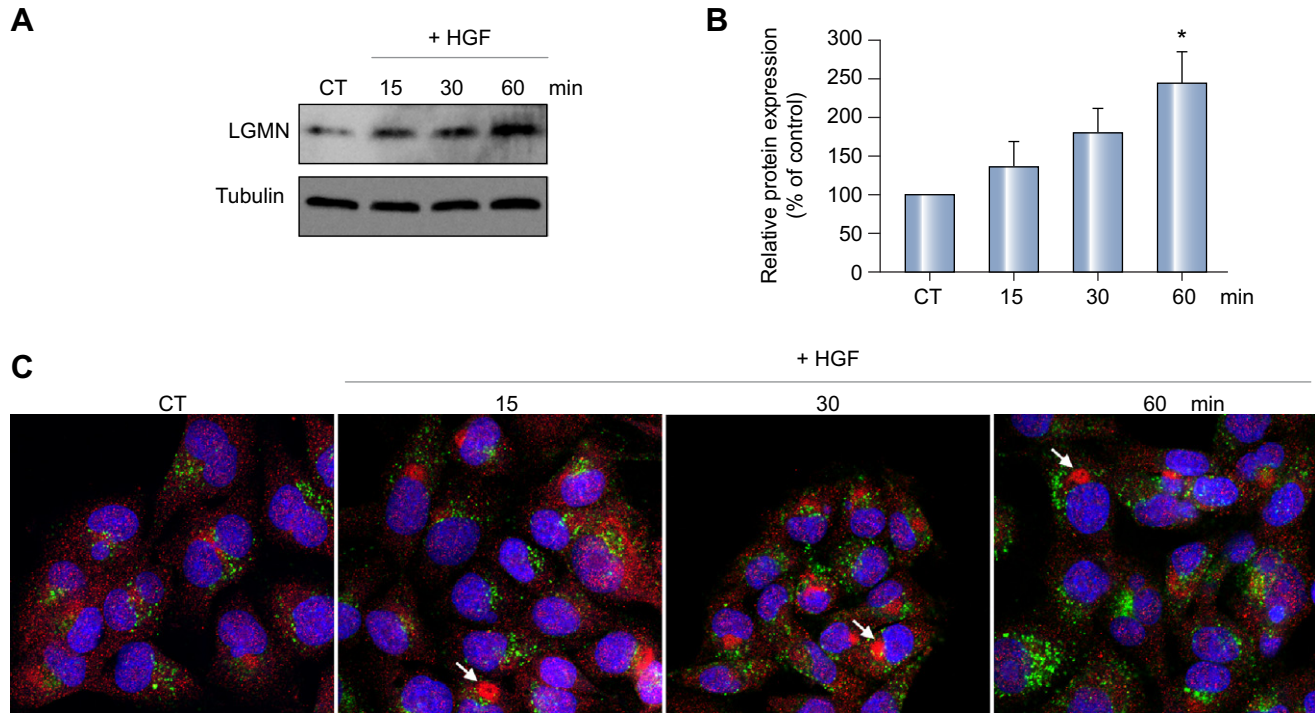


Fig. 3. HGF stimulation increases LGMN expression. (A) Western blot analysis of total cell lysates prepared from control (non-stimulated) cells and cells stimulated with HGF (100 ng/ml) for the indicated time periods demonstrates a time-dependent increase in LGMN expression. (B) Bar graph shows the densitometric quantification of four separate experiments ($p < 0.05$, one-way ANOVA). (C) LGMN localization is altered after HGF treatment. SKHep1 cells were stimulated as above and examined by confocal immunofluorescence. LGMN (red) is present in punctate structures that do not co-localize with the lysosomal marker Lamp-1 (green), in either control or HGF-stimulated cells. Nuclei are labeled by TO-PRO-3 (blue). Upon HGF stimulation, LGMN accumulates near the nucleus (arrows).

Mitotic index measurements

SKHep1 cells treated with siRNA were labeled for phospho-histone-3 (Upstate Biotechnology, Chicago, IL) by immunofluorescence and then examined by confocal microscopy. Mitotic cells were defined by the presence of DNA condensation and phospho-histone-3 positivity [35]. Mitotic index was calculated as the percentage of mitotic cells per total cell number. At least 20 fields representing a total of >100 cells were visualized for each condition.

Cell cycle analysis

SKHep1 cells transfected with siRNA were trypsinized, washed in phosphate-buffered saline (PBS), fixed with 70% Ethanol at 4 °C and then washed with PBS. After centrifugation cells were supplemented with RNase (100 µg/ml Sigma) for 5 min and stained with propidium iodide (50 µg/ml). DNA content was determined using a FACSCalibur (BD Biosciences), and the data were analyzed using Flowjo software.

Apoptosis assay

Apoptosis was measured using a caspase-3 activity kit with colorimetric detection (BD Biosciences). Apoptosis was induced using 500 nM staurosporine (Sigma-Aldrich) as a positive control.

Immunofluorescence in human tissue samples

Paraffin-embedded sections of hepatocellular carcinoma (HCC) human liver were pretreated with 10 mmol/L Tris, 1 mmol/L EDTA buffer at 100 °C, incubated with anti-LGMN, and then labeled with Alexa 488-conjugated secondary antibodies [36]. Nuclei were stained with TO-PRO3. To ensure specificity of staining, images were obtained using machine settings at which no fluorescence was detectable in negative controls labeled with secondary antibodies alone. Specimens were observed by confocal microscopy and quantified with ImageJ. The diagnosis of hepatocellular carcinoma was made in each case using standard histopathologic

criteria [37]. These included the presence of a discreet liver mass composed of proliferation of hepatocytes exhibiting a variety of disordered growth patterns. Loss of lobular architecture, thickened hepatocellular cell plates, aberrant arteries, abnormal cytologic inclusions, and nuclear pleomorphism were observed to varying degrees in each case. Reticulin stains were used to highlight abnormal cellular arrangements.

Legumain promoter luciferase assay

The plasmids pGL4.10[Luc2] and pRL-CMV, which provide constitutive expression of *Renilla* luciferase, were obtained from Promega (Madison, WI). For generation of the *LGMN* reporter vector, a 750 bp sequence upstream of the initiation codon of the *LGMN* gene was amplified by PCR from SKHep1 genomic DNA with the following primers: 5'-GGACCACCCAGAAACACC-3' and 5'-CTCGCTTAAGGGCCACTG-3'. The product of this reaction was used as a template in a second round of amplification using primers: 5'-GCGCTCGAGTTGGCATTCTAAATAGGGAAGTTAA-3' and 5'-GCGCAGATCTGCGTGGCATCTGCCAAAA-3', which introduced a 5' *XhoI* and 3' *BglII* restriction site, respectively. The fragment was cloned into the pGL4.10[Luc2] to generate the pLGMNprom vector whose identity was confirmed by automated sequencing. Lipofectamine 2000 was used to transfect SKHep1 cells with 10 µg of pLGMNprom alone or in combination with 3 µg of pPV-NLS-DsRed, which expresses a nuclear targeted parvalbumin tagged with DsRed. Luciferase activity was measured with a Dual-Luciferase Reporter Assay (Promega, Madison, WI). Luciferase activity was normalized by *Renilla* luciferase activity. Each assay was performed in triplicate and the data were compared to empty vector controls.

Statistical analysis

Results are expressed as mean ± SEM. Prism software (GraphPad Software, San Diego, CA) was used for data analysis. Statistical significance was tested using Student's *t*-test or one-way ANOVA followed by Bonferroni post-tests, and p value <0.05 was taken to indicate statistical significance.

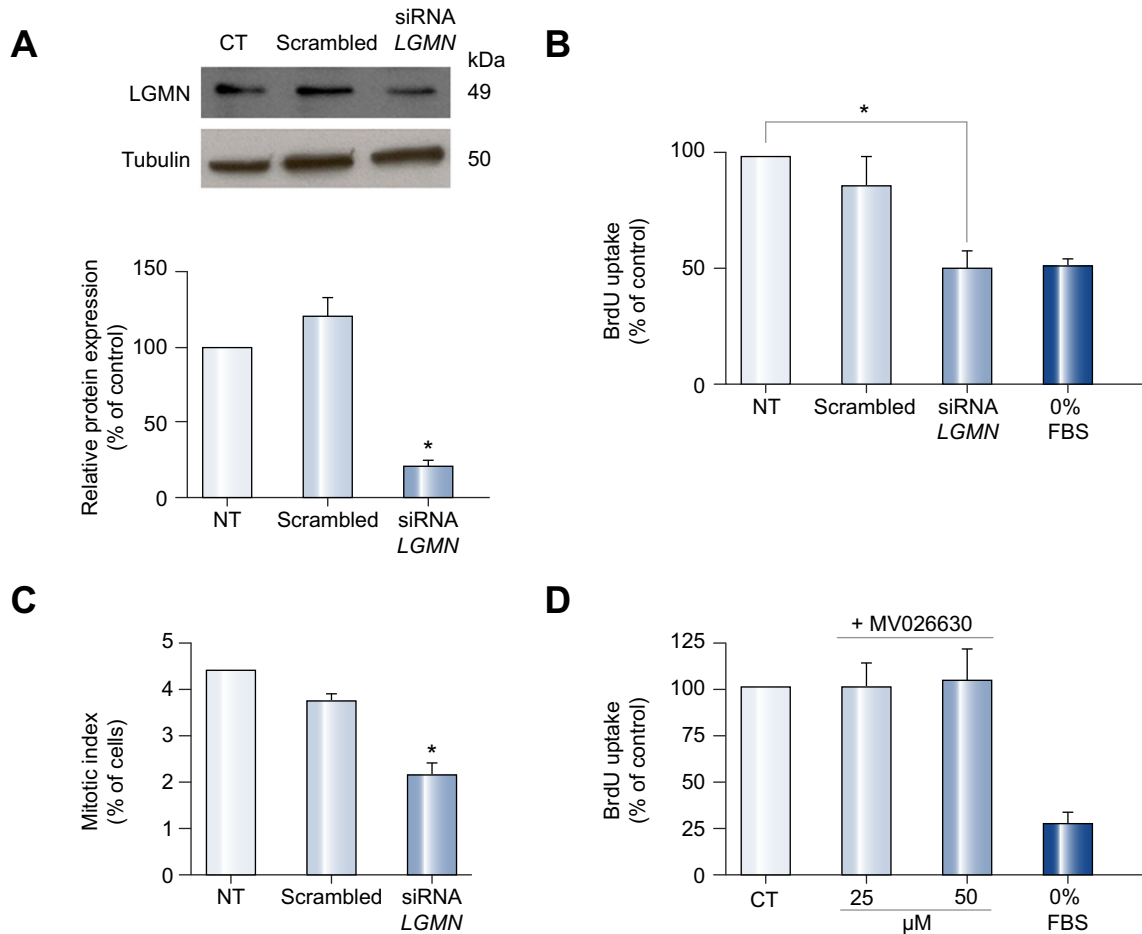


Fig. 4. Knock down of LGMN inhibits cell proliferation. (A) Silencing of LGMN. SKHeP1 cells were transfected with 20 nM siRNA for LGMN, and incubated for 72 h. Immunoblots demonstrate that LGMN but not scrambled siRNA knocks down LGMN expression. α -Tubulin serves as a loading control. Densitometry confirms reduction of LGMN to $21.5 \pm 3.2\%$ of non-transfected controls ($p < 0.0001$). Results are representative of three separate experiments. (B) Knockdown of LGMN decreases BrdU incorporation in SKHeP1 cells to $50.7 \pm 8.1\%$ of controls ($p < 0.0034$). (C) Mitotic SKHeP1 cells were identified by confocal imaging of phospho-histone-3 labeling measured 72 h after knockdown of LGMN. The mitotic index is decreased to $2.2 \pm 0.7\%$ of control in cells in which LGMN is silenced ($p < 0.0001$). A total of 300 cells were examined in three separate experiments. (D) Inhibition of LGMN activity with MV026630 at either 25 or 50 μ M does not alter BrdU uptake in SKHeP cells ($p > 0.05$).

Results

Identification of LGMN as a protein that is sensitive to nuclear Ca^{2+} by RaSH

To define the spectrum of gene expression changes occurring after buffering nuclear Ca^{2+} , a modified subtraction hybridization technique was used [32]. cDNAs libraries were obtained from SKHeP1 cells treated with pAd-PV-NLS-DsRed or pAd-PV-NLS-CD-DsRed. These constructs have been used previously to selectively buffer nuclear Ca^{2+} in SKHeP1 cells [6,9]. Two cDNA libraries were constructed, one with genes up-regulated and the second one with genes down-regulated when nuclear Ca^{2+} was buffered (Fig. 1). Colonies from the two subtractive libraries were isolated randomly and the PCR-amplified products were sequenced and compared with genes deposited in GenBank. One hundred and forty-five insert DNA fragments were amplified by PCR (data not shown). From this pool of positive clones, 13 differentially expressed clones were identified (Table 1). Among these 13 clones, expression was down-regulated in three and up-regulated in 10 when nuclear Ca^{2+} was buffered. Three of

these genes were chosen for validation by real time PCR: *LGMN*, *Transforming growth factor beta regulator 4*, and *Reticulon 4*. These three of the thirteen genes were studied further based on literature linking them to cell proliferation and tumor progression. However, additional experiments were only able to demonstrate that the expression of LGMN affected cell proliferation, so only that protein was studied in greater detail.

Buffering nuclear Ca^{2+} inhibits expression of LGMN

Real time PCR analysis showed that *LGMN* mRNA decreased by $97 \pm 2\%$ ($p < 0.0001$) when nuclear Ca^{2+} was buffered (Fig. 2A). A decrease in LGMN at the protein level was also observed 48 h after infection with the adenovirus PV-NLS. LGMN protein expression decreased by $52 \pm 9\%$ ($p < 0.01$) after nuclear Ca^{2+} was buffered (Fig. 2B). To confirm that expression of this gene was altered in SKHeP1 cells expressing PV fused to DsRed within the nucleus, confocal immunofluorescence was performed. Staining for LGMN (Fig. 2C) indicated that the expression of this protein was lower in cells expressing DsRed-tagged PV within the nucleus when compared to control cells transfected with DsRed

Research Article

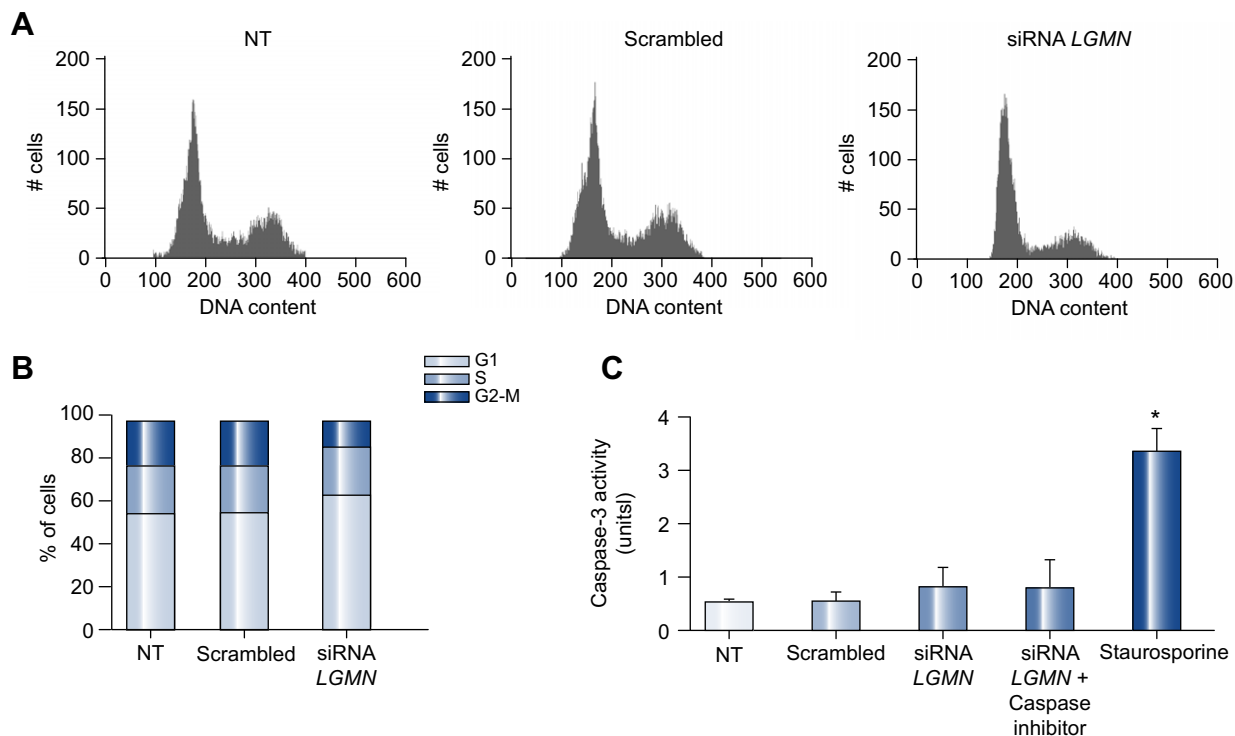


Fig. 5. Cell cycle kinetics after knockdown of LGMN. (A) Representative FACS cell cycle profiles of non-transfected (NT) and siRNA-transfected SkHep cells 72 h after treatment with scrambled or *LGMN* siRNA. (B) In cells in which *LGMN* was silenced, there was a reduction in the fraction of cells in G₂/M phase ($7.4 \pm 10.9\%$ in *LGMN* siRNA versus $25.6 \pm 3.5\%$ in non-transfected; mean \pm SD; $p < 0.05$), without a significant increase in the fraction of cells in G₁ or S phase. Cell cycle profiles were not changed in cells transfected with scrambled siRNA. Data are mean of three independent experiments. (C) Knockdown of *LGMN* does not induce apoptosis, as measured by caspase-3 activity. Staurosporine (500 nM) was used to induce apoptosis as a positive control for caspase-3, and a caspase-3 inhibitor was used as a negative control. Bar graph shows that caspase-3 activity was not increased in response to knockdown of *LGMN* ($p > 0.05$, by one-way ANOVA). Results are representative of four independent experiments (* $p < 0.001$).

alone (quantified in Fig. 2D). Because buffering of nuclear Ca^{2+} is associated with reduced *LGMN* mRNA levels, we investigated whether nuclear Ca^{2+} transcriptionally regulates *LGMN* expression. A sequence encompassing 750 bp upstream of the *LGMN* start codon was used as a putative promoter in a dual-reporter luciferase assay. Luciferase activity driven by the *LGMN* promoter was significantly reduced when nuclear Ca^{2+} was buffered by expression of parvalbumin in the nucleus (20.57 ± 5.34 pLGMN-prom alone as compared to 6.89 ± 0.88 pLGMNprom + PV-NLS; $p < 0.05$; Fig. 2E). These data show that buffering nuclear Ca^{2+} reduces *LGMN* expression, in part through transcription regulation. Next we examined whether hepatocyte growth factor (HGF), a potent mitogen for hepatocytes that also selectively increases nuclear Ca^{2+} in SKHep1 cells [17], modulates *LGMN* expression. HGF (100 ng/ml) promoted an increase in *LGMN* expression in a time-dependent manner, reaching its maximum at 60 min ($245.7 \pm 37.9\%$, $p < 0.05$; Fig. 3A and B). This increase in expression was associated with partial redistribution of *LGMN*, which changed from a punctuate pattern observed in non-stimulated cells to the formation of a large peri-nuclear aggregate in cells treated with HGF (Fig. 3C).

LGMN affects cell proliferation

Nuclear Ca^{2+} regulates proliferation of SKHep1 cells by controlling progression through the cell cycle [9]. Therefore, the relationship between *LGMN* expression and proliferation of these cells was investigated. RNA interference constructs decreased

LGMN expression by $78 \pm 6\%$ ($p < 0.0001$; Fig. 4A). Cell proliferation was assessed by BrdU incorporation in populations of cells in which *LGMN* was silenced. Knockdown of *LGMN* decreased BrdU incorporation by 49% ($p < 0.005$; Fig. 4B). The fraction of cells in mitosis also was quantified by calculation of the mitotic index. The fraction of cells in mitosis decreased when *LGMN* was silenced (Fig. 4C). Similarly, cell counting showed that proliferation of SKHep1 cells decreased after knockdown of *LGMN* (data not shown). Because *LGMN*'s only known biological effect is its endopeptidase activity, BrdU uptake was further investigated in SKHep1 cells in the presence of the chemical inhibitor of *LGMN*, MV026630 [38]. Inhibition of *LGMN* enzymatic activity did not alter BrdU incorporation ($p > 0.05$ by one-way ANOVA; Fig. 4D), suggesting that *LGMN*'s proliferative effect is independent of its endopeptidase activity. These results provide evidence that *LGMN* promotes cell proliferation and suggest that nuclear Ca^{2+} regulates proliferation of SKHep1 cells in part through modulation of *LGMN* expression.

Knockdown of LGMN alters the cell cycle profile rather than apoptosis

In order to understand why reduced expression of *LGMN* inhibited cell proliferation, we investigated whether the decreased cell proliferation was due to apoptosis or changes in the cell cycle profile. Flow cytometry was used to examine whether reduction in the expression of *LGMN* alters the distribution of cells through the phases of cell cycle. Cells were synchronized in G₀ by serum

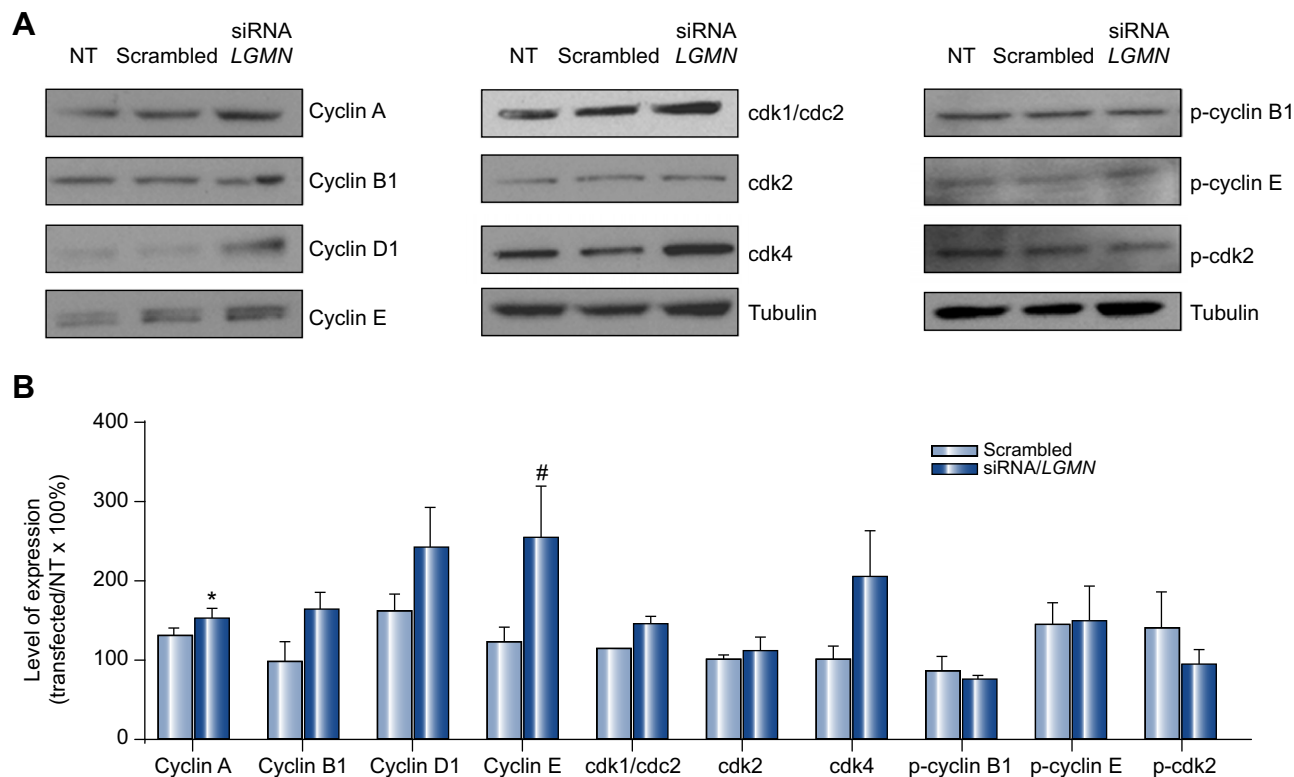


Fig. 6. Progression of cell cycle after knockdown of LGMN. (A) Immunoblot of total protein from SKHep1 cells tests the expression of various cell cycle regulatory proteins 72 h after knockdown of LGMN. (B) Densitometric analysis summarizes the results of the western blots. There was a significant increase in the expression of Cyclin A ($*p < 0.01$) and cyclin E ($**p < 0.05$) in cells transfected with LGMN siRNA relative to non-transfected. Expression of α -tubulin was used as an internal control for protein loading. Data are mean of three independent experiments.

starvation for 24 h, and then released into the cell cycle by the addition of serum. siRNA was transfected and after 72 h the cells were fixed and stained with propidium iodide and submitted to FACS analysis (Fig. 5A). In cells in which LGMN was silenced, there was a significant reduction in the fraction of cells in G₂/M (25 ± 2% of non-transfected cells, as compared to 7 ± 6% of siRNA-treated cells; $p < 0.05$). Despite the reduction in the fraction of cells in G₂/M phase, there was no significant increase in the fractions of cells in G₁ or S phase (Fig. 5B). No changes were observed in cells transfected with scrambled siRNA. Apoptosis was monitored by caspase-3 activation [39] and no increase was observed in cells treated with LGMN siRNA (Fig. 5C). Together, these findings suggest that absence of LGMN causes a decrease in SKHep1 cell proliferation that is not due to an increase in apoptosis.

Knockdown of LGMN modulates cell cycle proteins

The changes observed in the cell cycle profile after knock down of LGMN raises the question of whether the decrease in cell proliferation may be due to alterations in the expression of checkpoint proteins. To investigate this, we examined the expression of these proteins by Western blot (Fig. 6A). The expression of cyclin D1 and Cdk4, which form the complex that regulates the progression through G₁ phase, was unchanged, as was cyclin B1, which controls the G₂/M transition (Fig. 6A). However, the checkpoint proteins of S phase showed increased expression when LGMN was silenced (Fig. 6A); both cyclins A and E expressions were signifi-

cantly increased ($p < 0.05$; Fig. 6B). These increases in expression were not followed by an increase in phosphorylation or activity of CDK2 (Supplementary Fig. 1), nor were they associated with an increase in PCNA expression. Moreover, there was no change in either phosphorylation of cyclins B1 and E or expression of the Cdk inhibitors p21 and p27 (Fig. 6A and B and Supplementary Fig. 1A and B). Together, these findings suggest that LGMN has only minor effects on the expression profile of checkpoint proteins.

LGMN expression in normal human liver and hepatocellular carcinoma

Among the putative cDNAs identified by RaSH, LGMN is notable because this gene is highly expressed in several types of tumors. Its presence correlates with a poor prognosis and increased tumor invasiveness [29] and it can be used as a prognostic factor in breast cancer [30]. Expression of LGMN also may be involved in early development of colorectal cancer [40]. Therefore, we investigated LGMN expression in hepatocellular carcinoma (HCC). Liver resection specimens from patients diagnosed with HCC were examined by confocal immunofluorescence. Three samples which contain both normal and tumor tissue from each of five different patients were examined. LGMN expression was increased in tumor cells (53.9 ± 6.5 a.u.) when compared to normal hepatocytes (38.3 ± 4.3 a.u.) in the same tissue samples ($p < 0.01$ by paired t -test, Fig. 7). These results suggest that LGMN expression is increased in hepatocellular carcinoma, similar to

Research Article

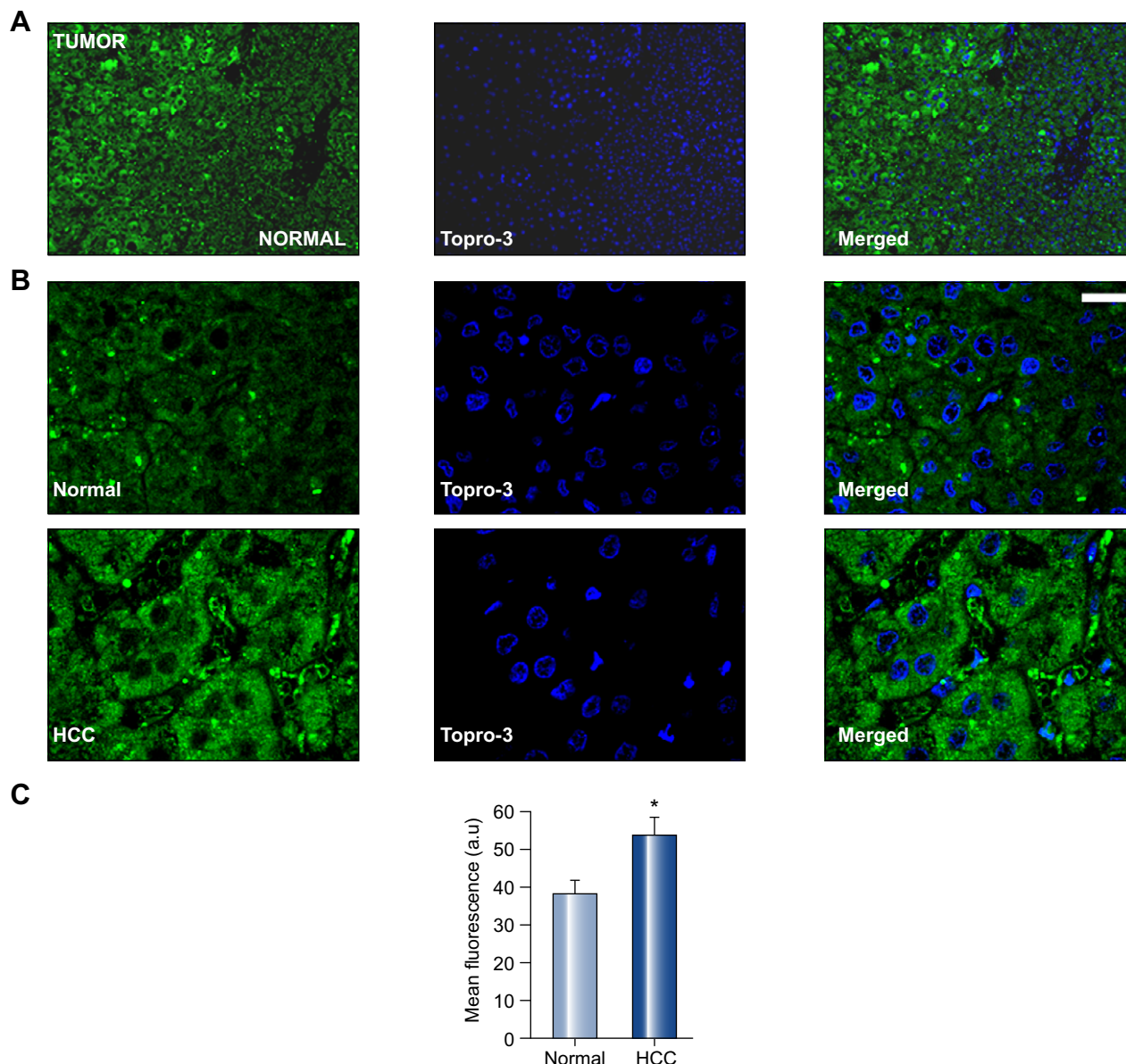


Fig. 7. Expression of LGMN is increased in hepatocellular carcinoma (HCC). Confocal immunofluorescence images were obtained from paraffin-embedded surgical specimens of tumors from patients with HCC. Immunohistochemical staining was performed to determine the expression of LGMN (green) in tumor cells and in nearby normal hepatocytes. To-Pro-3 was used to identify cell nuclei (blue). (A) Low-power (10 \times) image of carcinoma cells and normal hepatocytes in the same field of view shows that LGMN staining is increased in the HCC. (B) Higher magnification (63 \times) images confirm increased the expression of LGMN and show that it is distributed throughout the cytoplasm in HCC (scale bar = 30 μ m). Findings are representative of what was observed in three fields each of specimens from five separate patients. (C) Quantification of the average fluorescence in normal and HCC affected areas in the same specimen shows a significant increase in LGMN expression in the carcinoma cells (53.9 \pm 4.8 a.u.) as compared to normal hepatocytes (38.3 \pm 3.1 a.u.; p < 0.01, paired t test).

what has been observed in other solid tumors, and is consistent with the idea that the positive effects of LGMN on cell proliferation may promote carcinogenesis.

Discussion

Intracellular Ca²⁺ signals regulate cell growth [41], and in hepatocytes, nuclear rather than cytoplasmic Ca²⁺ is responsible for this regulation [18]. The nucleus contains the machinery needed to

generate Ca²⁺ signals, and can form these signals independent of Ca²⁺ signals in the cytoplasm [15,33]. Hepatic mitogens such as insulin [18] and HGF [17] selectively activate this machinery. Buffering nuclear Ca²⁺ inhibits the growth of liver tumors in particular [9]. Specifically, liver tumors implanted in nude mice grew much more slowly when expressing parvalbumin in their nuclei, but not in their cytosol [9]. The proteins that link nuclear Ca²⁺ signals to cell proliferation have not been identified, although such Ca²⁺ signals have effects that would be expected to stimulate cell proliferation. For example, nuclear Ca²⁺ activates the

transcription factors CREB [5] and Elk-1 [6] and stimulates the intranuclear activity of PKC [15] and CaMK-IV [14]. The current work identifies the expression of LGMN as a novel target of nuclear Ca^{2+} , and further shows that inhibition of LGMN expression impairs cell proliferation. Moreover, our findings show that the LGMN promoter is sensitive to nuclear Ca^{2+} , and a bioinformatics analysis identified a putative Elk-1 binding site on the promoter (not shown), so it is possible that nuclear Ca^{2+} regulates LGMN expression through Elk-1.

The findings that LGMN expression is increased in HCC or after treatment of SKHep1 cells with HGF suggest that LGMN may play a role in carcinogenesis in the liver. Although buffering nuclear Ca^{2+} and knockdown of LGMN each reduce cell proliferation, reduction of LGMN expression does not exactly mimic the effects of PV-NLS. For example, transfection of cells with PV-NLS increases the fraction of cells in G_2 , and this is associated with a block in early prophase and an increase in the mitotic index [9]. In contrast, *LGMN* siRNA reduces both the fraction of cells in G_2 and the mitotic index. Furthermore, PV-NLS reduces phospho-Cdk1 but does not alter cyclin expression, whereas *LGMN* siRNA increases expression of cyclins A and E. These results are counterintuitive to the classical model of cell cycle regulation [42] and findings in mouse hepatocytes during liver regeneration [43], both of which predict increased proliferation in cells with higher levels of cyclins due to prolonged CDK2 activation. However, the increased expression of cyclins A and E observed here was not followed by increased CDK2 activity [44]. This unexpected finding is supported by one report demonstrating that cyclin E overexpression promotes cell cycle arrest [45]. Alternatively, the increased expression of cyclin E observed here could be a compensatory up-regulation triggered by the decrease in cell proliferation after knock down of LGMN. Taken together, these results suggest that LGMN has only a minor effect on cell cycle kinetics, and so nuclear Ca^{2+} may act on cell proliferation only in part by regulating LGMN expression.

LGMN is an asparaginyl endopeptidase that hydrolyzes peptides and proteins on the carboxyl side of asparagine residues [24]. Studies in *LGMN* knockout mice have determined that LGMN is expressed predominantly in late endosomes and lysosomes, where it is involved in processing of cathepsins and lysosomal degradation [27]. LGMN is highly expressed in carcinomas of the breast, colon, and prostate, and in several central nervous system neoplasms, compared with the corresponding normal tissues, in which there is little or no LGMN expression [29]. These findings in other types of tumors are similar to what we report here in HCC. *LGMN* knockout mice have hepatomegaly, which is attributed to extramedullary hematopoiesis rather than hepatocyte proliferation because liver histology in these mice is normal [46]. However, the incidence of spontaneous HCC has not been studied in these animals, nor has LGMN expression been studied in xenograft models of liver tumors. LGMN is also involved in extracellular matrix remodeling, including fibronectin degradation, which is enhanced by LGMN over-expression [28]. LGMN-containing vesicles are localized to the invading edge of tumor cells, and tumor cells that over-express LGMN have increased invasive and migratory activity [29]. Collectively, these findings had been interpreted to suggest that LGMN promotes neoplasia by creating a tumor micro-environment that facilitates metastatic behavior. However, the current work suggests that LGMN may have direct effects on cell proliferation as well. Moreover, LGMN co-localizes with integrins [29], which also can directly

modulate cell growth. Further work will be needed to understand how LGMN enhances cell proliferation in the liver.

Conflict of interest

The underlying research reported in the study was funded by the NIH Institutes of Health.

Financial support

This work was supported by grants from HHMI (MF Leite), CNPq (CAD Jardim and MF Leite), CAPES (VA Andrade), and FAPEMIG (MF Leite), and NIH Grants DK45710, DK57751, DK61747, and DK34989 (MH Nathanson). Confocal imaging was supported by CEMEL (UFMG).

Acknowledgments

The authors thank Ewa Menet (Cell Sorter Facility, Yale School of Medicine) for assistance with FACS experiments.

Supplementary data

Supplementary data associated with this article can be found, in the online version, at doi:10.1016/j.jhep.2010.12.022.

References

- [1] Minagawa N, Nagata J, Shibao K, Masyuk AI, Gomes DA, Rodrigues MA, et al. Cyclic AMP regulates bicarbonate secretion in cholangiocytes through release of ATP into bile. *Gastroenterology* 2007;133:1592–1602.
- [2] Nathanson MH, Gautam A, Bruck R, Isales CM, Boyer JL. Effects of Ca^{2+} agonists on cytosolic Ca^{2+} in isolated hepatocytes and on bile secretion in the isolated perfused rat liver. *Hepatology* 1992;15:107–116.
- [3] Nathanson MH, Gautam A, Ng OC, Bruck R, Boyer JL. Hormonal regulation of paracellular permeability in isolated rat hepatocyte couplets. *Am J Physiol* 1992;262:G1079–G1086.
- [4] Hajneczky G, Robb-Gaspers LD, Seitz MB, Thomas AP. Decoding of cytosolic calcium oscillations in the mitochondria. *Cell* 1995;82:415–424.
- [5] Hardingham GE, Chawla S, Johnson CM, Bading H. Distinct functions of nuclear and cytoplasmic calcium in the control of gene expression. *Nature* 1997;385:260–265.
- [6] Pusch T, Wu JJ, Zimmerman TL, Zhang L, Ehrlich BE, Berchtold MW, et al. Epidermal growth factor-mediated activation of the ETS domain transcription factor Elk-1 requires nuclear calcium. *J Biol Chem* 2002;277:27517–27527.
- [7] Mendes CC, Gomes DA, Thompson M, Souto NC, Goes TS, Goes AM, et al. The type III inositol 1,4,5-trisphosphate receptor preferentially transmits apoptotic Ca^{2+} signals into mitochondria. *J Biol Chem* 2005;280:40892–40900.
- [8] Minagawa N, Kruglov EA, Dranoff JA, Robert ME, Gores GJ, Nathanson MH. The anti-apoptotic protein Mcl-1 inhibits mitochondrial Ca^{2+} signals. *J Biol Chem* 2005;280:33637–33644.
- [9] Rodrigues MA, Gomes DA, Leite MF, Grant W, Zhang L, Lam W, et al. Nucleoplasmic calcium is required for cell proliferation. *J Biol Chem* 2007;282:17061–17068.
- [10] Leite MF. Ca^{2+} signaling in the liver. In: Arias IM, editor. *The liver biology and pathobiology*. Wiley; 2009. p. 485–510.
- [11] Leite MF, Hirata K, Pusch T, Burgstahler AD, Okazaki K, Ortega JM, et al. Molecular basis for pacemaker cells in epithelia. *J Biol Chem* 2002;277:16313–16323.
- [12] Carrion AM, Link WA, Ledo F, Mellstrom B, Naranjo JR. DREAM is a Ca^{2+} -regulated transcriptional repressor. *Nature* 1999;398:80–84.
- [13] Thompson M, Andrade VA, Andrade SJ, Pusch T, Ortega JM, Goes AM, et al. Inhibition of the TEF/TEAD transcription factor activity by nuclear calcium and distinct kinase pathways. *Biochem Biophys Res Commun* 2003;301:267–274.

Research Article

- [14] Deisseroth K, Heist EK, Tsien RW. Translocation of calmodulin to the nucleus supports CREB phosphorylation in hippocampal neurons. *Nature* 1998;392:198–202.
- [15] Echevarria W, Leite MF, Guerra MT, Zipfel WR, Nathanson MH. Regulation of calcium signals in the nucleus by a nucleoplasmic reticulum. *Nat Cell Biol* 2003;5:440–446.
- [16] Berridge MJ, Bootman MD, Roderick HL. Calcium signalling: dynamics, homeostasis and remodelling. *Nat Rev Mol Cell Biol* 2003;4:517–529.
- [17] Gomes DA, Rodrigues MA, Leite MF, Gomez MV, Varnai P, Balla T, et al. C-Met must translocate to the nucleus to initiate calcium signals. *J Biol Chem* 2008;283:4344–4351.
- [18] Rodrigues MA, Gomes DA, Andrade VA, Leite MF, Nathanson MH. Insulin induces calcium signals in the nucleus of rat hepatocytes. *Hepatology* 2008;48:1621–1631.
- [19] Maniatis AJ, Chen CS, Ingber DE. Demonstration of mechanical connections between integrins, cytoskeletal filaments, and nucleoplasm that stabilize nuclear structure. *Proc Natl Acad Sci USA* 1997;94:849–854.
- [20] Kembhavi AA, Buttle DJ, Knight CG, Barrett AJ. The two cysteine endopeptidases of legume seeds: purification and characterization by use of specific fluorometric assays. *Arch Biochem Biophys* 1993;303:208–213.
- [21] Chen JM, Dando PM, Rawlings ND, Brown MA, Young NE, Stevens RA, et al. Cloning, isolation, and characterization of mammalian legumain, an asparaginyl endopeptidase. *J Biol Chem* 1997;272:8090–8098.
- [22] Caffrey CR, Mathieu MA, Gaffney AM, Salter JP, Sajid M, Lucas KD, et al. Identification of a cDNA encoding an active asparaginyl endopeptidase of *Schistosoma mansoni* and its expression in *Pichia pastoris*. *FEBS Lett* 2000;466:244–248.
- [23] Oliver EM, Skuce PJ, McNair CM, Knox DP. Identification and characterization of an asparaginyl proteinase (legumain) from the parasitic nematode, *Haemonchus contortus*. *Parasitology* 2006;133:237–244.
- [24] Chen JM, Dando PM, Stevens RA, Fortunato M, Barrett AJ. Cloning and expression of mouse legumain, a lysosomal endopeptidase. *Biochem J* 1998;335:111–117.
- [25] Manoury B, Hewitt EW, Morrice N, Dando PM, Barrett AJ, Watts C. An asparaginyl endopeptidase processes a microbial antigen for class II MHC presentation. *Nature* 1998;396:695–699.
- [26] Manoury B, Mazzeo D, Li DN, Billson J, Loak K, Benaroch P, et al. Asparagine endopeptidase can initiate the removal of the MHC class II invariant chain chaperone. *Immunity* 2003;18:489–498.
- [27] Shirahama-Noda K, Yamamoto A, Sugihara K, Hashimoto N, Asano M, Nishimura M, et al. Biosynthetic processing of cathepsins and lysosomal degradation are abolished in asparaginyl endopeptidase-deficient mice. *J Biol Chem* 2003;278:33194–33199.
- [28] Morita Y, Araki H, Sugimoto T, Takeuchi K, Yamane T, Maeda T, et al. Legumain/asparaginyl endopeptidase controls extracellular matrix remodeling through the degradation of fibronectin in mouse renal proximal tubular cells. *FEBS Lett* 2007;581:1417–1424.
- [29] Liu C, Sun C, Huang H, Janda K, Edgington T. Overexpression of legumain in tumors is significant for invasion/metastasis and a candidate enzymatic target for prodrug therapy. *Cancer Res* 2003;63:2957–2964.
- [30] Gawenda J, Traub F, Luck HJ, Kreipe H, von Wasielewski R. Legumain expression as a prognostic factor in breast cancer patients. *Breast Cancer Res Treat* 2007;102:1–6.
- [31] Luo Y, Zhou H, Krueger J, Kaplan C, Lee SH, Dolman C, et al. Targeting tumor-associated macrophages as a novel strategy against breast cancer. *J Clin Invest* 2006;116:2132–2141.
- [32] Jiang H, Kang DC, Alexandre D, Fisher PB, RaSH, a rapid subtraction hybridization approach for identifying and cloning differentially expressed genes. *Proc Natl Acad Sci USA* 2000;97:12684–12689.
- [33] Leite MF, Thrower EC, Echevarria W, Koulen P, Hirata K, Bennett AM, et al. Nuclear and cytosolic calcium are regulated independently. *Proc Natl Acad Sci USA* 2003;100:2975–2980.
- [34] Krasinska L, Besnard E, Cot E, Dohet C, Mechali M, Lemaitre JM, et al. Cdk1 and Cdk2 activity levels determine the efficiency of replication origin firing in *Xenopus*. *EMBO J* 2008;27:758–769.
- [35] Hendzel MJ, Wei Y, Mancini MA, Van Hooser A, Ranalli T, Brinkley BR, et al. Mitosis-specific phosphorylation of histone H3 initiates primarily within pericentromeric heterochromatin during G2 and spreads in an ordered fashion coincident with mitotic chromosome condensation. *Chromosoma* 1997;106:348–360.
- [36] Shibao K, Hirata K, Robert ME, Nathanson MH. Loss of inositol 1,4,5-trisphosphate receptors from bile duct epithelia is a common event in cholestasis. *Gastroenterology* 2003;125:1175–1187.
- [37] Ishak KG, Goodman ZD, Stocker JT. Tumors of the liver and intrahepatic bile ducts. *Atlas of tumor pathology*. Washington: Armed Forces Institute of Pathology; 2001.
- [38] Loak K, Li DN, Manoury B, Billson J, Morton F, Hewitt E, et al. Novel cell-permeable acyloxymethylketone inhibitors of asparaginyl endopeptidase. *Biol Chem* 2003;384:1239–1246.
- [39] Boatright KM, Salvesen GS. Mechanisms of caspase activation. *Curr Opin Cell Biol* 2003;15:725–731.
- [40] Murthy RV, Arbman G, Gao J, Roodman GD, Sun XF. Legumain expression in relation to clinicopathologic and biological variables in colorectal cancer. *Clin Cancer Res* 2005;11:2293–2299.
- [41] Patel R, Holt M, Philipova R, Moss S, Schulman H, Hidaka H, et al. Calcium/calmodulin-dependent phosphorylation and activation of human Cdc25-C at the G2/M phase transition in HeLa cells. *J Biol Chem* 1999;274:7958–7968.
- [42] Hochegger H, Takeda S, Hunt T. Cyclin-dependent kinases and cell-cycle transitions: does one fit all? *Nat Rev Mol Cell Biol* 2008;9:910–916.
- [43] Nevzorova YA, Tschaharganeh D, Gassler N, Geng Y, Weiskirchen R, Scinski P, et al. Aberrant cell cycle progression and endoreplication in regenerating livers of mice that lack a single E-type cyclin. *Gastroenterology* 2009;137:691–703, e691–696.
- [44] Sherr CJ, Roberts JM. CDK inhibitors: positive and negative regulators of G1-phase progression. *Genes Dev* 1999;13:1501–1512.
- [45] Keck JM, Summers MK, Tedesco D, Ekholm-Reed S, Chuang LC, Jackson PK, et al. Cyclin E overexpression impairs progression through mitosis by inhibiting APC(Cdh1). *J Cell Biol* 2007;178:371–385.
- [46] Chan CB, Abe M, Hashimoto N, Hao C, Williams IR, Liu X, et al. Mice lacking asparaginyl endopeptidase develop disorders resembling hemophagocytic syndrome. *Proc Natl Acad Sci USA* 2009;106:468–473.

Mitochondrial Calcium Regulates Liver Regeneration Through the Modulation of Apoptosis

AQ1

Mateus T. Guerra,^{1,5*} Emerson A. Fonseca,^{1*} Flavia M. Melo,¹ Viviane A. Andrade,¹ Carla J. Aguiar,^{1,6} Lídia M. Andrade,^{1,7} Ana Cristina N. Pinheiro,¹ Marisa F. Casteluber,¹ Rodrigo R. Resende,⁸ Mauro C. X. Pinto,¹ Simone O. A. Fernandes,² Valbert N. Cardoso,² Elaine M. Souza-Fagundes,¹ Gustavo B. Menezes,³ Ana M. de Paula,⁴ Michael H. Nathanson,⁵ and Maria de Fátima Leite^{1,9}

AQ2

Subcellular Ca²⁺ signals control a variety of responses in the liver. For example, mitochondrial Ca²⁺ (Ca_{mit}²⁺) regulates apoptosis, whereas Ca²⁺ in the nucleus regulates cell proliferation. Because apoptosis and cell growth can be related, we investigated whether Ca_{mit}²⁺ also affects liver regeneration. The Ca²⁺-buffering protein parvalbumin, which was targeted to the mitochondrial matrix and fused to green fluorescent protein, was expressed in the SKHep1 liver cell line; the vector was called parvalbumin-mitochondrial targeting sequence-green fluorescent protein (PV-MITO-GFP). This construct properly localized to and effectively buffered Ca²⁺ signals in the mitochondrial matrix. Additionally, the expression of PV-MITO-GFP reduced apoptosis induced by both intrinsic and extrinsic pathways. The reduction in cell death correlated with the increased expression of antiapoptotic genes [B cell lymphoma 2 (bcl-2), myeloid cell leukemia 1, and B cell lymphoma extra large] and with the decreased expression of proapoptotic genes [p53, B cell lymphoma 2-associated X protein (bax), apoptotic peptidase activating factor 1, and caspase-6]. PV-MITO-GFP was also expressed in hepatocytes *in vivo* with an adenoviral delivery system. Ca_{mit}²⁺ buffering in hepatocytes accelerated liver regeneration after partial hepatectomy, and this effect was associated with the increased expression of Bcl-2 and the decreased expression of Bax. **Conclusion: Together, these results reveal an essential role for Ca_{mit}²⁺ in hepatocyte proliferation and liver regeneration, which may be mediated by the regulation of apoptosis. (HEPATOLOGY 2011;00:000–000)**

AQ4

Liver regeneration is a complex process triggered by acute damage to the organ and can be induced experimentally by chemical or surgical injuries that result in a loss of parenchymal cells (i.e., hepatocytes).¹ After partial hepatectomy (PH), liver mass restoration is achieved by a massive proliferation of hepatocytes, which switch from a quiescent phenotype to a

proliferative phenotype. This cell growth response is driven by a number of cytokines and growth factors, such as interleukin-6,² tumor necrosis factor (TNF),³ hepatocyte growth factor,⁴ and epidermal growth factor. Ca²⁺ signaling is one of the pathways activated during liver regeneration, and growth factors and hormones that promote Ca²⁺ release in hepatocytes, such as hepatocyte

Abbreviations: Ad, adenovirus; Ad-PV-MITO, parvalbumin-mitochondrial targeting sequence adenovirus; Ad-PV-MITO-GFP, parvalbumin-mitochondrial targeting sequence-green fluorescent protein adenovirus; AIF, apoptosis-inducing factor; Apaf-1, apoptotic peptidase activating factor 1; ATP, adenosine triphosphate; Bax, B cell lymphoma 2-associated X protein; Bcl-2, B cell lymphoma 2; Bcl-xL, B cell lymphoma extra large; BrdU, bromodeoxyuridine; Camit2+, mitochondrial Ca²⁺; cDNA, complementary DNA; CT, control; D, day; EGFR, epidermal growth factor receptor; ER, endoplasmic reticulum; GAPDH, glyceraldehyde 3-phosphate dehydrogenase; GFP, green fluorescent protein; IB, immunoblotting; Mcl-1, myeloid cell leukemia 1; MITO-GFP, mitochondrial targeting sequence-green fluorescent protein; MPO, myeloperoxidase; MTS, mitochondrial targeting sequence; OD, optical density; pAd-PV-MITO-GFP, parvalbumin-mitochondrial targeting sequence-green fluorescent protein adenovirus plasmid; PCNA, proliferating cell nuclear antigen; PCR, polymerase chain reaction; PH, partial hepatectomy; PI, propidium iodide; PV, parvalbumin; PV-MITO-GFP, parvalbumin-mitochondrial targeting sequence-green fluorescent protein; STA, staurosporine; ^{99m}Tc-phytate, phytate labeled with technetium-99m; TNF, tumor necrosis factor.

AQ3

From the ¹Department of Physiology and Biophysics, ²Radioisotope Laboratory, Department of Clinical and Toxicological Analysis, Faculty of Pharmacy, ³Department of Morphology, and ⁴Department of Physics, Federal University of Minas Gerais, Belo Horizonte, Minas Gerais, Brazil; ⁵Section of Digestive Diseases, Department of Internal Medicine, Yale University School of Medicine, New Haven, CT; ⁶Izabela Hendrix Methodist Institute, Belo Horizonte, Minas Gerais, Brazil; ⁷René Rachou Research Center, Oswaldo Cruz Foundation, Belo Horizonte, Minas Gerais, Brazil; ⁸Nanobiotechnology Laboratory, Federal University of São João del Rei, São João del Rei, Minas Gerais, Brazil; and ⁹Howard Hughes Medical Institute, Chevy Chase, MD.

Received January 4, 2011; accepted April 5, 2011.

growth factor, epidermal growth factor, and vasopressin, are potent mitogens for this cell type.⁵⁻⁷

Ca²⁺ signaling regulates a variety of cellular functions in the liver; these functions range from bile secretion to cell proliferation.^{8,9} This ability to regulate various functions is closely related to the subcellular compartments in which Ca²⁺ is released.¹⁰ For example, pericanalicular increases in Ca²⁺ regulate the targeting and canalicular insertion of multidrug resistance-associated protein 2,⁸ whereas nuclear Ca²⁺ signals regulate proliferation in liver cell lines.⁹ Mitochondria also participate in Ca²⁺ signaling. Mitochondrial Ca²⁺ (Ca_{mit}²⁺) signals depend on cytosolic Ca²⁺ because there is a close association between inositol 1,4,5-trisphosphate receptors within the endoplasmic reticulum (ER) and mitochondria¹¹; this permits the transmission of Ca²⁺ from the ER to the mitochondrial matrix.¹² Ca_{mit}²⁺ signals regulate apoptosis in various cell systems.^{13,14} This form of cell death is controlled in part by members of the B cell lymphoma 2 (Bcl-2) protein family, which directly modulate Ca²⁺ signaling.¹⁵ Proapoptotic members of this family induce cell death through either the enhancement of Ca²⁺ release from the ER or the facilitation of Ca²⁺ entry into mitochondria, which ultimately causes cytochrome C release and caspase activation. Conversely, prosurvival Bcl-2 proteins such as Bcl-2, B cell lymphoma extra large (Bcl-xL), and myeloid cell leukemia 1 (Mcl-1) work either by the direct modulation of the activity of the inositol 1,4,5-trisphosphate receptor or by the reduction of Ca²⁺ entry into mitochondria, which prevents the generation of proapoptotic Ca²⁺ signals.¹⁶⁻¹⁸ However, this interplay between Ca_{mit}²⁺ and apoptosis has not been studied in the liver in the context of liver regeneration. Therefore, we investigated the role of Ca_{mit}²⁺ in the regulation of liver regeneration.

Materials and Methods

Cell Lines and Materials. SKHep1 and HEK-293 cell lines were obtained from the American Type Cul-

ture Collection (Manassas, VA). Cells were grown at 37°C with 5% carbon dioxide/95% air in Dulbecco's modified Eagle's medium supplemented with 1% penicillin-streptomycin and 10% heat-inactivated fetal bovine serum (all from Gibco, Grand Island, NY). The pAc1GFP1-Mito vector was acquired from Clontech (Mountain View, CA). MitoTracker Red, Rhod-2/AM, the SuperScript first-strand synthesis system for real-time polymerase chain reaction (PCR), PCR Super-Mix, Lipofectamine, a caspase-9 detection kit, and antibodies against B cell lymphoma 2-associated X protein (Bax), Bcl-2, and c-Met were obtained from Invitrogen (Carlsbad, CA). Antibodies against β -actin, anti- γ -tubulin, adenosine triphosphate (ATP), and TNF- α were acquired from Sigma Aldrich (St. Louis, MO). Antibodies against proliferating cell nuclear antigen (PCNA) and epidermal growth factor receptor (EGFR) were obtained from Santa Cruz (Santa Cruz, CA) and Cell Signaling Technology (Boston, MA). Caspase-3 and caspase-8 detection kits were acquired from BD Biosciences (San Jose, CA). An apoptosis-inducing factor (AIF) reagent was obtained from Santa Cruz. Staurosporine (STA) was acquired from Calbiochem (San Diego, CA). All other reagents were of the highest quality that was commercially available.

Animals. Male Holtzman rats (40-50 g), which were obtained from CEBIO (Federal University of Minas Gerais, Belo Horizonte, Minas Gerais, Brazil), were used for all studies. The animals were maintained on a standard diet and were housed with a 12-hour light-dark cycle. The investigation conformed to the standards of *Guide for the Care and Use of Laboratory Animals* (National Institutes of Health publication 85-23, 1996 revision).

Plasmid and Adenovirus Constructs. Complementary DNA (cDNA) for the Ca²⁺ binding protein parvalbumin (PV) was subcloned between the *Bam*HI and *Age*I restriction sites of the pAc1GFP1-Mito vector. The resulting vector encoded PV, which was fused to the mitochondrial targeting sequence (MTS) and green

This work was supported by grants from the Howard Hughes Medical Institute (to Maria de Fátima Leite), Conselho Nacional de Desenvolvimento Científico e Tecnológico (to Maria de Fátima Leite and Rodrigo R. Resende), Fundação de Amparo à Pesquisa do Estado de Minas Gerais (to Maria de Fátima Leite and Rodrigo R. Resende), Coordenação de Aperfeiçoamento de Pessoal de Nível Superior (to Mateus T. Guerra, Viviane A. Andrade, Marisa F. Casteluber, and Rodrigo R. Resende), Instituto Nacional de Ciência e Tecnologia (to Carla J. Aguiar), and the National Institutes of Health (DK57751, DK45710, and DK34989 to Michael H. Nathanson).

**These authors contributed equally to this work.*

Address reprint requests to: Maria de Fátima Leite, Ph.D., Department of Physiology and Biophysics, Federal University of Minas Gerais, Avenida Antonio Carlos 6627, Pampulha, Belo Horizonte, Minas Gerais, Brazil 31270-901. E-mail: leitemd@netuno.lcc.ufmg.br; fax: +55 31 34092924.

Copyright © 2011 by the American Association for the Study of Liver Diseases.

View this article online at wileyonlinelibrary.com.

DOI 10.1002/hep.24367

Potential conflict of interest: Nothing to report.

Additional Supporting Information may be found in the online version of this article.

AQ4 fluorescent protein (GFP), and it was called parvalbumin-mitochondrial targeting sequence-green fluorescent protein (PV-MITO-GFP). A recombinant adenovirus was used to deliver the parvalbumin-mitochondrial targeting sequence-green fluorescent protein adenovirus plasmid (pAd-PV-MITO-GFP). The virus was amplified with HEK-293 cells and was purified with the VivaPure AdenoPack kit (Sartorius, Göttingen, Germany) according to the manufacturer's protocol. pAd-PV-MITO-GFP (3×10^9 pfu) was injected into rats by tail vein infusions, and the livers were processed at the indicated times.

Detection of Ca_{mit}^{2+} Signals. Cells were perfused with ATP (1 μ M), and Ca_{mit}^{2+} was monitored in SKHep1 cells with time-lapse confocal microscopy, as previously described.¹⁴ Transfected cells were identified with GFP fluorescence. MitoTracker Red and GFP colocalization images were collected as described previously.¹⁴

Immunoblots. Protein lysates from SKHep1 cells or the total liver were subjected to sodium dodecyl sulfate-polyacrylamide gel electrophoresis and were transferred to polyvinylidene fluoride membranes. Western blots were developed with the ECL Plus reagent. Densitometry was performed with ImageJ software (National Institutes of Health, Bethesda, MD).

AQ4 **Flow Cytometry.** For the determination of the proportion of dead cells, control SKHep1 cells and cells transfected with mitochondrial targeting sequence-green fluorescent protein (MITO-GFP) or PV-MITO-GFP were stimulated with 300 nM STA for 6 hours. The cells were trypsinized, fixed in 70% ethanol, and incubated with 0.5 mg/mL propidium iodide (PI). The cells were analyzed for GFP and PI fluorescence with the Becton Dickinson FACSCalibur system.

Real-Time PCR. Total RNA was isolated from SKHep1 cells with TRIzol, and cDNA was synthesized with the SuperScript II kit (Invitrogen). DNA templates were amplified by real-time PCR with the StepOnePlus real-time PCR system (Applied Biosystems, Foster City, CA) and the SYBR Green method.¹⁹ β -Actin was used as an internal control to normalize variations in the cDNA content. Experiments were performed in triplicate for each data point. The sequences of the primers are listed in Supporting Table 1.

Apoptosis Assay. Apoptosis through the intrinsic pathway was induced by a 6-hour treatment with 300 nM STA. For the induction of apoptosis through the extrinsic pathway, cells were stimulated with 100 ng/mL TNF- α for 24 hours. Apoptosis was measured with caspase-3, caspase-8, and caspase-9 kits and colorimetric detection, as previously described.^{9,19} Immuno-

fluorescence for AIF was used to evaluate the caspase-independent intrinsic pathway in cells treated with 300 nM STA for 6 hours. Images were obtained with a Zeiss LSM 510 confocal microscope.

Measurement of Bromodeoxyuridine (BrdU) Incorporation. Cell proliferation was measured by BrdU incorporation with an enzyme-linked immunosorbent assay (Roche Applied Science) according to the manufacturer's instructions. SKHep1 cells were plated onto 96-well culture plates, transfected with MITO-GFP or PV-MITO-GFP, and starved for 24 hours. The cells were then treated for 6 hours with 300 nM STA and were incubated 18 hours later with a BrdU labeling solution. BrdU incorporation was measured with a multiplate reader.

Intravital and Liver Section Confocal Microscopy. Rat liver intravital microscopy was performed as described previously with modifications.²⁰ Briefly, rats were anesthetized by an intraperitoneal injection of a mixture of 10 mg/kg xylazine hydrochloride and 200 mg/kg ketamine hydrochloride and were placed in a right lateral position on an adjustable microscope stage. A lateral abdominal incision was made to expose the liver surface, which was covered with a cover slip. The liver was visualized with an intravital multiphoton/confocal microscopy system based on a modified Olympus FV300 confocal microscope in an up-right configuration (a BX51 microscope). Images were obtained with the confocal laser at 488 nm or via multiphoton excitation at 840 nm with a UPlanFLN 10 \times /0.30 objective. For frozen liver section analysis, samples from rats injected with the adenovirus or saline were fixed, dehydrated in sucrose, and mounted for the visualization of GFP-positive cells with a Zeiss LSM 510 confocal microscope.

PH, Liver Histology, and Biochemical Analysis. Two-thirds hepatectomy (i.e., PH) was performed on adult male Holtzman rats as described.²¹ One day before PH, the parvalbumin-mitochondrial targeting sequence-green fluorescent protein adenovirus (Ad-PV-MITO-GFP) was injected into the tail vein. For histology, 8- μ m-thick liver cryostat sections were processed 24, 48, and 72 hours after PH for PCNA and hematoxylin-eosin staining. Serum samples were used to measure the levels of albumin, conjugated and total bilirubin, aminotransferases (aspartate aminotransferase and alanine aminotransferase), and alkaline phosphatase with commercial fluorometric kits according to the manufacturer's instructions.

Scintigraphic Imaging. Liver scintigraphy was performed with phytate labeled with technetium-99m (^{99m}Tc-phytate). Rats received 1.48 MBq of ^{99m}Tc-

phytate via the tail vein. Fifteen minutes after the administration of the radiopharmaceutical, the animals were anesthetized and placed in the prone position on a gamma camera equipped with a low-energy collimator (Nuclide TH 22, Mediso, Budapest, Hungary). Ten-minute static planar images were acquired with a 256 pixel \times 256 pixel matrix. The liver area (mm²) was determined by the amount of radioactivity uptake in the organ.

Determination of the Myeloperoxidase (MPO) Activity. Neutrophil accumulation in the liver was quantified with MPO activity assays as previously described.²² MPO activity was assayed with measurements of the variation in the optical density (OD) at 450 nm with tetramethylbenzidine (1.6 mM) and hydrogen peroxide (0.5 mM). The results are expressed as relative neutrophil numbers, and they were calculated by comparisons of tissue supernatant OD values with the OD values of a standard neutrophil curve (>95% purity).

Statistical Analysis. The results are expressed as means and standard errors of the mean. Prism (GraphPad Software, San Diego, CA) was used for data analysis. Statistical significance was tested with the Student *t* test or a one-way analysis of variance followed by Bonferroni posttests, and *P* < 0.05 was considered to indicate statistical significance.

Results

Targeted PV as a Ca_{mit}²⁺ Buffer. PV fused to an MTS and GFP was developed as a genetically encoded Ca_{mit}²⁺ buffer. GFP targeted to the mitochondrial matrix was used as a control (Fig. 1A). PV was effectively expressed in SKHep1 cells transfected with PV-MITO-GFP, as demonstrated by immunoblotting (Fig. 1B). Moreover, PV was correctly targeted to the mitochondrial matrix, as demonstrated by the colocalization of GFP and MitoTracker Red (Fig. 1C). For the evaluation of Ca²⁺ buffering by this construct, SKHep1 cells were stimulated with 1 μ M ATP, and Ca_{mit}²⁺ was measured by Rhod-2/AM confocal microscopy. ATP elicited a robust increase in Ca_{mit}²⁺ in control cells and in cells expressing GFP alone, but this was reduced by approximately 90% in cells expressing PV in mitochondria (n = 3, *P* < 0.001; Fig. 2). These results demonstrated that PV-MITO-GFP was correctly targeted to the mitochondrial matrix and efficiently buffered agonist-induced Ca_{mit}²⁺ signals.

Ca_{mit}²⁺ Buffering Attenuates Apoptotic Cell Death. Ca_{mit}²⁺ plays a crucial role in apoptosis, so we investigated the effect of Ca_{mit}²⁺ buffering on cell death.

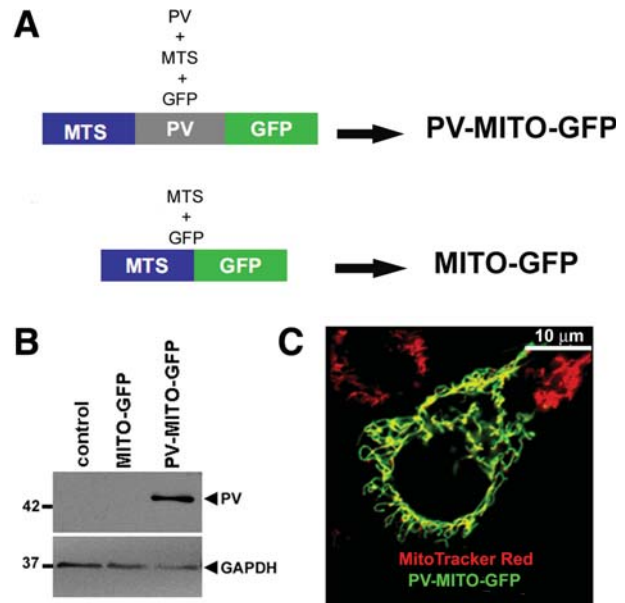


Fig. 1. Expression and mitochondrial localization of targeted PV-GFP fusion proteins. (A) Schematic view of mitochondrial PV expression and control vectors. (B) Exogenous expression of PV in SKHep1 cells. PV-MITO-GFP led to the expression of the 42-kDa fusion protein. (C) Subcellular localization of PV-MITO-GFP. Green indicates GFP, red indicates mitochondrial staining with MitoTracker Red, and yellow indicates colocalization of the two signals. In transfected SKHep-1 cells, the expression of PV-MITO-GFP was restricted to mitochondria. Abbreviation: GAPDH, glyceraldehyde 3-phosphate dehydrogenase.

A treatment with STA increased the percentage of dead cells to 19.1% \pm 3.7% (11.4% \pm 0.7% for unstimulated cells, *P* < 0.001, n = 3). Upon Ca_{mit}²⁺ buffering, the rate of cell death induced by STA was reduced to 7.7% \pm 2.2%, whereas the rate of cell death remained high (25.7% \pm 1.8%) in cells transfected with MITO-GFP (*P* < 0.001, n = 3; Fig. 3A). The role of Ca_{mit}²⁺ in cell death was further characterized by the evaluation of the intrinsic or extrinsic apoptotic pathways because the two pathways converge at the level of Ca_{mit}²⁺ signaling.²³ The intrinsic pathway was investigated through the measurement of caspase-9 and caspase-3 activity in SKHep1 cells stimulated with 100 nM STA for 6 hours. Caspase-9 activity was increased by 0.16% \pm 0.06% after the STA treatment and by 0.1% \pm 0.02% in control cells, and this was blocked by the expression of PV-MITO-GFP (*P* < 0.001, n = 3; Fig. 3B). Similarly, STA-induced caspase-3 activity was inhibited by Ca_{mit}²⁺ buffering (Fig. 3C). Caspase-3 activity was increased from 43.0 \pm 5.8 nmol/mg of protein in unstimulated cells to 97.5 \pm 9.2 nmol/mg of protein in the STA-treated cells. STA increased caspase-3 activity in MITO-GFP cells to 126.2 \pm 22.2 nmol/mg of protein, whereas the level of caspase-3 activity was 54.4 \pm 6.4 nmol/mg of

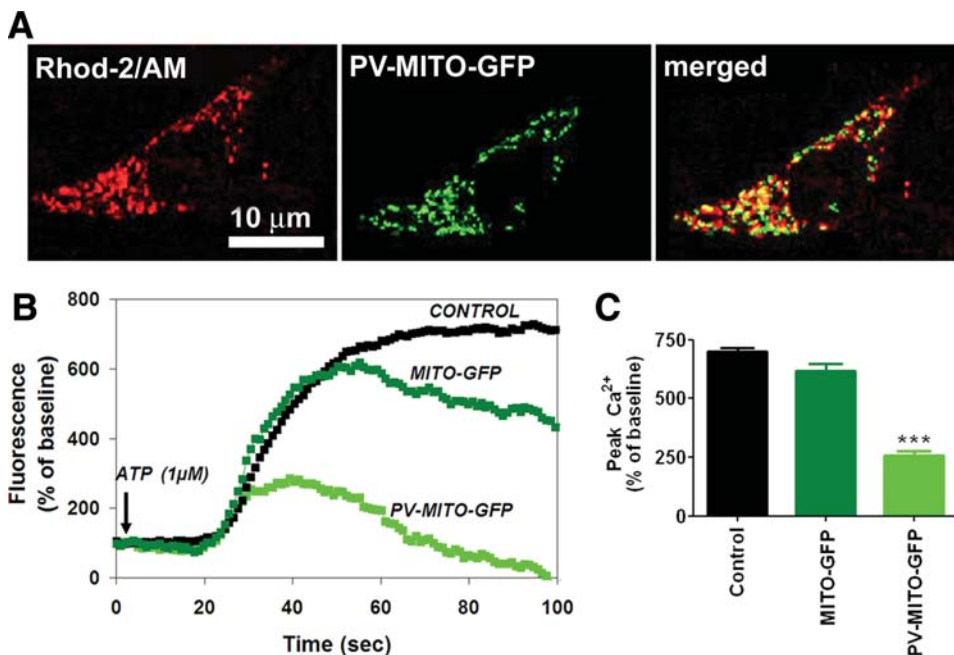


Fig. 2. PV buffers Ca²⁺_{mit} signaling. (A) Confocal images show SKHep1 cells expressing PV-MITO-GFP (green) loaded with the Ca²⁺_{mit} indicator Rhod-2/AM (red). (B) Representative changes in Ca²⁺_{mit} signals over time are shown. They were induced by ATP (1 μM) in control SKHep1 cells or cells transfected with the indicated vectors. Ca²⁺_{mit} signals were attenuated in cells expressing PV in mitochondria. (C) Peak Ca²⁺_{mit} signals were observed in three separate experiments for control SKHep1 cells, cells transfected with MITO-GFP, and cells transfected with PV-MITO-GFP (*P* < 0.001 versus control cells, *n* ≥ 70 cells for each experimental condition).

C
O
L
O
R

AQ9

protein in SKHep1 cells expressing PV-MITO-GFP (*P* < 0.001, *n* = 3; Fig. 3C). Next, we investigated whether the caspase-independent intrinsic pathway was also affected by Ca²⁺_{mit} buffering. Confocal immunofluorescence imaging of AIF demonstrated that targeting PV against mitochondria reduced the expression of this proapoptotic factor in comparison with SKHep1 cells transfected with the control construct MITO-GFP (Fig. 3D). These data show that the expression of PV in mitochondria protected cells from STA-induced cell death through the caspase-dependent and caspase-independent intrinsic apoptotic pathway. We also investigated whether PV-MITO affected the extrinsic apoptotic pathway. The activity of caspase-8 and caspase-3 was measured in control cells and in cells transfected with PV-MITO-GFP or MITO-GFP and treated with 100 ng/mL TNF-α for 6 hours. TNF-α increased caspase-8 and caspase-3 activity levels to 246.7 ± 15.2 and 63.3 ± 10.4 nmol/mg of protein, respectively; the levels of activity were 72.0 ± 2.6 and 25 ± 5 nmol/mg of protein, respectively, under control conditions. PV-MITO-GFP expression reduced the level of TNF-α-dependent caspase-8 activity to 150 ± 20 nmol/mg of protein (296.7 ± 30.5 nmol/mg of protein in MITO-GFP cells), and it completely abolished caspase-3 activity (*P* < 0.001, *n* = 3; Fig. 3E,F). These data demonstrate that Ca²⁺_{mit} buffering also prevents apoptotic cell death through the extrinsic pathway.

Apoptosis can be modulated through the expression of antiapoptotic and proapoptotic genes,²⁴ so we investigated whether alterations of Ca²⁺_{mit} handling could

affect the expression of such genes. Real-time PCR showed that Ca²⁺_{mit} buffering reduced the expression of several proapoptotic genes under the baseline or STA treatment conditions (Fig. 4A-D). The expression of each gene was normalized to its expression level in unstimulated, nontransfected cells. The expression of *p53* was reduced to 0.72 ± 0.03 au in PV-MITO-GFP cells in comparison with the control (*P* < 0.001, *n* = 3). After the STA treatment, the expression of *p53* increased to 2.2 ± 0.1 au in untransfected cells, whereas in PV-MITO-GFP cells, it remained at 1.08 ± 0.06 au (*P* < 0.001, *n* = 3; Fig. 4A). The expression of *bax* was reduced to 0.41 ± 0.04 au in PV-MITO-GFP cells in comparison with the control (*P* < 0.001), and after the STA treatment, the level of *bax* expression was 2.0 ± 0.2 au in nontransfected cells and 0.72 ± 0.06 au in PV-MITO-GFP cells (*P* < 0.001, *n* = 3; Fig. 4B). Although apoptotic peptidase activating factor 1 (*apaf-1*) expression was not altered between unstimulated control and transfected cells, after the STA treatment, *apaf-1* expression increased to 1.69 ± 0.07 au in control cells and remained at 0.83 ± 0.10 au in PV-MITO-GFP cells (*P* < 0.001, *n* = 3; Fig. 4C). The baseline level of caspase-6 expression was reduced to 0.75 ± 0.036 au in PV-MITO-GFP cells in comparison with the control (*P* < 0.001), and it increased to 1.98 ± 0.09 au in nontransfected cells (0.97 ± 0.03 au in PV-MITO-GFP cells, *P* < 0.001, *n* = 3; Fig. 4D). Conversely, the expression of genes encoding antiapoptotic proteins was up-regulated after Ca²⁺_{mit} buffering (Fig. 4E-G). *Bcl-2* gene expression

F4

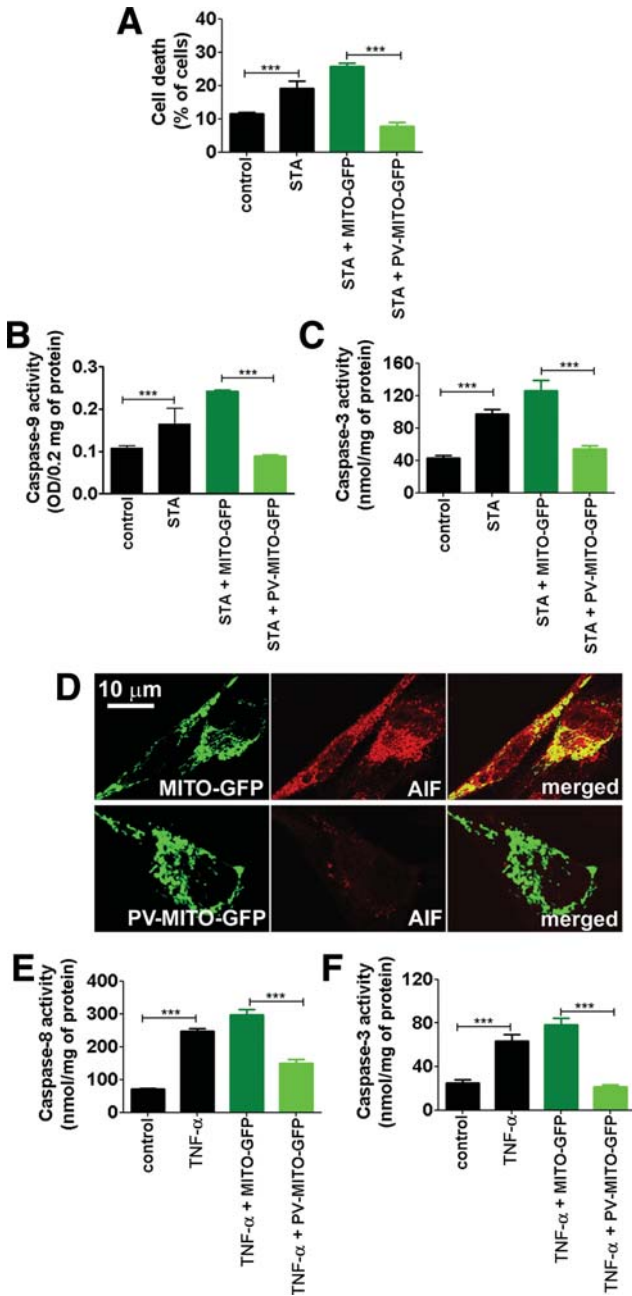


Fig. 3. Ca^{2+}_{mit} buffering reduces cell death. Control SKHep1 cells and cells transfected with MITO-GFP or PV-MITO-GFP were treated with 100 nM STA or 100 ng/mL TNF- α for 6 hours to activate intrinsic or extrinsic apoptotic pathways, respectively. (A) STA increased cell death in nontransfected SKHep1 cells ($P < 0.001$ versus controls), whereas cell death was reduced by Ca^{2+}_{mit} buffering ($P < 0.001$ versus MITO-GFP-transfected cells in the presence of STA, $n = 3$). (B,C) The expression of PV-MITO-GFP reduced the activation of the caspase-dependent intrinsic apoptotic pathway. Ca^{2+}_{mit} buffering reduced caspase-9 and caspase-3 activity ($P < 0.001$ versus MITO-GFP-transfected cells with STA, $n = 3$). (D) The expression of PV-MITO-GFP reduced the activation of the caspase-independent intrinsic pathway. Representative confocal images show SKHep1 cells transfected with MITO-GFP or PV-MITO-GFP (green) and stained with an antibody to AIF (red). Targeting PV against mitochondria reduced AIF expression. (E,F) The expression of PV-MITO-GFP inhibited apoptosis through the extrinsic pathway. The expression of PV-MITO-GFP decreased caspase-8 and caspase-3 activity ($P < 0.001$ versus MITO-GFP-transfected cells with TNF- α , $n = 3$).

increased to 1.21 ± 0.13 au in PV-MITO-GFP cells in comparison with the control ($P < 0.001$, $n = 3$) and remained higher upon STA treatment (1.19 ± 0.17 versus 0.63 ± 0.09 au in the control, $P < 0.001$, $n = 3$; Fig. 4E). Similarly, the expression of *mcl-1* and *bcl-xL* genes increased to 1.2 ± 0.06 and 1.41 ± 0.10 au, respectively, in PV-MITO-GFP cells and to 1.0 ± 0.05 and 1.0 ± 0.06 au, respectively, in the control ($P < 0.001$, $n = 3$). After the STA treatment, the expression levels of *mcl-1* and *bcl-xL* remained high (1.18 ± 0.06 and 1.26 ± 0.10 au, respectively) in PV-MITO-GFP cells (0.46 ± 0.02 and 0.73 ± 0.06 au in the control, $P < 0.001$, $n = 3$; Fig. 4F,G). To examine whether the expression of these genes was also altered at the protein level in SKHep1 cells expressing PV-MITO-GFP, we performed immunoblotting for the antiapoptotic protein Bcl-2 and the proapoptotic protein Bax (Fig. 4H-J). The expression of the Bcl-2 protein increased to 1.15 ± 0.09 au in cells expressing PV-MITO-GFP and to 0.56 ± 0.08 au in control cells ($P < 0.001$, $n = 3$), whereas the expression of the Bax protein decreased to 0.84 ± 0.09 au in cells expressing PV-MITO-GFP and to 1.14 ± 0.09 au in control cells ($P < 0.05$, $n = 3$). Similar results were observed in cells treated with STA. These findings suggest that Ca^{2+}_{mit} buffering directs the expression ratio of proapoptotic and antiapoptotic protein members toward a predominantly antiapoptotic pathway.

For the determination of whether the decrease in cell death observed in PV-MITO-GFP cells was associated with changes in proliferation, SKHep1 cells were synchronized in G_0 by serum withdrawal, transfected with the target constructs, and assayed for BrdU incorporation. No increase in cell proliferation was observed in PV-MITO-GFP cells in comparison with control cells or cells expressing MITO-GFP (supporting Fig. 1). However, with agonist-induced cell death, BrdU uptake was lower in cells expressing MITO-GFP versus cells expressing PV in the mitochondria ($51.1\% \pm 5.3\%$ for MITO-GFP versus $79.4\% \pm 3.6\%$ for PV-MITO-GFP, $P < 0.001$, $n = 3$). Together, these results suggest that Ca^{2+}_{mit} buffering preferentially prevents cells from undergoing apoptosis instead of stimulating proliferation.

Ca²⁺_{mit} Buffering Accelerates Liver Mass Restoration After PH. Liver regeneration requires both increased cell proliferation and reduced apoptosis.²⁵ The role of Ca^{2+}_{mit} signaling in apoptosis is well known, but its role in liver regeneration has not been studied. Therefore, we investigated the involvement of Ca^{2+}_{mit} in liver growth after two-thirds hepatectomy (i.e., PH). Adenoviruses encoding PV-MITO-GFP were injected

COLOR

AQ4

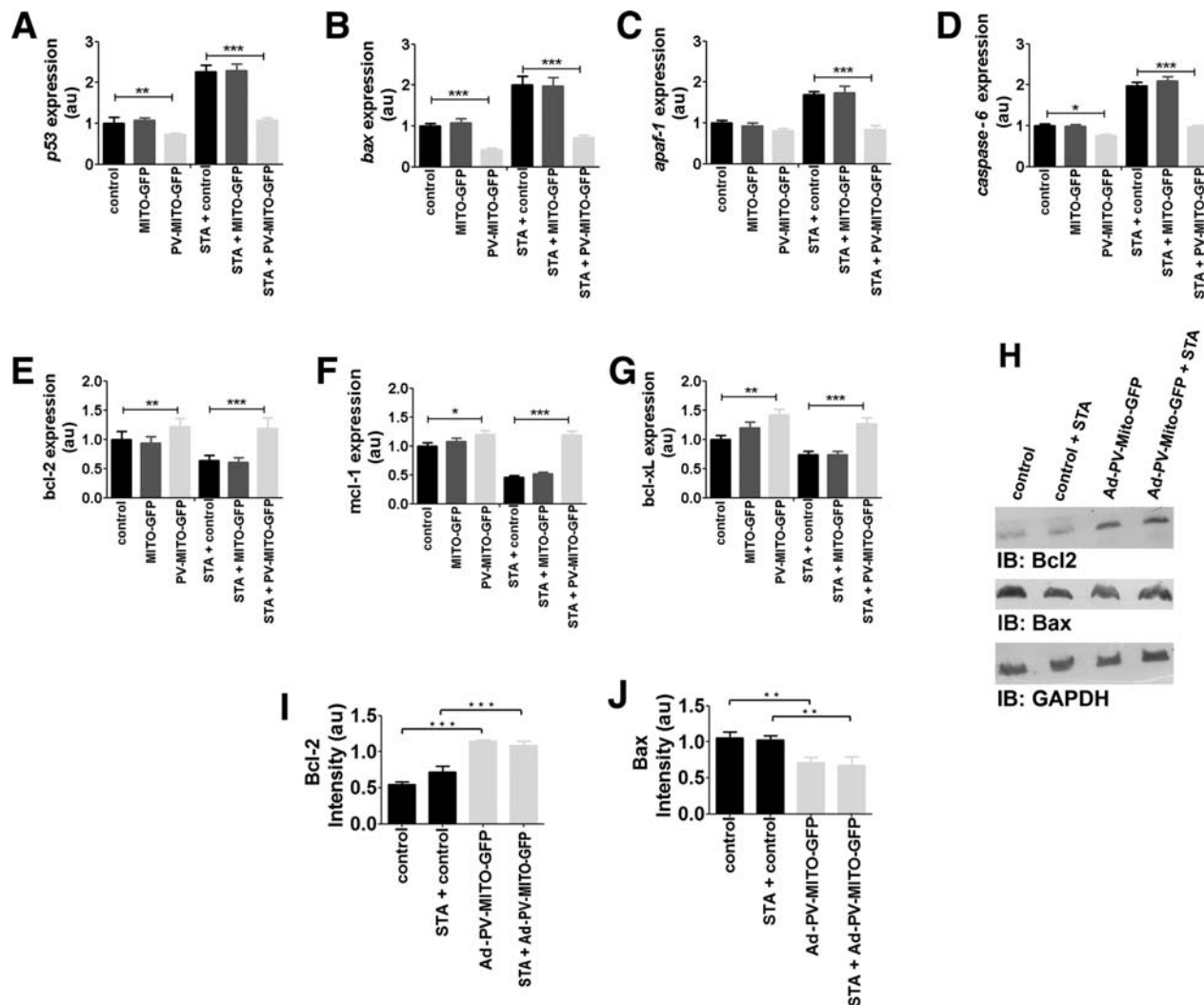


Fig. 4. Ca^{2+}_{mit} buffering alters the expression levels of proapoptotic and antiapoptotic genes. Control SKHep1 cells and cells transfected with either MITO-GFP or PV-MITO-GFP were incubated in the presence or absence of 300 nM STA for 6 hours. (A-D) After the STA treatment, Ca^{2+}_{mit} buffering down-regulated the expression levels of *p53*, *bax*, *apaf-1*, and *caspase-6* ($P < 0.001$ versus control cells treated with STA). (E-G) After the STA treatment, Ca^{2+}_{mit} buffering up-regulated the expression of *bcl-2*, *mcl-1*, and *bcl-xL* ($P < 0.001$ versus controls). (H) IB demonstrates that Ca^{2+}_{mit} buffering increased the expression of Bcl-2 and decreased the expression of Bax. (I,J) A densitometric analysis shows that the expression of Bcl-2 was increased and the expression of Bax was reduced with respect to controls ($P < 0.001$, $n = 3$). Abbreviations: GAPDH, glyceraldehyde 3-phosphate dehydrogenase; IB, immunoblotting.

into rats, and GFP fluorescence was used to monitor PV expression in the liver (Fig. 5A). PV was expressed throughout the liver lobule (Supporting Fig. 2). No fluorescence was observed in the livers of animals injected with a saline solution. Additionally, no GFP fluorescence was observed in the intestines of animals injected with Ad-PV-MITO-GFP (Supporting Fig. 3), and this demonstrated the preferential targeting of the vector to the liver. Confocal images of liver slices showed that PV was highly expressed in the mitochondria of hepatocytes (Fig. 5B). Moreover, immunoblotting confirmed PV expression in the liver after the adenovirus injection, whereas PV was not expressed in a control liver (Fig. 5C). Together, these data show that

the injected adenoviruses efficiently delivered the Ca^{2+} -buffering construct to hepatocytes *in vivo* and promoted the expression of PV in this cell type.

To investigate the role of Ca^{2+}_{mit} in liver regeneration, we performed PH 1 day after the Ad-PV-MITO-GFP injection, and liver regeneration was analyzed for 1 to 4 days after PH. The expression of PV-MITO-GFP significantly increased the liver area in comparison with the controls, mainly 24 to 48 hours after PH (Fig. 6). There was no difference in the liver area from day 1 to day 4 in sham-operated animals. However, 1 day after PH, the liver area was significantly smaller in PH rats versus animals injected with the adenovirus ($198.1\% \pm 1.06\%$ in the PH animals versus 257.2%

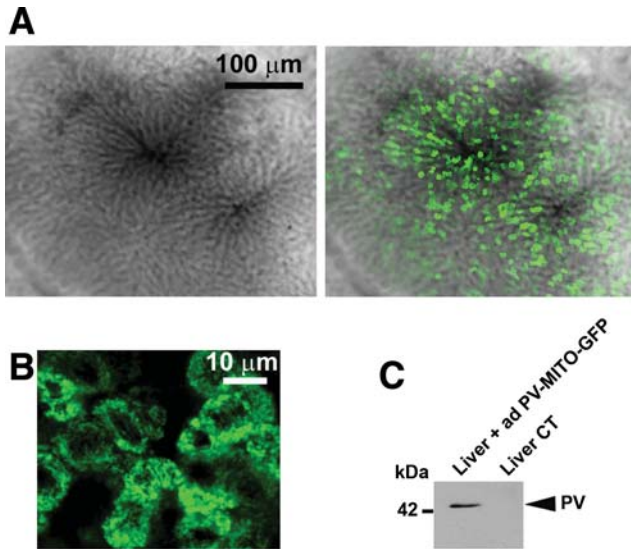


Fig. 5. Targeting PV expression in the rat liver. (A) Representative intravital confocal images of the hepatic lobule of a rat infected with Ad-PV-MITO-GFP show the expression of PV (green) in the liver 2 days after the adenovirus injection. (B) A representative confocal image of liver slices indicates the expression of PV (green) in hepatocytes. (C) A western blot analysis shows PV expression in the liver 2 days after the adenovirus infection. The tail vein injection of the adenovirus into rats led to the expression of PV in the liver. Abbreviation: CT, control.

± 3.4% in the PH/Ad-PV-MITO-GFP animals, $P < 0.05$, $n = 3$). The difference in the liver area was even more pronounced 2 days after PH ($208.2\% \pm 6.2\%$ in the PH animals versus $340.1\% \pm 1.8\%$ in the PH/Ad-PV-MITO-GFP animals, $P < 0.001$, $n = 3$). The PCNA labeling of liver slices similarly demonstrated that hepatocyte proliferation was accelerated by the buffering of Ca_{mit}^{2+} . The PCNA index peaked on day 1 in the PH/parvalbumin-mitochondrial targeting sequence adenovirus (Ad-PV-MITO) animals ($61.2\% \pm 2.2\%$, $n = 3$); the PH animals showed the maximum PCNA index on day 2 ($63.6\% \pm 4.0\%$, $n = 3$). These results indicate that Ca_{mit}^{2+} buffering accelerates liver regeneration after PH. This finding was further validated through measurements of the liver/body mass index after PH; this also demonstrated that liver regeneration occurred with accelerated kinetics in animals expressing PV in the mitochondria (Fig. 7A). One day after PH, the liver/body weight index was significantly smaller in PH rats versus PH animals injected with the adenovirus ($54.8\% \pm 4.3\%$ in the PH animals versus $63.2\% \pm 12.6\%$ in the PH/Ad-PV-MITO-GFP animals, $P < 0.01$, $n = 6$). Two days after PH, the liver/body weight index was $72.3\% \pm 6.9\%$ in the PH animals and $89.4\% \pm 8.8\%$ in the PH/Ad-PV-MITO-GFP animals ($P < 0.01$, $n = 6$). The accelerated

regeneration observed in the adenovirus-treated animals was not due to increased inflammation, as demonstrated by the measurement of the MPO activity and the histological examination of the livers from PH

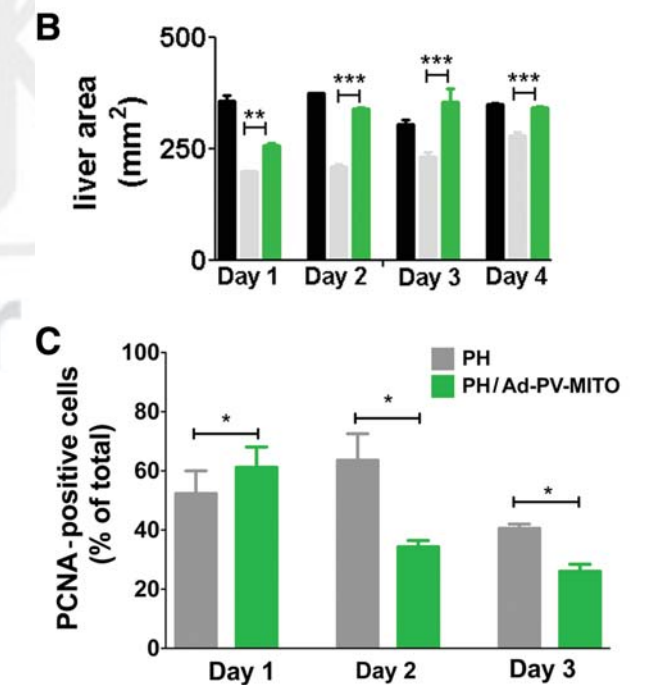
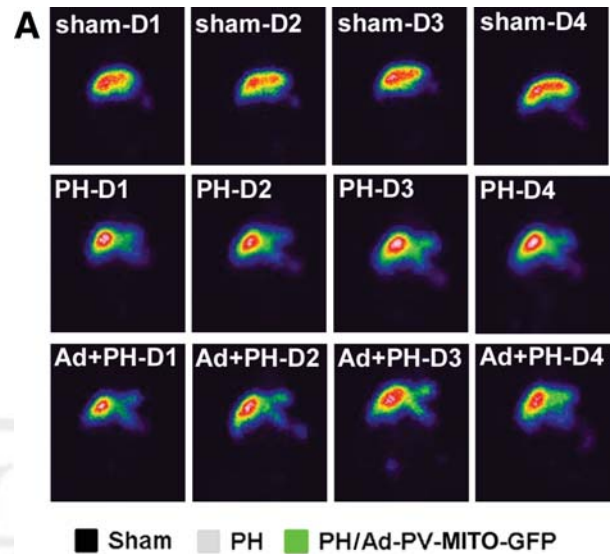


Fig. 6. Scintigraphic imaging of the liver area. (A) Representative scintigraphic images of sham-operated, control, and Ad-PV-MITO-GFP rats 1 to 4 days after PH. The liver area (mm^2) was determined by the amount of radioactivity uptake in the organ. (B) Quantification of the liver area demonstrated that Ca_{mit}^{2+} buffering accelerated liver growth after PH. (C) Proliferation was evaluated by PCNA staining of liver slices from PH and PH/Ad-PV-MITO rats. The PCNA index was increased 1 day after hepatectomy in the Ad-treated group versus the PH animals ($P < 0.05$) and reached its peak on day 2. On days 2 and 3, the PCNA index was significantly reduced in the group in which Ca_{mit}^{2+} was buffered in mitochondria ($P < 0.001$). Abbreviations: Ad, adenovirus; D, day.

COLOR

COLOR

AQ9

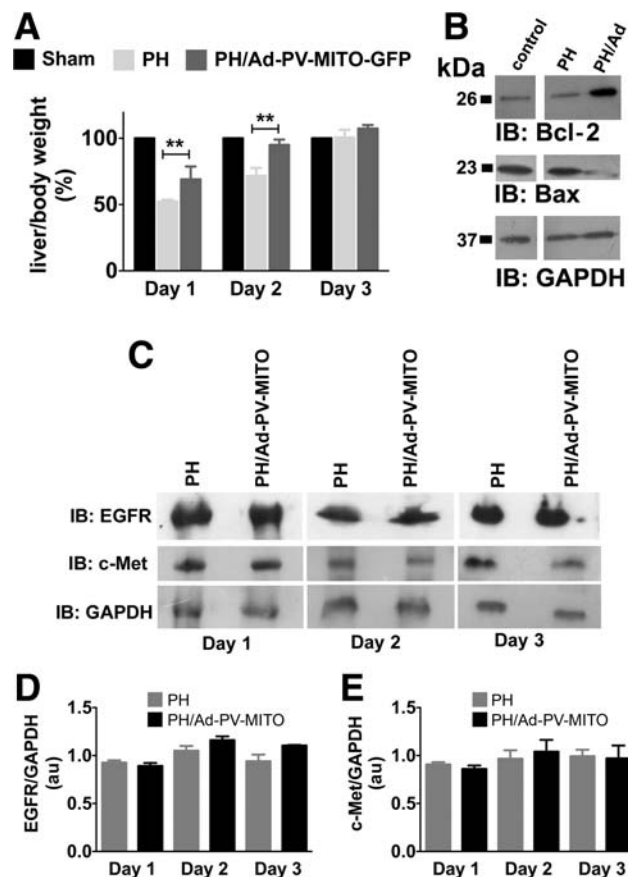


Fig. 7. The rate of liver regeneration is accelerated by the expression of PV-MITO-GFP. (A) Analysis of the liver/body weight index at the indicated times for sham-operated rats, PH rats, and rats infected with Ad-PV-MITO-GFP. Ca_{mit}^{2+} buffering increased the rate of liver regeneration by $16.7\% \pm 12.6\%$ 1 day after PH and by $23.5\% \pm 8.8\%$ 2 days after PH in comparison with PH alone, and the rate reached control levels 3 days after PH ($n = 6$ animals per condition). (B) Bcl-2 and Bax protein expression 2 days after PH demonstrated that Ca_{mit}^{2+} buffering increased the expression of Bcl-2 and decreased the expression of Bax ($n = 3$). (C) Representative western blots of EGFR and c-Met 1, 2, and 3 days after PH. GAPDH was used as a loading control. (D,E) A densitometric analysis of EGFR and c-Met shows no significant differences in the expression of these two receptors between PH livers and PH/Ad-PV-MITO livers during the course of liver regeneration. Abbreviations: Ad, adenovirus; GAPDH, glyceraldehyde 3-phosphate dehydrogenase; IB, immunoblotting.

AQ9

and PH/Ad-PV-MITO-GFP animals (Supporting Fig. 4). Liver weights returned to preoperative levels 3 days after PH. The liver histology and chemistry findings were similar in the control and PV-expressing animals 7 days after PH (Supporting Figs. 5 and 6). These data indicate that Ca_{mit}^{2+} homeostasis is important during liver regeneration.

To examine the mechanism by which Ca_{mit}^{2+} buffering accelerates liver regeneration, we investigated whether the expression of the antiapoptotic protein Bcl-2 and the expression of the proapoptotic protein Bax were altered in the livers of adenovirus-injected rats, as

observed in SKHep1 cells. Ca_{mit}^{2+} buffering increased the expression of Bcl-2 and reduced the expression of Bax (Fig. 7B). Because growth factor signaling might affect the expression of apoptotic proteins during liver regeneration,⁴ the expression of receptors for two essential liver mitogens, EGFR and c-Met, was assessed. They showed similar levels in PH and PH/Ad-PV-MITO-GFP animals during the 3 days after PH (Fig. 7C-E). Together, these results suggest that Ca_{mit}^{2+} buffering promotes liver regeneration by inhibiting apoptosis.

Discussion

Liver regeneration involves multiple factors and pathways¹ that result in increased proliferation and decreased apoptosis of hepatocytes.²⁵ Among the regulatory signaling pathways, a number of Ca^{2+} -mobilizing agonists are known to contribute to liver regeneration.^{6,26,27} Hepatocytes respond to such agonists by altering intracellular Ca^{2+} signaling, which propagates throughout the liver as intercellular Ca^{2+} waves^{28,29} that regulate several processes, including liver regeneration.⁶ Alterations in the Ca^{2+} signaling machinery have been reported to occur during liver regeneration,³⁰ and although recent studies have examined the role of nuclear and cytosolic Ca^{2+} signals in cell proliferation,^{9,31,32} the impact of Ca_{mit}^{2+} on liver regeneration has not been directly investigated. Here we have examined the role of Ca_{mit}^{2+} during liver regeneration after PH, and we have found that Ca_{mit}^{2+} buffering, at least in part by inhibiting apoptosis, accelerates regeneration.

Mitochondria play an integral role in Ca^{2+} signaling and have a key function in most forms of apoptosis.³³ Our results demonstrate that Ca_{mit}^{2+} buffering inhibits the intrinsic and extrinsic apoptotic pathways as well as the mitochondrial amplification loop; this was observed by the inhibition of caspase-8, caspase-9, and caspase-3 activation. This amplification is dependent on the release of cytochrome c from the mitochondrial matrix to the cytosol; there, it can further activate the effector caspases. Although we have not assessed the release of cytochrome C, we have found that Ca_{mit}^{2+} buffering inhibits the activation of caspase-9 by STA; this phenomenon is dependent on cytochrome C release from mitochondria.³⁴ We have also found that Ca_{mit}^{2+} buffering inhibits caspase-independent but AIF-dependent cell death. This is consistent with previous observations showing that the dysregulation of Ca^{2+} homeostasis is a prerequisite for AIF-mediated apoptosis.³⁵

Bcl-2 was the first gene identified as a regulator of apoptosis,³⁶ and subsequently, several *bcl-2* homologues were discovered that act as either proapoptotic

or antiapoptotic effectors. The present data are in agreement with previous observations demonstrating that the overexpression of *bcl-2*, *mcl-1*, and *bcl-xL*^{37,38} prevents cells from undergoing apoptosis, whereas *bax*, *apaf-1*, caspase-6, and *p53* function to promote cell death.³⁹ $\text{Ca}_{\text{mit}}^{2+}$ buffering also shifted the Bax/Bcl-2 ratio toward the antiapoptotic profile, and this resulted in the accelerated restoration of liver mass after PH. This agrees with recent proteomic data showing that apoptosis pathways are inhibited during liver regeneration.⁴⁰ Additionally, hepatocyte growth factor, an essential stimulus for liver regeneration, is known to have antiapoptotic activity in injured tissue.⁴¹ Similarly, TNF, another initiator of liver regeneration, also modulates apoptosis in addition to stimulating hepatocyte proliferation.⁴² Although our results suggest that $\text{Ca}_{\text{mit}}^{2+}$ buffering accelerates liver regeneration by inhibiting apoptosis, an effect on cell proliferation cannot be entirely excluded because Bax/Bcl-2 family proteins regulate liver regeneration independently of their role in modulating apoptosis in the liver.^{43,44} Moreover, $\text{Ca}_{\text{mit}}^{2+}$ buffering might also accelerate liver regeneration by modulating ATP production in the mitochondrial matrix because the activity of enzymes of the tricarboxylic acid cycle is regulated by Ca^{2+} .¹³

Heterologous expression of the Ca^{2+} binding protein PV has been widely used to study the role of Ca^{2+} signaling in the regulation of the cell cycle. PV was targeted to the nucleus or cytoplasm, and with this approach, the role of nuclear Ca^{2+} in regulating the cell cycle was established in a liver cell line.⁹ More recently, PV expression in the cytosol of hepatocytes *in vivo* demonstrated that cytosolic Ca^{2+} affects progression through the cell cycle after PH.³² Using PV targeted to the mitochondria, we have now shown that $\text{Ca}_{\text{mit}}^{2+}$ also regulates liver regeneration. Future advances in this field should lead to a better understanding of the ways in which these various Ca^{2+} compartments act in an integrated manner to regulate liver regeneration.

Acknowledgments: The authors thank Gilson Nogueira for his technical support and Soraya Smali for antibodies against Bax and Bcl-2 and useful discussions. Confocal imaging was supported by CEMEL (Federal University of Minas Gerais, Belo Horizonte, Minas Gerais, Brazil).

References

1. Fausto N, Campbell JS, Riehle KJ. Liver regeneration. *HEPATOLOGY* 2006;43:S45-S53.
2. Cressman DE, Greenbaum LE, DeAngelis RA, Ciliberto G, Furth EE, Poli V, et al. Liver failure and defective hepatocyte regeneration in interleukin-6-deficient mice. *Science* 1996;274:1379-1383.
3. Yamada Y, Kirillova I, Peschon JJ, Fausto N. Initiation of liver growth by tumor necrosis factor: deficient liver regeneration in mice lacking type I tumor necrosis factor receptor. *Proc Natl Acad Sci U S A* 1997;94:1441-1446.
4. Paranjpe S, Bowen WC, Bell AW, Nejak-Bowen K, Luo JH, Michalopoulos GK. Cell cycle effects resulting from inhibition of hepatocyte growth factor and its receptor c-Met in regenerating rat livers by RNA interference. *HEPATOLOGY* 2007;45:1471-1477.
5. Baffy G, Yang L, Michalopoulos GK, Williamson JR. Hepatocyte growth factor induces calcium mobilization and inositol phosphate production in rat hepatocytes. *J Cell Physiol* 1992;153:332-339.
6. Nicou A, Serriere V, Prigent S, Boucherie S, Combettes L, Guillon G, et al. Hypothalamic vasopressin release and hepatocyte Ca^{2+} signaling during liver regeneration: an interplay stimulating liver growth and bile flow. *FASEB J* 2003;17:1901-1903.
7. Tanaka Y, Hayashi N, Kaneko A, Ito T, Miyoshi E, Sasaki Y, et al. Epidermal growth factor induces dose-dependent calcium oscillations in single fura-2-loaded hepatocytes. *HEPATOLOGY* 1992;16:479-486.
8. Cruz LN, Guerra MT, Kruglov E, Mennone A, Garcia CR, Chen J, et al. Regulation of multidrug resistance-associated protein 2 by calcium signaling in mouse liver. *HEPATOLOGY* 2010;52:327-337.
9. Rodrigues MA, Gomes DA, Leite MF, Grant W, Zhang L, Lam W, et al. Nuclear calcium is required for cell proliferation. *J Biol Chem* 2007;282:17061-17068.
10. Leite MF, Thrower EC, Echevarria W, Koulen P, Hirata K, Bennett AM, et al. Nuclear and cytosolic calcium are regulated independently. *Proc Natl Acad Sci U S A* 2003;100:2975-2980.
11. de Brito OM, Scorrano L. Mitofusin 2 tethers endoplasmic reticulum to mitochondria. *Nature* 2008;456:605-610.
12. Csordas G, Varnai P, Golenar T, Roy S, Purkins G, Schneider TG, et al. Imaging interorganelle contacts and local calcium dynamics at the ER-mitochondrial interface. *Mol Cell* 2010;39:121-132.
13. Jouaville LS, Pinton P, Bastianutto C, Rutter GA, Rizzuto R. Regulation of mitochondrial ATP synthesis by calcium: evidence for a long-term metabolic priming. *Proc Natl Acad Sci U S A* 1999;96:13807-13812.
14. Mendes CC, Gomes DA, Thompson M, Souto NC, Goes TS, Goes AM, et al. The type III inositol 1,4,5-trisphosphate receptor preferentially transmits apoptotic Ca^{2+} signals into mitochondria. *J Biol Chem* 2005;280:40892-40900.
15. Rong Y, Distelhorst CW. Bcl-2 protein family members: versatile regulators of calcium signaling in cell survival and apoptosis. *Annu Rev Physiol* 2008;70:73-91.
16. Hanson CJ, Bootman MD, Distelhorst CW, Wojcikiewicz RJ, Roderick HL. Bcl-2 suppresses Ca^{2+} release through inositol 1,4,5-trisphosphate receptors and inhibits Ca^{2+} uptake by mitochondria without affecting ER calcium store content. *Cell Calcium* 2008;44:324-338.
17. White C, Li C, Yang J, Petrenko NB, Madesh M, Thompson CB, et al. The endoplasmic reticulum gateway to apoptosis by Bcl-X(L) modulation of the $\text{InoP}3\text{R}$. *Nat Cell Biol* 2005;7:1021-1028.
18. Minagawa N, Kruglov EA, Dranoff JA, Robert ME, Gores GJ, Nathanson MH. The anti-apoptotic protein Mcl-1 inhibits mitochondrial Ca^{2+} signals. *J Biol Chem* 2005;280:33637-33644.
19. Aguiar CJ, Andrade VL, Gomes ER, Alves MN, Ladeira MS, Pinheiro AC, et al. Succinate modulates Ca^{2+} transient and cardiomyocyte viability through PKA-dependent pathway. *Cell Calcium* 2010;47:37-46.
20. McDonald B, Pittman K, Menezes GB, Hirota SA, Slaba I, Waterhouse CC, et al. Intravascular danger signals guide neutrophils to sites of sterile inflammation. *Science* 2010;330:362-366.
21. Higgins G, Anderson R. Experimental pathology of the liver. I. Restoration of the liver of the white rat following partial surgical removal. *Arch Pathol* 1931;12:186-202.
22. Soares AC, Pinho VS, Souza DG, Shimizu T, Ishii S, Nicolli JR, et al. Role of the platelet-activating factor (PAF) receptor during pulmonary infection with gram negative bacteria. *Br J Pharmacol* 2002;137:621-628.
23. Joseph SK, Hajnoczky G. IP3 receptors in cell survival and apoptosis: Ca^{2+} release and beyond. *Apoptosis* 2007;12:951-968.

AQ8

24. Youle RJ, Strasser A. The BCL-2 protein family: opposing activities that mediate cell death. *Nat Rev Mol Cell Biol* 2008;9:47-59.
25. Michalopoulos GK, DeFrances MC. Liver regeneration. *Science* 1997; 276:60-66.
26. Cruise JL, Muga SJ, Lee YS, Michalopoulos GK. Regulation of hepatocyte growth: alpha-1 adrenergic receptor and ras p21 changes in liver regeneration. *J Cell Physiol* 1989;140:195-201.
27. Thevananther S, Sun H, Li D, Arjunan V, Awad SS, Wyllie S, et al. Extracellular ATP activates c-jun N-terminal kinase signaling and cell cycle progression in hepatocytes. *HEPATOLOGY* 2004;39:393-402.
28. Hirata K, Puls T, O'Neill AF, Dranoff JA, Nathanson MH. The type II inositol 1,4,5-trisphosphate receptor can trigger Ca²⁺ waves in rat hepatocytes. *Gastroenterology* 2002;122:1088-1100.
29. Thomas AP, Renard-Rooney DC, Hajnoczky G, Robb-Gaspers LD, Lin C, Rooney TA. Subcellular organization of calcium signalling in hepatocytes and the intact liver. *Ciba Found Symp* 1995;188: 18-35.
30. Nicou A, Serriere V, Hilly M, Prigent S, Combettes L, Guillon G, et al. Remodelling of calcium signalling during liver regeneration in the rat. *J Hepatol* 2007;46:247-256.
31. Soliman EM, Rodrigues MA, Gomes DA, Sheung N, Yu J, Amaya MJ, et al. Intracellular calcium signals regulate growth of hepatic stellate cells via specific effects on cell cycle progression. *Cell Calcium* 2009; 45:284-292.
32. Lagoudakis L, Garcin I, Julien B, Nahum K, Gomes DA, Combettes L, et al. Cytosolic calcium regulates liver regeneration in the rat. *HEPATOLOGY* 2010;52:602-611.
33. Pinton P, Giorgi C, Siviero R, Zecchini E, Rizzuto R. Calcium and apoptosis: ER-mitochondria Ca²⁺ transfer in the control of apoptosis. *Oncogene* 2008;27:6407-6418.
34. Li P, Nijhawan D, Budihardjo I, Srinivasula SM, Ahmad M, Alnemri ES, et al. Cytochrome c and dATP-dependent formation of Apaf-1/caspase-9 complex initiates an apoptotic protease cascade. *Cell* 1997;91: 479-489.
35. Norberg E, Gogvadze V, Ott M, Horn M, Uhlen P, Orrenius S, et al. An increase in intracellular Ca²⁺ is required for the activation of mitochondrial calpain to release AIF during cell death. *Cell Death Differ* 2008;15:1857-1864.
36. Reed JC. Bcl-2 and the regulation of programmed cell death. *J Cell Biol* 1994;124:1-6.
37. Boise LH, Gonzalez-Garcia M, Postema CE, Ding L, Lindsten T, Turka LA, et al. bcl-x, a bcl-2-related gene that functions as a dominant regulator of apoptotic cell death. *Cell* 1993;74:597-608.
38. Kozopas KM, Yang T, Buchan HL, Zhou P, Craig RW. MCL1, a gene expressed in programmed myeloid cell differentiation, has sequence similarity to BCL2. *Proc Natl Acad Sci U S A* 1993;90:3516-3520.
39. Degterev A, Yuan J. Expansion and evolution of cell death programmes. *Nat Rev Mol Cell Biol* 2008;9:378-390.
40. Deng X, Li W, Chen N, Sun Y, Wei H, Jiang Y, et al. Exploring the priming mechanism of liver regeneration: proteins and protein complexes. *Proteomics* 2009;9:2202-2216.
41. Miyazawa K. Hepatocyte growth factor activator (HGFA): a serine protease that links tissue injury to activation of hepatocyte growth factor. *FEBS J* 2010;277:2208-2214.
42. Cosgrove BD, Cheng C, Pritchard JR, Stolz DB, Lauffenburger DA, Griffith LG. An inducible autocrine cascade regulates rat hepatocyte proliferation and apoptosis responses to tumor necrosis factor-alpha. *HEPATOLOGY* 2008;48:276-288.
43. Bailly-Maitre B, Bard-Chapeau E, Luciano F, Droin N, Bruey JM, Faustin B, et al. Mice lacking bi-1 gene show accelerated liver regeneration. *Cancer Res* 2007;67:1442-1450.
44. Vail ME, Chaisson ML, Thompson J, Fausto N. Bcl-2 expression delays hepatocyte cell cycle progression during liver regeneration. *Oncogene* 2002;21:1548-1555.

Author Proof

Insulin Induces Calcium Signals in the Nucleus of Rat Hepatocytes

Michele A. Rodrigues,^{1,2} Dawidson A. Gomes,^{1,2} Viviane A. Andrade,³ M. Fatima Leite,² and Michael H. Nathanson¹

Insulin is an hepatic mitogen that promotes liver regeneration. Actions of insulin are mediated by the insulin receptor, which is a receptor tyrosine kinase. It is currently thought that signaling via the insulin receptor occurs at the plasma membrane, where it binds to insulin. Here we report that insulin induces calcium oscillations in isolated rat hepatocytes, and that these calcium signals depend upon activation of phospholipase C and the inositol 1,4,5-trisphosphate receptor, but not upon extracellular calcium. Furthermore, insulin-induced calcium signals occur in the nucleus, and are temporally associated with selective depletion of nuclear phosphatidylinositol bisphosphate and translocation of the insulin receptor to the nucleus. These findings suggest that the insulin receptor translocates to the nucleus to initiate nuclear, inositol 1,4,5-trisphosphate-mediated calcium signals in rat hepatocytes. This novel signaling mechanism may be responsible for insulin's effects on liver growth and regeneration. (HEPATOLOGY 2008;48:1621-1631.)

See Editorial on Page 1383

Insulin regulates a wide variety of biological functions in the liver, including glucose uptake,¹ regulation of gene expression,² and promotion of cell growth.³⁻⁵ The biological actions of insulin are initiated by binding to the insulin receptor, a heterotetrameric receptor tyrosine kinase (RTK) composed of two extracellular α -subunits and two transmembrane β -subunits.⁶ The α -subunit possesses insulin-binding activity whereas the β -subunit has intrinsic protein tyrosine kinase activity. Binding of insulin to the α -subunit of its receptor activates the protein tyrosine kinase and results in phosphorylation of tyrosine residues of the β -subunit and of several

endogenous substrates. These substrates include proteins containing a *src*-homology 2 domain such as phosphatidylinositol 3-kinase and phospholipase C (PLC).⁷ PLC hydrolyzes phosphatidylinositol 4,5-bisphosphate (PIP₂), generating two intracellular products: inositol 1,4,5-trisphosphate (InsP₃), a universal calcium-mobilizing second messenger, and diacylglycerol, an activator of protein kinase C. Like insulin, Ca²⁺ also regulates glucose metabolism,⁸ gene expression,^{9,10} and cell growth.^{11,12} Although it has not been established how a single second messenger coordinates such diverse effects within a cell, there is increasing evidence that the spatial and temporal patterns of Ca²⁺ signals may determine their specificity. Ca²⁺ signaling patterns can vary in different regions of the cell, and increases in Ca²⁺ in the nucleus have specific biological effects that differ from the effects of increases in cytosolic Ca²⁺.^{9,10,13-15} The mechanisms and pathways that promote localized increases in free Ca²⁺ levels in the nucleus have not been entirely defined. It is currently thought that signaling via the insulin receptor occurs only at the plasma membrane, where it binds to insulin.¹⁶ Here we investigate whether and how insulin signaling occurs in the nucleus of hepatocytes, where its downstream messenger Ca²⁺ may act.

Abbreviations: c-met; hepatocyte growth factor receptor; Gab1, CRB2-associated binding protein 1; EGF, epidermal growth factor; FGF, fibroblast growth factor; InsP₃, inositol 1,4,5-trisphosphate; KCl, potassium chloride; MKK1, mitogen-activated protein kinase kinase 1; mRFP, monomeric red fluorescent protein; PIP₂, phosphatidylinositol 4,5-bisphosphate; PLC, phospholipase C; RTK, receptor tyrosine kinase.

From the¹Department of Internal Medicine, Yale University School of Medicine, New Haven, CT; ²Department of Physiology and Biophysics and ³Department of Biochemistry and Immunology, Federal University of Minas Gerais, Belo Horizonte, Brazil.

Received December 4, 2007; accepted May 11, 2008.

Supported by National Institutes of Health (NIH) grants DK57751, DK34989, and DK45710, and by grants from the Conselho Nacional de Desenvolvimento Científico e Tecnológico, Fundação de Amparo à Pesquisa do Estado de Minas Gerais, and the Howard Hughes Medical Institute.

Address reprint requests to: Michael H. Nathanson, Digestive Diseases Section, Room TAC S241D, Yale University School of Medicine, New Haven, CT 06520-8019. E-mail: michael.nathanson@yale.edu; fax: 203-785-4306.

Copyright © 2008 by the American Association for the Study of Liver Diseases.

Published online in Wiley InterScience (www.interscience.wiley.com).

DOI 10.1002/hep.22424

Potential conflict of interest: Nothing to report.

Materials and Methods

Cells and Cell Culture. Hepatocytes were isolated from the livers of male Sprague-Dawley rats (190-200 g; Charles River Laboratories, Wilmington, MA) by collagenase perfusion as described.¹⁷ Primary hepatocytes were cultured at 37°C in 5% CO₂/95% O₂ in Williams' medium E containing 10% fetal bovine serum, 50 units/mL

penicillin, and 50 g/mL streptomycin (Invitrogen, Carlsbad, CA) and plated on collagen-coated coverslips (50 μ g/mL) (BD Biosciences, San Jose, CA). Hepatocytes were used 4–6 hours after isolation. Viability of the hepatocytes was greater than 85% and was measured by trypan blue exclusion.^{18,19} SkHep1 cells, a human liver cancer cell line, were cultured at 37°C in 5% CO₂ in Dulbecco's modified Eagle's medium (Invitrogen) containing 10% fetal bovine serum, 1 mM sodium pyruvate, 50 units/mL penicillin, and 50 g/mL streptomycin (Invitrogen).

Detection of Ca²⁺ Signals. Nuclear and cytosolic Ca²⁺ were monitored in individual cells by time-lapse confocal microscopy, as described.^{14,20} For Ca²⁺ imaging, cells were incubated with fluo-4/AM (6 μ M) (Invitrogen) for 30 minutes at 37°C, then coverslips containing the cells were transferred to a custom-built perfusion chamber on the stage of a Zeiss LSM 510 confocal microscope (Thornwood, NY) and the perfusion chamber was maintained at 37°C. The cells were stimulated with insulin (1–500 nM) or vasopressin (10 nM) (Sigma, Saint Louis, MO). In selected experiments cells were perfused for 10 minutes with the PLC inhibitor U-73122 (1 μ M) or pretreated for 30 minutes with the InsP3 receptor inhibitor xestospongin C (2.5 μ M) (Sigma). Fluo-4 fluorescence was monitored using a 40 \times , 1.2 NA objective lens, and images were collected at a rate of 1–5 frames/second. Changes in fluorescence F were normalized by the initial fluorescence (F_0) and were expressed as $(F/F_0) \times 100\%$.¹¹

InsP3 Buffer Constructs. The InsP3 binding domain (residues 224–605) of the human type I InsP3 receptor was tagged with monomeric red fluorescent protein (mRFP) and then the nuclear localization signal was subcloned to generate the nuclear InsP3 buffer expression vector. The nuclear exclusion signal sequence derived from mitogen-activated protein kinase kinase 1 was subcloned in the InsP3 binding domain tagged with the mRFP construct to generate the cytoplasmic InsP3 buffer expression vector, as described.²¹

Immunoblotting. Primary hepatocyte immunoblots were performed as described.²² Briefly, cells were washed twice with ice-cold phosphate-buffered saline, harvested by scraping, and lysed in a lysis buffer (20 mM [4-(2-hydroxyethyl)-1-piperazine ethanesulfonic acid], pH 7.0, 10 mM KCl, 2 mM MgCl₂, 0.5% Nonidet P-40). After incubation on ice for 10 minutes, the cells were homogenized by vortex. The homogenate was centrifuged at 1,500g for 5 minutes to sediment the nuclei. The supernatant was then centrifuged at a maximum speed of 16,100g for 20 minutes, and the resulting supernatant formed the non-nuclear fraction. The nuclear pellet was washed three times with lysis buffer to remove any contamination from cytoplasmic membranes, and the purity of the nuclei was confirmed by light micros-

copy. To extract nuclear proteins, the isolated nuclei were resuspended in NETN buffer (150 mM NaCl, 1 mM EDTA, 20 mM Tris-HCl, pH 8.0, 0.5% Nonidet P-40), and the mixture was sonicated briefly to aid nuclear lysis. Nuclear lysates were collected after centrifugation at 16,100g for 20 minutes at 4°C. Protease and phosphatase inhibitors (Sigma) were added to all buffers. Blots were visualized by enhanced chemiluminescence, and quantitatively analyzed using a GS-700 imaging densitometer. The purity of nuclear and non-nuclear fractions was confirmed using Lamin B1 (Abcam, Cambridge, MA) as a nuclear marker and α -Tubulin (Sigma) as a non-nuclear (cytosolic) marker.²³ The phosphorylated form of the insulin receptor was detected by immunoprecipitation of the receptor, followed by blotting with a monoclonal antibody directed against phosphotyrosine residues (Millipore, Billerica, MA).

Detection of PIP₂. A PI(4,5)P₂ Mass Strip Kit (Echelon, Salt Lake City, UT) was used for isolation and PIP₂ detection. Isolated hepatocytes were starved in serum-free William's E medium for 3 hours. Cells were incubated without or with insulin (10 nM) for 10 minutes or vasopressin (10 nM) for 1 minute, and then the medium was aspirated and cellular material precipitated by the immediate addition of 3 mL ice-cold 0.5 M trichloroacetic acid. The lysis buffer was used to prepare the nuclear and non-nuclear cell fractions, as described above.²² Briefly, cell membranes were disrupted to release cytoplasmic contents. Intact nuclei were recovered from the cytoplasmic extract by centrifugation, and then the nuclei were washed with phosphate-buffered saline and precipitated with 3 mL ice-cold 0.5 M trichloroacetic acid. Isolation of lipids was performed according to manufacturer instructions and as described.²⁴ The organic phase was collected into a clean tube and dried in a Speed Vac centrifuge. The pellet at this stage was faintly visible. The lipids were then resuspended by sonication in a cold water bath in 10 μ L of CHCl₃:methanol:H₂O (1:2:0.8), and spotted onto nitrocellulose membrane strips prespotted with PI(4,5)P₂ standards, PIP controls, and space for spotting unknown samples for probing with anti-PIP₂ monoclonal antibody (Echelon) to specifically detect PIP₂. Blots were visualized by enhanced chemiluminescence, and quantitatively analyzed using a GS-700 imaging densitometer (Bio-Rad, Hercules, CA).

Immunofluorescence. Confocal immunofluorescence was performed as described.^{14,20} Cells were double-labeled with a polyclonal antibody against insulin receptor B (BD Biosciences, CA), which is the predominant form of the receptor in hepatocytes,²⁵ and a monoclonal antibody against the nuclear membrane marker Lamin B1, and then incubated with secondary antibodies conjugated to Alexa 488 and 555 (Invitrogen), respectively. Images

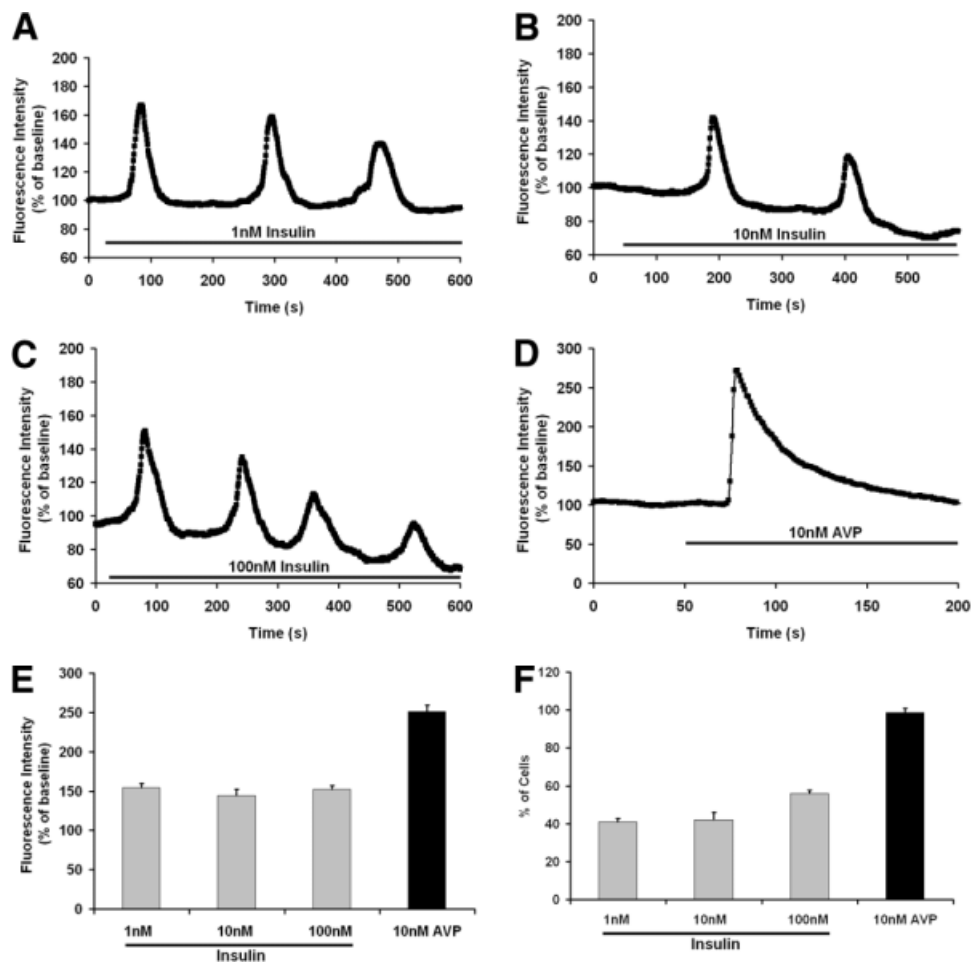


Fig. 1. Insulin induces calcium signaling in hepatocytes. (A-C) Insulin induces Ca²⁺ oscillations in primary rat hepatocytes. Ca²⁺ was monitored in individual hepatocytes 4-6 hours after isolation using the Ca²⁺ dye fluo-4 and time-lapse confocal microscopy. Tracings are shown from individual cells stimulated with 1, 10, or 100 nM insulin, respectively. No response was observed in cells stimulated with 0.1 nM insulin ($n = 30$; data not shown), and the response to 500 nM insulin was similar to the response shown here for 100 nM insulin ($n = 35$; data not shown). Stimulation with 1 and 10 nM insulin induced Ca²⁺ oscillations ($n = 58$). Stimulation with 100 nM insulin instead induced a sustained Ca²⁺ increase in some cells ($n = 25$; data not shown). Results are representative of what was observed in >25 responding cells under each condition. (D) Representative tracing of the Ca²⁺ signal induced by maximal (10 nM) stimulation with vasopressin. Note that the response begins and reaches its peak more rapidly in these cells than in cells stimulated with insulin. The result is representative of what was observed in $n = 90$ separate cells. (E) The amplitude of the Ca²⁺ signal induced by insulin is not concentration-dependent, and is significantly less than the amplitude of the Ca²⁺ signal induced by vasopressin ($*P < 0.001$; $n = 30$ in each group). (F) The fraction of cells responding to insulin is not concentration-dependent, and is significantly less than the fraction that responds to vasopressin ($*P < 0.001$; $n = 30$ in each group).

were collected with a Zeiss LSM 510 confocal microscope using a 63 \times , 1.4 NA objective lens with excitation at 488 nm and observation at 505-550 nm to detect Alexa 488, and excitation at 543 nm and observation at 560-610 nm to detect Alexa 555.

Statistical Analysis. Significance of changes in treatment groups relative to controls was determined by Student t test. Data are represented as mean \pm standard error.

Results

Insulin Induces Ca²⁺ Oscillations in Rat Hepatocytes. To examine Ca²⁺ signaling induced by insulin, freshly isolated rat hepatocytes were stimulated with a

range of insulin concentrations (0.1-100 nM) and observed by time-lapse confocal microscopy. Hepatocytes did not respond to 0.1 nM insulin ($n = 30$), but responded to all higher concentrations tested. The fraction of cells responding to insulin did not vary appreciably with increasing insulin concentrations; 41% of cells responded to stimulation with 1 nM insulin (Fig. 1A), 42% of cells responded to 10 nM insulin (Fig. 1B), and 56% of cells responded to maximal (100 nM) stimulation (Fig. 1C). Ca²⁺ oscillations were elicited in all responding cells stimulated with lower (1-10 nM) insulin concentrations, although higher insulin concentrations elicited Ca²⁺ oscillations in only 10% of responding cells, and instead

elicited a sustained increase in Ca^{2+} in the remaining 46% of responding cells (data not shown). Moreover, the response to 100 nM and 500 nM insulin was similar, suggesting that these findings represent the full range of insulin's effect on Ca^{2+} signals in hepatocytes. The frequency of Ca^{2+} oscillations (~ 5 mHz) was similar regardless of the insulin concentration. These findings show that insulin, like other Ca^{2+} agonists such as vasopressin, phenylephrine, angiotensin, and adenosine triphosphate,²⁶⁻²⁸ induces Ca^{2+} signals in hepatocytes that tend to be oscillatory at lower concentrations but can instead be sustained at higher concentrations. However, the frequency of insulin-induced Ca^{2+} oscillations was lower than has typically been reported for other agonists such as phenylephrine (10-50 mHz)^{26,27} and vasopressin (10-35 mHz).^{26,28} In addition, maximal concentrations of these other agonists generally elicit Ca^{2+} signals in >90% of hepatocytes,²⁶⁻²⁸ whereas insulin elicited Ca^{2+} signals in a much lower fraction of cells. Moreover, we stimulated cells with vasopressin (10 nM) and those results confirmed that $\sim 98\%$ of cells responded to that agonist, even though only half of the cells responded to insulin under the same experimental conditions. Vasopressin also induced a greater peak in fluorescence than what was observed in response to insulin stimulation (Fig. 1D). These findings demonstrate that insulin induces Ca^{2+} signals in hepatocytes, including Ca^{2+} oscillations, but that certain characteristics of these signals differ from what is elicited by stimulation of G protein-coupled receptors.

Insulin-Induced Ca^{2+} Signals Are Mediated by InsP3. Several maneuvers were performed to determine the mechanism by which insulin increases Ca^{2+} in hepatocytes. To determine the source of the Ca^{2+} , cells were stimulated in Ca^{2+} -free medium. Insulin induced Ca^{2+} oscillations even in Ca^{2+} -free medium (Fig. 2A), and Ca^{2+} signals were elicited in a similar fraction of cells regardless of the presence of extracellular Ca^{2+} (Fig. 2B). These findings demonstrate that insulin increases cytoplasmic Ca^{2+} by mobilizing intracellular Ca^{2+} stores. Most RTKs increase Ca^{2+} by activation of PLC γ , which forms InsP3 to bind to and release Ca^{2+} from InsP3 receptors in the endoplasmic reticulum.²⁹ Therefore, we stimulated hepatocytes with insulin in the presence of either the PLC inhibitor U-73122³⁰ or the InsP3 receptor inhibitor xestospongin C.³¹ Both U-73122 (Fig. 3A,B) and xestospongin C (Fig. 3C,D) eliminated insulin-induced Ca^{2+} signals in hepatocytes. Together, these findings suggest that insulin increases Ca^{2+} in hepatocytes through PLC- and InsP3-mediated release of intracellular Ca^{2+} stores.

Insulin-Induced Ca^{2+} Signals Begin in the Nucleus. Ca^{2+} signals in the nucleus and cytoplasm were moni-

tored simultaneously in hepatocytes ($n > 30$). The signals often had a similar temporal profile in both compartments (Fig. 4A), but the Ca^{2+} increase in the nucleus preceded the cytoplasmic increase in some cells, while in other cells an isolated increase in Ca^{2+} in the nucleus was observed (Fig. 4B). The kinetics of vasopressin-induced Ca^{2+} signals differed from this in two ways. First, insulin-induced signals often took up to 50 seconds from the time of onset to reach their peak amplitude (Figs. 1A-C and 4A), whereas the rise time of vasopressin-induced signals always was much shorter (~ 1 second; Fig. 1D), similar to what has been reported.¹⁸ Second, vasopressin-induced Ca^{2+} signals always began in the cytoplasm rather than the nucleus (Fig. 4C). These findings indicate that the subcellular kinetics of insulin-induced Ca^{2+} signals differ fundamentally from the kinetics of Ca^{2+} signals induced by vasopressin, which in turn suggests that insulin may increase Ca^{2+} through a mechanism based in the nucleus rather than in the cytoplasm.

The Insulin Receptor Translocates to the Nucleus. Ca^{2+} signals are initiated in hepatocytes when PIP_2 is hydrolyzed to form InsP3.¹⁸ Both the nucleus and the cytoplasm contain the machinery needed to form InsP3-mediated Ca^{2+} signals, including PLC, PIP_2 , and the InsP3 receptor,³² so we examined the effects of insulin on total cellular and nuclear pools of PIP_2 . Insulin reduced the nuclear pool by $38.9 \pm 7.1\%$ ($P < 0.05$) without significantly reducing total cellular PIP_2 (Fig. 5). For comparison, vasopressin reduced total cellular PIP_2 by $35.2 \pm 7.8\%$ ($P < 0.05$) without significantly reducing nuclear PIP_2 . To demonstrate more directly that the insulin receptor forms InsP3 in the nucleus, we targeted the ligand binding domain (residues 224-605) of the type 1 InsP3 receptor³³ to the cytoplasm or nucleus using a nuclear exclusion signal or nuclear localization signal sequence, respectively, plus mRFP to verify localization.²¹ These targeted InsP3 buffer constructs were expressed in the SkHep1 liver cell line, to circumvent technical difficulties associated with transient transfection of primary hepatocytes. It has previously been shown that the cytoplasmic but not the nuclear InsP3 buffer blocks vasopressin-induced Ca^{2+} signals in SkHep1 cells, reflecting the fact that G protein-coupled receptors such as the vasopressin V_{1a} receptor activate PLC and form InsP3 at the plasma membrane.²¹ In contrast, Ca^{2+} signals induced by insulin (100 nM) were nearly abolished in cells expressing the nuclear InsP3 buffer ($P < 0.005$), but were not affected by expression of the cytoplasmic buffer (Fig. 6). Together, these results show that insulin hydrolyzes PIP_2 and increases InsP3 only in the nucleus, and that Ca^{2+} signals throughout the cell result from this. To investigate why insulin preferentially forms InsP3 and increases Ca^{2+} in the nucleus, we

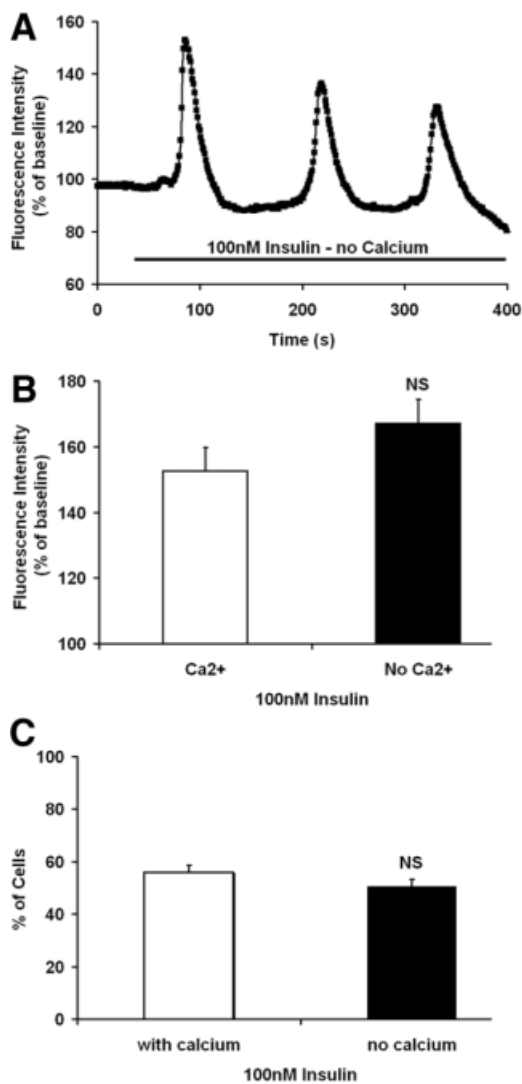


Fig. 2. Insulin-induced Ca²⁺ signals do not depend on extracellular Ca²⁺. (A) Insulin (100 nM) induces Ca²⁺ oscillations in a hepatocyte placed in Ca²⁺-free medium fortified with 1 mM ethylene glycol tetraacetic acid (EGTA). The result is representative of what was observed in 30 cells. (B) The amplitude of the Ca²⁺ signal induced by insulin is not decreased in Ca²⁺-free medium (n = 10 in each group). (C) The fraction of cells responding to insulin is not decreased in Ca²⁺-free medium (n = 10 in each group).

examined the location of the insulin receptor during cell stimulation. Immunoblots of non-nuclear and nuclear fractions showed that the insulin receptor was in the non-nuclear fraction of hepatocytes prior to stimulation with insulin. However, the receptor appeared in the nuclear fraction within 2.5 minutes of stimulation, and was detectable within the nucleus until 20 minutes after stimulation (Fig. 7A,B). Similarly, the phosphorylated (active) form of the insulin receptor was absent from the nucleus of hepatocytes prior to stimulation with insulin, but was detected there afterwards (Fig. 7C). To confirm the immunoblot findings, confocal immunofluorescence microscopy was used to monitor the

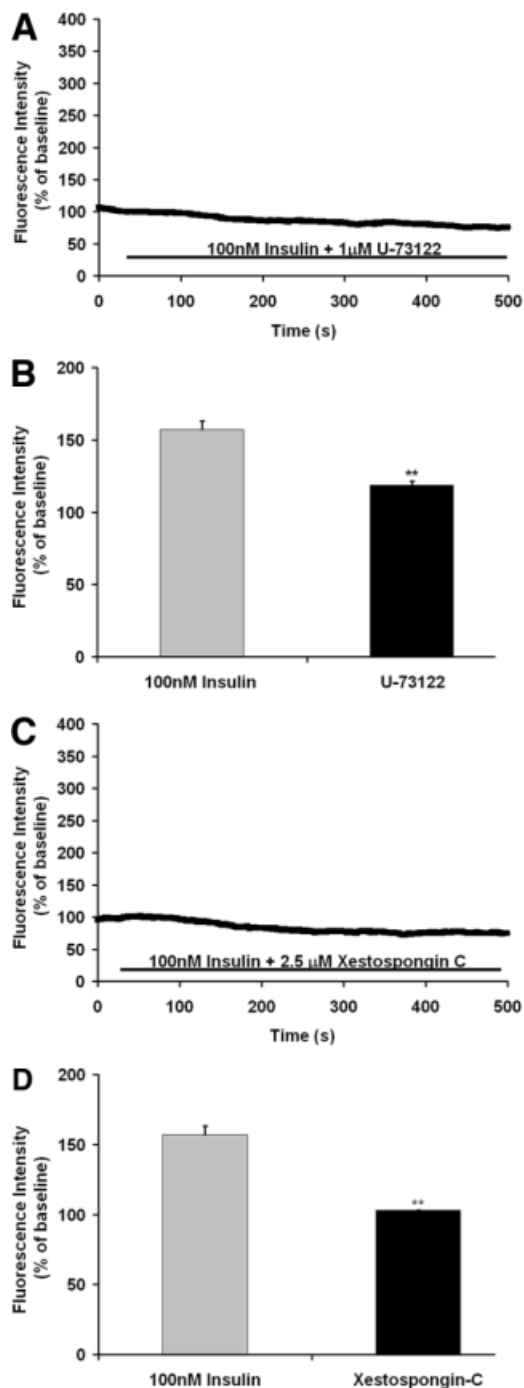


Fig. 3. Insulin-induced Ca²⁺ signals depend on PLC and InsP3. (A) The Ca²⁺ signal induced by insulin (100 nM) is blocked by the PLC inhibitor U-73122 (1 µM). The result is representative of what was observed in 56 cells. (B) Bar graph summary showing that the amplitude of the Ca²⁺ signal induced by insulin is significantly reduced by U-73122 (**P < 0.001; n = 18 in each group). (C) The Ca²⁺ signal induced by insulin (100 nM) is blocked by the InsP3 receptor inhibitor xestospongine C (2.5 µM). The result is representative of what was observed in 73 cells. (D) Bar graph summary showing that the amplitude of the Ca²⁺ signal induced by insulin is significantly reduced by xestospongine C (**P < 0.001; n = 25 in each group).

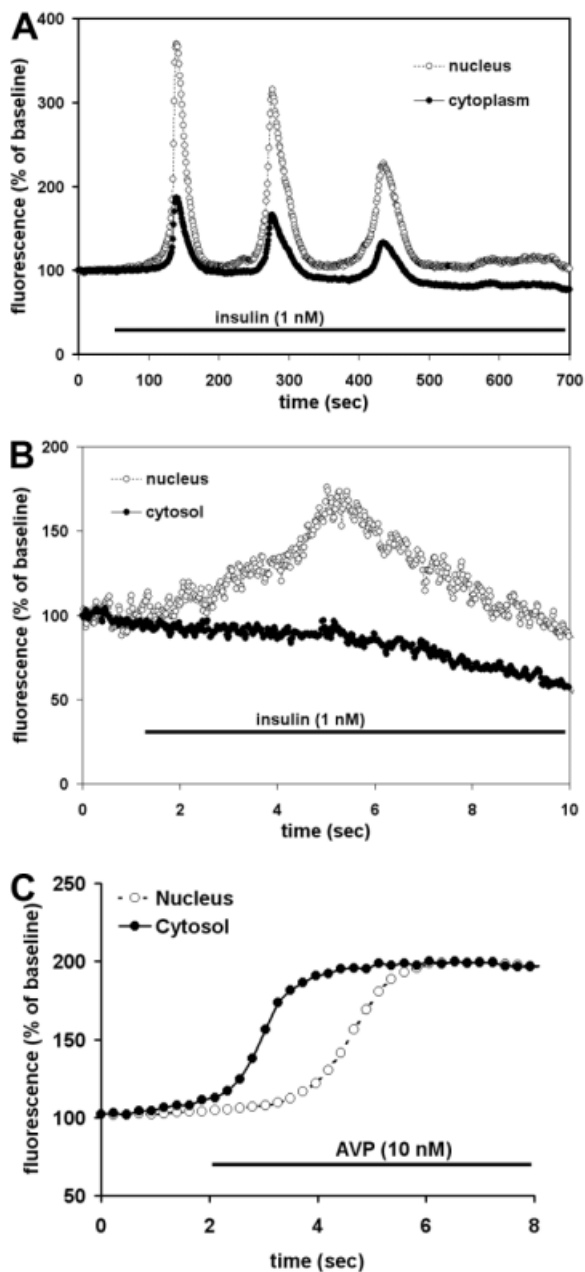


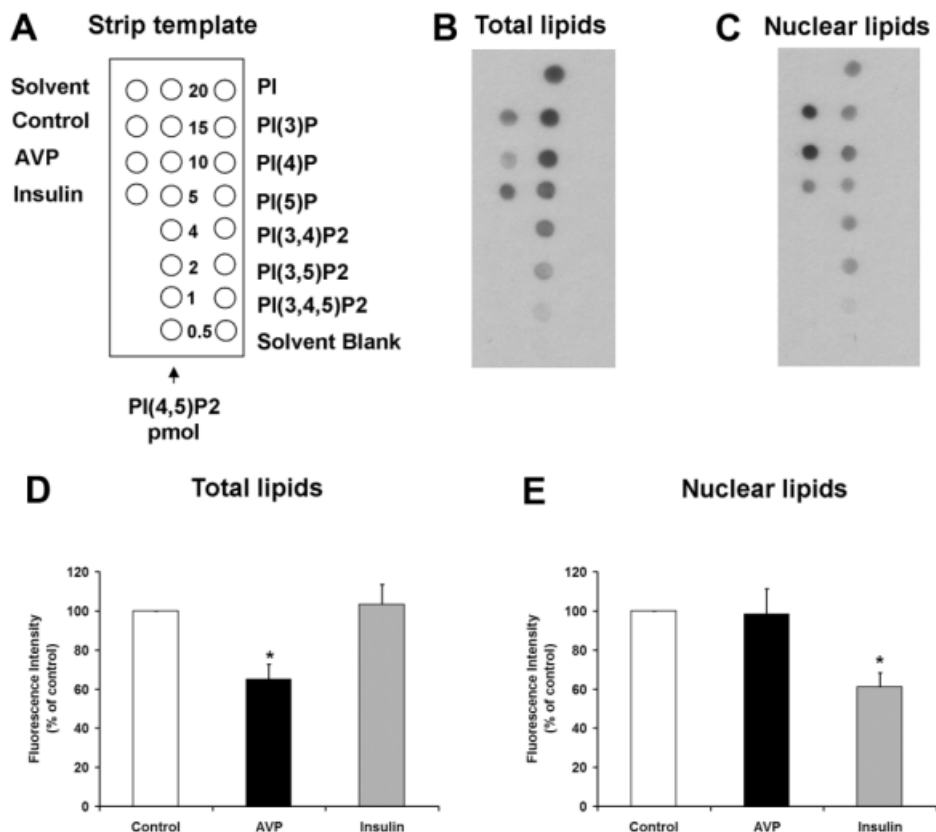
Fig. 4. Insulin-induced Ca^{2+} signals begin in the nucleus. (A) Examination of the nuclear and cytosolic components of the insulin-induced Ca^{2+} signal reveal that the Ca^{2+} increase occurs in both regions of the hepatocyte. The image is representative of what was observed in >90 cells. (B) Insulin can induce isolated Ca^{2+} increases in the nucleus. All cells responded to insulin in this fashion, with sequential increases in Ca^{2+} in the nucleus and then cytosol, or with a simultaneous increase in Ca^{2+} in the nucleus and cytosol. Note the expanded time scale relative to (A) of this figure and in Figs. 1-3. (C) The vasopressin-induced Ca^{2+} signal begins in the cytosol rather than the nucleus, similar to what has been reported.^{18,19} Because the fluorescence intensity of fluo-4 differs in the nucleus and cytosol,²⁰ fluorescence here was rescaled so that the nuclear and cytosolic signals would have the same baseline and peak values, to facilitate direct comparison of the time course of each tracing. Results are representative of what was observed in at least 25 cells in each group.

subcellular distribution of the insulin receptor. Confocal imaging demonstrated that the insulin receptor was at the plasma membrane or within the cytoplasm but absent from the nucleus prior to stimulation (Fig. 8A, top panels). Within 5 minutes of exposure to 10 nM insulin, the insulin receptor could also be detected at the nuclear envelope and within the nuclear interior (Fig. 8A, bottom panels). Three-dimensional (3D) reconstruction of serial confocal immunofluorescence images confirmed that the receptor could be identified within the nuclear interior of cells stimulated with insulin (Fig. 8B). Together, these findings demonstrate that stimulation of hepatocytes with insulin induces the insulin receptor to translocate to the nucleus, and this is associated with selective hydrolysis of nuclear PIP_2 and formation of InsP_3 -dependent Ca^{2+} signals within the nucleus.

Discussion

Insulin is a potent mitogen for hepatocytes *in vitro*⁴ and also plays a role in liver regeneration *in vivo*.³⁴ Insulin also plays an essential role in the growth and proliferation of hepatocytes in certain cell culture systems.³⁵ Insulin acts through the insulin receptor, which is a RTK, and evidence from other RTKs suggests that translocation to the nucleus may be a common feature for this class of receptors. A number of RTKs have been found in the nucleus, including receptors for growth hormone, several cytokines, epidermal growth factor (EGF), hepatocyte growth factor, and fibroblast growth factor (FGF).^{21,36,37} Phosphorylated EGF receptor can be found in the nucleus within 1-2 minutes of stimulation with EGF, and reaches peak levels within 15 minutes.³⁶ Phosphorylated hepatocyte growth factor receptor (c-met) appears in the nucleus within a similar time frame after stimulation with hepatocyte growth factor, and its appearance there has been linked to intranuclear formation of InsP_3 and initiation of Ca^{2+} signals within the nucleus.²¹ Translocation of the FGF receptor to the nucleus occurs over a longer time scale, reaching peak amounts after 3-4 hours.³⁷ Although these previous studies have demonstrated that RTKs can translocate to the nucleus in cell lines, the current work provides evidence that this also occurs in primary hepatocytes. Intranuclear RTKs can serve functional effects as well. For example, EGF receptors in the nucleus act as a transcription factor that promotes expression of cyclin D1³⁶ and COX-2,³⁸ each of which may contribute to the mitogenic effects of EGF. The mechanism by which RTKs reach the nucleus is not known, although transport of the FGF receptor to the nucleus depends on importin β , rather than the presence of a nuclear localization sequence on either the receptor or its ligand,³⁷ and transport of c-met to the nucleus depends upon both importin β and the adaptor protein GRB2-associated binding

Fig. 5. Insulin selectively hydrolyzes nuclear PIP₂. Immunoassay of total (B) and nuclear (C) lipids, plus a key to the strip template (A). The lipid samples were spotted onto nitrocellulose membranes, as illustrated by the strip template, and the PIP₂ levels were detected using an anti-PIP₂ monoclonal antibody. This antibody reacts with a higher degree of specificity to PI(4,5)P₂ than to other inositol polyphosphates (right column). A total of 20 pmol of each of the other PIP controls was used. (D) Densitometric measurement shows that arginine vasopressin (AVP) hydrolyzes 35.2 ± 7.8% of PIP₂ in whole cell preparations (n = 3, *P < 0.05), whereas insulin does not hydrolyze significant amounts of total cellular PIP₂. (E) Insulin hydrolyzes 38.9 ± 7.1% of PIP₂ in the nucleus (n = 3, *P < 0.05), whereas vasopressin stimulation does not hydrolyze significant amounts of nuclear PIP₂. Total and nuclear lipids were isolated 10 minutes after stimulation of hepatocytes with insulin (10 nM) or 1 minute after stimulation with vasopressin (10 nM). Data are mean ± standard error of the mean (SEM).



protein 1 (Gab1).²¹ Early studies based on binding of radiolabeled insulin to nuclear membranes,³⁹ plus autoradiographic studies of hepatocytes and hepatocyte lysates using photolabeled insulin receptors,⁴⁰ suggested that the insulin receptor can be intranuclear. This conclusion was questioned in later work using immunoblot and immunoelectron microscopic techniques,⁴¹ which had led many to conclude instead that the insulin receptor does not translocate to the nucleus.⁴² Similarly, previous evidence had suggested that the insulin receptor does not activate PLC, leading to the widely held conclusion that insulin does not stimulate the PLC/InsP₃/Ca²⁺ signaling pathway.^{43,44} However, recent studies have shown an increase in InsP₃ in rat epididymal cells stimulated with insulin,⁴⁵ as well as an increase in PLC activity in insulin-stimulated adipocytes.⁴⁶ Moreover, PLC γ coprecipitates with the insulin receptor, providing additional evidence that this receptor induces phospholipid hydrolysis.⁷ Finally, insulin has been reported to increase cytosolic Ca²⁺ in primary hepatocytes by triggering Ca²⁺ influx,⁴⁷ but the current work provides evidence that insulin instead mobilizes intracellular Ca²⁺ stores in hepatocytes, through a PLC-dependent and InsP₃-dependent mechanism. The current findings provide both structural and functional evidence that the insulin receptor moves to and acts within the nucleus in hepatocytes. Structural evi-

dence includes immunoblots showing that total as well as phosphorylated insulin receptor accumulates in the nucleus, plus confocal immunofluorescence localization of the receptor within the nucleus. Functional evidence includes studies showing that insulin selectively hydrolyzes the nuclear pool of PIP₂, plus Ca²⁺ imaging studies showing that insulin-induced Ca²⁺ signals can begin in the nucleus, and that these signals depend on intranuclear rather than cytoplasmic InsP₃. Thus, previous studies plus the current work together suggest that insulin induces its receptor to move to the nucleus in hepatocytes, and this translocation is associated with PLC-mediated hydrolysis of nuclear PIP₂, leading to formation of InsP₃-mediated Ca²⁺ signals. Because Ca²⁺ signals within the nucleus are particularly important for cell growth,¹¹ the effect of insulin on nuclear Ca²⁺ signaling may explain insulin's action as a mitogen. The metabolic effects of insulin in the liver are mediated by Akt/protein kinase B, and these effects are enhanced in the liver-specific Gab1 knockout mouse.⁴⁸ Since Gab1 may mediate nuclear translocation of RTKs,²¹ this suggests that the metabolic effects of insulin may be mediated by the non-nuclear insulin receptor, while the effects of insulin on growth and regeneration may be mediated by the insulin receptor that reaches the nucleus.

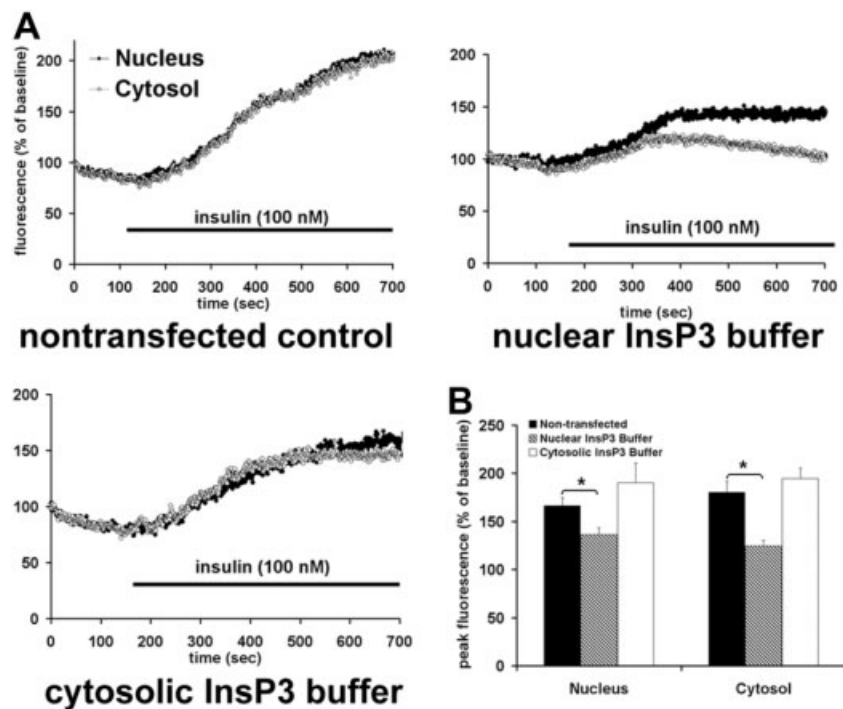


Fig. 6. Insulin generates InsP3 in the nucleus rather than the cytoplasm. (A) Insulin-induced Ca^{2+} signals are attenuated by the nuclear but not the cytosolic InsP3 buffer. SkHep1 cells loaded with fluo-4 were stimulated with insulin (100 ng/mL) while examined by time-lapse confocal microscopy. Graphical representation of the nuclear and cytosolic Ca^{2+} signal detected in a representative cell from each experimental group stimulated with insulin is shown. Ca^{2+} increases in the nucleus and cytosol are similar in nontransfected cells and in cells expressing the InsP3 buffer targeted to the cytosol, but Ca^{2+} signals in both compartments are attenuated when the InsP3 buffer is targeted to the nucleus. (B) Summary of InsP3 buffer studies confirms that insulin-induced Ca^{2+} signaling are significantly attenuated by buffering nuclear but not cytosolic InsP3. Values are mean \pm standard error of the mean (SEM) of the peak fluo-4 fluorescence attained during the observation period (expressed as % of baseline) and include the response from 23 nontransfected cells, seven cells expressing the InsP3 buffer targeted to the nucleus, and five cells expressing the InsP3 buffer targeted to the cytosol (* $P < 0.005$).

There is increasing evidence that the subcellular pattern of Ca^{2+} signals dictates the cellular effects of this second messenger. The InsP3 receptor is the only intracellular Ca^{2+} release channel in hepatocytes,¹⁸ so the subcellular distribution of this receptor determines the form of Ca^{2+} signals in these cells. For example, the type II InsP3 receptor, which is the principle isoform in hepatocytes, is most concentrated in the region of the endoplasmic reticulum beneath the canalicular membrane.^{18,19} Agonists such as vasopressin, angiotensin, or adenosine triphosphate increase InsP3 in the cytosol, and so the resulting Ca^{2+} signal takes the form of a Ca^{2+} wave that begins in the canalicular region, where the InsP3 receptor is most concentrated.¹⁸ This Ca^{2+} wave directs exocytosis⁴⁹ and fluid and electrolyte secretion.⁵⁰ Reduced expression of InsP3 receptors in hepatocytes impairs the formation of Ca^{2+} waves,⁵¹ but simple redistribution of the receptors away from the canalicular region impairs Ca^{2+} wave formation as well.¹⁹ This subcellular organization of the Ca^{2+} signaling machinery is relevant for the regulation of secretion, because treatment of cholangiocytes with small interfering RNA to decrease expression of

apical InsP3 receptors in these cells results in impaired bicarbonate secretion.⁵² Expression of apical InsP3 receptors is also decreased or absent in bile ducts of patients with cholestatic disorders such as primary biliary cirrhosis, sclerosing cholangitis, and biliary atresia,⁵³ although it has not yet been established that this loss of InsP3 receptors is responsible for the development of cholestasis in these disorders. Localization of InsP3 receptors to other microdomains can affect cell function as well. For example, the type III InsP3 receptor colocalizes more effectively than either the type I or II isoform of the receptor with mitochondria.⁵⁴ This is associated with more efficient transmission of Ca^{2+} signals into the mitochondria, which in turn is more effective at inducing apoptosis.⁵⁴ A number of Ca^{2+} -mediated events occur in the nucleus; including: activation of cyclic adenosine monophosphate response element-binding transcription factor¹⁰ and the Elk-1 transcription factor⁹; translocation of nuclear protein kinase C to the region of the nuclear envelope¹⁴; and regulation of progression of the cell cycle through prophase.¹¹ Although Ca^{2+} can spread passively from the cytosol into the nucleus under certain circumstances,^{55,56}

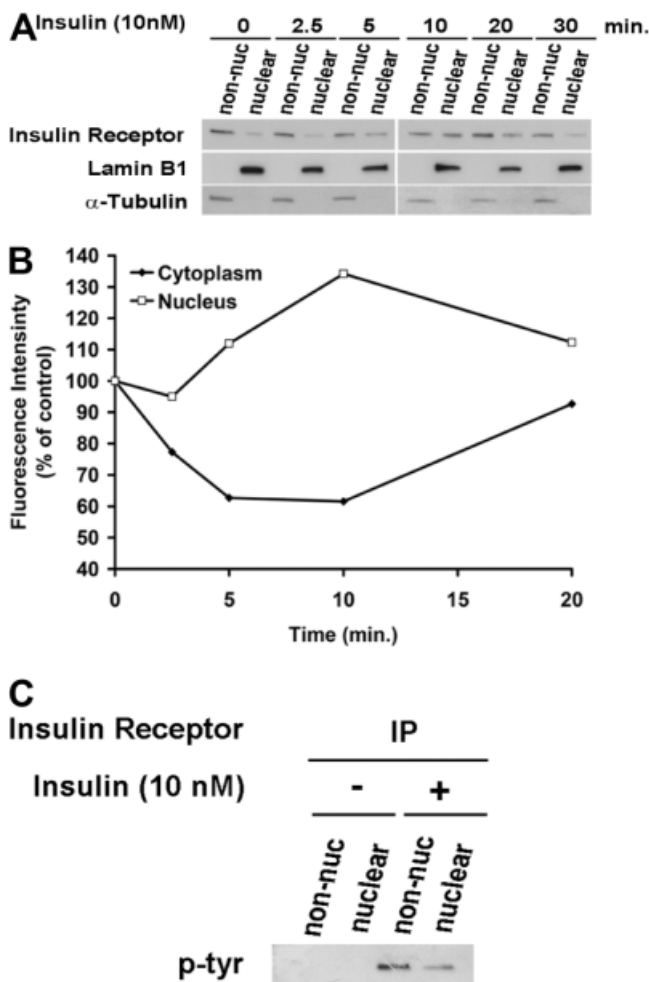


Fig. 7. The insulin receptor translocates to the nucleus. (A) Immunoblots show the insulin receptor in nuclear and non-nuclear fractions of primary hepatocytes before and at serial time points after stimulation with insulin (10 nM). Trace amounts of the receptor are found in the nucleus at baseline, and this increases within 5 minutes and reach peak intensity within 10 minutes of stimulation. Blots are representative of what was observed in $n = 3$ separate experiments. Alpha-tubulin and Lamin B were used as purity controls for the non-nuclear and nuclear fraction, respectively.²³ (B) Densitometric measurement of subcellular fractions of the insulin receptor. The amount of the insulin receptor in the nucleus is maximal within 10 minutes of stimulation ($n = 3$). Note that the increase in insulin receptor in the nucleus is transient and is temporally associated with a transient decrease in the receptor elsewhere in the cell. Measurements were normalized by alpha-tubulin and Lamin B levels in non-nuclear and nuclear fractions, respectively. Values are representative of what was observed in three separate experiments. (C) The phosphorylated insulin receptor reaches the nucleus. Insulin receptor was immunoprecipitated from the non-nuclear and nuclear fractions of hepatocytes before and 5 minutes after stimulation with insulin (10 nM), then probed with a phospho-tyrosine-specific antibody. The phosphorylated receptor is found after but not before stimulation with insulin in both cell fractions.

intracellular InsP3 can increase Ca^{2+} directly within the nucleus as well, in both isolated nuclei and in nuclei within intact cells.^{14,57} This is because the nuclear envelope⁵⁷ and the nucleoplasmic reticulum¹⁴ both express

InsP3 receptors, and these receptors can release Ca^{2+} into the nucleoplasm. How much InsP3 receptor is expressed in the nucleus? Although immunofluorescence studies suggest that the InsP3 receptor in hepatocytes is most concentrated in the pericanalicular region,¹⁸ quantitative immunoblots show that the ratio of nuclear:cytosolic InsP3 receptors is nearly 20:1.¹⁴ This ratio reflects InsP3 receptor concentration relative to other proteins in each compartment, but since there is presumably much less total protein per unit volume in the nucleus than in the cytoplasm, this may explain why immunofluorescence studies instead suggest that there is more InsP3 receptor in the cytoplasm. In any case, several mechanisms have been identified to control Ca^{2+} release from nuclear InsP3 receptors. The three InsP3 receptor isoforms have distinct sensitivities to InsP3, so targeting a more sensitive isoform to the nucleus will enable InsP3-mediated Ca^{2+} signals to occur preferentially in the nucleus, relative to the cytosol.²⁰ Alternatively, selective hydrolysis of the nuclear pool of PIP₂ will lead to local intranuclear formation of InsP3, so that Ca^{2+} will be released preferentially from

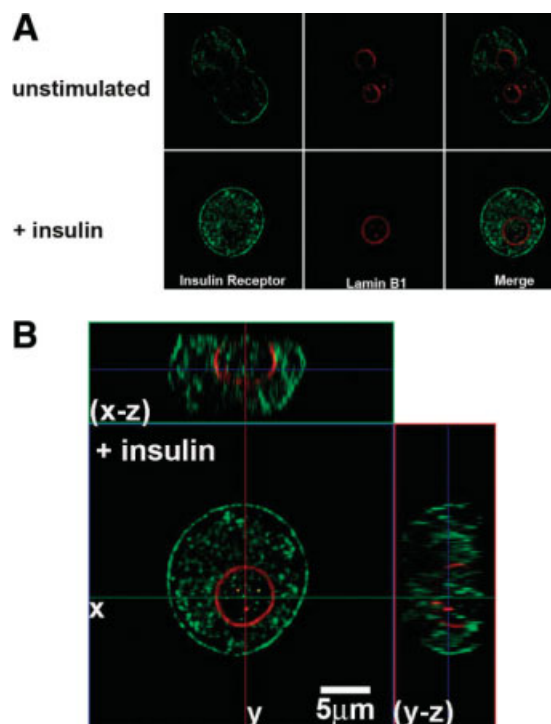


Fig. 8. The insulin receptor translocates to the nucleus. (A) Confocal immunofluorescence images of the insulin receptor before and 5 minutes after stimulation with insulin (10 nM), respectively. Insulin receptor labeling is in green and the nuclear envelope is stained with Lamin B1 in red. Note that the receptor initially labels the plasma membrane and is heterogeneously distributed in the cytosol as well, but is excluded from the nuclear interior until after stimulation with insulin. (B) Serial confocal sections were collected for three-dimensional reconstruction. These double-labeled images confirm that the receptor is heterogeneously distributed within the nuclear interior after stimulation with insulin.

nuclear InsP3 receptors. In particular, RTKs may selectively activate nuclear isoforms of PLC, particularly PLC β 1, and may also induce PLC γ 1 to translocate to the nucleus.^{58,59} The current work suggests that the insulin receptor may also act in this fashion. Although insulin-induced Ca²⁺ signals begin before peak accumulation of the insulin receptor occurs within the nucleus, there is likely a threshold relationship rather than a linear relationship between accumulation of insulin receptor within the nucleus and triggering of Ca²⁺ signals, just as there is a threshold, "all-or-none" relationship between accumulation of InsP3 and initiation of Ca²⁺ signals in the cytoplasm.⁶⁰ Therefore, although the increase in intranuclear insulin receptor does not become measurable for several minutes, smaller amounts, especially of the phosphorylated receptor, may be sufficient to generate enough InsP3 to initiate Ca²⁺ signals. Further work is needed to determine the mechanism by which the insulin receptor moves to the nucleus in hepatocytes and to demonstrate that this is responsible for insulin's mitogenic effects.

Acknowledgment: We thank Kathy Harry for hepatocyte isolations.

References

- Saltiel AR, Kahn CR. Insulin signalling and the regulation of glucose and lipid metabolism. *Nature* 2001;414:799-806.
- Rosen OM. After insulin binds. *Science* 1987; 237:1452-1458.
- Straus DS. Growth-stimulatory actions of insulin in vitro and in vivo. *Endocr Rev* 1984;5:356-369.
- Koontz JW, Iwahashi M. Insulin as a potent, specific growth factor in a rat hepatoma cell line. *Science* 1981;211:947-949.
- Block GD, Locker J, Bowen WC, Petersen BE, Katyal S, Strom SC, et al. Population expansion, clonal growth, and specific differentiation patterns in primary cultures of hepatocytes induced by HGF/SF, EGF and TGF alpha in a chemically defined (HGM) medium. *J Cell Biol* 1996;132:1133-1149.
- De Meyts P, Whittaker J. Structural biology of insulin and IGF1 receptors: implications for drug design. *Nat Rev Drug Discov* 2002;1:769-783.
- Eichhorn J, Kayali AG, Austin DA, Webster NJ. Insulin activates phospholipase C-gamma1 via a PI-3 kinase dependent mechanism in 3T3-L1 adipocytes. *Biochem Biophys Res Commun* 2001;282:615-620.
- Nathanson MH, Rios-Velez L, Burgstahler AD, Mennone A. Communication via gap junctions modulates bile secretion in the isolated perfused rat liver. *Gastroenterology* 1999;116:1176-1183.
- Pusl T, Wu JJ, Zimmerman TL, Zhang L, Ehrlich BE, Berchtold MW, et al. Epidermal growth factor-mediated activation of the ETS domain transcription factor Elk-1 requires nuclear calcium. *J Biol Chem* 2002;277:27517-27527.
- Hardingham GE, Chawla S, Johnson CM, Bading H. Distinct functions of nuclear and cytoplasmic calcium in the control of gene expression. *Nature* 1997;385:260-265.
- Rodrigues MA, Gomes DA, Leite MF, Grant W, Zhang L, Lam W, et al. Nucleoplasmic calcium is required for cell proliferation. *J Biol Chem* 2007;282:17061-17068.
- Poenie M, Alderton J, Tsien RY, Steinhardt RA. Changes of free calcium levels with stages of the cell division cycle. *Nature* 1985;315:147-149.
- Carrión AM, Link WA, Ledo F, Mellstrom B, Naranjo JR. DREAM is a Ca²⁺-regulated transcriptional repressor. *Nature* 1999;398:80-84.
- Echevarria W, Leite MF, Guerra MT, Zipfel WR, Nathanson MH. Regulation of calcium signals in the nucleus by a nucleoplasmic reticulum. *Nat Cell Biol* 2003;5:440-446.
- Thompson M, Andrade VA, Andrade SJ, Pusl T, Ortega JM, Goes AM, et al. Inhibition of the TEF/TEAD transcription factor activity by nuclear calcium and distinct kinase pathways. *Biochem Biophys Res Commun* 2003;301:267-274.
- Saltiel AR, Pessin JE. Insulin signaling pathways in time and space. *Trends Cell Biol* 2002;12:65-71.
- Boyer JL, Phillips JM, Graf J. Preparation and specific applications of isolated hepatocyte couplets. *Methods Enzymol* 1990;192:501-516.
- Hirata K, Pusl T, O'Neill AF, Dranoff JA, Nathanson MH. The type II inositol 1,4,5-trisphosphate receptor can trigger Ca²⁺ waves in rat hepatocytes. *Gastroenterology* 2002;122:1088-1100.
- Nagata J, Guerra MT, Shugrue CA, Gomes DA, Nagata N, Nathanson MH. Lipid rafts establish calcium waves in hepatocytes. *Gastroenterology* 2007;133:256-267.
- Leite MF, Thrower EC, Echevarria W, Koulen P, Hirata K, Bennett AM, et al. Nuclear and cytosolic calcium are regulated independently. *Proc Natl Acad Sci U S A* 2003;100:2975-2980.
- Gomes DA, Rodrigues MA, Leite MF, Gomez MV, Varnai P, Balla T, et al. c-Met must translocate to the nucleus to initiate calcium signals. *J Biol Chem* 2008;283:4344-4351.
- Hsu SC, Hung MC. Characterization of a novel tripartite nuclear localization sequence in the EGFR family. *J Biol Chem* 2007;282:10432-10440.
- Lo HW, Ali-Sayed M, Wu Y, Bartholomeusz G, Hsu SC, Hung MC. Nuclear-cytoplasmic transport of EGFR involves receptor endocytosis, importin beta1 and CRM1. *J Cell Biochem* 2006;98:1570-1583.
- Gray A, Olsson H, Batty IH, Priganica L, Peter DC. Nonradioactive methods for the assay of phosphoinositide 3-kinases and phosphoinositide phosphatases and selective detection of signaling lipids in cell and tissue extracts. *Anal Biochem* 2003;313:234-245.
- Serrano R, Villar M, Martinez C, Carrascosa JM, Gallardo N, Andres A. Differential gene expression of insulin receptor isoforms A and B and insulin receptor substrates 1, 2 and 3 in rat tissues: modulation by aging and differentiation in rat adipose tissue. *J Mol Endocrinol* 2005;34:153-161.
- Nathanson MH, Burgstahler AD, Fallon MB. Multistep mechanism of polarized Ca²⁺ wave patterns in hepatocytes. *Am J Physiol* 1994;267(Pt 1):G338-G349.
- Woods NM, Cuthbertson KS, Cobbold PH. Repetitive transient rises in cytoplasmic free calcium in hormone-stimulated hepatocytes. *Nature* 1986;319:600-602.
- Rooney TA, Sass EJ, Thomas AP. Characterization of cytosolic calcium oscillations induced by phenylephrine and vasopressin in single fura-2-loaded hepatocytes. *J Biol Chem* 1989;264:17131-17141.
- Divecha N, Banfic H, Irvine RF. The polyphosphoinositide cycle exists in the nuclei of Swiss 3T3 cells under the control of a receptor (for IGF-I) in the plasma membrane, and stimulation of the cycle increases nuclear diacylglycerol and apparently induces translocation of protein kinase C to the nucleus. *EMBO J* 1991;10:3207-3214.
- Hirata K, Nathanson MH, Burgstahler AD, Okazaki K, Mattei E, Sears ML. Relationship between inositol 1,4,5-trisphosphate receptor isoforms and subcellular Ca²⁺ signaling patterns in nonpigmented ciliary epithelia. *Invest Ophthalmol Vis Sci* 1999;40:2046-2053.
- Gafni J, Munsch JA, Lam TH, Catlin MC, Costa LG, Molinski TF, et al. Xestospingins: potent membrane permeable blockers of the inositol 1,4,5-trisphosphate receptor. *Neuron* 1997;19:723-733.
- Irvine RF. Nuclear lipid signalling. *Nat Rev Mol Cell Biol* 2003;4:349-360.
- Balla A, Tuymetova G, Barshishat M, Geiszt M, Balla T. Characterization of type II phosphatidylinositol 4-kinase isoforms reveals association of the enzymes with endosomal vesicular compartments. *J Biol Chem* 2002;277:20041-20050.
- Michalopoulos GK, DeFrances MC. Liver regeneration. *Science* 1997; 276:60-66.

35. Michalopoulos G, Pitot HC. Primary culture of parenchymal liver cells on collagen membranes. Morphological and biochemical observations. *Exp Cell Res* 1975;94:70-78.
36. Lin SY, Makino K, Xia W, Matin A, Wen Y, Kwong KY, et al. Nuclear localization of EGF receptor and its potential new role as a transcription factor. *Nat Cell Biol* 2001;3:802-808.
37. Reilly JF, Maher PA. Importin beta-mediated nuclear import of fibroblast growth factor receptor: role in cell proliferation. *J Cell Biol* 2001;152:1307-1312.
38. Wang SC, Lien HC, Xia W, Chen IF, Lo HW, Wang Z, et al. Binding at and transactivation of the COX-2 promoter by nuclear tyrosine kinase receptor ErbB-2. *Cancer Cell* 2004;6:251-261.
39. Wong KY, Hawley D, Vigneri R, Goldfine ID. Comparison of solubilized and purified plasma membrane and nuclear insulin receptors. *Biochemistry* 1988;27:375-379.
40. Podlecki DA, Smith RM, Kao M, Tsai P, Huecksteadt T, Brandenburg D, et al. Nuclear translocation of the insulin receptor. A possible mediator of insulin's long term effects. *J Biol Chem* 1987;262:3362-3368.
41. Soler AP, Thompson KA, Smith RM, Jarett L. Immunological demonstration of the accumulation of insulin, but not insulin receptors, in nuclei of insulin-treated cells. *Proc Natl Acad Sci U S A* 1989;86:6640-6644.
42. Wells A, Marti U. Signalling shortcuts: cell-surface receptors in the nucleus? *Nat Rev Mol Cell Biol* 2002;3:697-702.
43. Taylor D, Uhing RJ, Blackmore PF, Prpic V, Exton JH. Insulin and epidermal growth factor do not affect phosphoinositide metabolism in rat liver plasma membranes and hepatocytes. *J Biol Chem* 1985;260:2011-2014.
44. Nishibe S, Wahl MI, Hernandez-Sotomayor SM, Tonks NK, Rhee SG, Carpenter G. Increase of the catalytic activity of phospholipase C-gamma 1 by tyrosine phosphorylation. *Science* 1990;250:1253-1256.
45. Farese RV, Kuo JY, Babischkin JS, Davis JS. Insulin provokes a transient activation of phospholipase C in the rat epididymal fat pad. *J Biol Chem* 1986;261:8589-8592.
46. Koepfer-Hobelsberger B, Wieland OH. Insulin activates phospholipase C in fat cells: similarity with the activation of pyruvate dehydrogenase. *Mol Cell Endocrinol* 1984;36:123-129.
47. Benzeroual K, Van de WG, Meloche S, Mathe L, Romanelli A, Haddad P. Insulin induces Ca²⁺ influx into isolated rat hepatocyte couplets. *Am J Physiol* 1997;272(Pt 1):G1425-G1432.
48. Bard-Chapeau EA, Hevener AL, Long S, Zhang EE, Olefsky JM, Feng GS. Deletion of Gab1 in the liver leads to enhanced glucose tolerance and improved hepatic insulin action. *Nat Med* 2005;11:567-571.
49. Ito K, Miyashita Y, Kasai H. Micromolar and submicromolar Ca²⁺ spikes regulating distinct cellular functions in pancreatic acinar cells. *EMBO J* 1997;16:242-251.
50. Kasai H, Augustine GJ. Cytosolic Ca²⁺ gradients triggering unidirectional fluid secretion from exocrine pancreas. *Nature* 1990;348:735-738.
51. Hernandez E, Leite MF, Guerra MT, Kruglov EA, Bruna-Romero O, Rodrigues MA, et al. The spatial distribution of inositol 1,4,5-trisphosphate receptor isoforms shapes Ca²⁺ waves. *J Biol Chem* 2007;282:10057-10067.
52. Minagawa N, Nagata J, Shibao K, Masyuk AI, Gomes DA, Rodrigues MA, et al. Cyclic AMP regulates bicarbonate secretion in cholangiocytes through release of ATP into bile. *Gastroenterology* 2007;133:1592-602.
53. Shibao K, Hirata K, Robert ME, Nathanson MH. Loss of inositol 1,4,5-trisphosphate receptors from bile duct epithelia is a common event in cholestasis. *Gastroenterology* 2003;125:1175-1187.
54. Mendes CC, Gomes DA, Thompson M, Souto NC, Goes TS, Goes AM, et al. The type III inositol 1,4,5-trisphosphate receptor preferentially transmits apoptotic Ca²⁺ signals into mitochondria. *J Biol Chem* 2005;280:40892-40900.
55. Lipp P, Thomas D, Berridge MJ, Bootman MD. Nuclear calcium signalling by individual cytoplasmic calcium puffs. *EMBO J* 1997;16:7166-7173.
56. Fox JL, Burgstahler AD, Nathanson MH. Mechanism of long-range Ca²⁺ signalling in the nucleus of isolated rat hepatocytes. *Biochem J* 1997;326(Pt 2):491-495.
57. Gerasimenko OV, Gerasimenko JV, Tepikin AV, Petersen OH. ATP-dependent accumulation and inositol trisphosphate- or cyclic ADP-ribose-mediated release of Ca²⁺ from the nuclear envelope. *Cell* 1995;80:439-444.
58. Xu A, Suh PG, Marmy-Conus N, Pearson RB, Seok OY, Cocco L, et al. Phosphorylation of nuclear phospholipase C beta1 by extracellular signal-regulated kinase mediates the mitogenic action of insulin-like growth factor I. *Mol Cell Biol* 2001;21:2981-2990.
59. Klein C, Gensburger C, Freyermuth S, Nair BC, Labourdette G, Malviya AN. A 120 kDa nuclear phospholipase Cgamma1 protein fragment is stimulated in vivo by EGF signal phosphorylating nuclear membrane EGFR. *Biochemistry* 2004;43:15873-15883.
60. Parker I, Ivorra I. Localized all-or-none calcium liberation by inositol trisphosphate. *Science* 1990;250:977-979.

Highly efficient siRNA delivery system into human and murine cells using single-wall carbon nanotubes

This article has been downloaded from IOPscience. Please scroll down to see the full text article.

2010 Nanotechnology 21 385101

(<http://iopscience.iop.org/0957-4484/21/38/385101>)

View [the table of contents for this issue](#), or go to the [journal homepage](#) for more

Download details:

IP Address: 150.164.34.151

The article was downloaded on 08/09/2010 at 15:23

Please note that [terms and conditions apply](#).

Highly efficient siRNA delivery system into human and murine cells using single-wall carbon nanotubes

M S Ladeira¹, V A Andrade¹, E R M Gomes¹, C J Aguiar¹,
E R Moraes¹, J S Soares², E E Silva², R G Lacerda², L O Ladeira²,
A Jorio², P Lima³, M Fatima Leite^{1,4}, R R Resende^{2,5} and
S Guatimosim¹

¹ Department of Physiology and Biophysics, Federal University of Minas Gerais, Belo Horizonte, MG, 31270-901, Brazil

² Department of Physics, Federal University of Minas Gerais, Belo Horizonte, MG, 31270-901, Brazil

³ Department of Biosystems Engineering, Federal University of São João Del Rei, São João Del Rei, MG, 36307-352, Brazil

⁴ Howard Hughes Medical Institute, 4000 Jones Bridge Road, Chevy Chase, 20815-6789 MD, USA

⁵ Department of Biochemistry, Federal University of São João Del Rei, Advanced Center of Health, Divinópolis, MG, 35501-296, Brazil

E-mail: rresende@hotmail.com and guatimosim@icb.ufmg.br

Received 29 June 2010

Published 27 August 2010

Online at stacks.iop.org/Nano/21/385101

Abstract

Development of RNA interference (RNAi) technology utilizing short interfering RNA sequences (siRNA) has focused on creating methods for delivering siRNAs to cells and for enhancing siRNA stability *in vitro* and *in vivo*. Here, we describe a novel approach for siRNA cellular delivery using siRNA coiling into carboxyl-functionalized single-wall carbon nanotubes (SWCNTs). The CNT–siRNA delivery system successfully demonstrates nonspecific toxicity and transfection efficiency greater than 95%. This approach offers the potential for siRNA delivery into different types of cells, including hard-to-transfect cells, such as neuronal cells and cardiomyocytes. We also tested the CNT–siRNA system in a non-metastatic human hepatocellular carcinoma cell line (SKHep1). In all types of cells used in this work the CNT–siRNA delivery system showed high efficiency and apparent no side effects for various *in vitro* applications.

1. Introduction

In recent years, carbon-nanotube-based carriers are one of the non-viral vectors that have gained increasing interest as a safer and cost-effective delivery system for gene materials including plasmid DNA (pDNA) and oligonucleotides (ODN) as well as proteins and peptides. Carbon nanotubes (CNTs) have beneficial qualities such as low toxicity, low immunogenicity (Liu *et al* 2008, Cherukuri *et al* 2006) and biocompatibility (Dubin *et al* 2008). Moreover, they offer the possibility of functionalization that can easily form polyelectrolyte complexes with negatively charged nucleotides by electrostatic interaction. Previously, some studies evaluated the ability

of multi-wall carbon nanotubes (MWCNTs) and single-wall carbon nanotubes (SWCNTs) covalently or electrostatically linked to chemical groups as transfection agents to deliver gene materials including pDNA, ODN, proteins and peptides (Kam *et al* 2005, Rege *et al* 2006, Zhang *et al* 2006, Krajcik *et al* 2008). Previous work using an immortalized HeLa cell line (Kam *et al* 2005) reported a covalent conjugation of siRNA to phospholipid-functionalized SWCNTs via cleavable disulfide linkage. By using this approach they have shown highly efficient delivery of siRNA by SWCNTs, and achieved a more potent RNAi functionality than a widely used commercial agent. By using the same functionalization technique of siRNA conjugation through disulfide linkages specific knockdown of

target gene in T-cells transfected with SWCNTs–siRNA was obtained (Liu *et al* 2007). Interestingly, the authors failed to see a knockdown effect when using liposome-based carriers.

Moreover, another study reported that positively charged –CONH–(CH₂)₆–NH³⁺Cl-functionalized SWCNTs were able to bind and efficiently carry siRNA into tumor cells. (Zhang *et al* 2006). Recently, another study used a chemical functionalization of SWCNTs with hexamethylenediamine (HMDA) and poly(diallyldimethylammonium) chloride (PDDA) to bind negatively charged siRNA. PDDA–HMDA–SWCNTs were able to carry siRNA into cardiomyocytes and efficiently knock down targeted genes ERK1 and ERK2. Importantly, the complex PDDA–HMDA–SWCNTs showed no cytotoxic effects on cardiomyocytes (Krajcik *et al* 2008).

Here, we report a new strategy for delivering siRNA into hard-to-transfect cells by using carboxylic-functionalized SWCNTs. To compare the delivery efficiency in a stable cell line, we used the SKHep1 cell culture. We further report that carboxylic-SWCNTs represent an efficient non-cytotoxic system for carrying siRNA.

2. Experimental details

2.1. Materials

If not otherwise indicated, all reagents were purchased from Sigma.

2.2. Carbon nanotube synthesis

SWCNTs were prepared by the arc discharge method using a Co/Ni (0.6/0.6 at.%) catalyst with helium at a total pressure 500 Torr, with the arc generated by a current of 200 A/20 V (Trigueiro *et al* 2007, Da Silva *et al* 2009). After the synthesis, an indispensable as-grown SWCNT purification (~95%) process was performed. One gram of SWCNTs was refluxed with 3 M HNO₃ at 120 °C during 32 h, centrifuged at 7000 rpm and washed with distilled water in order to purify the SWCNTs. Nitric acid oxidation on the carbon nanotubes exhibits a dual role: this treatment was performed to decorate the SWCNT surface with –COOH groups and also to afford short SWCNTs (length 50–500 nm). The final solution was dried during 12 h in an oven at 60 °C. At the end, 0.75 g of high purity COOH-SWCNTs was obtained.

2.3. RNAi preparation

For siRNA studies, potential target sites within the rat inositol 1,4,5-triphosphate receptor (InsP3R) genes were selected and then searched with NCBI Blast to confirm specificity for each InsP3R isoform. The siRNAs for the type I and II InsP3R were prepared by a transcription-based method using the Silencer kit according to the manufacturer's instructions (Ambion Inc., Austin, TX). The sense and antisense oligonucleotides of siRNAs were, respectively, as follows: type I, 5'-AAAGTTGTAGCTGCTGGTGCCTCCTGTCCTC-3' and 5'-AAAGCACCAGCAGCTACAA CTCCTGTCCTC-3'; type II, 5'-AACAGCCTAATCAAGATCTCCCCTGTCTC-3' and 5'-AAGGAGATCTTGATTAGGCTGCCTGTCTC-3'.

2.4. Transfection solutions

A stable aqueous solution of short single-wall CNTs (~length 200 nm) was prepared with high purity short COOH-SWCNTs dissolved in MilliQ water. The solution was sonicated for 3 h followed by centrifugation (15 700g). 50 or 100 nM of siRNA for each InsP3R isoform was added to 50 μl (dose 1) or 100 μl (dose 2) of a CNT aqueous solution, sonicated for 30 min and added to the cell medium. CNT concentration in the cell's medium was respectively 0.0125 and 0.0250 mg ml⁻¹. For RNAi preparation the cells were washed and supplied with 1 ml of fresh tissue culture medium. 50 or 100 nM of siRNA for the InsP3R-II isoform was added to 3 μl (concentration 1) or 6 μl (concentration 2) of transfection reagent (RNAifect, QIAGEN) and then the volume was completed to 100 μl with tissue culture medium. The mixture was incubated for 15 min at 37 °C for complex formation, and then 900 μl of tissue culture medium was added to the mixture and this solution was placed dropwise onto the cells. The cells were incubated at 37 °C in an atmosphere of 5% CO₂ for 48 h prior to use, as previously shown (Mendes *et al* 2005).

2.5. SKHep1 cell culture

SKHep1 cells (American Type Culture Collection—Manassas, VA) were cultured in Dulbecco's modified Eagle's medium (DMEM) (GIBCO BRL, Frederick, MD) supplemented with 10% fetal bovine serum and antibiotics. Cells were incubated at 37 °C in an atmosphere of 5% CO₂ for 48 h.

2.6. Cardiomyocyte cell culture

Neonatal cardiomyocytes were isolated from hearts of three-day-old Wistar rats, as previously described (Guatimosim *et al* 2008). Briefly, cells were resuspended in DMEM supplemented with 10% fetal bovine serum (FBS) (GIBCO BRL, Frederick, MD), 100 units ml⁻¹ penicillin, 100 μg ml⁻¹ streptomycin. Cardiomyocytes were plated into fibronectin-coated culture dishes or flasks and incubated at 37 °C in 5% CO₂ incubator. Two days after plating, cells were rinsed with DMEM and fed for another 24 h with regular culture medium, now including 20 μg ml⁻¹ cytosine β-D-arabinofuranoside (ARAC) to inhibit growth of non-cardiomyocyte cells. The cultured cardiomyocytes were used in experiments on the fourth day of culture.

2.7. Rat dorsal root ganglion (DRG) neuron cell culture

Male Wistar rats (220–280 g) were sacrificed by decapitation, and dorsal root ganglia dissected out and maintained in HEPES-buffered saline (HBS) containing (in mM): NaCl 140, KCl 2.5, Hepes 10, Glucose 7.5, pH adjusted to 7.4 with NaOH. Ganglia were cleaned of connective tissue and sectioned prior to 20 min enzymatic treatment with Papain (1 μg ml⁻¹), activated by cystein (0.03 μg ml⁻¹) in HBS. The ganglia were washed with enzyme-free HBS followed by 20 min treatment with 2.5 μg ml⁻¹ collagenase (Type 1A) in HBS. During enzymatic treatment, tubes were gently agitated to avoid settling and adherence of the tissue.

Enzymatic treatment was halted by washing the ganglia with DMEM containing 10% FBS. Digested ganglia fragments were triturated through pipettes fire polished to an inner tip diameter of 2 mm until dissociated. The cell suspension obtained was plated onto glass cover slips previously treated with polylysine (MW 70 000–150 000, 20 $\mu\text{g ml}^{-1}$, 12 h at 4 °C) followed by laminin (20 $\mu\text{g ml}^{-1}$, 6 h at 4 °C). The cultures were stored at 37 °C in a 5% CO₂ incubator to allow the cells to settle and adhere to the cover slips.

2.8. Immunofluorescence

Immunofluorescence to detect the subcellular distribution of InsP3R isoform was performed, as described previously (Mendes *et al* 2005). Briefly, cardiomyocytes, DRG and SKHep1 cells were fixed in 4% paraformaldehyde, followed by cell permeabilization in 0.5% Triton X-100. After a blocking step, cells were incubated with primary antibody against specific InsP3R isoforms and then rinsed with phosphate-buffered saline and 1% bovine serum albumin. The specimens were then incubated with Alexa 488 secondary antibody (Invitrogen) and/or co-labeled with Alexa 633 (Invitrogen). A Zeiss LSM 510 confocal microscope (Thorwood, NY) was used for all imaging studies. Images were obtained by excitation at 488 nm and observation at 505–550 nm to detect Alexa 488. Each InsP3R isoform was labeled using isoform-specific antibodies. Type I InsP3R antibodies were from affinity-purified specific rabbit polyclonal antiserum directed against the 19 C-terminal residues of the mouse type I InsP3R (Hagar *et al* 1998) and were produced by Research Genetics (Huntsville, AL). Type II InsP3R antibodies were from affinity-purified specific rabbit polyclonal antiserum directed against the 18 C-terminal residues of the rat type II InsP3R (Wojcikiewicz 1995) and were kindly provided by Richard Wojcikiewicz (SUNY, Syracuse, NY).

2.9. RNA extraction, reverse transcription and real-time PCR

cDNA templates were amplified by real-time PCR on the 7000 Sequence Detection System (ABI Prism, Applied Biosystems, Foster City, CA) using the Syber green method as described (Resende *et al* 2008, Soares *et al* 2007). Sets of primers were chosen for type II InsP3R, forward, 5' AGCACATTACGGCGAATCCT 3' and reverse 5' CCTGACAGAGGTCGGTTCACA 3', and type III InsP3R, forward 5' CGGAGCGCTTCTTCAAGGT 3' and reverse 5' TGACAGCGACCGTGGACTT 3', and type II RyR, forward 5' CCGCATCGACAAGGACAAA 3' and reverse 5' TGAGGGCTTTTCTGAGCAT 3', and for β -actin, forward 5' GACGGCCAGGTCATCACTATTG 3' and reverse 5' AGGAAGGCTGGAAAAGAGCC 3' to give PCR products less than 100 base pairs in length. Primers and probes were custom synthesized by Integrated DNA Technologies (Coralville, IA).

Gene expression profile in SKHep1 cells incubated or not with SWCNTs (0.0250 mg ml⁻¹) was performed with primers selected and searched with NCBI Blast to confirm specificity. Genes were selected for: G1/S phase-associated genes (cyclin

D1, cyclin D2, cdk4, cyclin E1, cyclin E2, and cdk2), S phase-associated genes (cyclin A1, and cdk2), G2 phase-associated genes (cyclin A2, and cyclin D3), M phase-associated genes (cyclin B1, and cyclin B2), cell cycle inhibitors such as p16INK4a, p15INK4b and p19INK4d. A panel of apoptotic (p53, Apaf-1, caspase 6 and bax) and anti-apoptotic genes (mdm2, p21CIP/WAF) were also chosen for this study.

Total RNA from SKHep1 cells was isolated using the TRIzol reagent (Invitrogen). Contaminating DNA was removed by DNase I (Ambion Inc., Austin, TX) treatment and integrity of the isolated RNA was analyzed on a 2% SYBR[®] safe DNA-stained agarose gel (Invitrogen, Carlsbad, CA). Three micrograms of total RNA from each sample were used in each case as template for cDNA synthesis in the presence of 50 ng of random primers and 200 units of RevertAid[™] H Minus Moloney murine leukemia virus reverse transcriptase (Fermentas Inc., Hanover, MD) in a total volume of 20 μl for 45 min at 42 °C. Complementary DNA was amplified in a 10 μl volume containing 6 μl of 2x TaqMan Universal PCR Master Mix (Applied Biosystems, Foster City, CA), 100 nM probe (Applied Biosystems, Foster City, CA) and 300 nM of each primer. After a denaturing step at 95 °C for 10 min, 50 cycles were performed at 95 °C for 15 s and then 60 °C for 1 min. Mathematical analysis of the results was performed as recommended by the manufacturer.

2.10. Measurement of beating frequency

Cells were loaded with the fluorescent Ca²⁺ dye Fluo/4 AM and beating frequency was acquired with a Zeiss LSM 510 confocal microscope (Guatimosim *et al* 2008).

2.11. Live/dead cell viability assay

Viability assay was performed in neonatal cardiomyocytes with a live/dead assay kit from Invitrogen (Invitrogen, Carlsbad, CA). Cell medium was removed and cells were washed twice with PBS, and 2 ml of Hepes solution containing 0.5 μl of calcein AM and 1.0 μl of ethidium homodimer was added in each cell well and stored for 30 min at 37 °C in a 5% CO₂ incubator. Live and dead cells were observed with a BioRad MRC-1024 confocal microscope (Hercules, CA). Values were expressed as the number of living cells divided by the total number of cells. All experiments were carried out in triplicate.

2.12. Flow cytometry

SKHep1 cells were analyzed by a Becton-Dickinson FAC-Scan instrument after incubation with COOH-SWCNTs (0.0250 mg ml⁻¹) for 6, 12, 24 or 48 h. The cells were washed, trypsinized to detach them from the plate surface and washed with PBS, followed by 2 min centrifugation (1000 rpm). Anexin-V-FITC (50 $\mu\text{g ml}^{-1}$) and propidium iodide (100 $\mu\text{g ml}^{-1}$) were added to the cell in the presence of the binding buffer and allowed to react for 10 min at room temperature. The data presented here represent the mean fluorescence obtained from a population of 50 000 cells.

2.13. Raman spectrophotometry

Confocal Raman measurements were performed on an inverted optical microscope with the addition of an x, y stage for raster-scanning samples. The sample was excited with an He–Ne laser (632.8 nm), focused onto the surface of the sample using an oil objective with 60 \times magnification, NA = 1.4. The Raman scattered light was recorded using: (i) a single-photon counting avalanche photodiode (APD) filtered at the frequency of the CNT G band (1580 cm^{-1}) for Raman imaging and (ii) a spectrograph with a charge-coupled device (CCD) for spectral information.

3. Results

Here we showed an examination of CNT properties by checking simultaneously its biocompatibility and efficiency as an siRNA delivery method. In this study, we used three distinct cell types (DRG, neonatal cardiomyocytes and SKHep1 cells) in order to evaluate the potential of purified short SWCNTs as siRNA carriers. An effort was made in order to select cell types with distinct characteristics to investigate the physiological potential of CNTs as transfection agents for clinical therapy. In addition, these cells express different isoforms of InsP3R. Moreover, cardiomyocytes and dorsal root ganglion (DRG) neuron cells have in common the feature of being hard to transfect, which has limited their use in siRNA studies. For siRNA experiments the target gene of choice was the InP3R.

3.1. Effects of CNTs on cell viability

SKHep1 cells are a liver-derived epithelial cell line, capable of proliferating, that are not polarized. These cells express two different types of InsP3Rs, type II and type III (Leite *et al* 2002), therefore representing a valuable model to investigate the cytotoxicity and specificity of CNT–siRNA complexes.

A critical aspect that plays an important role in determining CNT toxicity is related to its biocompatibility. Therefore, we first evaluated the effect of CNTs on gene expression levels of regulators of cell cycle and apoptosis control factors in SKHep 1 cells. For that, cells were treated with a solution of functionalized CNTs (carboxylic-SWCNTS 0.0250 mg ml^{-1}) for 48 h and gene expression levels were evaluated by real-time PCR. Table 1 shows mRNA levels of a panel of 21 genes assessed by real-time PCR. Gene list includes regulators of cell cycle, pro-apoptotic and inhibitor of apoptosis genes. The analyses showed that regulators of cell cycle genes G1/S phase-associated genes (cyclin D1, cyclin D2, cdk4, cyclin E1, cyclin E2, and cdk2), S phase-associated genes (cyclin A1, and cdk2), and G2 phase-associated genes (cyclin A2) were up-regulated, while M phase-associated genes (cyclin B1, and cyclin B2) were down-regulated, suggesting that SKHep1 cells were arrested in the G1 phase in the presence of CNTs. Both apoptosis-related genes such as p53, Apaf-1, caspase 6 and bax, and anti-apoptotic genes (p21CIP/WAF, mdm2, p19ARF) were up-regulated suggesting that SWCNTs do not induce apoptosis in SKHep1 cells.

To investigate the functional consequence of these changes in mRNA levels, we performed FACS in SKHep 1 cells

Table 1. Effects of CNTs on mRNA relative expression levels of regulators of cell cycle and apoptosis-related genes.

Genes	Control	CNT
Cyclin A1	1.87	2.61
Cyclin A2	1.70	2.60
Cyclin B1	1.60	0.76
Cyclin B2	1.43	0.74
Cyclin D1	5.34	30.69
Cyclin D2	110.36	250.83
Cyclin D3	1.08	0.99
Cyclin E1	7.90	162.42
Cyclin E2	6.87	122.11
cdk2	2.33	11.91
cdk4	3.90	6.22
p15INK	2.90	1.95
p16INK	1.015	1.47
p19INK	0.95	0.32
p53	1.14	3.07
p21CIP/WAF	0.91	16.41
Apaf-1	0.99	1.48
Caspase6	0.83	1.09
Bax	1.23	1.80
mdm2	0.53	1.36
p19ARF	0.70	0.73

exposed or not to functionalized CNTs (0.0250 mg ml^{-1}). As shown in figures 1(A) and (B) no significant difference was observed between untreated control cells and cells incubated with functionalized CNTs at the different exposure times tested (6, 12, 24 and 48 h).

In this study, therefore, we expanded previous findings by showing that CNTs do not affect cellular viability. Although gene expression levels of important cellular pro-apoptotic genes and cell cycle regulators were altered in SKHep 1 cells exposed to CNTs, we also noted a higher expression of survival genes, which may have compensated the increased expression of death genes. This data was confirmed by FACS, which showed no effect of CNTs on SKHep 1 cell viability. These data correlated with findings from a previous study (Shi Kam *et al* 2004) showing that the uptake of SWCNTs did not adversely affect HL60 cells at equivalent CNT concentration used in this work. Taken together, our data show that, although functionalized CNTs alter gene expression, these changes do not lead to reduced cellular viability. Next, we assessed the potential of SWCNTs as siRNA carriers.

3.2. SWCNT–siRNA complex efficiently reduces InsP3R expression levels in SKHep1 cells

Ca^{2+} regulates multiple processes within an individual cell. Among intracellular Ca^{2+} channels the InsP3R family is widely expressed in excitable as well as non-excitable cells. In SKHep1 cells, for instance, InsP3Rs are distributed throughout the cytosol and the nucleus (Echevarria *et al* 2003, Mendes *et al* 2005) and Ca^{2+} signaling depends entirely on InsP3R-generated Ca^{2+} signals. Therefore, we next investigated the efficiency of our CNT–InsP3R–siRNA complex in SKHep1 cells. To achieve maximum effectiveness of exogenously introduced siRNAs, transfection optimization experiments are required, since failure to optimize critical transfection

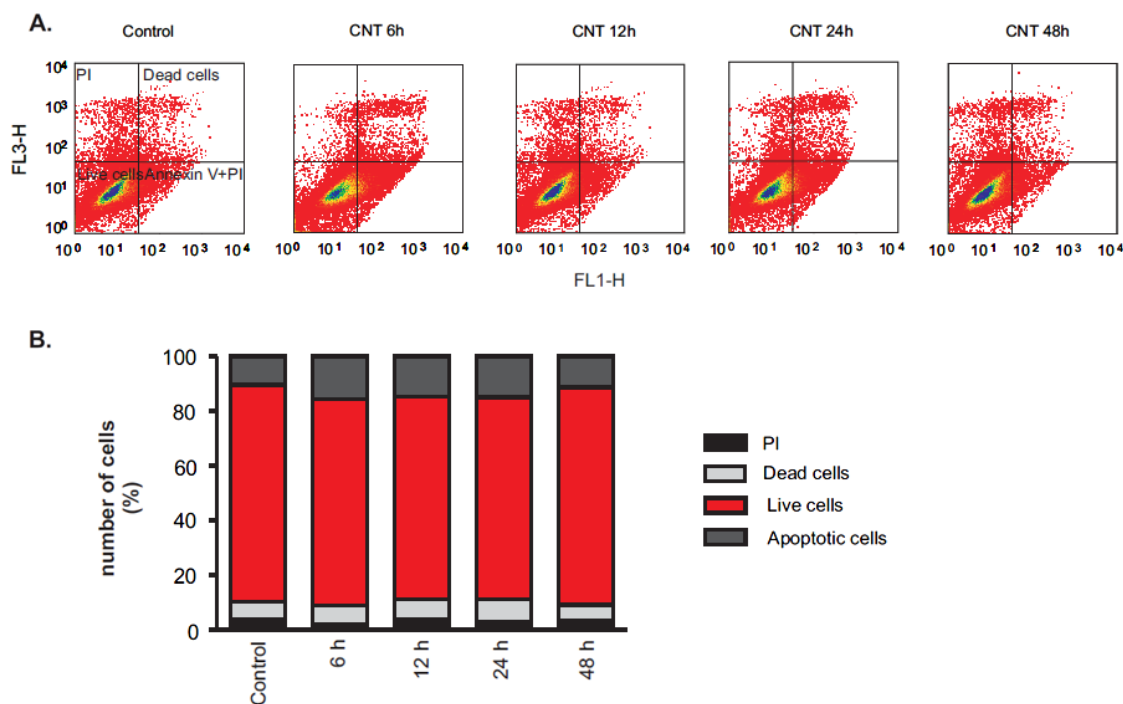


Figure 1. CNTs do not affect SKHeP 1 cell viability. Cellular viability was assessed by FACS in cells incubated with CNTs (0.025 mg ml^{-1}) for 6, 12, 24 and 48 h. (A) Representative FACS analyses shown in the histogram format. (B) Bar graph showing that SKHeP 1 cell viability is not altered by CNT exposure at different time points.

(This figure is in colour only in the electronic version)

parameters can render RNAi effects undetectable in cell culture. In order to determine the optimal time that provides maximum gene knockdown, while maintaining an acceptable level of viability for the particular cell type, we exposed cells to the CNT–siRNA–InsP3R-II complex for 2, 6, 24 and 48 h, and we performed quantitative real-time PCR experiments. Cell medium was changed to remove the transfection complex after each time point, and siRNA silencing efficiency was measured 48 h after transfection began. As shown in figure 2, higher InsP3R gene knockdown was achieved when cells were exposed to the CNT–siRNA–InsP3R-II complex for 24 and 48 h. CNTs alone did not interfere with InsP3R mRNA levels.

In order to confirm this data, we performed immunofluorescence experiments in SKHeP1 cells stained with anti-InsP3R antibodies. As shown in figure 3(A), InsP3R-II protein levels were significantly reduced in cells treated for 48 h with the CNT–siRNA–InsP3R-II complex, when compared to control untreated cells. Quantitative real-time PCR experiments also corroborated this data (figure 3(B)). We next compared the efficiency of the CNT–siRNA–InsP3R-II complex to an available commercial method (RNAifect, Qiagen). For this experiment, two different dilutions of RNAifect (3 and $6 \mu\text{l}$) were used, according to the manufacturer's instructions, in conjunction with 50 or 100 nM InsP3R-II siRNA. Under these conditions significant reduction of InsP3R-II mRNA was observed (figure 3(B)). For CNT–siRNA experiments four different combinations were evaluated. All combinations led to reduced InsP3R-II mRNA levels, with higher efficiency observed in the cells transfected with the complex formed by

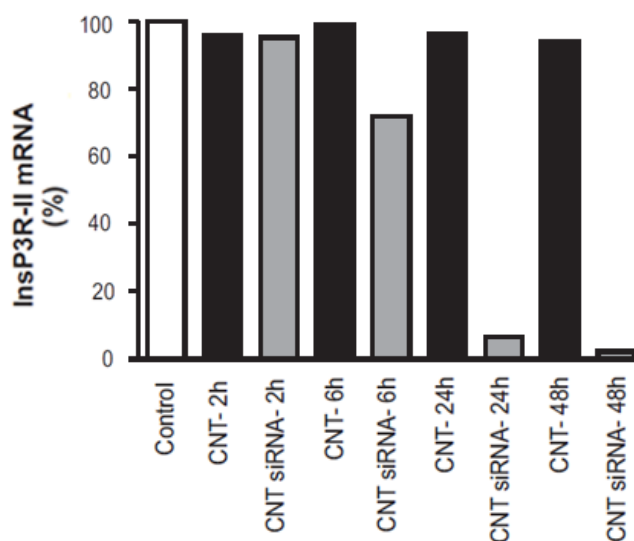


Figure 2. Time dependence of CNTs as siRNA carriers. Cells were incubated with transfection complex (CNT–siRNA–InsP3R-II) for 2, 6, 24 and 48 h, after which media was replaced by regular culture media. InsP3R-II mRNA levels were examined 48 h after transfection began. Significant InsP3R-II gene knockdown was observed in cells incubated with transfection complex for 24 and 48 h.

combination of 100 nM siRNA and $0.0250 \text{ mg ml}^{-1}$ CNTs. Since type III InsP3R is also found in this cell type, we decided to assess whether our silencing complex targeted to InsP3R-II would affect InsP3R-III mRNA expression levels. As shown in

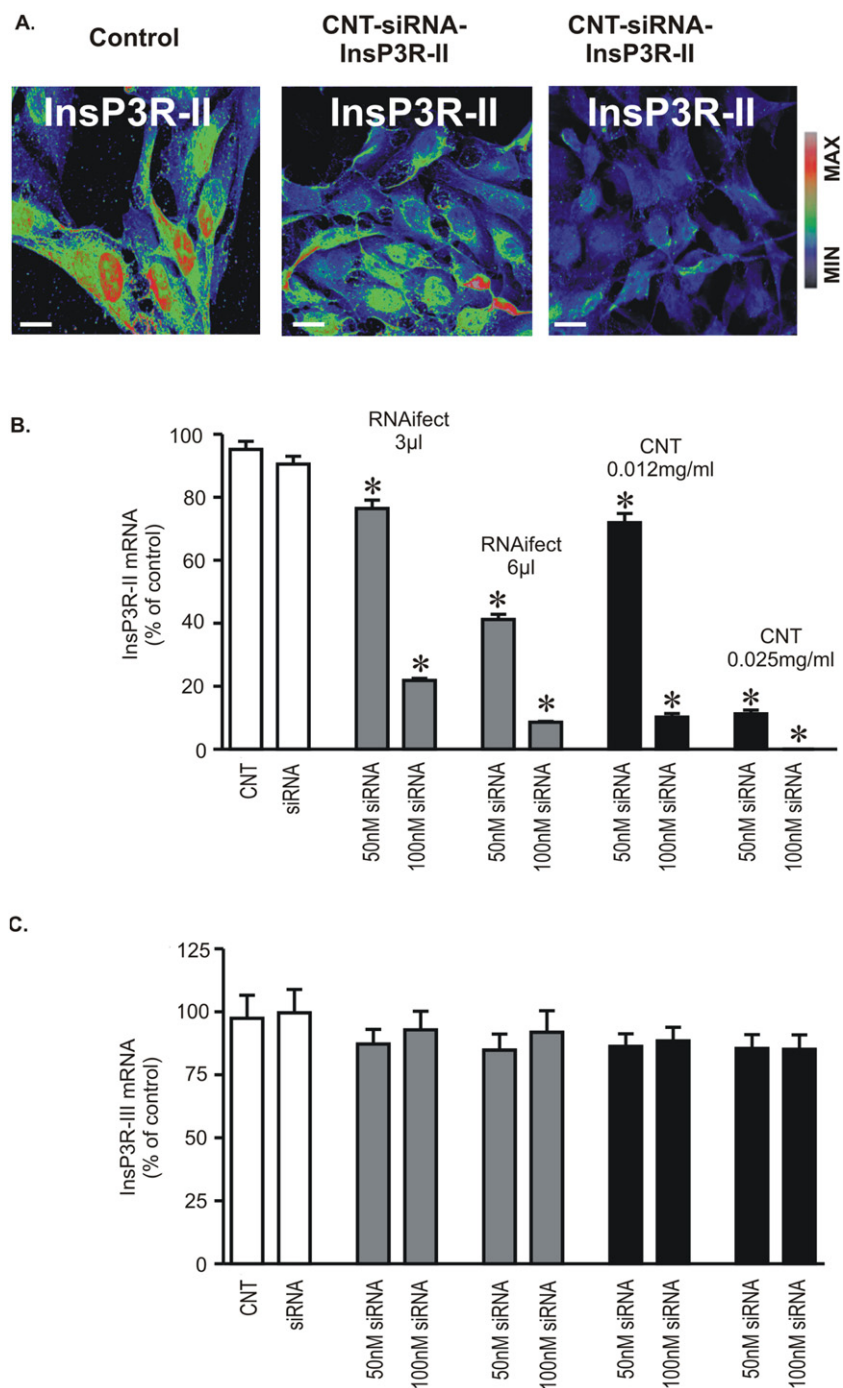


Figure 3. CNT–siRNA–InsP3R-II complex reduces InsP3R-II expression levels in SKHep1 cells. (A) Representative confocal images showing InsP3R-II labeled cells. InsP3R-II staining was significantly reduced in SKHep1 cells transfected with CNT–siRNA–InsP3R-II (middle and right panels) when compared to control cells (left panel). Confocal images were collected 48 h after transfection began. Final concentration of 50 nM (middle panel) or 100 nM siRNA (right panel) were efficiently delivered by CNTs in SKHep 1 cells. Images were pseudocolored according to the color scale. Scale bar = 10 μ m. (B) and (C) Real-time PCR comparing type II and type III InsP3R mRNA expression levels following siRNA transfection using CNTs or a lipid-based gene transfer system as RNA carriers. siRNA:RNAiVect reagent combination was evaluated at ratios of 50 nM:3 μ l, 100 nM:3 μ l, 50 nM:6 μ l and 100 nM:6 μ l. For CNT–siRNA complex formation different concentrations of CNT (0.0125 or 0.025 mg ml⁻¹) were added to the diluted siRNA (50 or 100 nM final concentration). Both transfection agents were efficient in suppressing InsP3R-II gene expression in SKHep1 cells. (C) InsP3R-III transcript levels were not altered in cells transfected with InsP3R-II siRNA.

figure 3(C), InsP3R-II silencing was achieved without any impact on InsP3R-III message level. Moreover, we observed a dose dependence on silencing efficiency, since a higher CNT to siRNA ratio produced more efficient knocking down, with

no apparent impact on nonspecific gene silencing or toxicity. This finding is consistent with the idea that nanotube uptake into the cells increases as a function of nanotube concentration in the medium (Cherukuri *et al* 2004).

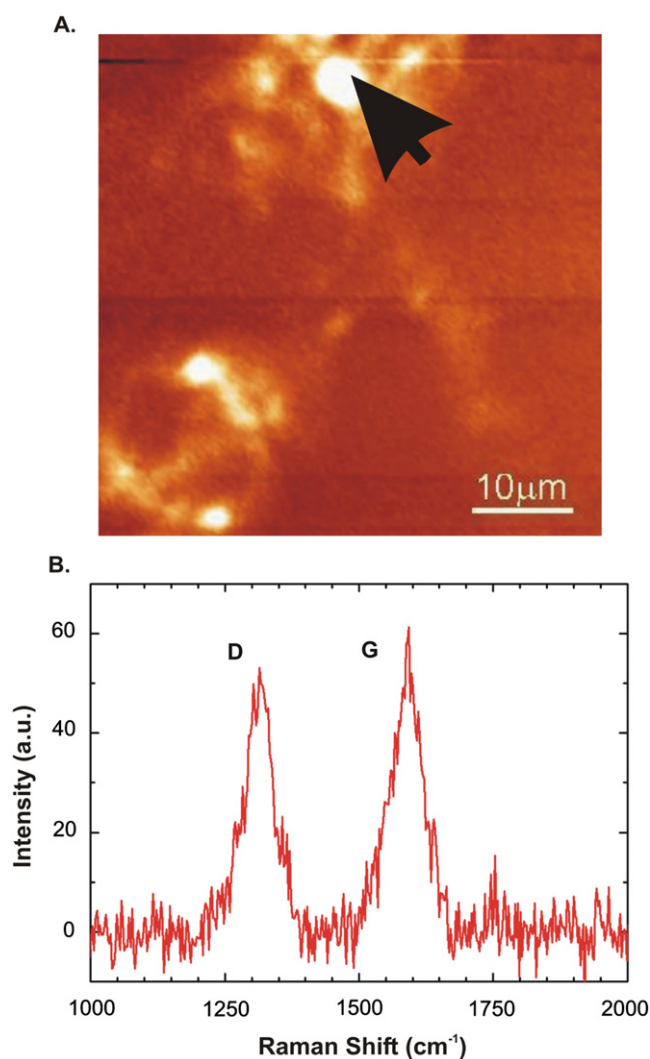


Figure 4. CNTs can be uptaken by neonatal cardiomyocytes. The G band Raman peak at 1590 cm^{-1} was used for CNT detection in this cell. (A) The plot of the carbon nanotube G band Raman intensity (degree of yellow) gives the CNT concentration inside the neonatal cardiomyocyte. (B) Representative Raman spectrum of neonatal cardiomyocytes exposed to CNTs (0.025 mg ml^{-1}) for 48 h taken from the area marked by the black arrow. The G and D carbon nanotube Raman peaks are highlighted.

3.3. Neonatal cardiomyocyte viability is not affected by internalized CNTs

In order to assess whether functionalized CNTs are also capable of carrying siRNA into neonatal cardiomyocytes, we first evaluated the internalization potential of CNTs into this cell type. Cardiomyocytes were incubated with 0.025 mg ml^{-1} CNTs for 48 h and then examined by Raman spectroscopy. Figure 4 panels (A) and (B) show the presence of CNTs inside neonatal cardiomyocytes, confirming the ability of CNTs to enter this cell.

In contrast to SKHeP 1 cells that are capable of proliferating, neonatal cardiomyocytes irreversibly withdraw from the cell cycle soon after birth and lose the cell proliferative activity (Campa *et al* 2008). Therefore, to evaluate CNT effects on cellular viability we used a

fluorescence-based live/dead assay (figure 5(A)). The bar graph in figure 5(B) shows that incubation of neonatal cardiomyocytes with a higher dose of CNTs (0.050 mg ml^{-1}) does not alter the proportion of live/dead cells when compared with untreated cells.

Neonatal cardiomyocytes beat spontaneously when maintained in culture, as a result of intracellular Ca^{2+} increase known as Ca^{2+} transient. In cardiomyocytes, $[\text{Ca}^{2+}]_i$ transients are induced by a Ca^{2+} influx triggering a large Ca^{2+} release from the sarcoplasmic reticulum (SR) (Lukyanenko *et al* 2001). To evaluate whether CNTs affect normal physiological behavior of cardiomyocytes, we recorded Ca^{2+} transients in Fluo-4/AM loaded cells after CNT exposure (final concentration 0.050 mg ml^{-1} for 48 h). As shown in figures 5(C) and (D), beating frequency was not different between neonatal cardiomyocytes treated or not with CNTs. In conclusion, no apparent change in cellular viability was observed in cardiomyocytes, even when a higher dose of CNTs was used (0.05 mg ml^{-1}). Taken together, these data present strong evidence that CNTs can enter inside cardiomyocytes with minimal side effects to the cells.

3.4. Efficient *InsP3R-II* silencing in neonatal cardiomyocytes

In order to investigate whether CNTs can efficiently deliver siRNAs inside neonatal cardiomyocytes, we transfected cells with the CNT-siRNA-InsP3R-II complex. In cardiomyocytes InsP3R-II is the predominant isoform and its distribution has been reported both in the sarcoplasmic reticulum and in the nuclear region (Garcia *et al* 2004, Guatimosim *et al* 2008). We exposed cardiomyocytes to the CNT-siRNA-InsP3R-II complex (0.0250 mg ml^{-1} and 100 nM of siRNA) and evaluated, by immunofluorescence using specific anti-InsP3R-II antibody, the expression levels of this receptor in the cell. As expected, InsP3R-II was found in the cytosol and nuclear envelope of control cells exposed to CNTs (figure 6(A)). In cells treated with the CNT-siRNA-InsP3R-II complex, InsP3R-II labeling was significantly reduced when compared to control cells. To investigate if InsP3R-II silencing affected the expression levels of other proteins in the cells, we analyzed the cellular distribution of another intracellular Ca^{2+} release channel in cardiomyocytes, RyR-II. RyR-II is the main Ca^{2+} release channel found in the sarcoplasmic reticulum of cardiomyocytes. In cells treated with the CNT-siRNA-InsP3R-II complex RyR-II immunostaining was not altered. Real-time quantitative PCR experiments corroborated these findings showing a significant silencing of InsP3R-II mRNA when cells were transfected with CNT-siRNA-InsP3R-II complex (figure 6(B)). Silencing efficiency exhibited a dose dependence since cells incubated with a higher proportion of CNTs to siRNA presented more reduced InsP3R-II mRNA levels. We also compared the efficiency of CNTs as an siRNA carrier to RNAiVect. CNT efficiency was almost two times higher than that obtained with the RNAiVect-siRNA-InsP3R-II complex (figure 6(B)). Accordingly, InsP3R-II silencing was achieved in neonatal cardiomyocytes without any impact on RyR-II mRNA levels (figure 6(C)). Interestingly, CNT efficiency as a transfection agent, when compared to a commercial agent, was more apparent in a hard-to-transfect cell type, such as cardiomyocytes, than in SKHeP 1 cells.

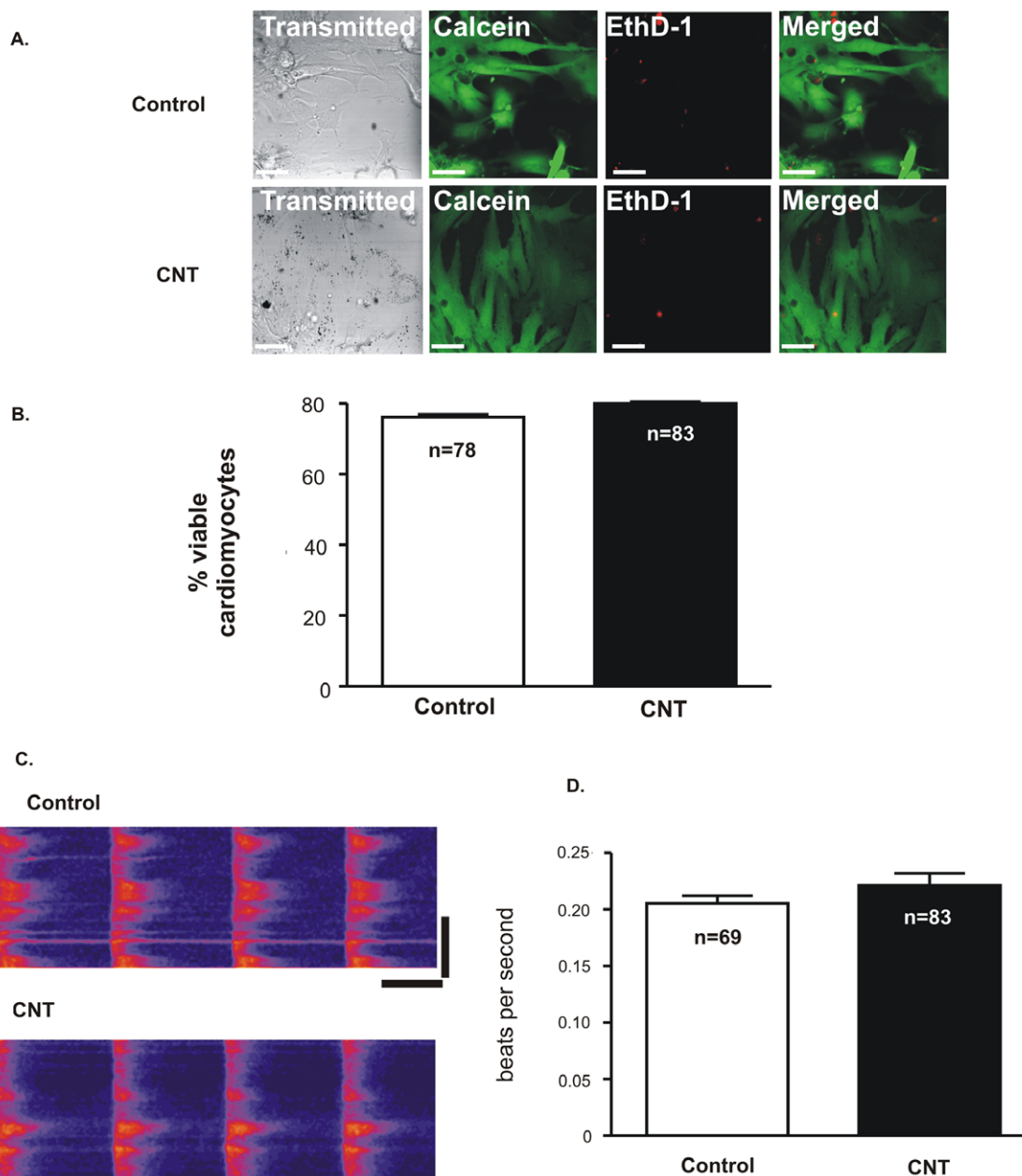


Figure 5. CNTs do not alter cardiomyocyte dynamics. (A) Cardiomyocytes were submitted to fluorescence-based live/dead viability assay. Dead cells were labeled with EthD-1 (red) and living cells were labeled with calcein AM (green). Images of neonatal cardiomyocytes exposed or not (untreated control) to CNTs (0.05 mg ml^{-1}) for 48 h were collected in a confocal microscope. (B) Averaged bar graph shows that cell viability is not altered by CNTs. Values are presented as mean \pm S.E.M. of three independent experiments. n = number of cells. (C) Representative line-scan confocal image of cells incubated or not with CNT solution. Neonatal cardiomyocyte beating frequency was monitored in Fluo-4/AM loaded cells following incubation with CNTs (0.05 mg ml^{-1}) for 48 h. (D) Averaged bar graph shows that CNTs do not alter cardiomyocyte beating frequency. The data shown is representative of three independent experiments. n = number of cardiomyocytes analyzed. Scale bar = $10 \mu\text{m}$.

3.5. Silencing efficiency of SWCNT-siRNA complex in DRG cells

In DRG neurons the InsP3R-I is the major isoform (Dent *et al* 1996). To evaluate the efficiency of CNTs as siRNA carriers in another hard-to-transfect cell, we performed immunofluorescence experiments in DRG neurons maintained in culture for 48 h in the presence of the CNT-siRNA-InsP3R-I complex formed by a combination of $0.0250 \text{ mg ml}^{-1}$ CNTs

to 100 nM siRNA. As shown in figure 7(A) DRG neurons express InsP3R-I in the cytosol and in the nucleus (Dent *et al* 1996, Blackshaw *et al* 2000). Significant reduction of InsP3R-I was observed in DRG cells exposed to the CNT-siRNA-InsP3R-I complex, when compared to CNT-exposed control cells. The transmitted image presented in figure 7(B) shows the uptake of the CNT-siRNA-InsP3R-I complex by DRG neurons. Panel 7(B) shows that DRG cells retain their morphological structure in the presence of CNTs.

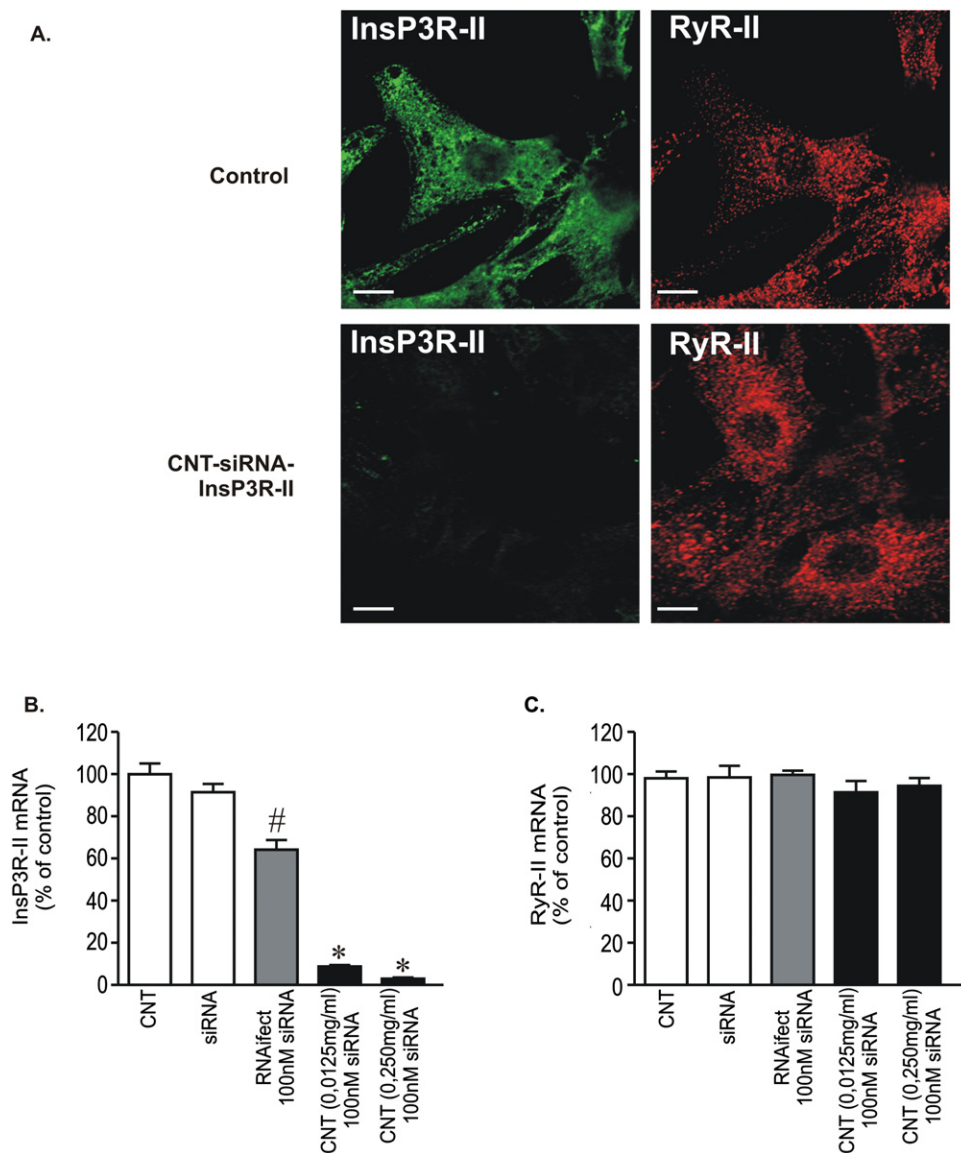


Figure 6. Efficient reduction of InsP3R-II expression in neonatal cardiomyocytes after CNT-siRNA-InsP3R-II complex transfection. (A) (top) Representative immunofluorescence of neonatal cardiomyocytes double-labeled with anti-InsP3R-II (green, left panel) and anti-RyR-II antibodies (red, right panel). (Bottom) Representative immunofluorescence of neonatal cardiomyocytes following transfection with CNT-siRNA-InsP3R-II complex for 48 h and double-labeled with anti-InsP3R-II (green, left panel) and anti-RyR-II antibodies (red, right panel). CNT efficiently delivered InsP3R-II siRNA (100 nM) into cardiomyocytes and reduced InsP3R-II expression in these cells. RyR-II immunolocalization was not altered in CNT-siRNA-InsP3R-II cardiomyocytes. Scale bar = 10 μm . (B) Forty eight hours following transfection with siRNA complexed with CNT or with a lipid-based gene transfer system (RNAiVect), cells were harvested, mRNA was isolated and real-time PCR was performed to determine the InsP3R-II expression levels. Real-time PCR assay shows that cells transfected with a combination of 3 μl RNAiVect and 100 nM siRNA presented a 30% reduction in InsP3R-II mRNA levels. For CNT-siRNA complex formation different concentrations of CNT (0.0125 or 0.025 mg ml^{-1}) were added to the diluted 100 nM final concentration of InsP3R-II siRNA. InsP3R-II gene was suppressed with higher efficiency in neonatal cardiomyocytes transfected with CNT-siRNA-InsP3R-II complex than with RNAiVect. (C) RyR-II transcript levels were determined in the same samples as in (B). RyR-II mRNA expression levels were not affected by incubation with RNAiVect or CNT-siRNA-InsP3R-II complex. The data shown are mean values \pm S.E.M of at least two independent experiments. # = $p < 0.05$ and * = $p < 0.001$ when compared with control data.

4. Discussion

Here we showed an examination of CNT properties by checking simultaneously its biocompatibility and efficiency as an siRNA delivery method. In this work, we were able to visualize an efficient knockdown of the siRNA target to the InsP3R isoform into three distinct cell types (DRG, neonatal

cardiomyocytes and SKHepl cells) by using purified short CNTs.

Strategies aimed to increase CNT delivery efficiency are constantly under investigation. A previous study has reported a highly efficient molecular delivery of DNA plasmid, based on the penetration of nickel-embedded CNTs into targeted cell membranes by magnetic field driving (Cai *et al* 2005). Other

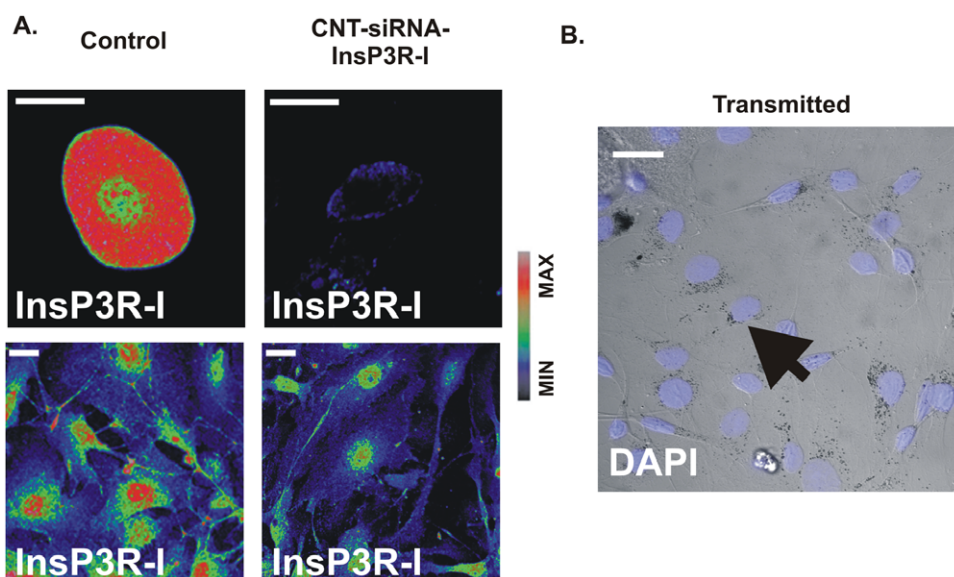


Figure 7. CNT–siRNA–InsP3R-I complex reduces InsP3R-I expression levels in DRG-transfected cells. (A) Immunofluorescence images of InsP3R-I labeled cells. CNT–siRNA was formed by a combination of 0.025 mg ml^{-1} CNT and 100 nM siRNA. CNTs efficiently delivered siRNA into DRG cells leading to decreased InsP3R-I expression levels. Images are pseudocolored according to the color scale. (B) Transmitted image of DRG cells showing the presence of CNT in the cytoplasm (arrow). Cell nucleus was labeled with Dapi (blue). Scale bar = $10 \mu\text{m}$.

groups have also used different strategies to deliver siRNA into mammal cells by chemically modifying CNTs with groups that could be covalently or electrostatically linked to the siRNA (Kam *et al* 2005, Rege *et al* 2006, Zhang *et al* 2006, Krajcik *et al* 2008). In fact, it has been shown that positively charged CNTs successfully mediate targeted gene interference when complexed with an siRNA concentration of 2 nM (Zhang *et al* 2006). While these approaches were efficient, they required complex modifications of the CNTs, which may have increased contamination with residues. Furthermore, most of these studies used immortalized cell lines that, in general, are considered easy to transfect (Kam *et al* 2005). The delivery efficiency presented by CNTs can be explained, at least in part, by its larger aspect ratio when compared to classical delivery systems, such as liposomes. It allows for more siRNA load and more efficient permeation through cell membranes (Kam and Dai 2006). In fact, CNTs can efficiently deliver siRNA into human T-cells and microglia, whereas conventional transfection vectors such as lipofectamine show little effect in the internalization of siRNA in these cell types (Liu *et al* 2007, Kateb *et al* 2007). A dependence of the delivery ability of nanotubes on functionalization and the degree of hydrophilicity has been reported previously (Liu *et al* 2007). Accordingly, hydrophobic interactions are an underlying factor in nanotube-mediated molecular delivery, suggesting that a balanced chemical functionalization should be achieved in order to handle solubility without impairing their ability to enter inside the cell (Liu *et al* 2007).

Although the biological effects of CNTs still remain unclear, evidence in support of non-cellular toxicity of CNTs is found in the literature (Shi Kam *et al* 2004, Pantarotto *et al* 2004, Zhang *et al* 2006, Liu *et al* 2007, Cui *et al* 2007, Dumortier *et al* 2006, Kateb *et al* 2007). In this study

we expanded this data by showing that CNTs do not affect cellular viability in spite of changing gene expression levels of important cellular pro-apoptotic genes and cell cycle regulators in SKHep 1 cells. However, we also noted a higher expression of survival genes, which may have compensated the increased expression of death genes. This data was confirmed by FACS, which showed no effect of CNTs on SKHep 1 cells viability. These data correlated with findings from a previous study (Shi Kam *et al* 2004) showing that the uptake of SWCNTs did not adversely affect HL60 cells at equivalent CNT concentration used in this work. No apparent change in cellular viability was also observed in cardiomyocytes, even when a higher dose of CNTs was used (0.05 mg ml^{-1}). Two lines of evidence support this assumption: (i) cardiomyocyte beating rate was not affected by CNT exposure and (ii) live/dead experiments indicated that exposure of cardiomyocytes to CNTs did not alter the percentage of live cells. This data is in line with a previous report showing a lack of toxicity of functionalized CNTs in cardiomyocytes (Krajcik *et al* 2008). Besides RyR immunolabeling or mRNA levels were similar in cardiomyocytes treated or not with CNTs.

Another important issue is the location of CNTs inside the cells. By using fluorescence microscopy, it has been reported the presence of CNTs inside phagosomes of a macrophage-like cell, with no apparent toxicity (Cherukuri *et al* 2004). Although some reports described that CNTs can enter the nucleus, its presence in the nucleus is still controversial (Mu *et al* 2009). We have observed the presence of CNTs in the cytosol of all cells studied, although the specific localization was not determined. More work is necessary in order to answer this question.

Surprisingly, 96% silence of the expression of InsP3R-II was achieved in cardiomyocytes, an amount which was

never reached by a commercially available method, until now. Moreover, we observed an efficient gene silencing by increasing the ratio of CNTs to siRNA, with no apparent impact on nonspecific gene silencing or toxicity. This finding is consistent with the idea that nanotube uptake into the cells increases as a function of nanotube concentration in the medium (Cherukuri et al 2004).

Different from our work, CNT preparations generally using side groups containing large carbon strain make siRNA binding to CNTs difficult. Furthermore, the increase in the number of positive charges on the CNT surface may cause a strong interaction between siRNA and CNTs, which may cause the release of siRNA from the complex difficult once inside the cell. The use of siRNA carriers based on short single-wall CNTs (length 50–500 nm) with just a few chemical groups such as COOH– or NH₃– is expected to overcome these problems by achieving three major goals: reduction of toxicity, enhancement of the stability of siRNA and increase of siRNA permeation into cells. In addition, CNT efficiency as a transfection agent was more apparent in a hard-to-transfect cell type, such as cardiomyocytes, than in SKHeP 1 cells.

In conclusion, short single-wall carboxylated-CNT–siRNA represents a very effective RNAi carrier to different cell types, providing an efficient silencing of the target gene with high specificity and large reduction in toxicity.

Acknowledgments

This work was supported by Instituto do Milênio/CNPq–MCT, Instituto Nacional de Ciência e Tecnologia de Nanomateriais de Carbono–CNPq (Conselho Nacional de Desenvolvimento Científico e Tecnológico) and Rede Mineira de Biotecnologia e Bioensaios (FAPEMIG), Brazil. RRR, SG, RGL, MFL and LOL are grateful for grants from CNPq (Conselho Nacional de Desenvolvimento Científico e Tecnológico) and FAPEMIG (Fundação de Amparo à Pesquisa do Estado de Minas Gerais), Brazil. We also would like to thank Bernardo R A Neves for the AFM measurements and Débora Pereira for helping with the functionalization experiments. MSL is a recipient of a CAPES PhD fellowship at the Post-graduation Program in Biological Science: Physiology and Pharmacology at UFMG.

References

- Blackshaw S, Sawa A, Sharp A H, Ross C A, Snyder S H and Khan A A 2000 Type 3 inositol 1,4,5-trisphosphate receptor modulates cell death. *FASEB J.* **14** 1375–9
- Cai D, Mataraza J M, Qin Z H, Huang Z, Huang J, Chiles T C, Carnahan D, Kempa K and Ren Z 2005 Highly efficient molecular delivery into mammalian cells using carbon nanotube sparring. *Nat. Methods* **2** 449–54
- Campa V M, Gutierrez-lanza R, Cerignoli F, Diaz-trelles R, Nelson B, Tsuji T, Barcova M, Jiang W and Mercola M 2008 Notch activates cell cycle reentry and progression in quiescent cardiomyocytes. *J. Cell Biol.* **183** 129–41
- Cherukuri P, Bachilo S M, Litovsky S H and Weisman R B 2004 Near-infrared fluorescence microscopy of single-walled carbon nanotubes in phagocytic cells. *J. Am. Chem. Soc.* **126** 15638–9
- Cherukuri P, Gannon C J, Leeuw T K, Schmidt H K, Smalley R E, Curley S A and Weisman R B 2006 Mammalian pharmacokinetics of carbon nanotubes using intrinsic near-infrared fluorescence. *Proc. Natl Acad. Sci. USA* **103** 18882–6
- Cui D, Tian F, Coyer S R, Wang J, Pan B, Gao F, He R and Zhang Y 2007 Effects of antisense-myc-conjugated single-walled carbon nanotubes on HL-60 cells. *J. Nanosci. Nanotechnol.* **7** 1639–46
- Da Silva E E, Della Colleta H H M, Ferlauto AS, Moreira R L, Resende R R, Oliveira S, Kitten G T, Lacerda R G and Ladeira L O 2009 Nanostructured 3D collagen/nanotube biocomposites for future bone regeneration scaffolds. *Nano Res.* **2** 462–73
- Dent M A, Raisman G and Lai F A 1996 Expression of type 1 inositol 1,4,5-trisphosphate receptor during axogenesis and synaptic contact in the central and peripheral nervous system of developing rat. *Development* **122** 1029–39
- Dubin R A, Callegari G, Kohn J and Neimark A 2008 Carbon nanotube fibers are compatible with mammalian cells and neurons. *IEEE Trans. Nanobiosci.* **7** 11–4
- Dumortier H, Lacotte S, Pastorin G, Marega R, Wu W, Bonifazi D, Briand J P, Prato M, Muller S and Bianco A 2006 Functionalized carbon nanotubes are non-cytotoxic and preserve the functionality of primary immune cells. *Nano Lett.* **6** 1522–8
- Echevarria W, Leite M F, Guerra M T, Zipfel W R and Nathanson M H 2003 Regulation of calcium signals in the nucleus by a nucleoplasmic reticulum. *Nat. Cell Biol.* **5** 440–6
- Garcia K D, Shah T and Garcia J 2004 Immunolocalization of type 2 inositol 1,4,5-trisphosphate receptors in cardiac myocytes from newborn mice. *Am. J. Physiol. Cell Physiol.* **287** C1048–57
- Guatimosim S et al 2008 Nuclear Ca(2+) regulates cardiomyocyte function. *Cell Calcium* **44** 230–42
- Hagar R E, Burgstahler A D, Nathanson M H and Ehrlich B E 1998 Type III InsP3 receptor channel stays open in the presence of increased calcium. *Nature* **396** 81–4
- Kam N W, Liu Z and Dai H 2005 Functionalization of carbon nanotubes via cleavable disulfide bonds for efficient intracellular delivery of siRNA and potent gene silencing. *J. Am. Chem. Soc.* **127** 12492–3
- Kam N W S and Dai H 2006 Single walled carbon nanotubes for transport and delivery of biological cargos. *Phys. Status Solidi b* **243** 3561–6
- Kateb B, Van handel M, Zhang L, Bronikowski M J, Manohara H and Badie B 2007 Internalization of MWCNTs by microglia: possible application in immunotherapy of brain tumors. *Neuroimage* **37** (suppl 1) S9–17
- Krajcik R, Jung A, Hirsch A, Neuhuber W and Zolk O 2008 Functionalization of carbon nanotubes enables non-covalent binding and intracellular delivery of small interfering RNA for efficient knock-down of genes. *Biochem. Biophys. Res. Commun.* **369** 595–602
- Leite M F, Hirata K, Pusch T, Burgstahler A D, Okazaki K, Ortega J M, Goes A M, Prado M A, Spray D C and Nathanson M H 2002 Molecular basis for pacemaker cells in epithelia. *J. Biol. Chem.* **277** 16313–23
- Liu Z, Davis C, Cai W, He L, Chen X and Dai H 2008 Circulation and long-term fate of functionalized, biocompatible single-walled carbon nanotubes in mice probed by Raman spectroscopy. *Proc. Natl Acad. Sci. USA* **105** 1410–5
- Liu Z, Winters M, Holodniy M and Dai H 2007 siRNA delivery into human T cells and primary cells with carbon-nanotube transporters. *Angew. Chem. Int. Edn Engl.* **46** 2023–7
- Lukyanenko V, Viatchenko-Karpinski S, Smirnov A, Wiesner T F and Gyorke S 2001 Dynamic regulation of sarcoplasmic reticulum Ca(2+) content and release by luminal Ca(2+)-sensitive leak in rat ventricular myocytes. *Biophys. J.* **81** 785–98
- Mendes C C, Gomes D A, Thompson M, Souto N C, Goes T S, Goes A M, Rodrigues M A, Gomez M V, Nathanson M H and Leite M F 2005 The type III inositol 1,4,5-trisphosphate receptor preferentially transmits apoptotic Ca2+ signals into mitochondria. *J. Biol. Chem.* **280** 40892–900

- Mu Q, Broughton D L and Yan B 2009 Endosomal leakage and nuclear translocation of multiwalled carbon nanotubes: developing a model for cell uptake *Nano Lett.* **9** 4370–5
- Pantarotto D, Briand J P, Prato M and Bianco A 2004 Translocation of bioactive peptides across cell membranes by carbon nanotubes *Chem. Commun. (Camb)* **16**–7
- Rege K, Viswanathan G, Zhu G, Vijayaraghavan A, Ajayan P M and Dordick J S 2006 *In vitro* transcription and protein translation from carbon nanotube–DNA assemblies *Small* **2** 718–22
- Resende R R, Gomes K N, Adhikari A, Britto L R and Ulrich H 2008 Mechanism of acetylcholine-induced calcium signaling during neuronal differentiation of P19 embryonal carcinoma cells *in vitro Cell Calcium* **43** 107–21
- Shi Kam N W, Jessop T C, Wender P A and Dai H 2004 Nanotube molecular transporters: internalization of carbon nanotube–protein conjugates into mammalian cells *J. Am. Chem. Soc.* **126** 6850–1
- Soares F A, Segundo G R, Alves R, Ynoue L H, Resende R O, Sopelete M C, Silva D A, Sung S S and Taketomi E A 2007 Indoor allergen sensitization profile in allergic patients of the allergy clinic in the University Hospital in Uberlandia, Brazil *Rev. Assoc. Med. Bras.* **53** 25–8
- Trigueiro J P *et al* 2007 Purity evaluation of carbon nanotube materials by thermogravimetric, TEM, and SEM methods. *J. Nanosci. Nanotechnol.* **7** 3477–86
- Wojcikiewicz R J 1995 Type I, II, and III inositol 1,4,5-trisphosphate receptors are unequally susceptible to down-regulation and are expressed in markedly different proportions in different cell types *J. Biol. Chem.* **270** 11678–83
- Zhang Z, Yang X, Zhang Y, Zeng B, Wang S, Zhu T, Roden R B, Chen Y and Yang R 2006 Delivery of telomerase reverse transcriptase small interfering RNA in complex with positively charged single-walled carbon nanotubes suppresses tumor growth *Clin. Cancer Res.* **12** 4933–9

Metadata of the chapter that will be visualized in Online

Series Title	
Chapter Title	Signaling Pathways in Biliary Epithelial Cells
Chapter SubTitle	
Copyright Year	2010
Copyright Holder	Springer-Verlag Berlin Heidelberg
Corresponding Author	Family Name Nathanson Particle Given Name Michael H. Suffix Division Department of Medicine Organization Yale University School of Medicine Address 1 , Gilbert Street , Room TAC S241D, 06520-8019, New Haven, CT, USA Email michael.nathanson@yale.edu
Author	Family Name Leite Particle Given Name M. Fatima Suffix Division Department of Medicine Organization Yale University School of Medicine Address 1 , Gilbert Street , Room TAC S241D, 06520-8019, New Haven, CT, USA Email
Author	Family Name Andrade Particle Given Name Viviane A. Suffix Division Department of Medicine Organization Yale University School of Medicine Address 1 , Gilbert Street , Room TAC S241D, 06520-8019, New Haven, CT, USA Email
Abstract	Biliary epithelial cells, or cholangiocytes, line the lumen of the biliary tree. Like hepatocytes, cholangiocytes are a polarized epithelium with structural features that include well-defined apical and basolateral membrane domains. Cholangiocytes constitute approximately 5% of the mass of the liver and play an important role in the formation of bile by altering primary canalicular bile through a series of secretory and reabsorptive events. These events are regulated by peptide hormones, nucleotides, bile salts, growth factors, cytokines, and neurotransmitters that bind to and stimulate specific apical or basolateral surface membrane receptors, which in turn initiate intracellular signal transduction pathways that regulate cell function. In addition to their role in the modification of ductal bile, cholangiocytes participate in the detoxification of xenobiotics [1].

Signaling Pathways in Biliary Epithelial Cells

2

M. Fatima Leite, Viviane A. Andrade, and Michael H. Nathanson

4 Introduction

Biliary epithelial cells, or cholangiocytes, line the lumen of the biliary tree. Like hepatocytes, cholangiocytes are a polarized epithelium with structural features that include well-defined apical and basolateral membrane domains. Cholangiocytes constitute approximately 5% of the mass of the liver and play an important role in the formation of bile by altering primary canalicular bile through a series of secretory and reabsorptive events. These events are regulated by peptide hormones, nucleotides, bile salts, growth factors, cytokines, and neurotransmitters that bind to and stimulate specific apical or basolateral surface membrane receptors, which in turn initiate intracellular signal transduction pathways that regulate cell function. In addition to their role in the modification of ductal bile, cholangiocytes participate in the detoxification of xenobiotics [1].

In the adult liver, cholangiocytes are mitotically dormant [2]. Cholangiocyte proliferation may include some combination of proliferation of preexisting ductules, progenitor cell activation, and appearance of intermediate hepatocytes. Proliferating cholangiocytes display enhanced secretory activity. This may serve to compensate for the impaired secretion of injured cells and maintain biliary mass and secretory function during disease states [2]. Cholangiocytes are the primary target of injury in a variety of cholestatic liver diseases, such as sclerosing cholangitis, primary biliary cirrhosis, cystic fibrosis, and biliary atresia. There is evidence

that signaling pathways are altered in such disorders, which may contribute to the secretory defects that characterize these diseases. Cholestatic disorders represent the main indication for liver transplantation in pediatrics and are a common indication in adults [3, 4].

This chapter will systematically review the membrane receptors and associated intracellular signaling pathways that regulate cholangiocyte function, and will discuss the alterations that occur in these signaling pathways in cholangiopathic diseases.

Membrane Receptors

Several well-characterized families of membrane receptors have been identified in cholangiocytes. The receptors that associate with guanosine triphosphate (GTP)-binding regulatory proteins, or G proteins, constitute the largest family.

Members of the G protein-coupled receptor family share structural and functional similarities, and contain seven hydrophobic membrane-spanning domains plus a cytoplasmic site for binding to G proteins. At least fifteen G proteins have been identified and each consists of a heterotrimeric complex consisting of alpha, beta, and gamma subunits. The alpha subunit has intrinsic GTPase activity at the guanine nucleotide binding site, plus a specific binding site for the receptor and effector proteins. When a ligand binds to the receptor, guanosine diphosphate (GDP) rapidly exchanges for GTP, which allows the G protein to dissociate from the receptor and the alpha subunit to dissociate from the beta-gamma subunits. The dissociated subunits then activate effector proteins such as adenylate cyclase, phospholipase C (PLC) or other hydrolyses, which in turn generates or activates signaling molecules such as cyclic adenosine

M. H. Nathanson (✉)
Department of Medicine, Yale University School of Medicine,
1, Gilbert Street, Room TAC S241D, New Haven,
CT 06520-8019, USA
e-mail: michael.nathanson@yale.edu

J.-F. Dufour, P.-A. Clavien (eds.), *Signaling Pathways in Liver Diseases*,
DOI: 10.1007/978-3-642-00150-5_2, © Springer-Verlag Berlin Heidelberg 2009

66 monophosphate (cAMP), cAMP-dependent protein
 67 kinase A (PKA), inositol 1,4,5-trisphosphate (InsP3),
 68 1-2 diacylglycerol (DAG), cytoplasmic calcium (Ca_i^{2+}),
 69 or protein kinase C (PKC). G protein-coupled receptors
 70 that have been identified in cholangiocytes include the
 71 secretin receptor, the bombesin receptor, the vasoactive
 72 intestinal peptide (VIP) receptor, the M3 muscarinic
 73 acetylcholine receptor, the gastrin receptor, the α_{1B} and
 74 α_2 adrenergic receptors, the somatostatin receptor, the
 75 type A and B endothelin receptors, the serotonin recep-
 76 tor, and several subtypes of the P2Y nucleotide recep-
 77 tor. Cholangiocytes also express all four subtypes of the
 78 histamine receptor. These subtypes are classified as
 79 H1R, H2R, H3R, and H4 and have been identified in
 80 both small and large cholangiocytes [5]. Under normal
 81 conditions, the predominant histamine receptors in cho-
 82 langiocytes are H1R, which increases cytoplasmic Ca^{2+}
 83 via Gq, and H2R, which increases cAMP via Gs.
 84 Activation of H1R is associated with calmodulin-
 85 dependent stimulation of calmodulin-dependent protein
 86 kinase (CaMK) and activation of cAMP-response ele-
 87 ment binding protein (CREB), which results in cholan-
 88 giocyte proliferation [6]. Following bile duct ligation,
 89 expression shifts to H3R and H4R, both of which inhibit
 90 cAMP formation [7]. This serves to inhibit PKA activa-
 91 tion, which decreases activation of ERK 1/2 and Elk-1,
 92 which in turn retards proliferation of cholangiocytes
 93 [7]. Functional evidence suggests that cholangiocytes
 94 can signal via the endocannabinoid system as well,
 95 which consists of the G protein-coupled cannabinoid
 96 receptors Cb1 and Cb2 that are activated by anandamide
 97 (AEA). These receptors could be of relevance in the
 98 pathogenesis of liver fibrosis and portal hypertension
 99 [8]. For example, treatment of cholangiocytes with
 100 AEA impairs cholangiocyte proliferation after extrahe-
 101 patic biliary obstruction [9]. Activation of this pathway
 102 involves the accumulation of reactive oxygen species
 103 and activation and nuclear translocation of thioredoxin
 104 1 (TRX1), where it interacts with redox factor 1 (Ref1)
 105 to modulate the DNA-binding activity of the activator
 106 protein 1 (AP-1) transcription factor complex [9].
 107 Activation of Cb receptors and of the endocannabinoid
 108 pathway thus plays a role in the suppression of cholan-
 109 giocyte proliferation.

110 Non-G protein-coupled receptors have also been
 111 identified in cholangiocytes. This broad group includes
 112 receptors for epidermal growth factor (EGF), nerve
 113 growth factor, insulin, interleukins, and lipopolysac-
 114 charides. These receptors typically have a single

115 plasma membrane spanning domain and possess
 116 ligand-activated tyrosine kinase activity. Such receptor
 117 tyrosine kinases stimulate several downstream signal
 118 transduction pathways, including those associated with
 119 phosphatidyl inositol metabolism and the mitogen-
 120 activated protein kinase (MAPK) cascade. The MAPK
 121 pathway requires several steps for activation, involving
 122 autophosphorylation of the tyrosine kinase receptor
 123 that provides recognition and binding sites for the src
 124 homology (SH2) domain of the adaptor molecule Grb2.
 125 This in turn causes the binding of another protein, SOS,
 126 at the SH3 domain of Grb2, required for activation of
 127 the ras proto-oncogene. Ras triggers the Ras/Raf/MEK/
 128 MAPK cascade reaction [10]. The serine/threonine
 129 protein kinases of the Raf family (Raf-1, B-Raf, and
 130 A-Raf) play a key role in growth factor signaling by the
 131 phosphorylation and stimulation of MEK, then MAPK
 132 [11, 12] and subsequently, by the intranuclear activa-
 133 tion of transcription factors, including Elk-1, myc, fos,
 134 and jun [13]. This signaling pathway induces a variety
 135 of biological responses, including cell proliferation,
 136 differentiation, and apoptosis. ERK signaling further-
 137 more undergoes spatial control by Sef, an inhibitor that
 138 acts as a molecular switch for ERK by specifically
 139 inhibiting nuclear translocation of ERK without inhib-
 140 iting its activity in the cytoplasm [14]. The Ras/Raf/
 141 MEK/MAPK cascade reaction also can be modulated
 142 via cross talk with other intracellular signaling path-
 143 ways. In some cells, including cholangiocytes, cAMP/
 144 PKA signaling inhibits MAPK activity through the inhi-
 145 bition of Raf-1 and B-Raf activation [15, 16]. On the
 146 other hand, stimulation of cytokine receptor C-X-C
 147 motif chemokine receptor 4 (CXCR4) via the CXC
 148 chemokine ligand 12 (CXCL12) plays an important role
 149 in cholangiocarcinoma cell invasion by induction of the
 150 ERK1/2 and AKT pathways [17]. Inflammation signals
 151 mediated by the inflammatory cytokine IL-6 also induce
 152 the ERK and AKT pathways and enhance expression of
 153 the anti-apoptotic protein Mcl-1 in cholangiocarcinoma
 154 cells, thereby enhancing their survival [18].

155 Bile acids activate several membrane receptors in
 156 cholangiocytes. Bile acids activate the epidermal
 157 growth factor receptor (EGFR), which occurs through
 158 a TGF α -dependent mechanism [13, 19]. Bile acids also
 159 regulate the expression of death receptor 5/TRAIL-
 160 receptor 2 via a c-Jun N-terminal kinase-dependent
 161 pathway and modulate the IGF1 system [20]. This
 162 effect depends upon the hydrophobicity of the bile salt,
 163 with deoxycholate exerting a maximal effect and

2 Signaling Pathways in Biliary Epithelial Cells

164 ursodeoxycholate exerting no measurable effect. This
165 pathway protects cholangiocytes as well as hepato-
166 cytes against bile acid-induced cytotoxicity [20, 21].
167 Finally, there is an evidence that bile salts may activate
168 the cystic fibrosis transmembrane conductance regula-
169 tor (CFTR) Cl^- channel [22]. CFTR and the apical
170 sodium-dependent bile acid transporter (ASBT) colo-
171 calize on the apical membrane of large cholangiocytes
172 [23] and evidence suggests that taurocholate directly
173 modulates gating of the CFTR Cl^- channel [22].

174 Cholangiocytes express not only cell membrane
175 receptors, but also intracellular steroid hormone recep-
176 tors. Steroid hormones enter cells by passive diffusion
177 across the plasma membrane in order to bind to their
178 intracellular receptor. Receptor binding results in a con-
179 formational change that increases the affinity of the
180 receptor to bind to DNA. Specific binding sites are
181 present on regulatory regions of genes, which serve to
182 alter transcription and thus protein synthesis. Steroid
183 receptors characterized in cholangiocytes include the α
184 and β estrogen receptors ($\text{ER}\alpha$ and β , respectively)
185 [24]. Cholangiocarcinomas express $\text{ER}\alpha$ and β , insulin-
186 like growth factor 1 (IGF1) and IGF1 receptor (IGF1R).
187 In these cells, estrogens cooperate with IGF1 and their
188 receptor to modulate tumor growth [25]. Estrogens also
189 induce the expression of vascular endothelial growth
190 factor receptor (VEGFR) and may enhance cell prolif-
191 eration on that basis as well [24–26].

192 Cyclic Adenosine 3', 5'-Monophosphate 193 (cAMP)

194 Adenylate cyclase is a membrane-bound enzyme that
195 can be regulated by alpha subunits of two G proteins,
196 G_i and G_s . G_i inhibits adenylate cyclase activity, while
197 G_s catalyzes the formation of cAMP from adenosine
198 triphosphate (ATP). Cyclic AMP then activates PKA,
199 which in turn phosphorylates a range of intracellular
200 proteins, triggering a series of events that lead to spe-
201 cific cellular responses, such as ion secretion, absorp-
202 tion, and motility. Specific effects of cAMP in
203 cholangiocytes include stimulation of exocytosis [27],
204 opening of aquaporin water channels [28, 29], activa-
205 tion of the cystic fibrosis transmembrane conductance
206 regulator (CFTR) Cl^- channel [30, 31], and activation of
207 $\text{Cl}^-/\text{HCO}_3^-$ exchange [32, 33]. Increases in cAMP in
208 cholangiocytes, increase ductular bile flow in isolated

209 bile duct units [32–35], but not in the intact, perfused
210 rat liver [36]. This apparent inconsistency may be
211 explained by the observation that ductular secretion in
212 rats accounts for only ~10% of total bile flow [37].

213 Secretin receptors belong to the class of G protein-
214 coupled receptors that activate adenylate cyclase to
215 increase cAMP formation [38, 39]. Activation of the
216 secretin receptor does not affect Ca_i^{2+} in isolated bile
217 duct cells [40], nor does it affect cAMP production in
218 hepatocytes [38]. Thus, in the liver these receptors are
219 expressed only by cholangiocytes [38] and are local-
220 ized to the basolateral membrane of these cells.
221 Stimulation of secretin receptors induces ductal secre-
222 tion by activation of CFTR. Among the different types
223 of ion channels expressed by cholangiocytes, CFTR
224 has been investigated most extensively and appears to
225 be largely responsible for secretin-stimulated increases
226 in apical Cl^- secretion. Phosphorylation by PKA
227 increases the open probability of plasma membrane
228 CFTR channels, which is the mechanism by which
229 cAMP increases apical Cl^- secretion through this ion
230 channel [41]. Activation of CFTR is also associated
231 with ductular bicarbonate excretion, since forskolin, a
232 direct activator of adenylyl cyclase, alkalinizes the lumen
233 of isolated bile duct units [35]. Studies in isolated cho-
234 langiocytes and bile duct units suggest that Cl^- secre-
235 tion via CFTR is linked to $\text{Cl}^-/\text{HCO}_3^-$ exchange [32, 34],
236 and that this linkage leads to net secretion of HCO_3^- by
237 bile duct epithelia [42]. However, work in the intact,
238 perfused liver instead suggests that secretin-induced
239 HCO_3^- secretion depends on the activation of Cl^- chan-
240 nels, but not on $\text{Cl}^-/\text{HCO}_3^-$ exchange [36]. In fact,
241 direct evidence in other systems similarly shows that
242 CFTR can regulate bicarbonate efflux directly, rather
243 than through activation of $\text{Cl}^-/\text{HCO}_3^-$ exchange [43–46].
244 It has been suggested that these apparent differences
245 between in vitro and in vivo studies may be related to
246 paracrine effects as well as vascular factors that alter
247 signaling and secretion in vivo. Yet another possible
248 mechanism for cAMP-mediated ductular HCO_3^- secre-
249 tion has been delineated in microdissected, microper-
250 fused intrahepatic bile ductal units (IBDUs). In this
251 experimental system, forskolin-induced alkalinization
252 of the ductular lumen could be inhibited by knock-
253 down of the apical, type III inositol 1,4,5-trisphosphate
254 receptor (InsP_3R) in cholangiocytes or by hydrolysis of
255 luminal ATP, inhibition of apical P2Y nucleotide
256 receptors, or buffering of cytosolic Ca^{2+} signals [47].
257 These findings suggest that cAMP-induced ductular

258 HCO_3^- secretion depends on an autocrine signaling
259 pathway that involves CFTR-mediated apical secre-
260 tion of ATP, which leads to the stimulation of apical
261 P2Y receptors, and then to the activation of apical,
262 type III InsP_3Rs [47]. Regardless of the mechanism, it
263 is well accepted that increases in cAMP lead to HCO_3^-
264 excretion in cholangiocytes.

265 Water movement into the ductular lumen is
266 increased by the increase in cAMP in cholangiocytes
267 [34, 35]. Cholangiocytes contain secretory vesicles that
268 are enriched in aquaporin-1, a water-selective channel
269 protein, as well as CFTR, other Cl^- channels and the
270 $\text{Cl}^-/\text{HCO}_3^-$ exchanger [48]. Secretin or dibutyl cAMP
271 causes a rapid redistribution of these secretory vesicles
272 from the cell interior to the apical membrane of cho-
273 langiocytes, leading to ion-driven water-transport and
274 ductal bile secretion [27, 28, 48, 49].

275 Hormonal stimulation can serve not only to increase
276 cAMP-mediated secretion in cholangiocytes, but also
277 to decrease it. For instance, somatostatin acts on cho-
278 langiocytes via SSTR2 somatostatin receptors to
279 increase cGMP, which inhibits secretin-stimulated
280 cAMP synthesis, thereby decreasing bile formation
281 through a combination of events that involve inhibition
282 of ductal fluid secretion and stimulation of ductal fluid
283 absorption [50]. Gastrin and endothelin-1, hormones
284 that activate the PLC pathway, also inhibit secretin-
285 stimulated secretion. Like somatostatin, gastrin and
286 endothelin-1 inhibit secretin-induced ductal bile secre-
287 tion by binding to their specific cholangiocyte recep-
288 tors, which links to decreased expression of the secretin
289 receptor and a decrease in secretin-stimulated cAMP
290 formation [49, 51–53].

291 Cyclic AMP has effects not only on secretion but
292 also on proliferation. Administration of a cell-permeant
293 form of cAMP enhances proliferation of cholangio-
294 cytes after bile duct ligation, whereas, the neuroendo-
295 crine hormone serotonin inhibits proliferation.
296 Serotonin acts on cholangiocytes through both the 1A
297 and 1B subtypes of its receptor. Animals subjected to
298 bile duct ligation are treated with serotonin receptor
299 agonists; there is a strong reduction in secretin-induced
300 bile flow, HCO_3^- secretion, cAMP synthesis, and PKA
301 activity [54]. Therefore, activation of the serotonin 1A
302 and 1B receptor in cholangiocytes inhibits prolifera-
303 tion by reducing cAMP formation and subsequent acti-
304 vation of PKA.

305 Bombesin, VIP, and ATP each stimulate cholangi-
306 cyte secretory responses similar to the effect of

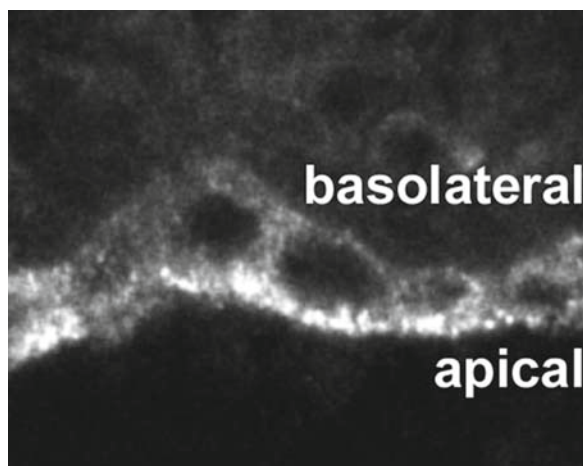
secretin, but unlike secretin, the effects of these agents
do not appear to be mediated by cAMP [55–57]. The
signaling pathways involved in such cAMP-indepen-
dent secretory responses in cholangiocytes are not well
characterized yet, but seems likely that Cl^- channels
other than CFTR are involved. In fact, a number of
other types of Cl^- channels have been identified in cho-
langiocytes [58], but the exact role of these channels in
ductular secretion remains unclear.

Cytosolic Ca^{2+}

316
317 Phosphatidylinositol 4,5-bisphosphate (PIP_2) is a
318 membrane lipid that is a substrate for PLC. Once it has
319 been activated by a specific class of G protein-coupled
320 receptors, PLC cleaves PIP_2 into two signaling mole-
321 cules, DAG and InsP_3 . DAG is lipophilic and remains
322 at the membrane, where it activates PKC. InsP_3 is a
323 water-soluble molecule that diffuses through the cyto-
324 sol to interact with the InsP_3R , which stimulates the
325 release of Ca^{2+} from intracellular Ca^{2+} stores into the
326 cytosol. Three isoforms of the InsP_3R have been iden-
327 tified and are termed type I, type II, and type III.
328 Although the three isoforms have a high degree of
329 sequence homology and behave as InsP_3 -gated intracel-
330 lular Ca^{2+} release channels, they differ in sensitivity
331 to InsP_3 , with the type II isoform being the most sensi-
332 tive, followed by the type I, and then the type III [59].
333 The open probability of each isoform of InsP_3R is fur-
334 ther regulated by Ca^{2+} itself, but the effect of Ca^{2+} on
335 each isoform appears to be distinct [60, 61]. InsP_3R
336 isoforms are expressed in relatively unique proportions
337 in different tissues and have specific subcellular pat-
338 terns of distribution as well. The behavior of the
339 InsP_3R is also altered by tissue-specific expression of
340 various cofactors that interact with and modify the
341 behavior of the InsP_3R . For example, chromogranin A
342 and chromogranin B each binds to the ER luminal
343 aspect of the InsP_3R and increases the open probabili-
344 ty of the receptor [62, 63]. Chromogranin A is found in
345 cholangiocytes but not hepatocytes [64], while chro-
346 mogranin B is not found in the liver. The differences in
347 behavior of each InsP_3R isoform, along with tissue-
348 specific patterns of distribution of the isoforms and
349 their cofactors, suggest that these factors may permit
350 tissue-specific patterns of Ca^{2+} signaling. Rat cholangi-
351 cytes express all three isoforms of InsP_3R [65]. The

2 Signaling Pathways in Biliary Epithelial Cells

AQ2



AQ1

Fig. 2.1 The type III InsP3 receptor is concentrated in the apical region of cholangiocytes. Image shows confocal immunofluorescence labeling of a section through rat liver. The tissue was labeled with a monoclonal antibody directed against the N-terminal region of the type III InsP3R (image provided courtesy of Dr. Keiji Hirata)

352 type III InsP3R is expressed most heavily and is con- 380
 353 centrated apically (Fig. 2.1) while type I and type II 381
 354 InsP3R are expressed to a similar extent and are dis- 382
 355 tributed uniformly throughout the cytosol. Human 383
 356 cholangiocytes, like rat cholangiocytes, express all 384
 357 three InsP3R isoforms, and express the type III iso- 385
 358 form most heavily [66]. NRC cells, a polarized rat cho- 386
 359 langiocyte cell line, express the type III InsP3R almost 387
 360 exclusively, and this isoform is concentrated apically 388
 361 in these cells, just as in primary cholangiocytes [65]. 389

362 The ryanodine receptor (RyR) is a separate intracel- 390
 363 lular Ca^{2+} release channel that plays a major role in 391
 364 cytosolic Ca^{2+} signaling. Like the InsP3R, the RyR has 392
 365 three isoforms, each of which displays distinct func- 393
 366 tional properties. It was believed initially that RyRs 394
 367 regulate Ca^{2+} signaling only in myocytes, whereas 395
 368 InsP3Rs regulate Ca^{2+} signaling in nonexcitable cells 396
 369 such as epithelia. However, many cell types express 397
 370 both RyR and InsP3R [67, 68] including a number of 398
 371 polarized epithelia [69, 70]. Each RyR isoform is acti- 399
 372 vated by a process known as Ca^{2+} -induced Ca^{2+} release 400
 373 (CICR). The type II and III RyRs also are sensitive to 401
 374 cyclic adenosine diphosphate (ADP)-ribose (cADPr) 402
 375 [71, 72]. Cholangiocytes from rat liver do not express 403
 376 RyR, but faint expression of type I RyR can be detected 404
 377 in NRC cells by RT-PCR [65]. 405

378 Cytosolic Ca^{2+} signals are encoded through signaling 406
 379 patterns such as Ca^{2+} waves and Ca^{2+} oscillations, and 407

both of these types of Ca^{2+} signals occur in cholangio- 380
 cytes [40, 65]. The ability to form Ca^{2+} waves in cholan- 381
 giocytes and other polarized epithelia is thought to 382
 depend on the pattern of expression of InsP3R isoforms 383
 [73]. Specifically, Ca^{2+} waves begin in the apical region 384
 of cholangiocytes, where the type III InsP3R is concen- 385
 trated [65]. This association is observed in other epithelia 386
 as well [74, 75], and indeed the single-channel behavior 387
 of the type III receptor suggests that it may trigger Ca^{2+} 388
 waves [60]. Ca^{2+} signals can spread among neighboring 389
 cholangiocytes. This effect is mediated by gap junctions 390
 in most epithelia [76], including cholangiocytes [77]. 391
 The types of Ca^{2+} release channels in the basolateral 392
 region may also affect the formation of Ca^{2+} waves. For 393
 example, in pancreatic acinar cells all three InsP3R iso- 394
 forms are concentrated in the apical region, whereas the 395
 RyR is basolateral [69]. In contrast, the type III isoform 396
 of the InsP3R predominates in the apical region while 397
 expression of the other isoforms is not limited to this 398
 region in both cholangiocytes and nonpigmented epithe- 399
 lial cells of the ocular ciliary body [65, 74]. 400

Formation of polarized Ca_i^{2+} waves may be impor- 401
 tant for regulation of secretion in particular. Ca_i^{2+} 402
 waves regulate secretion in several ways, including 403
 activation of specific transporters and ion channels 404
 [78], and stimulation of vesicle fusion with the plasma 405
 membrane [79]. Vesicle fusion can in turn promote 406
 secretion either via exocytic release of vesicles con- 407
 tents [80], or by inserting additional transporters or 408
 channels into the plasma membrane, as occurs with 409
 canalicular transporters in the hepatocyte [81]. In cho- 410
 langiocytes, ductular secretion depends upon apical 411
 insertion of water channels [28, 29] and other mem- 412
 brane fusion events [27, 82]. In these cells, Ca_i^{2+} regu- 413
 lates ductular secretion through pathways that differ 414
 from those activated by cAMP. Ca_i^{2+} directly activates 415
 apical Ca^{2+} -dependent Cl^- channels that are distinct from 416
 CFTR [31, 83], so that either Ca^{2+} or cAMP can mediate 417
 apical bicarbonate secretion [36, 84]. However, Ca^{2+} may 418
 also potentiate cAMP-mediated secretion. In particular, 419
 activation of M3 muscarinic receptors by acetylcholine 420
 enhances secretin-induced cAMP formation [85, 86] 421
 and accelerates secretin-induced Cl^-/HCO_3^- exchange 422
 [32]. This is mediated by calcineurin and inhibited by 423
 cyclosporin [32]. This effect has been observed in the 424
 intact, perfused liver as well, but only if secretin is 425
 administered before cyclosporin [36]. 426

Ca^{2+} oscillations can be induced in cholangiocytes by 427
 either ATP or acetylcholine. ATP-induced oscillations 428

429 have been observed both in individual cholangiocytes
 430 within isolated bile duct units and in NRC cells [40, 65,
 431 77]. This Ca_i^{2+} signaling pattern is concentration-depend-
 432 ent, since lower concentration of ATP predominantly
 433 induces Ca_i^{2+} oscillations, whereas, higher concentra-
 434 tions predominantly induce single increases in Ca_i^{2+} [40].
 435 ATP is a signaling molecule in virtually all types of tis-
 436 sues, and at least 18 types of purinergic receptors have
 437 been identified. Cholangiocytes and biliary cell lines
 438 express P2X receptors [84, 87], which are ATP-gated
 439 cation channels, as well as P2Y receptors [84, 88], which
 440 are G protein-coupled receptors that increase Ca_i^{2+} via
 441 InsP3. However, ATP-induced Ca^{2+} signaling in chol-
 442 angocytes occurs principally via apical P2Y1, P2Y2,
 443 P2Y4, and P2Y6 subtypes of the P2Y receptor [89, 90].

444 Individual hepatocytes can release nucleotides in
 445 amounts sufficient to induce Ca_i^{2+} signals in cocultured
 446 bile duct cells [91], and measurable amounts of ATP
 447 can be detected in rodent and human bile [92, 93].
 448 Thus, one possible mechanism for paracrine regulation
 449 of Ca^{2+} signaling in cholangiocytes may be for hepa-
 450 tocytes to signal to cholangiocytes through release of
 451 nucleotides into bile, followed by activation of api-
 452 cal P2Y receptors. Stimulation of cholangiocyte P2Y
 453 receptors in turn results in InsP3-mediated increases in
 454 cytosolic Ca^{2+} , leading to ductular bicarbonate secre-
 455 tion [84]. Autocrine regulation of Ca^{2+} signaling in cho-
 456 langiocytes may occur through a related mechanism in
 457 which cAMP induces CFTR-mediated release of ATP
 458 into bile [47], as described above. Cholangiocytes
 459 also express basolateral P2Y receptors [40, 84], which
 460 may mediate signaling from neural or vascular tissues.
 461 However, signaling via basolateral nucleotide receptors
 462 is attenuated by the expression of NTPDases by portal
 463 fibroblasts [94]. Cholangiocytes express multiple P2Y
 464 receptor subtypes [84]. P2Y12 receptors are expressed
 465 in the primary cilia on the apical surface of chol-
 466 angocytes. Cilia are sensory organelles which respond
 467 to chemical, osmotic, and mechanical stimuli [95].
 468 Unlike most other P2Y receptors, the P2Y12 recep-
 469 tor is a G protein-coupled receptor associated with
 470 cAMP instead of Ca^{2+} signaling [96]. The expression
 471 of P2Y12 receptors in rat cholangiocytes links specifi-
 472 cally to the chemo-sensory function of primary cilia
 473 [96]. Stimulation of P2Y12 receptors in rat cholangi-
 474 ocytes by either ADP or ATP- γ S activates G_i and thus
 475 inhibits forskolin-induced formation of cAMP [96].
 476 Cholangiocyte cilia also express TRPV4, a member of
 477 the transient receptor potential (TRP) superfamily of

Ca^{2+} channels. Activation of this channel via hypotonic 478
 stimuli induces an increase in cytosolic Ca^{2+} , as well as 479
 apical release of ATP and an increase in HCO_3^- secre- 480
 tion [95]. Therefore, stimulation of primary cilia acti- 481
 vates a variety of signaling pathways in cholangiocytes, 482
 which depends in part upon the type of stimulus [95]. 483

484 Most studies of Ca^{2+} signaling in cholangiocytes 484
 have examined signals induced by hormones and other 485
 humoral factors. However, increasing evidence sug- 486
 gests that neurotransmitters regulate Ca^{2+} signals in 487
 bile ducts as well. Acetylcholine activates M3 muscar- 488
 inic receptors [85] to induce Ca^{2+} waves and oscilla- 489
 tions in isolated bile duct units [40, 65]. Unlike ATP, 490
 acetylcholine induces Ca^{2+} oscillations that have no 491
 clear concentration dependence [40]. Ca^{2+} signals 492
 induced by both ATP and acetylcholine mediate ductu- 493
 lar bicarbonate secretion, however [36, 84]. Additional 494
 studies of the role of cholinergic innervation have been 495
 performed by examining the effect of vagotomy on 496
 cholangiocytes. Bile duct ligation induces proliferation 497
 of cholangiocytes and enhances their response to secre- 498
 tin, but vagotomy impairs this response, in part by 499
 enhancing apoptosis of cholangiocytes [86]. Vagotomy 500
 also eliminates the choleric response to secretin that 501
 is induced by bile duct ligation [86]. Interestingly, this 502
 effect is reversed by forskolin, which may be consis- 503
 tent with the idea that cholinergic stimulation serves in 504
 part to potentiate formation of cAMP in cholangiocytes 505
 [85]. Adrenergic stimulation also increases Ca_i^{2+} in 506
 cholangiocytes. The α_1 -adrenergic agonist phenyleph- 507
 rine potentiates secretin-stimulated ductal secretion 508
 through a Ca^{2+} - and PKC-dependent amplification of 509
 the adenylyl cyclase system [97]. Cholangiocytes 510
 express dopamine receptors as well, and stimulation of 511
 these receptors inhibits rather than stimulates secretion 512
 induced by secretin and cAMP. This effect appears to 513
 be mediated by increases in cytosolic Ca^{2+} and Ca^{2+} - 514
 dependent activation of PKC [97]. Thus, distinct Ca^{2+} 515
 agonists may have opposing effects on ductal secre- 516
 tion. Although the basis for this is not known, one pos- 517
 sibility would be that different agonists activate distinct 518
 isoforms of PKC, which may be a downstream effector 519
 for Ca^{2+} in the cholangiocyte. 520

521 Ca^{2+} signaling in cholangiocytes also is involved in 521
 apoptosis. A number of pro- and antiapoptotic proteins 522
 exhibit their effects by modulating Ca^{2+} signals. A par- 523
 ticularly important example is Mcl-1, a member of the 524
 Bcl-2 family which is the primary antiapoptotic protein 525
 in cholangiocytes [18]. Mcl-1 exerts its anti-apoptotic 526

2 Signaling Pathways in Biliary Epithelial Cells

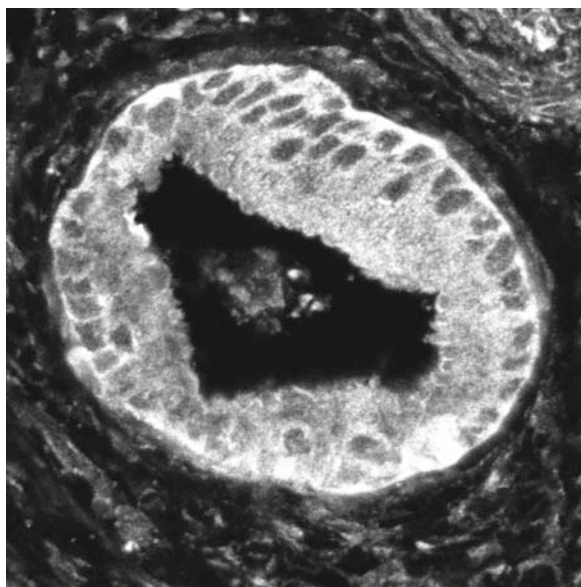


Fig. 2.2 The antiapoptotic protein Mcl-1 is heavily expressed in human cholangiocarcinoma. Confocal immunofluorescence image was obtained from a surgical resection specimen. Note that Mcl-1 is distributed diffusely throughout the cytosol, with some patchy areas of increased expression (image provided courtesy of Dr. Noritaka Minagawa)

AQ2

AQ1

527 activity in cholangiocytes as well as in the Mz-Cha-1
528 cholangiocarcinoma cell line through inhibition of
529 mitochondrial Ca^{2+} signals [98]. Overexpression of this
530 protein is thought to be important for development of
531 cholangiocarcinoma (Fig. 2.2) [99].

532 **Protein Kinase C**

533 DAG is formed along with InsP3 upon hydrolysis of
534 PIP_2 by PLC, and DAG acts to activate PKC. PKC
535 isoforms have been grouped into three classes [100],
536 which include conventional, nonconventional, and
537 atypical isoforms. $PKC\alpha$, $PKC\beta$, and $PKC\gamma$ are the
538 conventional isoforms, and are activated by Ca_i^{2+} and
539 DAG. These isoforms are involved in the regulation
540 of gene expression, secretion, and modulation of ion
541 channels, cell proliferation, and differentiation. For
542 example, gastrin inhibits cholangiocyte proliferation
543 and secretion following bile duct ligation by activa-
544 tion of $PKC\alpha$ [101]. Stimulation of α_1 -adrenergic
545 receptors by phenylephrine induces membrane trans-
546 location of $PKC\alpha$ as well as β -II, and this has been
547 associated with potentiation of secretin-stimulated

ductal secretion [102]. This is thought to induce 548
maximal bicarbonate excretion in proliferating ducts, 549
which may provide a compensatory mechanism for 550
the impaired secretion that occurs in ductular damage 551
[102]. Cholangiocytes also express prolactin receptors, 552
which stimulate growth by an autocrine mechanism 553
involving phosphorylation of $PKC\beta$ -I and dephos- 554
phorylation of $PKC\alpha$ [103]. Progesterone increases 555
cholangiocyte proliferation by activation of nuclear 556
(PR-A and PR-B) and plasma membrane (PRGMC1, 557
PRGMC2, and mPR) progesterone receptors. The 558
effects of this receptor have been examined in cho- 559
langiocytes from normal and bile duct ligated rats, as 560
well as in the NRC cell line [104]. The therapeutic bile 561
acids ursodeoxycholic acid (UDCA) and tauroursode- 562
oxycholic acid (TUDCA) similarly inhibit cholangio- 563
cyte proliferation after bile duct ligation by increasing 564
cytosolic Ca_i^{2+} and activating $PKC\alpha$. Specifically, both 565
UDCA and its taurine conjugate induce an immediate 566
and sustained increase in Ca_i^{2+} [101, 105]. This is asso- 567
ciated with redistribution of $PKC\alpha$ from the cytoplasm 568
to the plasma membrane, which is required for activa- 569
tion of this kinase [101]. In contrast, both taurocholic 570
acid (TCA) and tauroolithocholic acid (TLCA) increase 571
cholangiocyte proliferation after bile duct ligation. 572
Neither of these bile acids increases Ca_i^{2+} or activates 573
 PKC in cholangiocytes. Like $PKC\alpha$, $PKC\gamma$ appears to 574
play an inhibitory role in cholangiocytes. For exam- 575
ple, dopaminergic agonists inhibit secretin-stimulated 576
ductal secretion by decreasing cAMP formation and 577
inducing Ca^{2+} -mediated activation of $PKC\gamma$ [97]. Thus, 578
while certain Ca^{2+} agonists such as acetylcholine and 579
ATP stimulate secretion in cholangiocytes, other Ca^{2+} 580
agonists such as gastrin, dopamine, and certain bile 581
acids instead are inhibitory. Evidence at present sug- 582
gests that agonist-specific activation of various PKC 583
isoforms may in part be responsible for these differen- 584
tial, agonist-specific effects of Ca^{2+} . 585

586 **MAPK Signaling**

The MAPK pathways are important for the normal and 587
abnormal regulation of cell growth, and are often acti- 588
vated by stimulation of receptor tyrosine kinases. Certain 589
inflammatory mediators can stimulate receptor tyrosine 590
kinases. Lipopolysaccharide stimulates the release of 591
IL-6, transforming growth factor (TGF- β), interleukin 592

593 8 (IL-8), tumor necrosis factor (TNF- α), and platelet-
594 derived growth factor (PDGF). These factors can interact
595 with cholangiocytes in an autocrine/paracrine fashion to
596 regulate cholangiocyte intracellular responses [106].

597 Secreted IL-6 stimulates cholangiocyte IL-6 recep-
598 tors in an autocrine fashion, inducing activation of
599 MAPK as well as members of the STAT family of
600 transcription factors [107]. IL-6 increases cholangio-
601 cyte proliferation via this mechanism, since, IL-6
602 activates the p44/p42 and p38 MAPK signaling path-
603 way [107]. The p44/p42 MAPK signaling cascade
604 can be activated by mitogenic stimulation of nonma-
605 lignant human cholangiocytes, although the p38
606 MAPK pathway is activated by mitogenic stimulation
607 of malignant but not nonmalignant cholangiocytes.
608 p38 MAPK signaling affects the growth of malignant
609 cholangiocytes by dysregulation of the eukaryotic
610 initiation factor, eIF-4E [108]. The eIF-4E is known
611 to bind the cap structure of eukaryotic messenger
612 RNAs, mediating the recruitment of ribosomes to
613 messenger RNA, a rate-limiting step for translation
614 [108]. Thus, protein synthesis is decreased after stim-
615 ulation with mitogens in cholangiocarcinoma cells
616 with a functional impairment in p38 MAPK activa-
617 tion, due to impaired initiation of translation [108].
618 Because of the importance of translational regulation
619 in promoting tumor growth, the translational appara-
620 tus could represent an attractive target for therapeutic
621 intervention in the treatment or prevention of cholan-
622 giocarcinoma. Activation of p38 MAPK by IL-6 also
623 plays a role in inhibiting apoptosis. Cholangiocarcinoma
624 cells secrete IL-6, which upregulates expression of
625 Mcl-1, thereby inhibiting apoptosis through STAT 3
626 and Akt [18, 109]. Mcl-1, furthermore, inhibits apop-
627 totic Ca²⁺ signals in mitochondria, suggesting that it
628 inhibits apoptosis in cholangiocytes through a range
629 of complementary effects [98].

630 Cholangiocarcinoma growth is regulated in part by
631 the sympathetic nervous system, although this may
632 involve MAPK signaling as well. The α_2 adrenorecep-
633 tor agonist UK-14304 inhibits growth in the Mz-ChA-1
634 and TFK-1 cholangiocarcinoma cell lines, which ele-
635 vates cAMP, and in turn substantially inhibits Raf-1
636 and B-Raf-1 activity induced by EGF. This is associ-
637 ated with sustained inhibition of MAPK activity and
638 decreased cholangiocyte proliferation [16]. Thus, α_2 -
639 adrenergic receptor stimulation inhibits cholangiocar-
640 cinoma growth through modulation of Raf-1 and
641 B-Raf-1 activities [16].

Cholangiocarcinoma growth may also be regu- 642
643 lated in part by other inflammatory mediators. 644
645 Activation of inducible nitric oxide (NO) synthase 644
645 (iNOS) can result in the generation of NO in suffi- 645
646 cient amounts to damage DNA. In addition, activa- 646
647 tion of iNOS promotes upregulation of COX-2 in 647
648 immortalized mouse cholangiocytes, suggesting that 648
649 COX-2 and COX-2-derived prostanoids play a key 649
650 role in cholangiocarcinogenesis [110]. A subset of 650
651 cholangiocarcinomas harbor activating mutations in 651
652 the oncogenes *K-ras* and *Braf*, which potentiates 652
653 activation of the ERK1/2 pathway. Disruption of the 653
654 Ras/Raf/MAPK pathway through these mechanisms 654
655 may play a crucial role in regulating development of 655
656 cholangiocarcinoma [111]. 656

657 Together, these studies demonstrate that a number of 657
658 stimuli may converge to affect growth of cholangiocar- 658
659 cinomas via MAPK pathways. Although the fundamen- 659
660 tal role of MAPK signaling in growth of nonmalignant 660
661 cells has been established in many types of cells and 661
662 tissues, this topic has received little attention to date in 662
663 the cholangiocyte. 663

664 PI3-Kinase Signaling 664

665 Increases in cell volume are known to activate phos- 665
666 phatidylinositol 3-kinase (PI3-K) [112]. PI3-K is a 666
667 heterodimer that phosphorylates phosphatidylinositol 667
668 upon activation, producing distinct phospholipid sec- 668
669 ond messengers. Studies in a number of cell types 669
670 show that this kinase is involved in controlling cell 670
671 proliferation, organization of the actin cytoskeleton, 671
672 regulation of vesicle trafficking between intracellular 672
673 organelles, and a range of secretion-related processes 673
674 [113]. In hepatocytes, PI3-K is activated by certain 674
675 bile acids and plays an important role in the choleric 675
676 and anti-apoptotic effects of hydrophilic bile acids in 676
677 particular [113, 114]. In cholangiocytes, activation of 677
678 PI3-K is an early event in the modulation of cholangi- 678
679 cyte proliferation and secretion by bile acids [115]. 679
680 The activation of PI3-K that occurs in proliferating 680
681 cholangiocytes during cholestasis may result in part 681
682 from activation of the glucagon-like peptide 1 (GLP-1) 682
683 receptor [116]. TCA also increases DNA synthesis 683
684 via PI3-K in cholangiocytes, since, TCA-induced 684
685 DNA synthesis is abolished in cholangiocytes incu- 685
686 bated with the PI3-K inhibitor wortmannin [112]. 686

2 Signaling Pathways in Biliary Epithelial Cells

687 Experimental evidence further suggests that PI3-K
688 plays a role in the regulation of ATP release from cho-
689 langiocytes [117]. ATP release appears necessary for
690 cell volume regulation, so PI3-K may be a key media-
691 tor of this autocrine pathway [117].

692 **Pathological Conditions**

693 Alterations in signaling have been implicated in two
694 types of disorders in cholangiocytes: cholestatic secre-
695 tory disorders and disorders associated with changes in
696 cell proliferation. Cholestasis is one of the principal
697 manifestations of liver disease and often reflects
698 impaired ductular secretion due to cholangiocyte dys-
699 function [42]. In models of ductular cholestasis such as
700 bile duct ligation, expression of the secretin receptor
701 and cAMP formation is preserved and even enhanced,
702 so that stimulation with secretin leads to a massive,
703 bicarbonate-rich choleresis [38]. However, Ca^{2+} signal-
704 ing pathways are severely impaired in this and other
705 cholestatic models and disorders [118]. For example,
706 there is a marked loss of each InsP3R isoform in cho-
707 langiocytes 2 weeks after bile duct ligation. In particu-
708 lar, expression of the type III InsP3R, which is the
709 predominant isoform in cholangiocytes, is nearly
710 absent. This loss of InsP3Rs is associated with impaired
711 Ca_i^{2+} signaling and Ca^{2+} -mediated bicarbonate secre-
712 tion as well. InsP3R expression and inhibition of ductu-
713 lar secretion also occur after treatment with endotoxin,
714 indicating that loss of InsP3R expression occurs in ani-
715 mal models of both acute and chronic cholestasis [118].
716 Human liver biopsy specimens similarly show that
717 InsP3R expression is decreased in bile duct epithelia
718 from a range of human cholestatic disorders, including
719 primary biliary cirrhosis, sclerosing cholangitis, bile
720 duct obstruction, and biliary atresia [118]. This is in
721 contrast to patients with hepatitis C infection, in which
722 there is portal inflammation without bile duct damage,
723 and no loss in InsP3Rs is observed in cholangiocytes
724 [118]. Thus loss of InsP3Rs appears to be a general fea-
725 ture of ductular cholestasis rather than of portal inflam-
726 mation. This raises the hypothesis that Ca^{2+} -mediated
727 bicarbonate secretion is not just an alternative pathway
728 to secretion via cAMP/CFTR, but may in fact be impor-
729 tant for biliary bicarbonate secretion to occur under
730 normal conditions. Recent studies have supported this
731 hypothesis by demonstrating that knockdown of the

type III InsP3R in microperfused intrahepatic bile duct 732
segments impairs bicarbonate secretion [47]. However, 733
further work will be needed to understand how ductular 734
damage leads to loss of InsP3Rs in cholangiocytes. 735

Regulation of signaling pathways may provide 736
approaches to treat cholestasis. For example, the only 737
medical therapy of proven benefit in certain cholestatic 738
disorders is administration of UDCA, which promotes 739
bile flow and biliary bicarbonate excretion [119, 120]. 740
Several observations suggest that UDCA may act in part 741
through a novel series of signaling events in the chol- 742
angiocyte. First, this bile acid induces hepatocytes [93] as 743
well as cholangiocytes [121] to secrete ATP into bile. 744
Biliary ATP in turn activates apical purinergic receptors 745
on cholangiocytes, which induces Ca^{2+} signals and then 746
stimulates Ca^{2+} -dependent ductular Cl^- and HCO_3^- secre- 747
tion [47, 84, 93]. Another novel potential therapy for 748
cholestasis is based on the sulfonylurea glybenclamide. 749
Glybenclamide stimulates bile flow by up to 50% and 750
stimulates bicarbonate excretion as well in the isolated 751
perfused rat liver. This effect appears to be mediated at 752
the level of the cholangiocyte rather than the hepatocyte. 753
Moreover, glybenclamide stimulates ductular secretion 754
by activation of $Na^+K^+2Cl^-$ cotransport, rather than via 755
mechanisms involving cAMP or Ca_i^{2+} [122]. 756

The cAMP signaling pathway is important for the 757
regulation of cholangiocyte proliferation. Cholang- 758
iocytes undergo proliferation in response to events such 759
as bile duct ligation and partial hepatectomy [51, 123, 760
124]. Under such conditions, proliferation of cholangio- 761
cytes is associated with the increases in expression of the 762
secretin receptor, secretin-stimulated cAMP levels, and 763
ductal secretion [38, 51, 125, 126]. Moreover, upregula- 764
tion of cAMP-related pathways by chronic administra- 765
tion of forskolin is sufficient to induce cholangiocyte 766
hyperplasia similar to what is observed following bile 767
duct ligation [127]. Other signaling pathways regulate 768
bile duct cell growth as well. For example, chronic feed- 769
ing of certain bile acids, such as TCA and TLCA, also 770
induces proliferation of cholangiocytes [125]. Such bile 771
acids enter cholangiocytes through the apical Na^+ - 772
dependent bile acid transporter (ASBT), and then alter 773
cell proliferation by activating the PI3-K pathway in a 774
cAMP-independent mechanism [115]. Interestingly, the 775
bile acids UDCA and TUDCA decrease bile duct prolif- 776
eration following bile duct ligation [115, 127]. Adminis- 777
tration of either of these bile acids is associated with 778
decreased secretin receptor gene expression as well as 779
decreased secretin-induced cAMP synthesis [115, 127]. 780

781 The mechanism of inhibition of these bile acids requires
 782 Ca²⁺-dependent activation of PKC α [115].
 783 Biliary tract inflammation predisposes to the develop-
 784 ment of cholangiocarcinoma, and the signaling pathways
 785 involved in this have been investigated. Inflammation
 786 leads to activation of the p38 MAPK stress signaling
 787 pathway, which facilitates cell proliferation by transla-
 788 tional regulation of protein synthesis. Activation of p38
 789 MAPK signaling may thereby contribute to tumor growth.
 790 It has thus been suggested that gene silencing of cellular
 791 eIF-4E may be a useful strategy to limit tumor cell growth
 792 [108]. Based on such observations, gene therapy may
 793 become an approach to treat biliary tract malignancies,
 794 since cholangiocytes are accessible by percutaneous or
 795 endoscopic interventions, and the feasibility of introduc-
 796 ing genes into cholangiocytes via retrograde biliary infu-
 797 sion has been shown in animal models [128].

Summary

- 799 > Cholangiocytes are polarized and mitotically
800 dormant.
- 801 > Cholangiocytes express numerous G protein-
802 coupled receptors and non-G protein-coupled
803 receptors.
- 804 > Calcium and cAMP are the principal second
805 messengers of the cholangiocytes.
- 806 > Cholangiocytes are responsive to basolateral
807 as well as apical signals.
- 808 > ATP is an important extracellular signaling
809 molecule for cholangiocytes.
- 810 > Secretin is a major agonist for cAMP-medi-
811 ated Cl⁻ secretion.
- 812 > Cholestasis affects in particular calcium
813 signaling.

Multiple Choice Questions

- 814 1. Cholangiocytes express:
- 815 (a) Secretin receptor
 - 816 (b) Histamin 2 receptor
 - 817 (c) Serotonin receptor
 - 818 (d) M3 muscarinic acetylcholine receptor
 - 819 (e) All the above
 - 820

- 2. Which statement is not correct. In cholangiocytes,
 - (a) Endocannabinoids impair cholangiocyte prolif- 821
eration 822
 - (b) CXC Chemokine ligand 12 induces ERK and 823
Akt pathway 824
 - (c) IL-6 induces ERK and Akt pathway 825
826
 - (d) Estrogens induce the expression of VEGF 827
 - (e) EGF inhibits the Ras/Raf/MAPK cascade 828
- 3. In cholangiocytes cAMP
 - (a) Stimulates exocytosis 829
830
 - (b) Close aquaporin water channels 831
 - (c) Inhibits CL⁻/HCO₃⁻ exchange channel 832
 - (d) Blocks the effect of secretin 833
 - (e) Is increased by somatostatin via the SSTR2 834
- 3. Regarding the effects of bile acids in cholangiocytes:
 - (a) They activate EGFR through a TGF- α depen- 835
dent mechanism 836
837
 - (b) They Regulate the expression of death receptor 838
5/TRAIL-receptor 2 839
 - (c) They modulate the IGF1 system 840
 - (d) They activate CFTR 841
 - (e) All the above are correct 842
- 5. Which statement is correct:
 - (a) Cholangiocytes have basolateral cilia 843
844
 - (b) Cilia are sensory organelles 845
 - (c) P2Y12 receptors link primary cilia to calcium 846
signaling 847
 - (d) TRPV4 are Cl⁻ channels associated with cilia 848
 - (e) Cilia are responsive only to mechanical stimuli 849

Acknowledgments This work was supported by NIH grants 850
 TW01451, DK61747, DK45710, DK34989, and DK57751 and 851
 by a grant from the Howard Hughes Medical Institute. 852

References

853

- 1. Wise C, Pилanthanonnd M, Perry BF, Alpini G, McNeal M, 854
Glaser SS (2008) Mechanisms of biliary carcinogenesis and 855
growth. *World J Gastroenterol* 14:2986–2989 856
- 2. Gaudio E, Franchitto A, Pannarale L, Carpino G, Alpini G, 857
Francis H, Glaser S, Alvaro D, Onori P (2006) Cholangiocytes 858
and blood supply. *World J Gastroenterol* 12:3546–3552 859
- 3. Bogert PT, LaRusso NF (2007) Cholangiocyte biology. *Curr* 860
Opin Gastroenterol 23:299–305 861
- 4. Francis H, LeSage G, DeMorrow S, Alvaro D, Ueno Y, 862
Venter J, Glaser S, Mancino MG, Marucci L, Benedetti A, 863
Alpini G (2007) The alpha2-adrenergic receptor agonist UK 864
14, 304 inhibits secretin-stimulated ductal secretion by 865

2 Signaling Pathways in Biliary Epithelial Cells

- 866 downregulation of the cAMP system in bile duct-ligated
867 rats. *Am J Physiol Cell Physiol* 293:C1252–C1262
- 868 5. DeMorrow S, Francis H, Alpini G (2007) Biogenic amine
869 actions on cholangiocyte function. *Exp Biol Med* (Maywood)
870 232:1005–1013
- 871 6. Francis H, Glaser S, DeMorrow S, Gaudio E, Ueno Y,
872 Venter J, Dostal D, Onori P, Franchitto A, Marzioni M,
873 Vaculin S, Vaculin B, Katki K, Stutes M, Savage J, Alpini G
874 (2008) Small mouse cholangiocytes proliferate in response
875 to H1 histamine receptor stimulation by activation of the
876 IP3/CaMK I/CREB pathway. *Am J Physiol Cell Physiol*
877 295:C499–C513
- 878 7. Francis H, Franchitto A, Ueno Y, Glaser S, DeMorrow S,
879 Venter J, Gaudio E, Alvaro D, Fava G, Marzioni M,
880 Vaculin B, Alpini G (2007) H3 histamine receptor agonist
881 inhibits biliary growth of BDL rats by downregulation of the
882 cAMP-dependent PKA/ERK1/2/ELK-1 pathway. *Lab Invest*
883 87:473–487
- 884 8. Jimenez W (2005) Endocannabinoids and liver disease.
885 *Hepatology* 41:983–985
- 886 9. DeMorrow S, Francis H, Gaudio E, Ueno Y, Venter J, Onori
887 P, Franchitto A, Vaculin B, Vaculin S, Alpini G (2008)
888 Anandamide inhibits cholangiocyte hyperplastic prolifera-
889 tion via activation of thioredoxin 1/redox factor 1 and AP-1
890 activation. *Am J Physiol Gastrointest Liver Physiol* 294:
891 G506–G519
- 892 10. Vaillancourt RR, Gardner AM, Johnson GL (1994) B-Raf-
893 dependent regulation of the MEK-1/mitogen-activated pro-
894 tein kinase pathway in PC12 cells and regulation by cyclic
895 AMP. *Mol Cell Biol* 14:6522–6530
- 896 11. Hagemann C, Rapp UR (1999) Isozyme-specific functions of
897 Raf kinases. *Exp Cell Res* 253:34–46
- 898 12. Moodie SA, Willumsen BM, Weber MJ, Wolfman A (1993)
899 Complexes of Ras.GTP with Raf-1 and mitogen-activated
900 protein kinase kinase. *Science* 260:1658–1661
- 901 13. Vojtek AB, Der CJ (1998) Increasing complexity of the Ras
902 signaling pathway. *J Biol Chem* 273:19925–19928
- 903 14. Torii S, Kusakabe M, Yamamoto T, Maekawa M, Nishida E
904 (2004) Sef is a spatial regulator for Ras/MAP kinase signal-
905 ing. *Dev Cell* 7:33–44
- 906 15. Hafner S, Adler HS, Mischak H, Janosch P, Heidecker G,
907 Wolfman A, Pippig S, Lohse M, Ueffing M, Kolch W (1994)
908 Mechanism of inhibition of Raf-1 by protein kinase A. *Mol*
909 *Cell Biol* 14:6696–6703
- 910 16. Kanno N, LeSage G, Phinizy JL, Glaser S, Francis H, Alpini G
911 (2002) Stimulation of alpha2-adrenergic receptor inhibits
912 cholangiocarcinoma growth through modulation of Raf-1 and
913 B-Raf activities. *Hepatology* 35:1329–1340
- 914 17. Leelawat K, Leelawat S, Narong S, Hongeng S (2007) Roles
915 of the MEK1/2 and AKT pathways in CXCL12/CXCR4
916 induced cholangiocarcinoma cell invasion. *World J*
917 *Gastroenterol* 13:1561–1568
- 918 18. Kobayashi S, Werneburg NW, Bronk SF, Kaufmann SH,
919 Gores GJ (2005) Interleukin-6 contributes to Mcl-1 up-
920 regulation and TRAIL resistance via an Akt-signaling path-
921 way in cholangiocarcinoma cells. *Gastroenterology* 128:
922 2054–2065
- 923 19. Werneburg NW, Yoon JH, Higuchi H, Gores GJ (2003) Bile
924 acids activate EGF receptor via a TGF-alpha-dependent
925 mechanism in human cholangiocyte cell lines. *Am J Physiol*
926 *Gastrointest Liver Physiol* 285:G31–G36
20. Drudi MV, Mancino MG, Mancino A, Torrice A, Gatto M, 927
Attili AF, Alpini G, Alvaro D (2007) Bile salts regulate pro- 928
liferation and apoptosis of liver cells by modulating the 929
IGF1 system. *Dig Liver Dis* 39:654–662 930
21. Higuchi H, Grambihler A, Canbay A, Bronk SF, Gores GJ 931
(2004) Bile acids up-regulate death receptor 5/TRAIL- 932
receptor 2 expression via a c-Jun N-terminal kinase-depend- 933
ent pathway involving Sp1. *J Biol Chem* 279:51–60 934
22. Bijvelds MJ, Jorna H, Verkade HJ, Bot AG, Hofmann F, 935
Agellon LB, Sinaasappel M, De Jonge HR (2005) Activa- 936
tion of CFTR by ASBT-mediated bile salt absorption. *Am* 937
J Physiol Gastrointest Liver Physiol 289:G870–G879 938
23. Alpini G, Glaser SS, Robertson WE, Phinizy JL, Rodgers R, 939
Caligiuri A, LeSage GD (1997) Bile acids stimulate prolifera- 940
tive and secretory events in large but not small cholangiocytes. 941
Am J Physiol Gastrointest Liver Physiol 273:G518–G529 942
24. Alvaro D, Alpini G, Onori P, Perego L, Svegliata BG, 943
Franchitto A, Baiocchi L, Glaser SS, Le Sage G, Folli F, 944
Gaudio E (2000) Estrogens stimulate proliferation of intra- 945
hepatic biliary epithelium in rats. *Gastroenterology* 119: 946
1681–1691 947
25. Alvaro D, Barbaro B, Franchitto A, Onori P, Glaser SS, 948
Alpini G, Francis H, Marucci L, Sterpetti P, Ginanni- 949
Corradini S, Onetti MA, Dostal DE, De Santis A, Attili AF, 950
Benedetti A, Gaudio E (2006) Estrogens and insulin-like 951
growth factor 1 modulate neoplastic cell growth in human 952
cholangiocarcinoma. *Am J Pathol* 169:877–888 953
26. Mancino A, Mancino MG, Glaser SS, Alpini G, Bolognese A, 954
Izzo L, Francis H, Onori P, Franchitto A, Ginanni- 955
Corradini S, Gaudio E, Alvaro D (2008) Estrogens stimulate 956
the proliferation of human cholangiocarcinoma by inducing 957
the expression and secretion of vascular endothelial growth 958
factor. *Dig Liver Dis* 41:156–163 959
27. Kato A, Gores GJ, LaRusso NF (1992) Secretin stimulates 960
exocytosis in isolated bile duct epithelial cells by a cyclic 961
AMP-mediated mechanism. *J Biol Chem* 267:15523–15529 962
28. Marinelli RA, Pham L, Agre P, LaRusso NF (1997) Secretin 963
promotes osmotic water transport in rat cholangiocytes by 964
increasing aquaporin-1 water channels in plasma membrane. 965
Evidence for a secretin-induced vesicular translocation of 966
aquaporin-1. *J Biol Chem* 272:12984–12988 967
29. Roberts SK, Yano M, Ueno Y, Pham L, Alpini G, Agre P, 968
LaRusso NF (1994) Cholangiocytes express the aquaporin 969
CHIP and transport water via a channel-mediated mecha- 970
nism. *Proc Natl Acad Sci USA* 91:13009–13013 971
30. Cohn JA, Strong TV, Picciotto MR, Nairn AC, Collins FS, 972
Fitz JG (1993) Localization of the cystic fibrosis transmem- 973
brane conductance regulator in human bile duct epithelial 974
cells. *Gastroenterology* 105:1857–1864 975
31. Fitz JG, Basavappa S, McGill J, Melhus O, Cohn JA (1993) 976
Regulation of membrane chloride currents in rat bile duct 977
epithelial cells. *J Clin Invest* 91:319–328 978
32. Alvaro D, Cho WK, Mennone A, Boyer JL (1993) Effect of 979
secretin on intracellular pH regulation in isolated rat bile 980
duct epithelial cells. *J Clin Invest* 92:1314–1325 981
33. Boyer JL (1996) Bile duct epithelium: frontiers in transport 982
physiology. *Am J Physiol Gastrointest Liver Physiol* 270: 983
G1–G5 984
34. Mennone A, Alvaro D, Cho W, Boyer JL (1995) Isolation of 985
small polarized bile duct units. *Proc Natl Acad Sci USA* 986
92:6527–6531 987

- 988 35. Roberts SK, Kuntz SM, Gores GJ, LaRusso NF (1993) 1049
 989 Regulation of bicarbonate-dependent ductular bile secre- 1050
 990 tion assessed by luminal micropuncture of isolated rodent 1051
 991 intrahepatic bile ducts. *Proc Natl Acad Sci U S A* 90: 1052
 992 9080–9084 1053
- 993 36. Hirata K, Nathanson MH (2001) Bile duct epithelia regulate 1054
 994 biliary bicarbonate excretion in normal rat liver. *Gastroen- 1055*
 995 *terology* 121:396–406 1056
- 996 37. Alpini G, Lenzi R, Zhai WR, Slott PA, Liu MH, Sarkozi L, 1057
 997 Tavoloni N (1989) Bile secretory function of intrahepatic 1058
 998 biliary epithelium in the rat. *Am J Physiol Gastrointest Liver 1059*
 999 *Physiol* 257:G124–G133 1060
- 1000 38. Alpini G, Ulrich CD II, Phillips JO, Pham LD, Miller LJ, 1061
 1001 LaRusso NF (1994) Upregulation of secretin receptor gene 1062
 1002 expression in rat cholangiocytes after bile duct ligation. *Am 1063*
 1003 *J Physiol Gastrointest Liver Physiol* 266:G922–G928 1064
- 1004 39. Lenzen R, Alpini G, Tavoloni N (1992) Secretin stimulates 1065
 1005 bile ductular secretory activity through the cAMP system. 1066
 1006 *Am J Physiol Gastrointest Liver Physiol* 263:G527–G532 1067
- 1007 40. Nathanson MH, Burgstahler AD, Mennone A, Boyer JL 1068
 1008 (1996) Characterization of cytosolic Ca²⁺ signaling in rat 1069
 1009 bile duct epithelia. *Am J Physiol Gastrointest Liver Physiol 1070*
 1010 271:G86–G96 1071
- 1011 41. McGill JM, Basavappa S, Gettys TW, Fitz JG (1994) Secretin 1072
 1012 activates Cl⁻ channels in bile duct epithelial cells through a 1073
 1013 cAMP-dependent mechanism. *Am J Physiol Gastrointest 1074*
 1014 *Liver Physiol* 266:G731–G736 1075
- 1015 42. Roberts SK, Ludwig J, LaRusso NF (1997) The pathobiology 1076
 1016 of biliary epithelia. *Gastroenterology* 112:269–279 1077
- 1017 43. Lee MG, Choi JY, Luo X, Strickland E, Thomas PJ, Muallem S 1078
 1018 (1999) Cystic fibrosis transmembrane conductance regulator 1079
 1019 regulates luminal Cl⁻/HCO₃⁻ exchange in mouse submandibular 1080
 1020 and pancreatic ducts. *J Biol Chem* 274:14670–14677 1081
- 1021 44. Lee MG, Wigley WC, Zeng W, Noel LE, Marino CM, 1082
 1022 Thomas PJ, Muallem S (1999) Regulation of Cl⁻/HCO₃⁻ 1083
 1023 exchange by cystic fibrosis transmembrane conductance 1084
 1024 regulator expressed in NIH 3T3 and HEK 293 cells. *J Biol 1085*
 1025 *Chem* 274:3414–3421 1086
- 1026 45. Poulsen JH, Fischer H, Illek B, Machen TE (1994) 1087
 1027 Bicarbonate conductance and pH regulatory capability of 1088
 1028 cystic fibrosis transmembrane conductance regulator. *Proc 1089*
 1029 *Natl Acad Sci U S A* 91:5340–5344 1090
- 1030 46. Seidler U, Blumenstein I, Kretz A, Viellard-Baron D, 1091
 1031 Rossmann H, Colledge WH, Evans M, Ratcliff R, Gregor M 1092
 1032 (1997) A functional CFTR protein is required for mouse 1093
 1033 intestinal cAMP-, cGMP- and Ca(2+)-dependent. *J Physiol 1094*
 1034 505(Pt 2):411–423 1095
- 1035 47. Minagawa N, Nagata J, Shibao K, Masyuk AI, Gomes DA, 1096
 1036 Rodrigues MA, LeSage G, Akiba Y, Kaunitz JD, Ehrlich BE, 1097
 1037 LaRusso NF, Nathanson MH (2007) Cyclic AMP regulates 1098
 1038 bicarbonate secretion in cholangiocytes through release of 1099
 1039 ATP into bile. *Gastroenterology* 133:1592–1602 1100
- 1040 48. Tietz PS, Marinelli RA, Chen XM, Huang B, Cohn J, Kole J, 1101
 1041 McNiven MA, Alper S, LaRusso NF (2003) Agonist-induced 1102
 1042 coordinated trafficking of functionally related transport pro- 1103
 1043 teins for water and ions in cholangiocytes. *J Biol Chem 1104*
 1044 278:20413–20419 1105
- 1045 49. Tietz PS, Holman RT, Miller LJ, LaRusso NF (1995) 1106
 1046 Isolation and characterization of rat cholangiocyte vesicles 1107
 1047 enriched in apical or basolateral plasma membrane domains. 1108
 1048 *Biochemistry* 34:15436–15443 1109
50. Gong AY, Tietz PS, Muff MA, Splinter PL, Huebert RC, 1049
 Strowski MZ, Chen XM, LaRusso NF (2003) Somatostatin 1050
 stimulates ductal bile absorption and inhibits ductal bile 1051
 secretion in mice via SSTR2 on cholangiocytes. *Am J 1052*
Physiol Cell Physiol 284:C1205–C1214 1053
51. Alpini G, Glaser SS, Ueno Y, Pham L, Podila PV, Caligiuri A, 1054
 LeSage G, LaRusso NF (1998) Heterogeneity of the prolifer- 1055
 ative capacity of rat cholangiocytes after bile duct ligation. 1056
Am J Physiol Gastrointest Liver Physiol 274:G767–G775 1057
52. Caligiuri A, Glaser S, Rodgers RE, Phinizy JL, Robertson W, 1058
 Papa E, Pinzani M, Alpini G (1998) Endothelin-1 inhibits 1059
 secretin-stimulated ductal secretion by interacting with ETA 1060
 receptors on large cholangiocytes. *Am J Physiol Gastrointest 1061*
Liver Physiol 275:G835–G846 1062
53. Glaser SS, Rodgers RE, Phinizy JL, Robertson WE, 1063
 Lasater J, Caligiuri A, Tretjak Z, LeSage GD, Alpini G 1064
 (1997) Gastrin inhibits secretin-induced ductal secretion by 1065
 interaction with specific receptors on rat cholangiocytes. *Am 1066*
J Physiol Gastrointest Liver Physiol 273: G1061–G1070 1067
54. Marzioni M, Glaser S, Francis H, Marucci L, Benedetti A, 1068
 Alvaro D, Taffetani S, Ueno Y, Roskams T, Phinizy JL, Venter J, 1069
 Fava G, LeSage GD, Alpini G (2005) Autocrine/paracrine 1070
 regulation of the growth of the biliary tree by the neuroendo- 1071
 crine hormone serotonin. *Gastroenterology* 128:121–137 1072
55. Cho WK, Boyer JL (1999) Vasoactive intestinal polypeptide 1073
 is a potent regulator of bile secretion from rat cholangio- 1074
 cytes. *Gastroenterology* 117:420–428 1075
56. Cho WK, Mennone A, Rydberg SA, Boyer JL (1997) 1076
 Bombesin stimulates bicarbonate secretion from rat cholangan- 1077
 giocytes: implications for neural regulation of bile secretion. 1078
Gastroenterology 113:311–321 1079
57. Roman RM, Feranchak AP, Salter KD, Wang Y, Fitz JG 1080
 (1999) Endogenous ATP release regulates Cl⁻ secretion in 1081
 cultured human and rat biliary epithelial cells. *Am J Physiol 1082*
Gastrointest Liver Physiol 276:G1391–G1400 1083
58. Fitz JG (2002) Regulation of cholangiocyte secretion. *Semin 1084*
Liver Dis 22:241–249 1085
59. Newton CL, Mignery GA, S adhof TC (1994) Co-expression 1086
 in vertebrate tissues and cell lines of multiple inositol 1, 4, 1087
 5-trisphosphate (InsP3) receptors with distinct affinities for 1088
 InsP3. *J Biol Chem* 269:28613–28619 1089
60. Hagar RE, Burgstahler AD, Nathanson MH, Ehrlich BE 1090
 (1998) Type III InsP3 receptor channel stays open in the 1091
 presence of increased calcium. *Nature* 396:81–84 1092
61. Ramos-Franco J, Fill M, Mignery GA (1998) Isoform- 1093
 specific function of single inositol 1, 4, 5-trisphosphate 1094
 receptor channels. *Biophys J* 75:834–839 1095
62. Anyatonwu GI, Buck ED, Ehrlich BE (2003) Methane- 1096
 thiosulfonate ethylammonium block of amine currents 1097
 through the ryanodine receptor reveals single pore architec- 1098
 ture. *J Biol Chem* 278:45528–45538 1099
63. Thrower EC, Choe CU, So SH, Jeon SH, Ehrlich BE, Yoo 1100
 SH (2003) A functional interaction between chromogranin B 1101
 and the inositol 1, 4, 5-trisphosphate receptor/Ca²⁺ channel. 1102
J Biol Chem 278:49699–49706 1103
64. Libbrecht L, Desmet V, Van Damme B, Roskams T (2000) 1104
 The immunohistochemical phenotype of dysplastic foci in 1105
 human liver: correlation with putative progenitor cells. *J 1106*
Hepatol 33:76–84 1107
65. Hirata K, Dufour JF, Shibao K, Knickelbein R, O'Neill AF, 1108
 Bode HP, Cassio D, St-Pierre MV, LaRusso NF, Leite MF, 1109

2 Signaling Pathways in Biliary Epithelial Cells

- 1110 Nathanson MH (2002) Regulation of Ca(2+) signaling in rat
1111 bile duct epithelia by inositol 1, 4, 5-trisphosphate receptor
1112 isoforms. *Hepatology* 36:284–296
- 1113 66. Dufour J-F, Luthi M, Forestier M, Magnoni F (1999)
1114 Expression of inositol 1, 4, 5-trisphosphate receptor
1115 isoforms in rat cirrhosis. *Hepatology*
30:1018–1026
- 1116 67. Bennett DL, Cheek TR, Berridge MJ, De Smedt H, Parys JB,
1117 Missiaen L, Bootman MD (1996) Expression and function
1118 of ryanodine receptors in nonexcitable cells. *J Biol Chem*
1119 271:6356–6362
- 1120 68. Giannini G, Conti A, Mammarella S, Scrobogna M,
1121 Sorrentino V (1995) The ryanodine receptor/calcium chan-
1122 nel genes are widely and differentially expressed in murine
1123 brain and peripheral tissues. *J Cell Biol* 128: 893–904
- 1124 69. Leite MF, Dranoff JA, Gao L, Nathanson MH (1999)
1125 Expression and subcellular localization of the ryanodine
1126 receptor in rat pancreatic acinar cells. *Biochem J* 337(Pt 2):
1127 305–309
- 1128 70. Verma V, Carter C, Keable S, Bennett D, Thorn P (1996)
1129 Identification and function of type-2 and type-3 ryanodine
1130 receptors in gut epithelial cells. *Biochem J* 319:449–454
- 1131 71. Meszaros LG, Bak J, Chu A (1993) Cyclic ADP-ribose as an
1132 endogenous regulator of the non-skeletal type ryanodine
1133 receptor Ca²⁺ channel. *Nature* 364:76–79
- 1134 72. Sonleitner A, Conti A, Bertocchini F, Schindler H, Sorrentino
1135 V (1998) Functional properties of the ryanodine receptor type
1136 3 (RyR3) Ca²⁺ release channel. *EMBO J* 17:2790–2798
- 1137 73. Li W, Llopis J, Whitney M, Zlokarnik G, Tsien RY (1998)
1138 Cell-permeant caged InsP3 ester shows that Ca²⁺ spike fre-
1139 quency can optimize gene expression. *Nature* 392:936–941
- 1140 74. Hirata K, Nathanson MH, Burgstahler AD, Okazaki K,
1141 Mattei E, Sears ML (1999) Relationship between inositol 1,
1142 4, 5-trisphosphate receptor isoforms and subcellular Ca²⁺
1143 signaling patterns in nonpigmented ciliary epithelia. *Invest*
1144 *Ophthalmol Vis Sci* 40:2046–2053
- 1145 75. Nathanson MH, Fallon MB, Padfield PJ, Maranto AR (1994)
1146 Localization of the type 3 inositol 1, 4, 5-trisphosphate
1147 receptor in the Ca²⁺ wave trigger zone of pancreatic acinar
1148 cells. *J Biol Chem* 269:4693–4696
- 1149 76. Leite MF, Hirata K, Pusch T, Burgstahler AD, Okazaki K,
1150 Ortega JM, Goes AM, Prado MAM, Spray DC, Nathanson MH
1151 (2002) Molecular basis for pacemaker cells in epithelia.
1152 *J Biol Chem* 277:16313–16323
- 1153 77. Bode HP, Wang L, Cassio D, Leite MF, St-Pierre MV,
1154 Hirata K, Okazaki K, Sears ML, Meda P, Nathanson MH,
1155 Dufour JF (2002) Expression and regulation of gap junctions
1156 in rat cholangiocytes. *Hepatology* 36:631–640
- 1157 78. Kasai H, Augustine GJ (1990) Cytosolic Ca²⁺ gradients
1158 triggering unidirectional fluid secretion from exocrine pan-
1159 creas. *Nature* 348:735–738
- 1160 79. Ito K, Miyashita Y, Kasai H (1997) Micromolar and submi-
1161 cromolar Ca²⁺ spikes regulating distinct cellular functions
1162 in pancreatic acinar cells. *EMBO J* 16:242–251
- 1163 80. Fernandez-Chacon R, Konigstorfer A, Gerber S, Garcia J,
1164 Matos M, Stevens C, Brose N, Rizo J, Rosenmund C,
1165 Sudhof TC (2001) Synaptotagmin I functions as a calcium
1166 regulator of release probability. *Nature* 410:41–49
- 1167 81. Boyer JL, Soroka CJ (1995) Vesicle targeting to the apical
1168 domain regulates bile excretory function in isolated rat hepa-
1169 tocyte couplets. *Gastroenterology* 109:1600–1611
- 1170 82. Tietz PS, Alpini G, Pham LD, LaRusso NF (1995) Soma-
1171 tostatin inhibits secretin-induced ductal hyperchloresis and
exocytosis by cholangiocytes. *Am J Physiol Gastrointest* 1172
Liver Physiol 269:G110–G118 1173
83. McGill J, Basavappa S, Mangel AW, Shimokura GH, 1174
Middleton JP, Fitz JG (1994) Adenosine triphosphate activates 1175
ion permeabilities in biliary epithelial cells. *Gastroenterology* 1176
107:236–243 1177
84. Dranoff JA, Masyuk AI, Kruglov EA, LaRusso NF, 1178
Nathanson MH (2001) Polarized expression and function of 1179
P2Y ATP receptors in rat bile duct epithelia. *Am J Physiol* 1180
Gastrointest Liver Physiol 281:G1059–G1067 1181
85. Alvaro D, Alpini G, Jezequel AM, Bassotti C, Francia C, 1182
Fraiole F, Romeo R, Marucci L, LeSage G, Glaser SS, 1183
Benedetti A (1997) Role and mechanisms of action of ace- 1184
tylcholine in the regulation of rat cholangiocyte secretory 1185
function. *J Clin Invest* 100:1349–1362 1186
86. LeSage GD, Alvaro D, Benedetti A, Glaser S, Marucci L, 1187
Baiocchi L, Eisel W, Caligiuri A, Phinzy J, Rodgers R, 1188
Francis H, Alpini G (1999) Cholinergic system modulates 1189
growth, apoptosis, and secretion of cholangiocytes from bile 1190
duct-ligated rats. *Gastroenterology* 117:191–199 1191
87. Taylor AL, Schwiebert LM, Smith JJ, King C, Jones JR, 1192
Sorscher EJ, Schwiebert EM (1999) Epithelial P2X puriner- 1193
gic receptor channel expression and function. *J Clin Invest* 1194
104:875–884 1195
88. Basavappa S, Middleton J, Mangel AW, McGill JM, Cohn 1196
JA, Fitz JG (1993) Cl⁻ and K⁺ transport in human biliary cell 1197
lines. *Gastroenterology* 104:1796–1805 1198
89. Salter KD, Fitz JG, Roman RM (2000) Domain-specific 1199
purinergic signaling in polarized rat cholangiocytes. *Am* 1200
J Physiol Gastrointest Liver Physiol 278:G492–G500 1201
90. Sauzeau V, Le Jeune H, Cario-Toumaniantz C, Vaillant N, 1202
Gadeau AP, Desgranges C, Scalbert E, Chardin P, Pacaud P, 1203
Loirand G (2000) P2Y(1), P2Y(2), P2Y(4), and P2Y(6) 1204
receptors are coupled to Rho and Rho kinase activation in 1205
vascular myocytes. *Am J Physiol Heart Circ Physiol* 278:
1206 H1751–H1761 1207
91. Schlosser SF, Burgstahler AD, Nathanson MH (1996) 1208
Isolated rat hepatocytes can signal to nearby hepatocytes and 1209
bile duct cells by secretion of nucleotides. *Gastroenterology* 1210
110:A1315 1211
92. Chari RS, Schutz SM, Haebig JE, Shimokura GH, Cotton PB, 1212
Fitz JG, Meyers WC (1996) Adenosine nucleotides in bile. 1213
Am J Physiol Gastrointest Liver Physiol 270:G246–G252 1214
93. Nathanson MH, Burgstahler AD, Masyuk AI, LaRusso NF 1215
(2001) Stimulation of ATP secretion in the liver by therapeutic 1216
bile acids. *Biochem J* 358:1–5 1217
94. Dranoff JA, Kruglov EA, Robson SC, Braun N, Zimmermann H, 1218
Sevigny J (2002) The ecto-nucleoside triphosphate diphos- 1219
phohydrolase NTPDase2/CD39L1 is expressed in a novel 1220
functional compartment within the liver. *Hepatology* 36:
1221 1135–1144 1222
95. Gradilone SA, Masyuk AI, Splinter PL, Banales JM, 1223
Huang BQ, Tietz PS, Masyuk TV, LaRusso NF (2007) 1224
Cholangiocyte cilia express TRPV4 and detect changes in 1225
luminal tonicity inducing bicarbonate secretion. *Proc Natl* 1226
Acad Sci U S A 104:19138–19143 1227
96. Masyuk AI, Gradilone SA, Banales JM, Huang BQ, 1228
Masyuk TV, Lee SO, Splinter PL, Stroope AJ, LaRusso NF 1229
(2008) Cholangiocyte primary cilia are chemosensory organ- 1230
elles that detect biliary nucleotides via P2Y12 purinergic 1231
receptors. *Am J Physiol Gastrointest Liver Physiol* 295:
1232 G725–G734 1233

- 1234 97. Glaser S, Alvaro D, Roskams T, Phinizy JL, Stoica G, 1293
 1235 Francis H, Ueno Y, Barbaro B, Marzioni M, Mauldin J, 1294
 1236 Rashid S, Mancino MG, LeSage G, Alpini G (2003) 1295
 1237 Dopaminergic inhibition of secretin-stimulated choleresis 1296
 1238 by increased PKC-gamma expression and decrease of PKA 1297
 1239 activity. *Am J Physiol Gastrointest Liver Physiol* 284: 1298
 1240 G683–G694 1299
- 1241 98. Minagawa N, Kruglov EA, Dranoff JA, Robert ME, 1300
 1242 Gores GJ, Nathanson MH (2005) The anti-apoptotic pro- 1301
 1243 tein Mcl-1 inhibits mitochondrial Ca²⁺ signals. *J Biol 1302*
 1244 Chem 280:33637–33644 1303
- 1245 99. Harnois DM, Que FG, Celli A, LaRusso NF, Gores GJ 1304
 1246 (1997) Bcl-2 is overexpressed and alters the threshold for 1305
 1247 apoptosis in a cholangiocarcinoma cell line. *Hepatology 1306*
 1248 26:884–890 1307
- 1249 100. Nishizuka Y (1992) Membrane phospholipid degradation and 1308
 1250 protein kinase C for cell signalling. *Neurosci Res* 15:3–5 1309
- 1251 101. Alpini G, Baiocchi L, Glaser S, Ueno Y, Marzioni M, 1310
 1252 Francis H, Phinizy JL, Angelico M, LeSage G (2002) 1311
 1253 Ursodeoxycholate and tauroursodeoxycholate inhibit cho- 1312
 1254 langiocyte growth and secretion of BDL rats through acti- 1313
 1255 vation of PKC alpha. *Hepatology* 35:1041–1052 1314
- 1256 102. LeSage GD, Alvaro D, Glaser S, Francis H, Marucci L, 1315
 1257 Roskams T, Phinizy JL, Marzioni M, Benedetti A, 1316
 1258 Taffetani S, Barbaro B, Fava G, Ueno Y, Alpini G (2004) 1317
 1259 Alpha-1 adrenergic receptor agonists modulate ductal 1318
 1260 secretion of BDL rats via Ca²⁺- and PKC-dependent 1319
 1261 stimulation of cAMP. *Hepatology* 40:1116–1127 1320
- 1262 103. Taffetani S, Glaser S, Francis H, DeMorrow S, Ueno Y, 1321
 1263 Alvaro D, Marucci L, Marzioni M, Fava G, Venter J, 1322
 1264 Vaculin S, Vaculin B, Lam IP, Lee VH, Gaudio E, 1323
 1265 Carpino G, Benedetti A, Alpini G (2007) Prolactin stimu- 1324
 1266 lates the proliferation of normal female cholangiocytes by 1325
 1267 differential regulation of Ca²⁺-dependent PKC isoforms. 1326
 1268 *BMC Physiol* 7:6 1327
- 1269 104. Glaser S, DeMorrow S, Francis H, Ueno Y, Gaudio E, 1328
 1270 Vaculin S, Venter J, Franchitto A, Onori P, Vaculin B, 1329
 1271 Marzioni M, Wise C, Pилanthanonnd M, Savage J, Pierce L, 1330
 1272 Mancinelli R, Alpini G (2008) Progesterone stimulates the 1331
 1273 proliferation of female and male cholangiocytes via auto- 1332
 1274 crine/paracrine mechanisms. *Am J Physiol Gastrointest 1333*
 1275 Liver Physiol 295:G124–G136 1334
- 1276 105. Wang L, Piguat A-C, Tordjmann T, Dufour J-F (2005) 1335
 1277 Activation of CREB by TUDCA protects cholangiocytes 1336
 1278 from apoptosis induced by mTOR inhibition. *Hepatology 1337*
 1279 41:1241–1251 1338
- 1280 106. Berthiaume EP, Wands J (2004) The molecular pathogen- 1339
 1281 esis of cholangiocarcinoma. *Semin Liver Dis* 24:127–137 1340
- 1282 107. Park J, Gores GJ, Patel T (1999) Lipopolysaccharide 1341
 1283 induces cholangiocyte proliferation via an interleukin-6- 1342
 1284 mediated activation of p44/p42 mitogen-activated protein 1343
 1285 kinase. *Hepatology* 29:1037–1043 1344
- 1286 108. Yamagiwa Y, Marienfeld C, Tadlock L, Patel T (2003) 1345
 1287 Translational regulation by p38 mitogen-activated protein 1346
 1288 kinase signaling during human cholangiocarcinoma 1347
 1289 growth. *Hepatology* 38:158–166 1348
- 1290 109. Isomoto H, Kobayashi S, Werneburg NW, Bronk SF, 1349
 1291 Guicciardi ME, Frank DA, Gores GJ (2005) Interleukin 6 1350
 1292 upregulates myeloid cell leukemia-1 expression through a 1351
 STAT3 pathway in cholangiocarcinoma cells. *Hepatology* 42:1329–1338
110. Ishimura N, Bronk SF, Gores GJ (2005) Inducible nitric 1295
 oxide synthase up-regulates Notch-1 in mouse cholangio- 1296
 cytes: implications for carcinogenesis. *Gastroenterology* 128:1354–1368 1297
 1298
111. Schmitz KJ, Lang H, Wohlschlaeger J, Sotiropoulos GC, 1299
 Reis H, Schmid KW, Baba HA (2007) AKT and ERK1/2 1300
 signaling in intrahepatic cholangiocarcinoma. *World J 1301*
 Gastroenterol 13:6470–6477 1302
112. Folli F, Alvaro D, Gigliozzi A, Bassotti C, Kahn CR, 1303
 Pontiroli AE, Capocaccia L, Jezequel AM, Benedetti A 1304
 (1997) Regulation of endocytic-transcytotic pathways and 1305
 bile secretion by phosphatidylinositol 3-kinase in rats. 1306
Gastroenterology 113:954–965 1307
113. Misra S, Ujhazy P, Varticovski L, Arias IM (1999) 1308
 Phosphoinositide 3-kinase lipid products regulate ATP- 1309
 dependent transport by sister of P-glycoprotein and multidrug 1310
 resistance associated protein 2 in bile canalicular membrane 1311
 vesicles. *Proc Natl Acad Sci U S A* 96:5814–5819 1312
114. Rust C, Karnitz LM, Paya CV, Moscat J, Simari RD, 1313
 Gores GJ (2000) The bile acid taurochenodeoxycholate 1314
 activates a phosphatidylinositol 3-kinase-dependent sur- 1315
 vival signaling cascade. *J Biol Chem* 275:20210–20216 1316
115. Alpini G, Glaser S, Alvaro D, Ueno Y, Marzioni M, 1317
 Francis H, Baiocchi L, Stati T, Barbaro B, Phinizy JL, 1318
 Mauldin J, LeSage G (2002) Bile acid depletion and reple- 1319
 tion regulate cholangiocyte growth and secretion by a 1320
 phosphatidylinositol 3-kinase-dependent pathway in rats. 1321
Gastroenterology 123:1226–1237 1322
116. Marzioni M, Alpini G, Saccomanno S, Candelaresi C, 1323
 Venter J, Rychlicki C, Fava G, Francis H, Trozzi L, Glaser S, 1324
 Benedetti A (2007) Glucagon-like peptide-1 and its receptor 1325
 agonist exendin-4 modulate cholangiocyte adaptive response 1326
 to cholestasis. *Gastroenterology* 133:244–255 1327
117. Feranchak AP, Roman RM, Doctor RB, Salter KD, Toker A, 1328
 Fitz JG (1999) The lipid products of phosphoinositide 1329
 3-kinase contribute to regulation of cholangiocyte ATP and 1330
 chloride transport. *J Biol Chem* 274:30979–30986 1331
118. Shibao K, Hirata K, Robert ME, Nathanson MH (2003) Loss 1332
 of inositol 1, 4, 5-trisphosphate receptors from bile duct epi- 1333
 thelia is a common event in cholestasis. *Gastroenterology* 125:1175–1187 1334
 1335
119. Beuers U, Boyer JL, Paumgartner G (1998) Ursodeoxycholic 1336
 acid in cholestasis: potential mechanisms of action and 1337
 therapeutic applications. *Hepatology* 28:1449–1453 1338
120. Poupon RE, Poupon R, Balkau B (1994) Ursodiol for the 1339
 long-term treatment of primary biliary cirrhosis. *N Engl 1340*
 J Med 330:1342–1347 1341
121. Fiorotto R, Spirli C, Fabris L, Cadamuro M, Okolicsanyi L, 1342
 Strazzabosco M (2007) Ursodeoxycholic acid stimulates 1343
 cholangiocyte fluid secretion in mice via CFTR-dependent 1344
 ATP secretion. *Gastroenterology* 133:1603–1613 1345
122. Nathanson MH, Burgstahler AD, Mennone A, Dranoff JA, 1346
 Rios-Velez L (1998) Stimulation of bile duct epithelial 1347
 secretion by glybenclamide in normal and cholestatic rat 1348
 liver. *J Clin Invest* 101:2665–2676 1349
123. Alpini G, Lenzi R, Sarkozi L, Tavoloni N (1988) Biliary 1350
 physiology in rats with bile ductular cell hyperplasia. 1351

2 Signaling Pathways in Biliary Epithelial Cells

1352	Evidence for a secretory function of proliferated bile ductules. <i>J Clin Invest</i> 81:569–578	1362
1353		1363
1354	124. LeSage G, Glaser SS, Gubba S, Robertson WE, Phinzy JL, Lasater J, Rodgers RE, Alpini G (1996) Regrowth of the rat biliary tree after 70% partial hepatectomy is coupled to increased secretin-induced ductal secretion. <i>Gastroenterology</i> 111:1633–1644	1364
1355		1365
1356		1366
1357		1367
1358		1368
1359	125. Alpini G, Glaser SS, Ueno Y, Rodgers R, Phinzy JL, Francis H, Baiocchi L, Holcomb LA, Caligiuri A, LeSage GD (1999) Bile acid feeding induces cholangiocyte proliferation and secretion: evidence for bile acid-regulated ductal secretion. <i>Gastroenterology</i> 116:179–186	1369
1360		1370
1361		1371
	126. LeSage G, Glaser S, Alpini G (2001) Regulation of cholangiocyte proliferation. <i>Liver</i> 21:73–80	
	127. Kanno N, LeSage G, Glaser S, Alpini G (2001) Regulation of cholangiocyte bicarbonate secretion. <i>Am J Physiol Gastrointest Liver Physiol</i> 281:G612–G625	
	128. Hommel JD, Sears RM, Georgescu D, Simmons DL, DiLeone RJ (2003) Local gene knockdown in the brain using viral-mediated RNA interference. <i>Nat Med</i> 9:1539–1544	

Uncorrected Proof

Author Queries

[AQ1] Kindly provide complete details of “Keiji Hirata and Noritaka Minagawa” and add them to the reference list and number them.

[AQ2] Please provide better quality figures.